UNITED NATIONS EDUCATIONAL, SCIENTIFIC AND CULTURAL ORGANIZATION
INTERNATIONAL ATOMIC ENERGY AGENCY
INTERNATIONAL CENTRE FOR THEORETICAL PHYSICS
I.C.T.P., P.O. BOX 586, 34100 TRIESTE, ITALY, CABLE: CENTRATOM TRIESTE

H4.SMR/1013-10

SCHOOL ON THE USE OF SYNCHROTRON RADIATION IN SCIENCE AND TECHNOLOGY:
"John Fuggle Memorial"

3 November - 5 December 1997

Miramare - Trieste, Italy

Notes to Dr. Savoia's lectures

A. Savoia
Sincrotrone - Trieste
Trieste, Italy

INTERNATIONAL ATOMIC ENERGY AGENCY
UNITED NATIONS EDUCATIONAL, SCIENTIFIC AND CULTURAL ORGANIZATION
INTERNATIONAL CENTRE FOR THEORETICAL PHYSICS
I.C.T.P., P.O. BOX 586, 34100 TRIESTE, ITALY, CABLE: CENTRATOM TRIESTE

UNITED NATIONS INDUSTRIAL DEVELOPMENT ORGANIZATION

INTERNATIONAL CENTRE FOR SCIENCE AND HIGH TECHNOLOGY
c/o INTERNATIONAL CENTRE FOR THEORETICAL PHYSICS 34100 TRIESTE (ITALY) VIA GRIGNANO, 9 (ADRIATICO PALACE) P.O. BOX 586 TELEPHONE 040-224572 TELEFAX 040-224575 TELEX 460449 APH I

H4.SMR/877-2

THIRD SCHOOL ON THE USE OF SYNCHROTRON RADIATION IN SCIENCE AND TECHNOLOGY: *"JOHN FUGGLE MEMORIAL"*

30 October - 1 December 1995

Miramare - Trieste, Italy

Some Notes on the Designs of Beamlines for Soft X-ray Synchrotron Radiation in Sources of the 3rd Generation

W.B. Peatman
BESSY, Berlin - Germany

BESSY

NOTES 95

Some Notes on the Design of Beamlines for Soft X-ray Synchrotron Radiation Sources of the 3rd Generation

W.B. Peatman
Berliner Elektronenspeicherring-Gesellschaft
für Synchrotronstrahlung mbH (BESSY)
Lentzeallee 100, D-14195 Berlin, BRD

Revised Version November 1995

"NOTES 95": Some Notes on the Design of Beamlines for Soft X-ray Synchrotron Radiation Sources of the 3rd Generation

W.B. Peatman
Berliner Elektronenspeicherring-Gesellschaft
für Synchrotronstrahlung mbH (BESSY)
Lentzeallee 100, D-14195 Berlin, BRD

Table of Contents

* No text. References only (see 11)

List of Figures

List of Figures (con't)

List of Tables

Foreword

Up until the development of synchrotron radiation (SR) sources in the 1960's and 1970's research in the extreme VUV and soft x-ray range of the electromagnetic spectrum was limited to single wavelengths produced by line sources and to the helium continuum which produces 10 - 20 eV photons. Most research employing line sources was done without monochromators and without elaborate beamlines. Thus, in the 1970's the need for monochromators and optical systems to handle the continous radiation emitted from synchrotrons and storage rings marked a dramatic and abrupt change in the course of the development of practical optics. Although the theoretical basis for what was to come had long existed, the practical aspects of the design of optical systems for photon energies between 10 eV and 2000 eV, and of the manufacture of suitable optical elements for these energies had until that time never been in significant demand and had therefore been neglected.

Most of the original SR sources, which had been designed for the needs of high energy physics and not as light sources, have been succeeded by SR sources of the second generation: electron or positron storage rings with a relatively high brightness in the dipole magnets. BESSY in Berlin, Germany, offering user operation since 1982 is just one example of such an SR-Facility. The SR is emitted from electrons undergoing centripetal acceleration in the bending magnets. Since then still better sources of high brightness SR have been developed: wigglers and undulators. At present the world is experiencing a building boom of SR-sources of the third generation: storage rings in which the primary sources of SR are undulators and where wigglers and dipole sources take a secondary, albeit important role.

These notes are intended for those who have been intrusted with the design of the optical system which accepts SR from the source and brings it in the desired form to the experiment. We restrict ourselves to storage rings with an electron energy of 1.0-2.0 GeV and emphasize the development of high resolution monochromators for photon energies of ca. 10 - 1000 eV. The problems associated with high energy storage rings ($E_{el} > 3$ GeV) and with hard x-ray radiation are not dealt with here. The problem of heat loading of optical elements will only be alluded to and indeed chapters 7 - 10 will be handled only in that relevant references have been provided in part 11 for the reader's convenience. Similarly, many tables and figures will be found here for which there is little or no corresponding text. Their relevance should be evident from their placement in the development.

The number of references in chapter 11 is an indication of how many people have been making contributions to this field. In this revised edition of these "Notes", a few new references have been added. However, they are in no way exhaustive and reference should be made to the proceedings of the various SR instrumentation meetings both national and international.

Of essential importance for the present endeavour have been the discussions with colleagues in the experimental and machine groups here at BESSY as well as with friends and colleagues at sister institutions around the world. Their patience and interest is most gratefully acknowledged.

We hope the information provided here is found to be useful and request the reader to make known to the author errors and suggestions for improvement.

WBP, BESSY, Berlin
March 1992
Revised 1995

Chapter 1. Introduction

The main, distinguishing characteristics of synchrotron radiation (SR) are well known and can be illustrated by five particular parameters (Fig. 1.0.1). These characteristics refer specifically to SR emanating from dipole magnets. So-called insertion devices (ID's), described later, share some of them. Differences are pointed out here.

1) Its continuous spectrum from the infra red to soft or hard x-rays, depending upon the energy of the electrons. In the case of ID's, the spectrum is not continuous but is strongly peaked, depending upon the magnetic field strength of the ID.

2) The "spot light" nature of the emitted radiation, like the headlights of an auto at night, sweeping around the curves. i.e. The emission is highly directed and emanates from a (very) small source: the electron beam dimensions.

3) The time structure of the emitted SR. The electrons in the storage ring are grouped in bunches which are synchronous with the phase of the radio frequency cavity employed to pump energy back into them. This leads to the SR being emitted as pulses from each bunch as they pass by the viewer.

4) The high degree of polarisation of the SR, from plane polarised in the plane of the storage ring (from dipole magnets) to elliptically polarised above and below this plane. Polarised radiation from ID's can also be generated.

5) The characteristics of the SR can be exactly calculated if one knows the (exact) values of just three parameters: (a) the energy of the electrons, (b) the number of electrons (ring current) and (c) the radius of curvature of the electron trajectory or equally, the magnetic field strength at the point of emission of SR. Thus, SR can be a primary source of light from the IR to the (soft) x-ray region.

These aspects of SR are illustrated in figure 1.0.1, while the origin of the time structure is explained in figure 1.0.2. Figure 1.0.3 depicts the experimentally determined relationship between the number of electrons and

Fig. 1.0.1: Important Characteristics of Synchrotron Radiation

1) 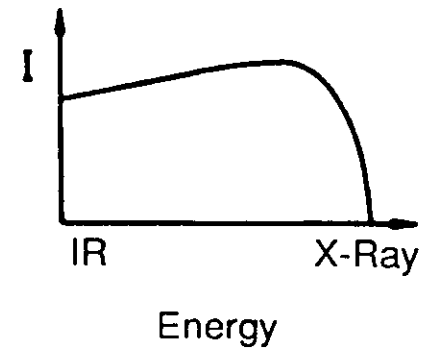

Continuous spectrum

2) 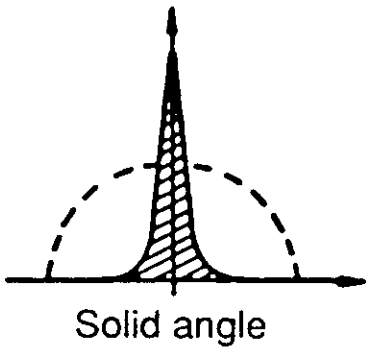

Emission in small solid angle

3) 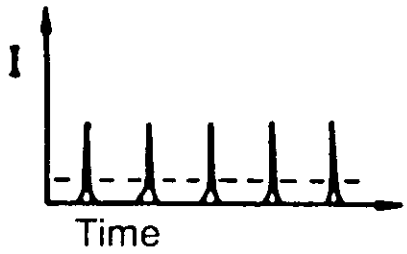

Pulsed time structure

4) 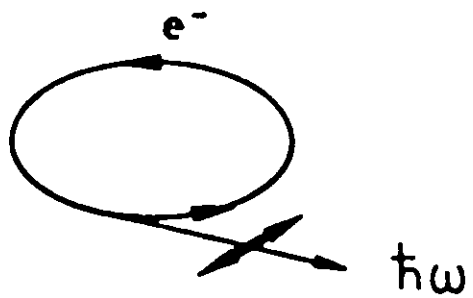

High degree of polarisation

5) Properties can be calculated/predicted

Figure 1.0.2: Time Structure of Synchrotron Radiation [2.12]

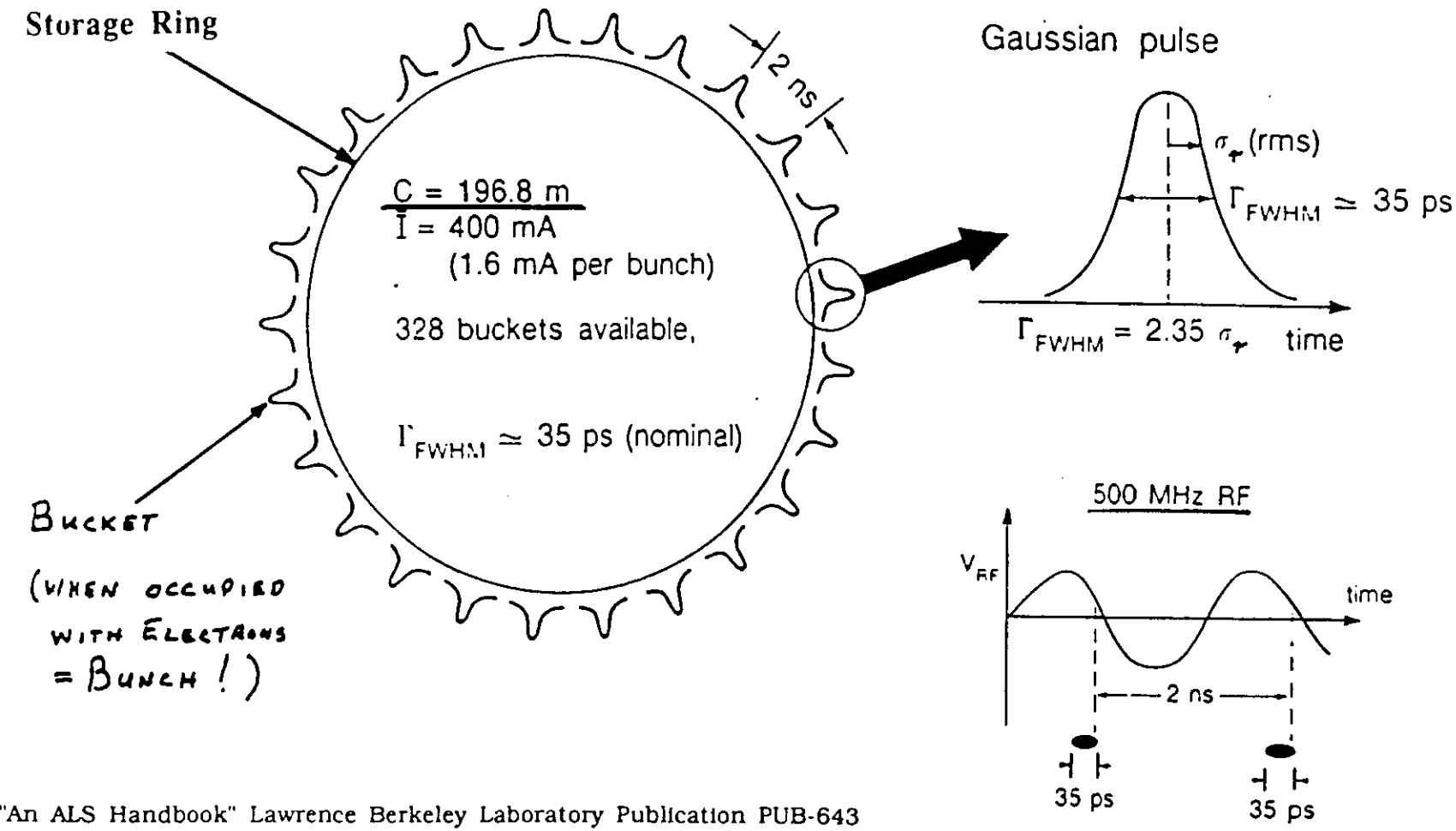

"An ALS Handbook" Lawrence Berkeley Laboratory Publication PUB-643
Rev. 2, April 1989

Figure 1.0.3: SR Intensity Versus Number of Electrons

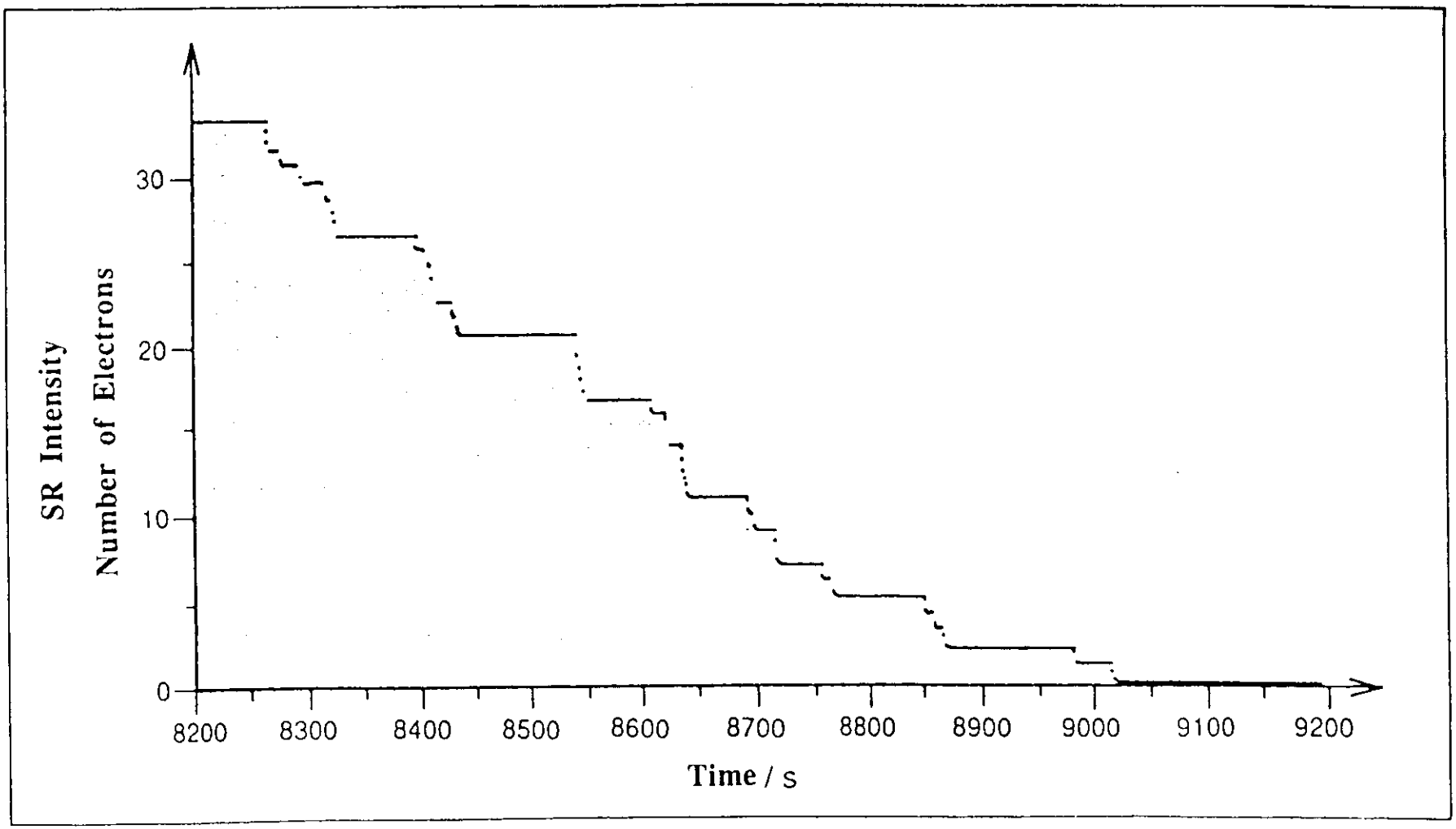

Figure 1.0.4: Synchrotron Radiation Sources

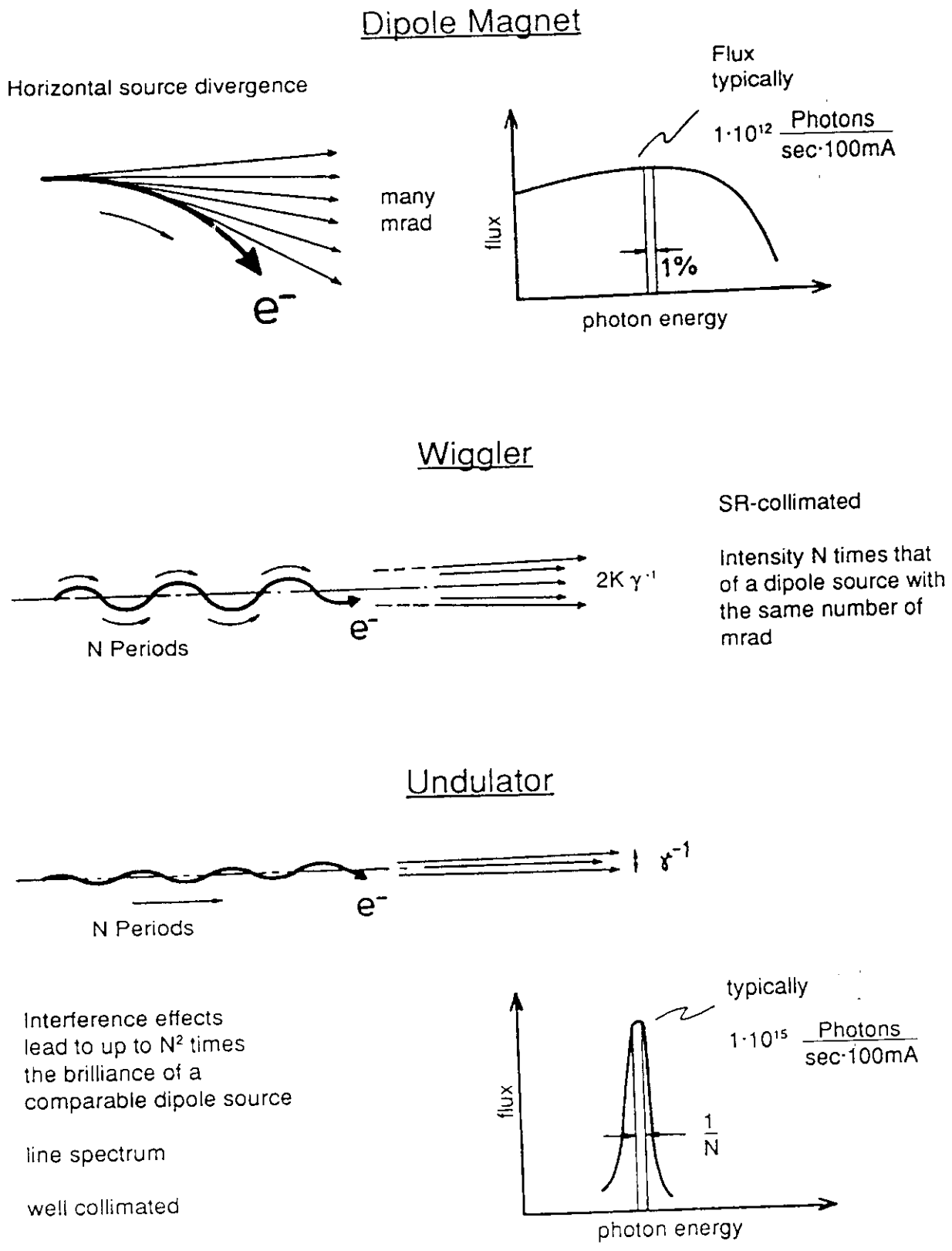

the intensity of the SR. The differences between dipole, wiggler and undulator radiation are shown in figure 1.0.4.

Finally, the high intensity of the SR together with the small source dimensions and the small solid angle into which the SR is emitted lead to a nearly ideal source for optical systems: a directed point source. These three quantities taken together are referred to as "Brilliance" or, in some parts of the SR community, as "Brightness". It has been the goal of the designers of synchrotron storage rings of the second and third generations to maximize the brilliance. It is the job of the beam line engineer or scientist to transfer this brilliance to the experiment. Thus, as many photons as possible of the desired energy should be transmitted from the source through the optical system to the experiment and refocussed there in as small a volume as possible. It was with this goal in mind that these notes were written!

1.1 Coupling the source to the experiment: Brilliance, Brightness and Flux

The word "brilliance" has already been mentioned without having been defined.

$$\text{Brilliance} = \frac{\text{Photons/sec}}{I} \cdot \frac{1}{\sigma_x \sigma_y \cdot \sigma_x' \sigma_y' \cdot BW}$$

where
- I = electron current in the storage ring
- $\sigma_x \sigma_y$ = the transverse area from which the SR is emitted
- $\sigma_x' \sigma_y'$ = the solid angle into which the SR is emitted
- BW = Bandwidth of the monochromator

In the USA the term "Brightness" is generally used for the above expression we call "Brilliance". This is unfortunate, since, in Europe the expression "Brightness" is also a defined quantity:

$$\text{Brightness} = \frac{\text{Photons/sec}}{I} \cdot \frac{1}{\sigma' x \cdot \sigma' y \cdot BW}$$

It has not been possible to get scientists to agree upon these definitions. Thus, one must be aware of the different definitions and stay awake!

Figure 1.1.1: The Practical Meaning of Brilliance

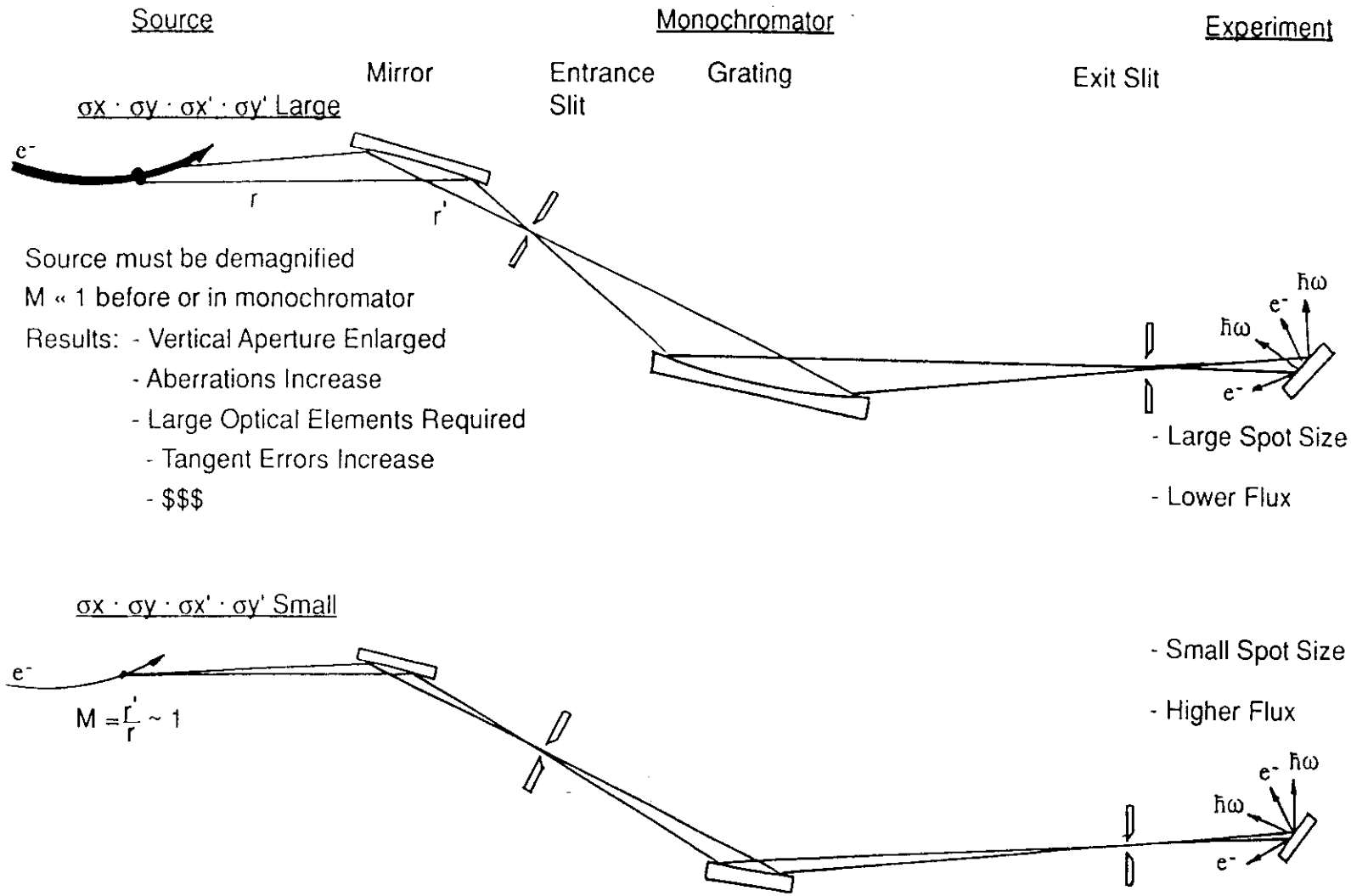

It is assumed here that all the above distributions are Gaussian.

In general, the researcher needs a certain minimum number of photons/sec or "flux" at his experiment. These photons will have been monochromatized to a greater or lesser extent (BW) and will be focussed down to a spot of some particular characteristics. Thus, where the researcher thinks of flux at his experiment, the beamline designer quickly discovers that the second half of the brilliance equation above is as important as the first half in determining the success or failure of his beamline design. But the brilliance equation given above is only the first link in the chain: the source. In order to optimize the coupling of the source to the experiment, the brilliance of the source must be conserved, as well as possible, as the SR is reflected and dispersed in the beamline. A bad optical design, faulty optical elements or instability of the various "links" are just a few of the things which irrevocably lead to loss of brilliance. Thus, in order to obtain a high flux of SR of the desired qualities at the experiment, a high brilliance source and a beamline in which this brilliance is conserved are required. Figure 1.1.1 illustrates the differences between a high brilliance system and one with a lower brilliance. Figure 1.1.2a shows the brilliance expected from a SR-facility of the third generation (the 1980's design of BESSY II. The 1990 design which is presently under construction is quite different!) [1.6]. In addition, the flux curves for the source are shown (Fig. 1.1.2b).

Regardless of the source, dipole, wiggler or undulator, the vertical source size stems primarily from the horizontal emittance of the storage ring, the horizontal to vertical coupling factor and the vertical β-function and is generally much smaller than the horizontal source size, typically by a factor of between 3 and 10 (see Chapter 2). If great importance is ascribed to energy resolution (BW), then the dispersive plane of the beamline should be vertical. For this reason, we will direct our energies in particular towards conserving vertical brilliance, in cases where energy resolution is to be optimized.

In order to illustrate some of the topics to be encountered in the subsequent chapers figures 1.1.3 - 1.1.4 are provided [1.7]. Figure 1.1.3 shows the spectral power distribution of undulator U-2.5 as originally planned for BESSY-II. The total power of 130 watts corresponds to the brightness and flux curves shown in figure 1.1.2a and b. Also shown in figure 1.1.3 is the

Figure 1.1.2: BESSY II: Brilliance and Flux

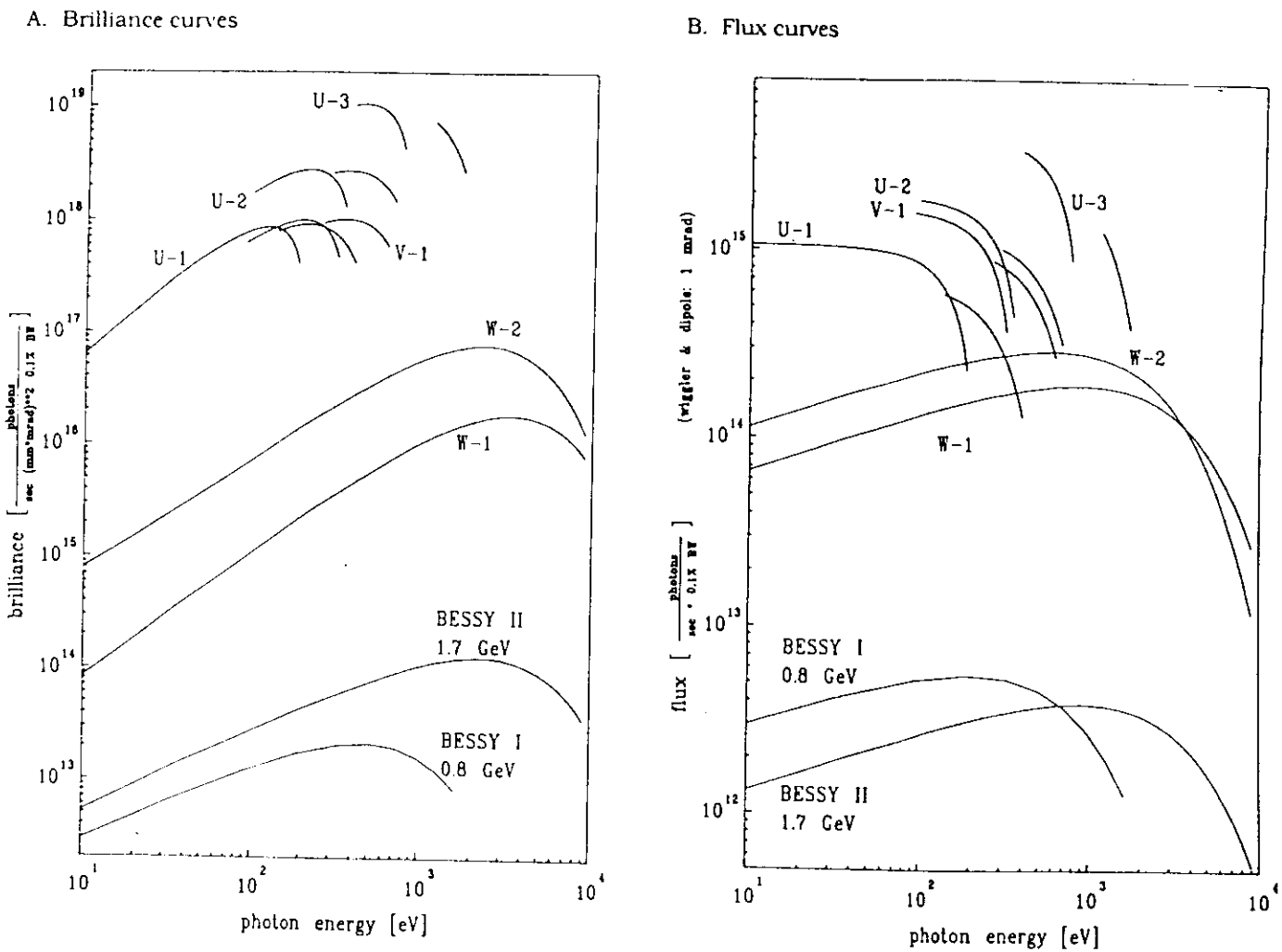

Fig. 1. (a) Brilliance curves for BESSY II (100 mA, 1.7 GeV) and BESSY I (300 mA, 0.8 GeV). (b) Flux curves for BESSY II and BESSY I as above. For complete details, see: "BESSY II, eine optimierte Undulator/Wiggler-Speicherring Lichtquelle für den VUV- und XUV-Spektralbereich."

Table 1.1.1 Thermal Loading of Optical Elements by Wiggler and Undulator Radiation [1.8, 1.9]

($K = 0.934\ B_{max}\ \lambda_o$)

a) Total power

$$P(W) = 12.7\ E^2 < B^2 > L\ I$$

b) Max. power per mrad (hor)

$$P_a\ (W/mrad) = 4.33\ E^3\ B_{max}\ I\ N$$

c) Max. power per solid angle

$$P_b\ (W/mrad^2) = 5.38\ E^4\ B_{max}\ I\ N$$

d) Max. power per mm (hor)

$$P_c\ (W/mm) = \frac{P_a\ (W/mrad)}{Z}$$

e) Max. power per mm^2

$$P_d\ (W/mm^2) = \frac{P_b\ (W/mrad^2)}{Z^2}$$

E = GeV
B = T
L = cm = $N\lambda_o$
N = No. of periods
λ_o = cm
I = A
Z = m (distance from source)

Figure 1.1.3: Spectral Power Distribution of Undulator U-2.5 [1.6b]

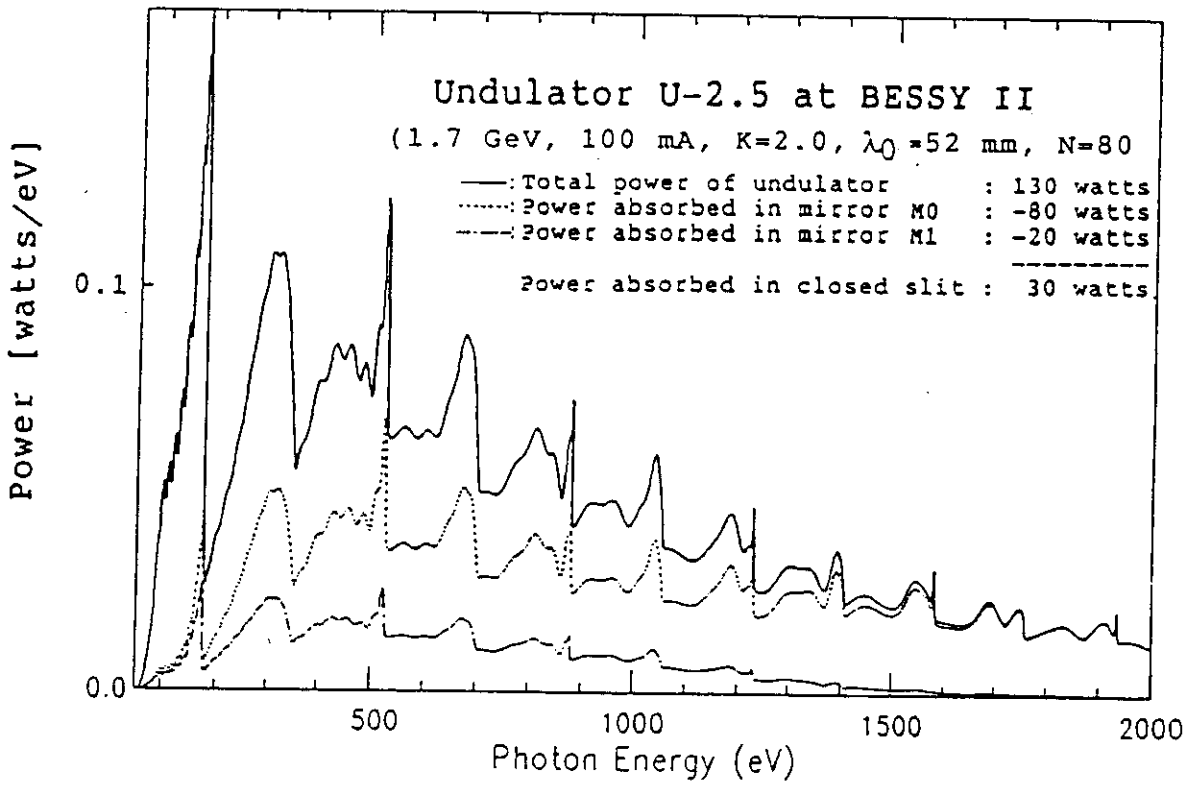

The spectral power distribution of undulator U-2.5 (λ_0 = 52 mm, N = 80) at BESSY II for 100 mA and K = 2. Also shown is the spectrum of the power absorbed in the mirror M0 and in M1.

Figure 1.1.4: Pre-Monochromator Optical System [1.7]

A. The Kirkpatrick-Baez pre-monochromator optical system.

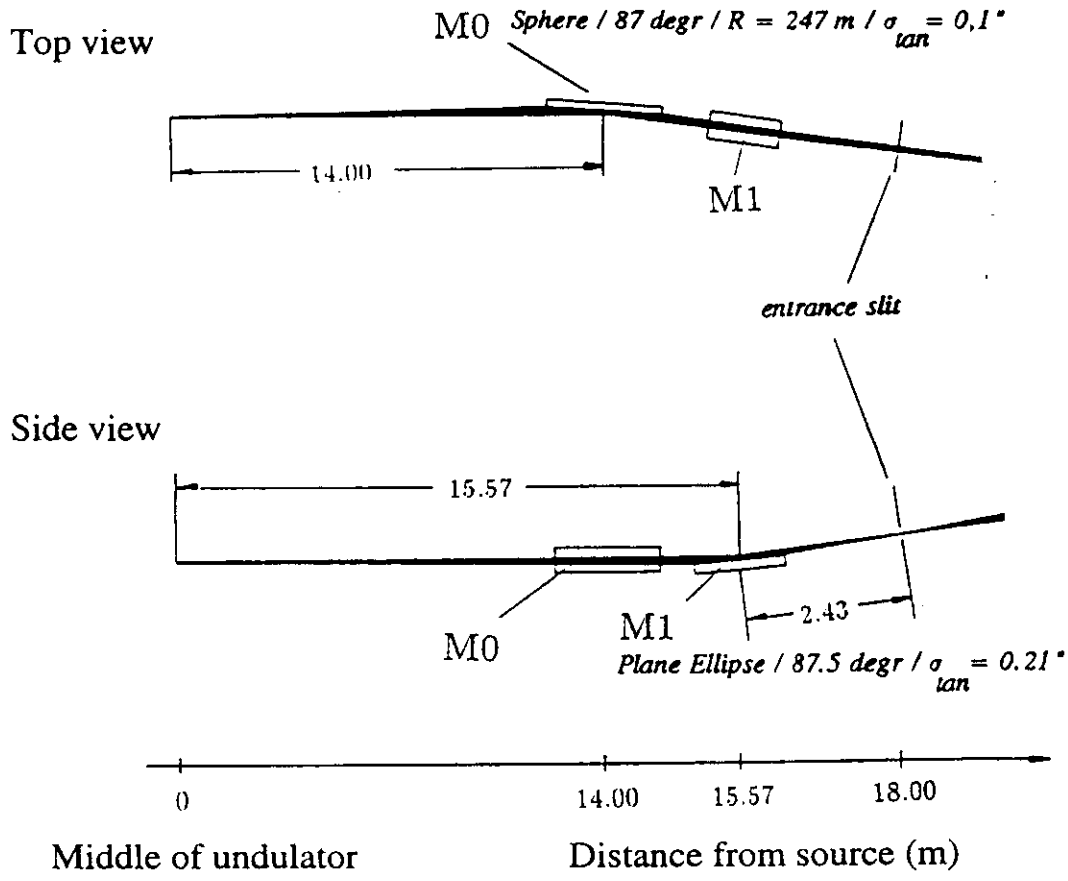

B. The effect of heat load on the premirror. The critical plane elliptical mirror, M1 (see above), showing schematically the deformation resulting from 20 W of heat absorbed.

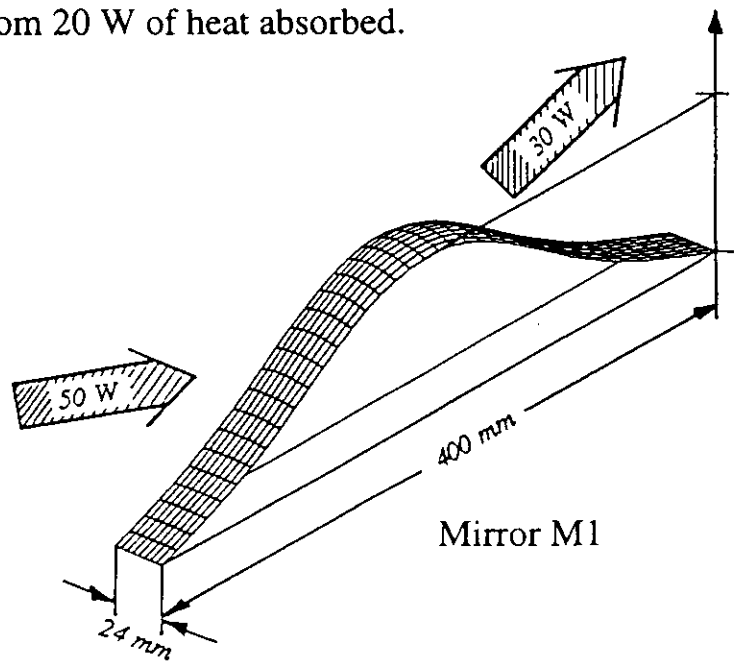

amount of power absorbed in the first two mirrors in the model beamline shown in figure 1.1.4a. For reasons to be given later (Chapter 5) the second of these mirrors is crucial for conserving vertical brilliance in this beamline. Figure 1.1.4b shows schematically the deformation of this mirror resulting from the heat absorbed in it (bottom curve of figure 1.1.3). Although the subject of heat loading will not be dealt with explicitly in these "Notes", references hereto are given under chapter 8. In Table 1.1.1 one can find the various power loading relationships for wigglers and undulators: total power, maximum (axial) power/mrad(hor), maximum power/mrad^2, maximum power/mm(hor) and maximum power/mm^2. Examples of these power relationships are to be found in chapter 2 (figure 2.5.2, table 2.5.2).

Whether the deformation of optical elements is caused by heat loading as shown or by manufacturing limits (figure errors) brilliance is degraded and some of the scientific potential of the source irretrievably lost. Thus, it is an exciting challenge for the designer of a beamline to keep all of the relevant parameters in mind and to optimize the entire system from the source to the experiment.

1.2 Tools necessary

1.2.1. Computer Codes

In order to design and optimize a beamline from the source to the experiment certain "tools" are highly desirable. With the availability of inexpensive, powerful computers along with the development and generally gratis distribution of various computer codes, one can maintain that the latter are indispensible. The amount of work required to familiarize oneself with, for example, a ray trace program is more than returned in the certainty it lends in the choice of optical elements and overall design. One cannot rely on intuition alone!

Similarly, computer codes are available which enable one to describe undulator sources in great detail and realism. Others are available to calculate the optical properties of reflectors from the optical constants. Still others will optimize the multitude of parameters in a monochromator for resolution. As mentioned above, most of these programs are available "free for the asking".

References are given in chapter 10 from which the authors and their addresses can be obtained.

Finally, it is possible to determine the effect of the power of the SR on the geometry of optical components and to develop cooling schemes to combat deformations due to heat. Such programs, called the finite element method (FEM) of analyses, are, however, much more difficult to use than the aforementioned ones and are generally available only at considerable cost.

1.2.2. Mechanical Tools

Once the theoretical design of the mirrors, gratings etc. has been optimized, they, their optical mounts and the vacuum vessels that house them should be examined with an eye towards aligning and adjusting them. Mirrored flats, fiducial marks, etc. can be provided by the manufacturer on mirrors and gratings in order to facilitate aligning them initially and maintaining alignment in routine operation. Windows, feedthroughs, adjustable apertures, moveable fluorescent screens, auxilliary optical components such as 90° prisms for peering into a beamline from the side should be brought into the design from the start.

The most common hardware "tools" which one employs to set up and align beamlines are the following:

Plumb line
50 m steel measuring tape
Machinists level
Vernier caliper
Red or green helium laser (low power) and adjustable tripod
Theodolyte and tripod
Levelling telescope and tripod
Autocollimator and tripod or stand
Various first surface mirrors, prisms, holders for same etc.

Other instruments are available for determining the profile and/or surface roughness of optical elements and although highly desirable are highly expensive.

1.3 Coordinate Systems, Distributions, Error Functions

1.3.1. Coordinate Systems. Storage Ring

There is no single generally accepted coordinate system for both storage ring geometry and optical geometry. Indeed, this statement holds for each area alone. In these notes we try to adhere to the convention that the vertical direction, i.e. perpendicular to the plane of the storage ring, is the "y" direction. In machine physics this is often designated as the "z" direction. The direction of propagation of electrons or photons is generally labled "s" by machine physicists, "r" in grating theory and in ray trace programs "z". For examples see figures 2.1.1, 4.2.1 and 5.4.1. The "right hand rule" for Cartesian coordinate systems is often violated. In addition, in ray trace programs the coordinate system is usually rotated according to the deflection plane of mirrors and gratings, meridional and sagittal maintaining their designators (y or z and x respectively) throughout the optical system (see section 1.3.2 below).

Thus, the reader being aware of this state of affairs should try to avoid being irritated or lead astray by it! One final point to this subject: in these "Notes" we try to adhere to the convention that a primed quantity refers to an angle and an unprimed quantity to a length. Thus σ' is (almost) always the standard deviation of an angle and σ that of a length. There are, however, a few exceptions, the main one being the definition of the arm lengths of an optical system, r and r' (chapters 4 and 5).

1.3.2. Ray Trace Program

For the ray trace programs, certain conventions must be established in order to maintain one's sanity in working through a multi-element beamline design. The definitions given in figure 1.3.1 for the BESSY ray trace program "RAY" are intended to fulfill this need. Be sure to note that "y always remains in the optical plane"!

Figure 1.3.1: Definition of Terms for the Ray Trace Program "RAY" [1.3]
Rotating Coordinate Systems

Note: "Y" always remains in the optical plane

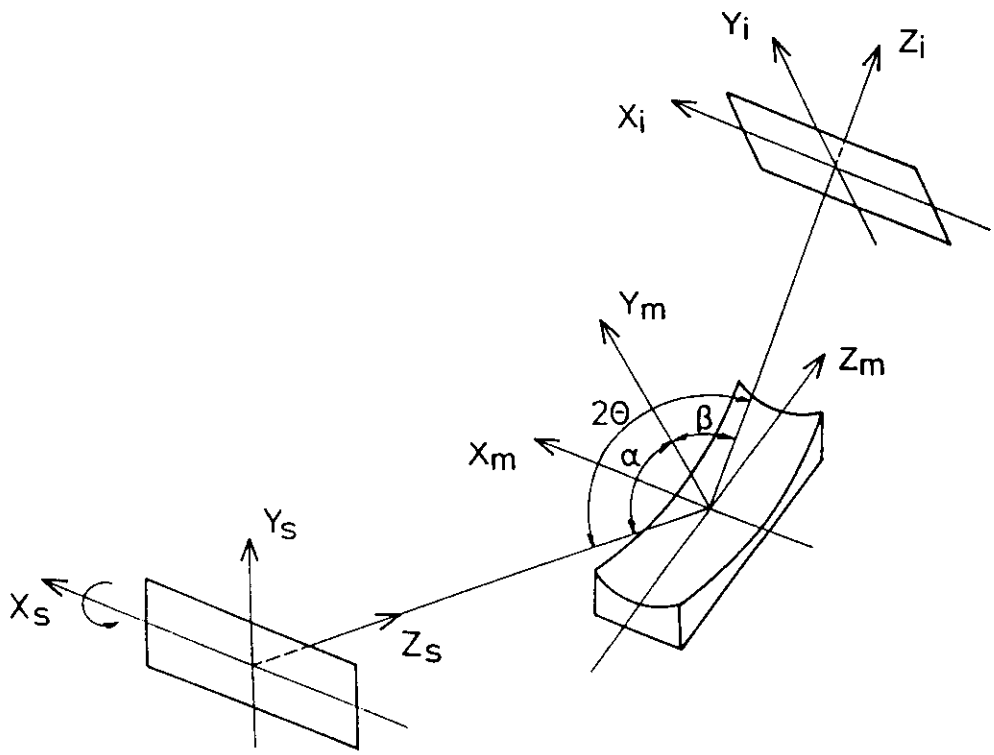

Vertical Deflection

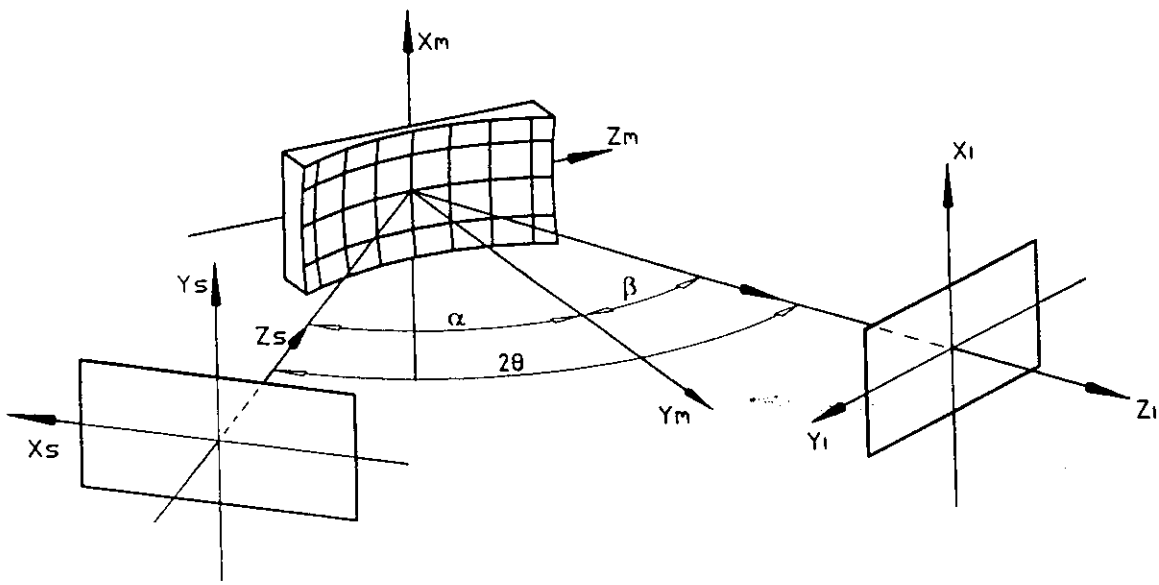

Horizontal Deflection

1.3.3. Distributions, Error Functions

In the development presented in these "Notes", we will either (a) derive the expressions for uncertainties in terms of the Gaußian or normal error distribution or (b) assume that a given distribution obeys it. In addition, for the convolution of the various functions used to describe a complete system, one often resorts to the statistics associated with randomly occuring errors according to Gauß. The definitions associated with these statistics are illustrated in table 1.3.1. In many real cases the relevant functions do not strictly obey these statistics, but for convenience the Gauß statistics are employed as a "best guess", which is certainly better than no estimate at all. Thus, for example, the ID source is described by Bessel functions. Useful approximations can be made to these functions. Depending upon who is making the approximations and how, the final approximate values of the quantities desired may deviate significantly from "deriver" to "deriver" . See, for example, section 2.5.2 and figure 2.5.4 for a direct comparison. The approximate values are both necessary and useful or beamline design. Exact values can be calculated in many cases but only with considerable effort and computer assistance. For ray trace calculations, as are necessary for beamline design, some sort of distribution function is required for a realistic definition of the source and of random surface errors of mirrors and gratings, etc.

In addition, the assumption of a Gaußian distribution makes the interpretation of measured or calculated data very easy: for a Gaußian distribution, the full width at half maximum (FWHM) is equal to 2.35 standard deviations (σ). In other cases we will be interested in the area under a distribution curve. We can utilize the fact that, again for a Gaußian distribution, 4 σ corresponds to 95 % of the area under the curve. See, for example, figures 2.5.3 a-d and tables 2.5.2 and 2.5.3 a-c. From the calculated data (figure 2.5.3 a-d) we can determine the asymptotic limit quite reliably and, taking 95 % of it, arrive at a σ value.

Table 1.3.1: Some Characteristics of a Gaußian Distribution

For randomly distributed errors, the scatter of measured values, x_i , about their average value, $\bar{x}$, obeys the relationship derived by Gauß (1808):

$$P(x) = \frac{1}{\sigma\sqrt{2\pi}} e^{\frac{-(x-\bar{x})^2}{2\sigma^2}} .$$

The variance, σ^2 , is defined as follows:

$$\sigma^2 \equiv \frac{1}{n-1} \sum_{i=1}^{n} (x_i - \bar{x})^2$$

where n is the number of trials and $\bar{x} = \frac{1}{n} \sum_{i=1}^{n} x_i$.

The standard deviation, σ , also known as the root mean square (rms) error, is defined in terms of the variance, σ^2 , above.

A plot of the distribution P(x) versus x is the familiar "bell" curve:

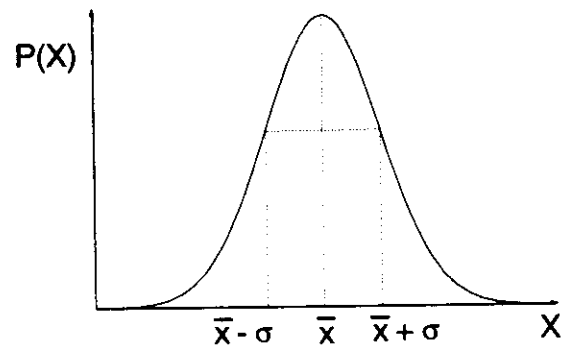

The following are useful relationships between σ and the area under the curve:

$\bar{x} \pm 1\sigma$	$\Rightarrow$	68.3 % of the area
$\bar{x} \pm \frac{2.35}{2}\sigma$	$\Rightarrow$	76.0 % of the area
$\bar{x} \pm 2\sigma$	$\Rightarrow$	95.4 % of the area
$\bar{x} \pm 3\sigma$	$\Rightarrow$	99.7 % of the area
$\bar{x} \pm \infty\sigma$	$\Rightarrow$	100 % of the area
2.35σ	$\Rightarrow$	Full width at half maximum of the curve, (FWHM) , sometimes designated as Δ .

1.4 Further remarks

1.4.1. Disturbing effects of wiggler/undulator operation

The installation of a wiggler or undulator in a storage ring presents particular problems to the ring designers: the symmetry of the ring is broken, a variable perturbation of the electron optics is introduced and the coupling of the horizontal equations of motion of the electrons with the vertical ones is increased due to magnet field errors and inhomogenieties in the multipole structures. Examples of the effects of undulator operation on some characteristics of the storage ring are shown in figure 1.4.1. These were observed on the first wiggler/undulator installed at BESSY and result largely from a residual skew quadrupole component in the magnet structure leading to an increase in the vertical beam dimension with increasing K value (decreasing gap) i.e. an increased coupling factor. Similarly, the beam lifetime is reduced with decreasing gap, probably resulting from tune shifts into less stable parts of tune space. Finally, the position and angle of the electron trajectories are momentarily affected by gap changes reflecting the time constant of the feedback electronics/steerer magnet orbit correction system.

All of the above problems become more severe as K increases. This, along with the fact that the power emitted from a wiggler/undulator is proportional to K^2 suggests that an upper limit be set on K in order to set an upper limit on the problems created. Supporting this suggestion is the fact that at least 50 % of the relative contributions of the odd harmonics from 1 to 11 are achieved for K values between 0.5 and 2.0. This is shown in figure 1.4.2 in which the function $F_k(K)$ is plotted as a function of K. $F_k(K)$ is the Bessel function giving the relative contribution of the odd harmonics to central intensity of the total spectrum according to

$$I_k(K) = 4.56 \times 10^6 \, N^2\gamma^2 I(A) F_k(K) \text{ photons/s}\cdot\text{mrad}^2\cdot 0.1\ \%\ \text{BW} \quad [2.1]$$

As seen in the figure, the higher the K value, the more unwanted harmonics are produced and with them unuseable power. This is also evident in measurements of the flux from an undulator as a function of K (figure 2.5.1b). In short, high K values increase the problems for the storage ring and heat loading of the optics without producing a commensurate increase in photon flux of the desired photons. An upper limit over which K can be

Figure 1.4.1: Disturbing Effects of Undulator Operation [2.10]

A. Vertical beam size as a function of the gap

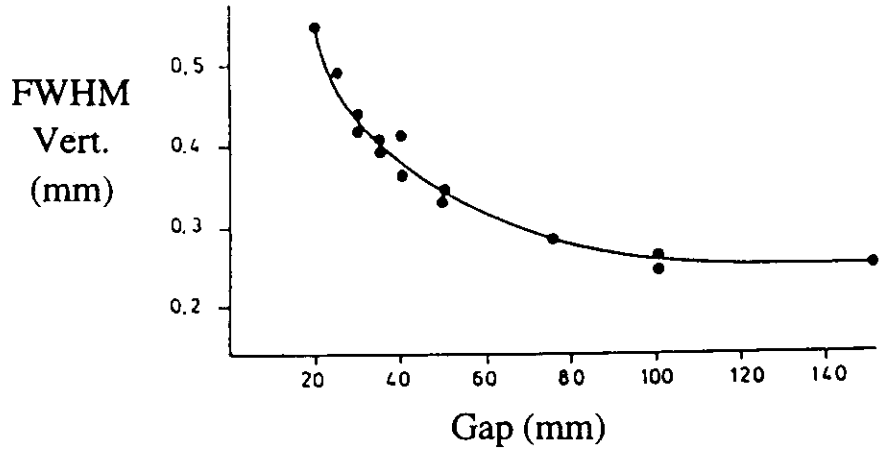

B. Beam lifetime as a function of the gap

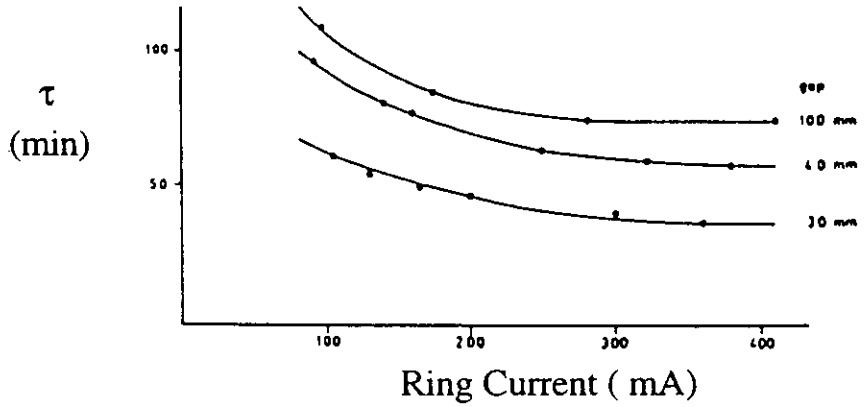

C. Beam position and angle of emission as gap is changed

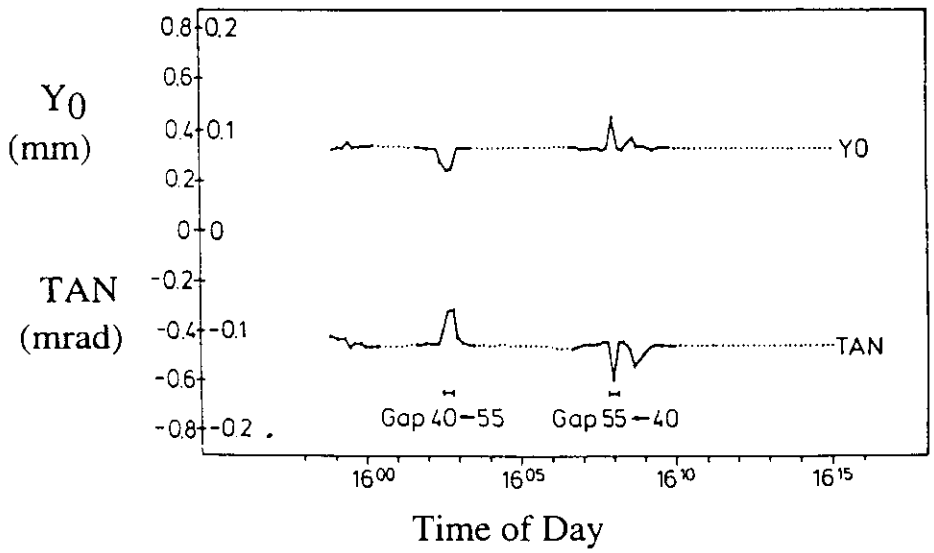

continuously scanned combined with fixed, higher K values for which the storage ring can be tuned would appear to be a reasonable solution to the problem.

1.4.2. Spectral purity

A common problem in the VUV, soft x-ray portion of the spectrum is the transmission of higher orders of radiation by the monochromator according to the grating equation: $k\lambda = \frac{1}{N}(\sin\alpha + \sin\beta)$ (see chapter 4.2). Thus, for a given grating line density, N, and incident and diffraction angles, α and β, a family of $k\lambda$ pairs will be transmitted where k, the order of the radiation equals $\pm$ 1, $\pm$ 2, $\pm$ 3 etc. A typical spectrum from an undulator with a toroidal grating monochromator is shown in figure 1.4.3. The higher order contributions are plainly to be seen. In the visible portion of the electromagnetic spectrum these orders can be separated with the help of filters or prisms. At short wavelengths, prisms do not exist and few filters are available. The principal method of suppressing the higher order light takes advantage of the energy dependence of the reflectivity from mirrors, higher energies being reflected less well for a given angle of incidence. Thus, it is possible to design a monochromator such that the angles of incidence favor the desired wavelengths and partially suppress the undesired ones. It is also possible to build two mirror systems explicitly for the purpose of suppressing higher order light. References for this subject are given under chapter 7.

1.4.3. Thermal problems

Here we refer not to the deformation of the optical surface of a mirror or grating but rather to the change in position of a mirror or grating in the beamline or of a magnet in the storage ring itself. Figure 1.4.4 shows the measured photon intensity behind a 20 μm slit as a function of time. Also shown is the temperature of the mirror/mirror mount used to focus the SR on the slit. The unambiguous correlation between the two shows that the thermally regulated cooling water is periodically deadjusting the position of the mirror, and this despite a thermal regulation to $\pm$ 0.5° C. The period of the thermoregulator is 6.5 minutes (figure 1.4.4a). By putting a buffer reservoir in the cooling line before the water reaches the mirror, the water of

Figure 1.4.2: The Function $F_k(K)$ for Odd Harmonics of Undulator Radiation [2.1]

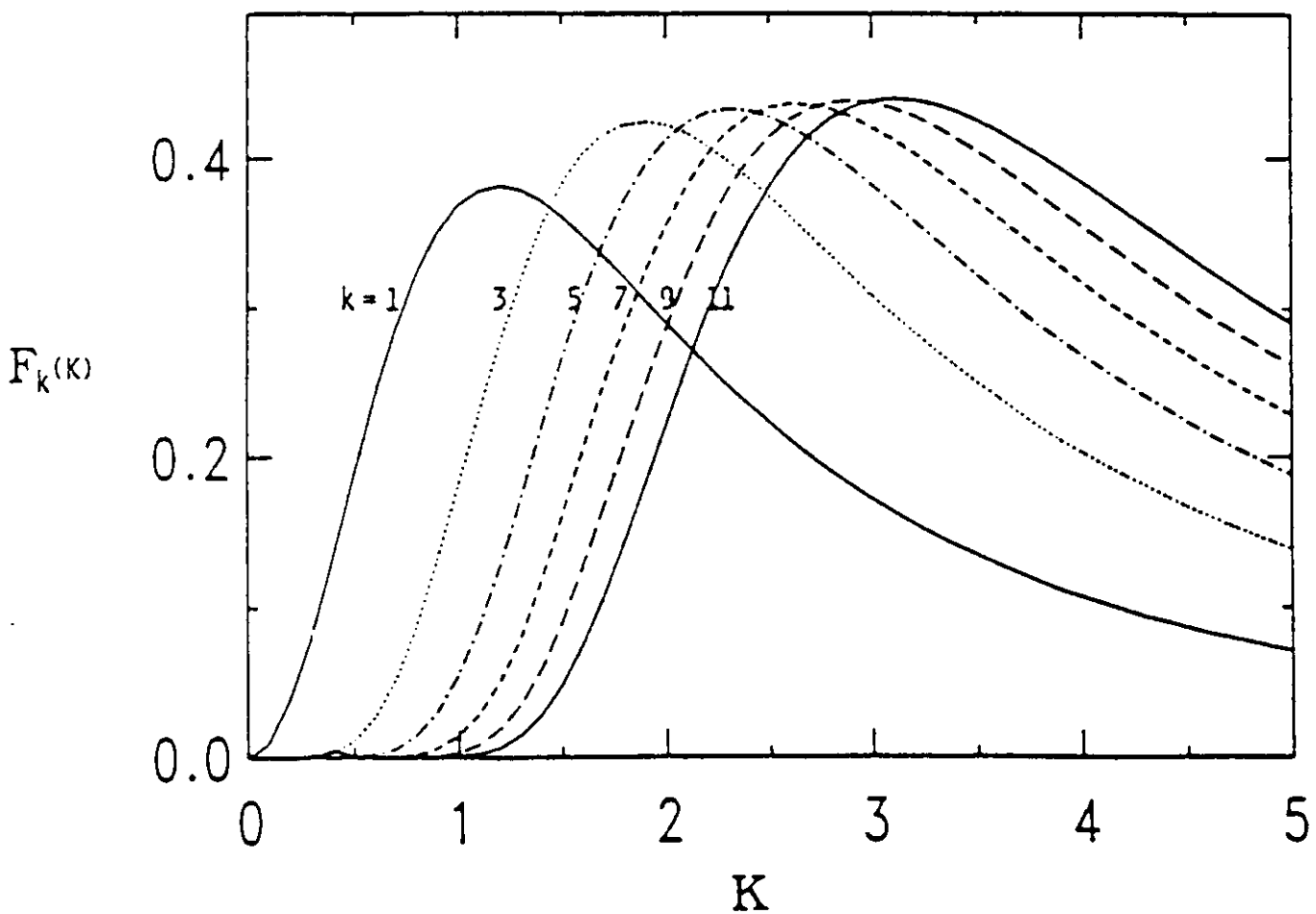

Figure 1.4.3: Undulator Radiation: A Mixed Pleasure [2.11]
Undulator spectra showing the presence of higher harmonics (Roman numerals) and higher orders (Arabic numerals). For a gap of 200 mm the photon flux comes from the neighboring dipoles.

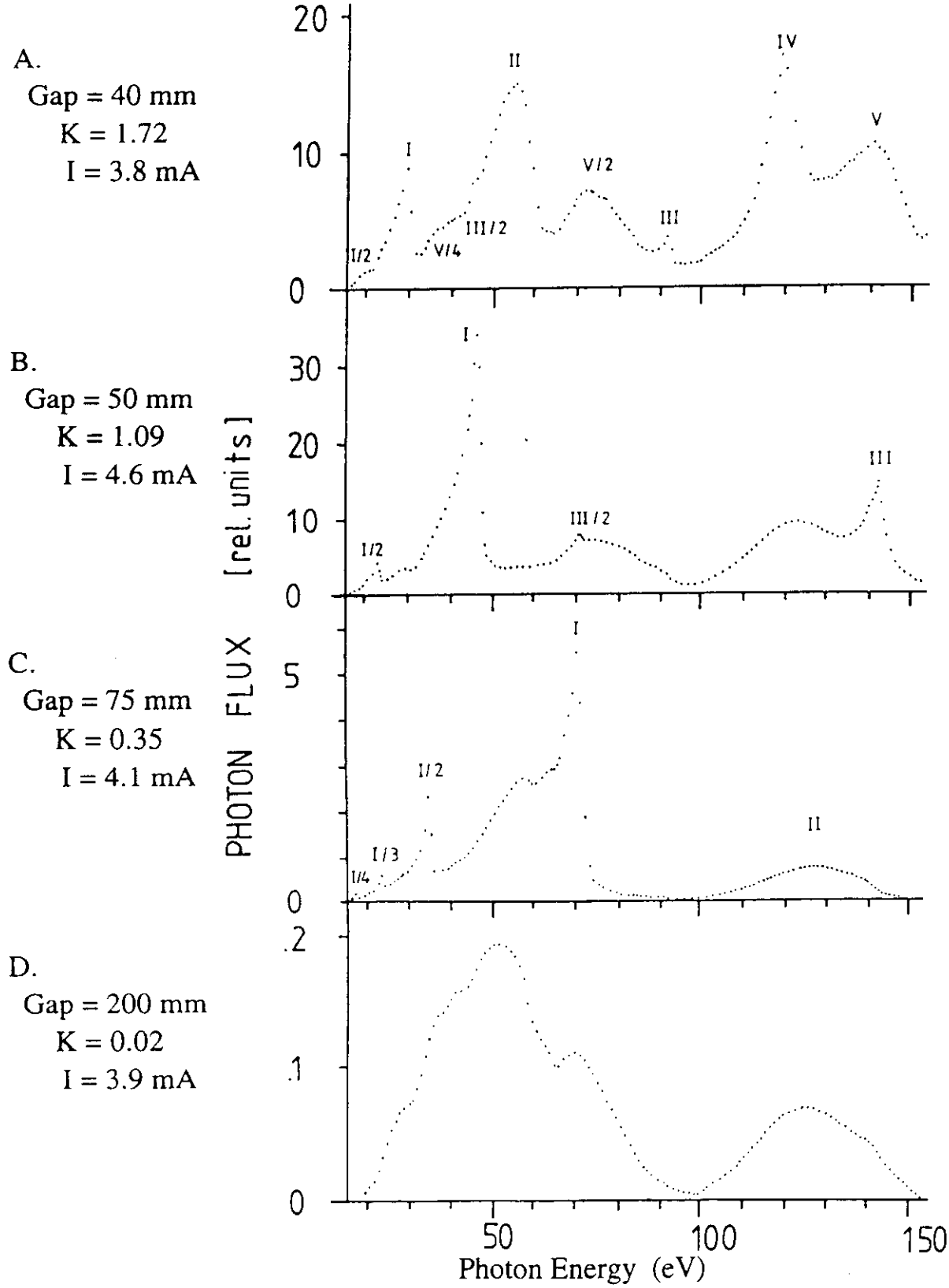

Figure 1.4.4: Temperature Stability: Mirror Cooling

The variation in intensity through a 20 μm slit compared with the temperature of the focussing mirror used to illuminate it. The cooling water temperature was regulated to (A) ± 0.5 ° C and (B) ± 0.05 ° C.

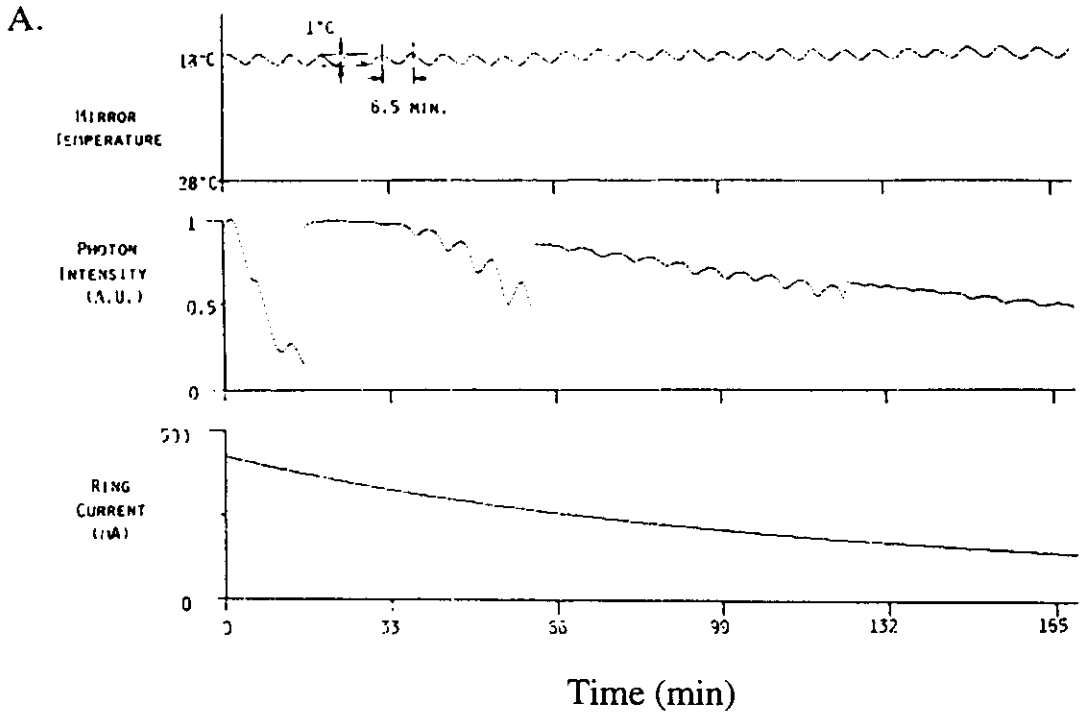

Figure 1.4.5: Temperature Stability: Magnet Cooling

A) Beam position and angle of SR emission: 8 AM - 8 PM 30.8.1991

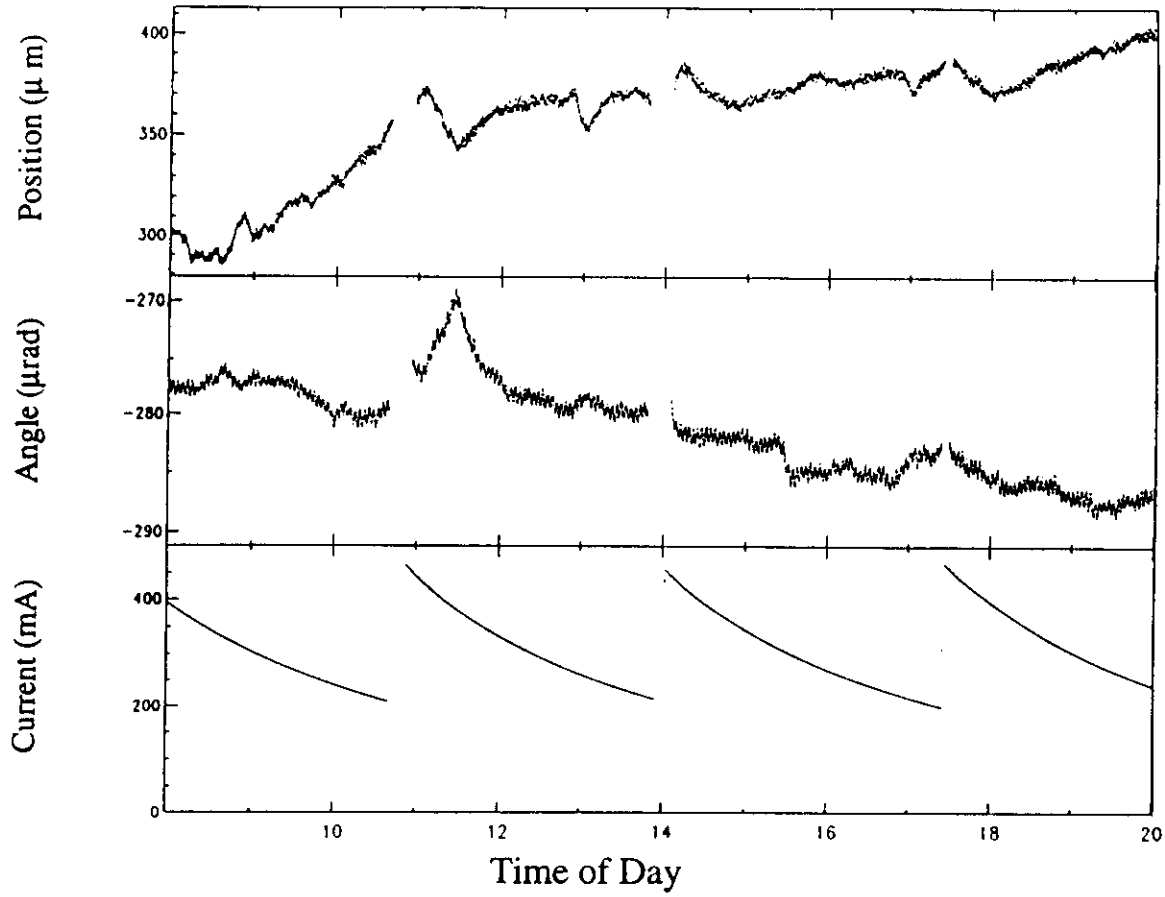

B) Expanded scale: 8 AM - 1:30 PM

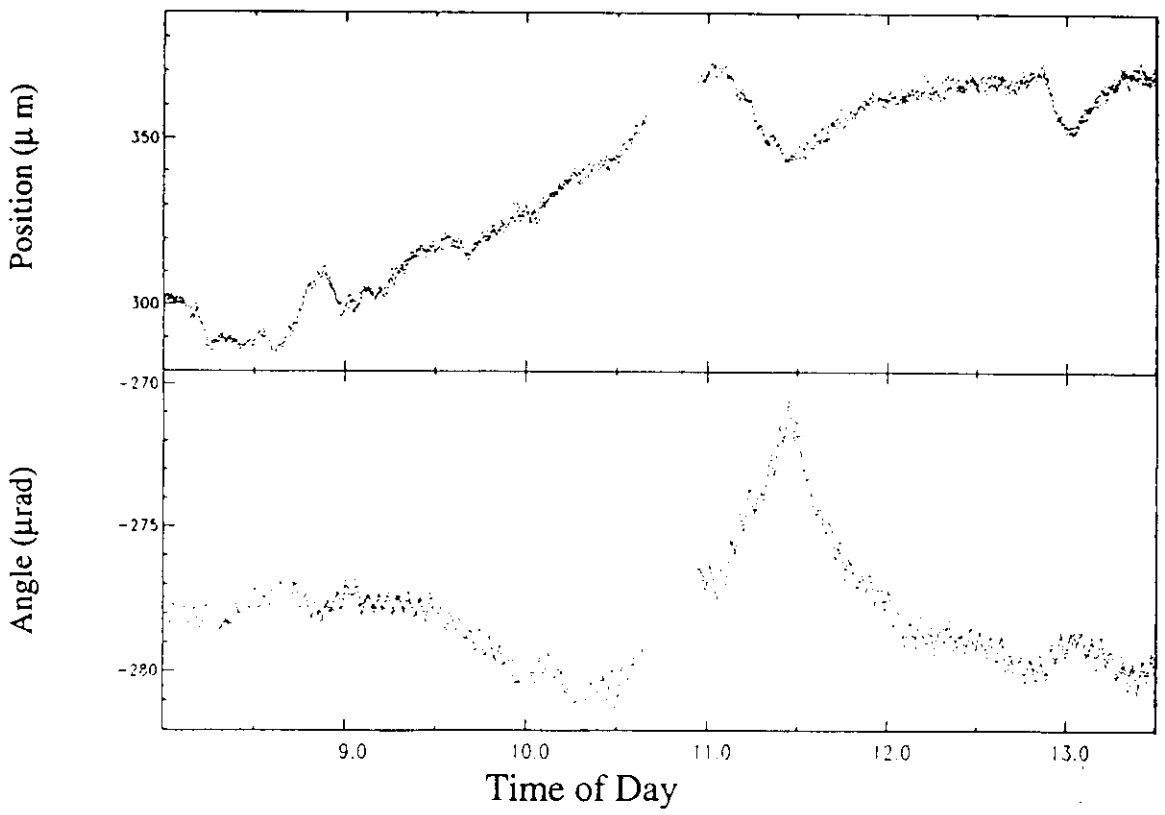

18°C ± 0.5°C is mixed producing a stable 18° ± 0.05°C or better regulation (figure 1.4.4b).

Similarly, the water cooling of magnets and consequently, of their support frames, can produce similar effects (figure 1.4.5). In these figures the position of the electron beam in a dipole magnet and the direction of the radiation emitted are shown as a function of time as measured with a SR-monitor system similar to that shown in figure 2.6.1. In the expanded scale of figure 1.4.5b one can clearly see the thermal cycle of the cooling water - with a period of about 3.3 minutes. In this case, the thermal "print through", although apparent, is harmless, being about 1 μrad peak to peak.

1.4.4. Cost

The cost of a beamline can vary widely, depending upon the pocketbook and the goals of the facility. There are all sorts of trade-offs one can make depending on the circumstances. Employing high quality and therefore expensive optical components with poorly designed holders and vessels makes no sense. If the beamline is intended to be in operation with as little "down time" as possible, suitable alignment equipment and adjustments should be provided, including such things as SR position monitors. The use of optical elements which are particularly expensive and difficult to align such as ellipsoidal mirrors should be justified by the (realistic) performance expected. The attainment of high resolution demands particular expenses and complexities. Such resolution is not always required nor desirable.

Thus, cost includes not only the initial investment but also the set-up and maintainence costs as well.

Chapter 2. Characteristics of Synchrotron Radiation Sources

For the design of any optical system, it is essential that the source of the radiation be known. Furthermore, for ray trace studies, the source must be mathematically defined so that the ray trace program can generate it or can accept it as a file. In the ray trace programs "RAY" and "SHADOW", various types of sources are offered via a menu. The input information required from the designer may vary in detail, but ultimately, the designer or the ray trace program must generate the following information:

1) The lateral size of the source in all three dimensions. These may be either rms or hard edge (step function) values. In general, Cartesian coordinates are used.
2) The angular divergence of the radiation in both vertical and horizontal planes.

In addition, characteristics such as the energy distribution and polarisation of the radiation as a function of emission angle are usually required. For dipole sources (s. figure 2.2.2) recent versions of the aforementioned ray trace programs automatically generate this information. For sources such as wigglers and undulators, referred to as "insertion devices" or "ID's" , special programs are usually required (see "SMUT", "URGENT" and "WAVE" ref. 2.3, 2.6 and 2.15). Such programs generate files which serve as source input files for the ray trace program.

For optical systems with a vertical dispersion plane, the vertical source size and divergence is most critical for resolution. Since the vertical source **size** in a storage ring is inherently smaller than the horizontal source **size** (see the factor "C" below in this section), vertically dispersing systems are most often encountered. There are, however, cases in which a horizontally dispersing system is more favorable.

Thus, the goal of this chapter is to be able to describe the source in a form suitable for ray tracing.

As seen in chapter 1, one of the primary advantages of SR is its inherent brilliance (often expressed as "high brightness". See chapter 1 section 1.1). The results from the large flux of photons produced by a source of small lateral size by electrons whose acceleration vectors are projected into a small solid angle in the forward direction. The latter two quantities are expressed by the "emittance" of the storage ring and is an invariant of the storage ring and its operating parameters:

Emittance = $\varepsilon = \sigma_e \, \sigma_e'$

where σ_e = lateral extent of the electron beam, generally resolved in σ_{eh} and σ_{ev} for the horizontal and vertical planes.

σ_e' = solid angle of the electron trajectories around the ideal trajectory. Again we have σ'_{eh} and σ'_{ev} .

With the help of the machine parameters it is easily possible to calculate σ_e and σ_e' as shown in this chapter. Since the two orthogonal lateral directions, x, in the plane of the ring, and y, perpendicular to it, are only weakly coupled it is useful to define a horizontal emittance, ε_x, and a vertical emittance, ε_y. Thus,

$$\varepsilon_y = C \cdot \varepsilon_x$$

where C corresponds to the coupling factor, also an invarient of the system. For storage rings designed explicity for the production of SR this coupling factor ranges between 0.01 and 0.1, and is a function primarily of the "goodness" of the alignment of the magnet fields in the ring. With perfect separation and alignment the coupling factor would be zero. The main contribution to misalignment comes from residual "skew-quadrupole" fields, expecially in insertion devices (I.D.'s): wigglers and undulators. Nevertheless, the vertical emittance can be kept much smaller than that in the ring plane making the vertical plane the logical one for dispersion in monochromators.

The definition of σ_e' given above should warn one that the definition of the radiation source is perhaps not so simple after all: for the design of the optical system, one needs the solid angle into which the photons are emitted. That may be quite different from σ_e' ! In a development similar to that for

the electron beam parameters, methods to determine the effective size and opening angles of the radiation, σ_r and σ'_r will be given. The effective parameters for the source for ray tracing are the Gaußian summation of the individual components: $\sqrt{\sigma^2 + \sigma'^2}$. We will define this quantity simply by σ'_i or by its components, σ'_{ih} and σ'_{iv} . The quantity σ'_{iv} is r.m.s. solid angle in the vertical direction into which the SR is emitted. It is the most important quantity in regard to the energy resolution of a beamline.

With this in mind, we give in the following pages the relevant parameters and formulas for calculating or otherwise obtaining σ_e, σ'_e, σ_r and σ_r' necessary for obtaining the optical characteristics of a beamline. These parameters are essential as the starting point for a quantitative examination of the optical characteristics of a beamline using ray traces.

2.1 Electron Beam

The lateral dimensions of the electron beam, σ_h and σ_v, and the angular deviation of the individual electrons from the ideal orbit σ_h' and σ_v' vary along the orbit in the ring, that is along the dimension "s". To determine them a knowledge of the Twiss parameters, $\alpha(s)$, $\beta(s)$ and $\gamma(s)$ as well as of the emittance, ε, the coupling factor, C, the dispersion, $\eta(s)$, and the momentum or energy spread, $\frac{\delta p}{p_o}$ or $\frac{\delta E}{E_o}$ respectively is required. The coupling factor mentioned above relates the vertical emittance to the horizontal and usually lies between 0.01 and 0.1. Similarly, the vertical dispersion is coupled to that in the horizontal plane and can only be determined on an operating ring. This latter coupling is a function of the position "s" along the orbit.

The Twiss parameters are defined as follows:

$\beta_x(s)$, $\beta_y(s)$ = horizontal and vertical beta functions

$$\alpha_x(s) = -\frac{1}{2}\frac{d\beta_x(s)}{ds} \quad ; \alpha_y(s) = -\frac{1}{2}\frac{d\beta_y(s)}{ds}$$

$$\gamma_x(s) = \frac{1 + \alpha_x(s)^2}{\beta_x(s)} \quad ; \gamma_y(s) = \frac{1 + \alpha_y(s)^2}{\beta_y(s)}$$

The beta functions reflect the focussing characteristics of the magnet lattice and are generally available for a given ring in the form shown in figure 2.1.1. As seen there they are relatively constant in the straight sections but can vary strongly in the dipole magnets. The horizontal dispersion, $\eta_x(s)$, is also shown in figure 2.1.1.

The values of the electron beam characteristics are obtained from the following relationships:

$$\sigma_{eh}(s) = \sqrt{\varepsilon_x \beta_x(s) + \left[\eta_x(s)\left(\frac{\delta p}{p_o}\right)\right]^2}$$

$$\sigma_{eh}'(s) = \sqrt{\varepsilon_x \gamma_x(s) + \left[\eta_x'(s)\left(\frac{\delta p}{p_o}\right)\right]^2}$$

and analogous expressions for $\sigma_{ev}(s)$, $\sigma_{ev}'(s)$.

Based on the experiences won on storage rings of the second generation, it is possible to make some assumptions which simplify the calculations [1.6b, 2.8]:

$C \approx 0.04$ is typical. It is essentially always between 0.10 and 0.01.

$\eta_y(s) \approx 0$, $\eta_y'(s) \approx 0$ generally true for the straight sections.

$\frac{\delta p}{p_o} \approx 3 \times 10^{-3}$ for normal multibunch operation. For very low currents it can be much smaller: $\approx 5 \times 10^{-4}$ [2.9].

2.1.1. Electron beam characteristics in the straight sections

In the straight sections of the storage ring (see figure 2.1.1)

$\eta_x(s) = \eta_x'(s) = 0$, $\eta_y(s) = \eta_y'(s) = 0$ (general design goal)

$\alpha_x(s) \approx 0$, $\alpha_y(s) \approx 0$ (exactly true only at center of straight)

Figure 2.1.1: Beta Functions and Dispersion for a TBA 10 Lattice [1.6b]

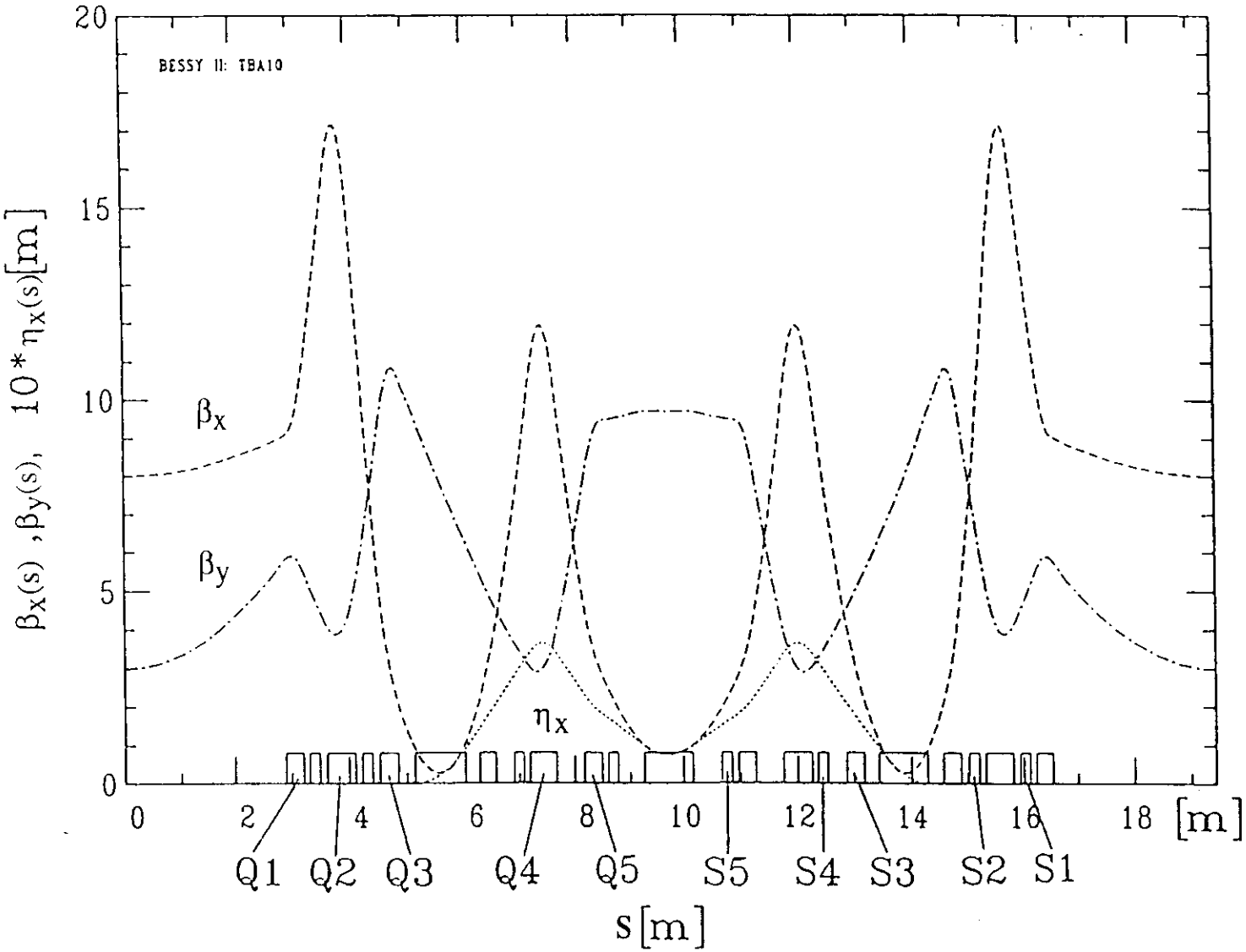

$$\gamma_x(s) = \frac{1}{\beta_x(s)} \qquad ; \gamma_y(s) = \frac{1}{\beta_y(s)}$$

and finally

$$\sigma_{eh}(s) = \sqrt{\varepsilon_x \beta_x(s)} \qquad ; \sigma'_{eh}(s) \approx \sqrt{\frac{\varepsilon_x}{\beta_x(s)}}$$

$$\sigma_{ev}(s) = \sqrt{\varepsilon_y \beta_y(s)} \qquad ; \sigma'_{ev}(s) \approx \sqrt{\frac{\varepsilon_y}{\beta_y(s)}}$$

For long undulators, that is for undulators that essentially take up the full length of the straight section, the parabolic form of the beta functions lead to α_x and α_y values which can deviate significantly from zero. However, such a correction is only needed for the most exact calculations

2.1.2. Electron beam characteristics in the dipole magnets

As seen in figure 2.1.1, the beta functions and the horizontal dispersion vary strongly with "s" in the curved sections of the storage ring. In the straight sections where ID's are located these parameters are generally constant. For an accurate calculation of the electron beam characteristics all the Twiss parameters must be evaluated and the full formulas used. Also to be seen in figure 2.1.1 is the fact that the β_x values may well exhibit a minimum in the middle of a dipole magnet making $\alpha_x = 0$ at that point while just before or after the middle point, 6° for the lattice shown, α_x becomes very significant, characteristic of strongly focussed storage ring lattices. In order to examine the variation of the various Twiss parameters with "s" and their effect on the electron beam characteristics, we have tabulated them in table 2.1.1 for four points in the storage ring [1.6b]. Also shown for all four points are the results obtained using only the emittance and the beta function for the calculations.

As will be seen in the ensuing sections, the σ'_{eh} and σ'_{ev} values are often considerably smaller than the corresponding σ'_{rh} and σ'_{rv} values in which case they can be neglected. Their relative magnitudes must be examined case for case.

Table 2.1.1 Calculation of the Electron Beam Characteristics at Different Points in the Ring+

Location	i	β_i(m)	α_i	γ_i(m^{-1})	η_i(m)	η_i'	Exact σ_i(mm)	Exact σ_i'(mrad)	Approximate* σ_i(mm)	Approximate* σ_i'(mrad)
Middle of straight	x	8	0	1/8	0	0	0.219	0.027	0.219	0.027
	y	3	0	1/3	0	0	0.027	0.009	0.027	0.009
Middle (6°) of Dipoles 1 + 3	x	0.25	0	1/0.25	0.024	0.088	0.082	0.306	0.039	0.155
	y	7.9	+1.8	1/1.9	-	-	0.044	0.011	0.044	0.006
Middle (6°) of Dipole 2	x	0.78	0	1/0.78	0.078	0	0.243	0.088	0.068	0.088
	y	9.6	0	1/9.6	-	-	0.048	0.005	0.048	0.005
9° in Dipole 1	x	0.56	-0.94	1/0.30	0.056	0.19	0.178	0.587	0.058	0.104
	y	7.0	+1.7	1/1.8	-	-	0.041	0.012	0.041	0.006

+ For $\varepsilon = \varepsilon_x = 6 \times 10^{-9}$ m·rad; C = 0.04, $\eta_y = 0$, $\delta p/p_o = 3 \times 10^{-3}$ and data of Fig. 2.1.1 [1.6b]

* Approximately: $\sigma_i(s) = \sqrt{\varepsilon_i \beta_i(s)}$; $\sigma_i'(s) = \sqrt{\varepsilon_i/\beta_i(s)}$; i = x, y

2.2 Dipole Magnet

a) Vertical opening angle of the radiation [2.1 pp 127-128]

$$\sigma'_{rv}\ (\text{mrad}) = \frac{570}{\gamma}\left(\frac{\lambda}{\lambda_c}\right)0.43$$

$$\text{for}\quad 0.2 < \frac{\lambda}{\lambda_c} < 100$$

$$\lambda_c\ (\text{Å}) = 5.59\ \rho/E^3 = 186/BE^2$$

$$\gamma = 1957\ E$$

$$\rho\ (\text{m}) = 33.35\ E/B$$

where

E = GeV
B = kG
ρ = m
I = Amp

b) Horizontal opening angle of the radiation, θ_{rh}, is defined by the geometry of front end, and can be up to 100 mrad and more. This is a hard edge and not an r.m.s. quantity and is hence defined as θ instead of σ.

c) Electron beam dimensions: see section 2.1.2

Typical values of electron beam characteristics are given in table 2.1.1.

d) Power emitted (total) $P(\text{kW}) = 88.5\ IE^4/\rho$
$= 2.65\ E^3IB$
Power (W/mrad) = P / 6.283
(There are 6283 mrad in a circle!)

e) Power (Watt/s·mrad·1 % BW) = $5.95 \times 10^{-15}\left(\frac{\gamma^4 I}{\rho}\right) G_2$ watt/s

Figure 2.2.1: Functions G_2 (λ/λc) and F (λ/λc) [2.1]

S. Krinsky et al.

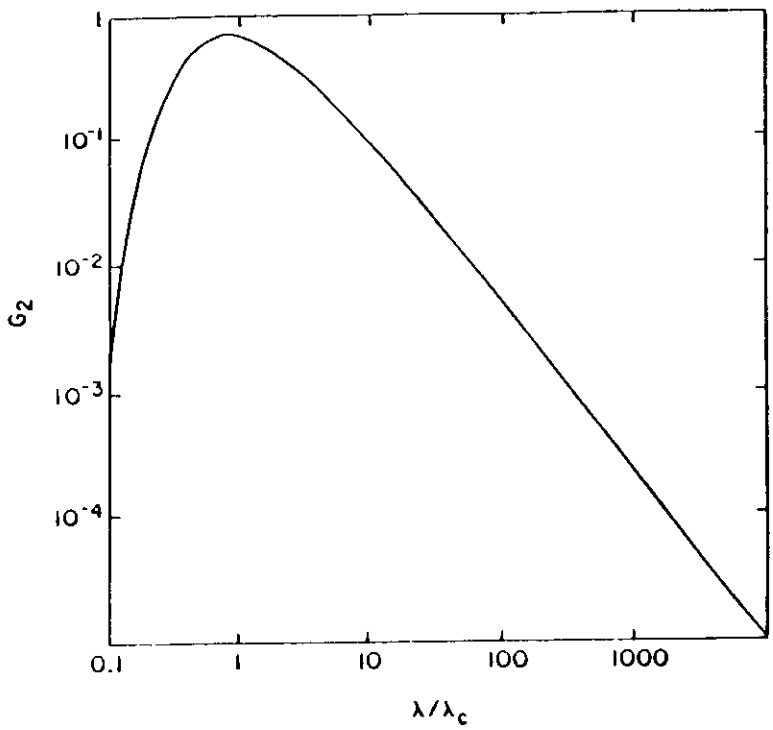

a) Function $G_2(\lambda/\lambda_c)$ of eq. (9) for the radiated power.

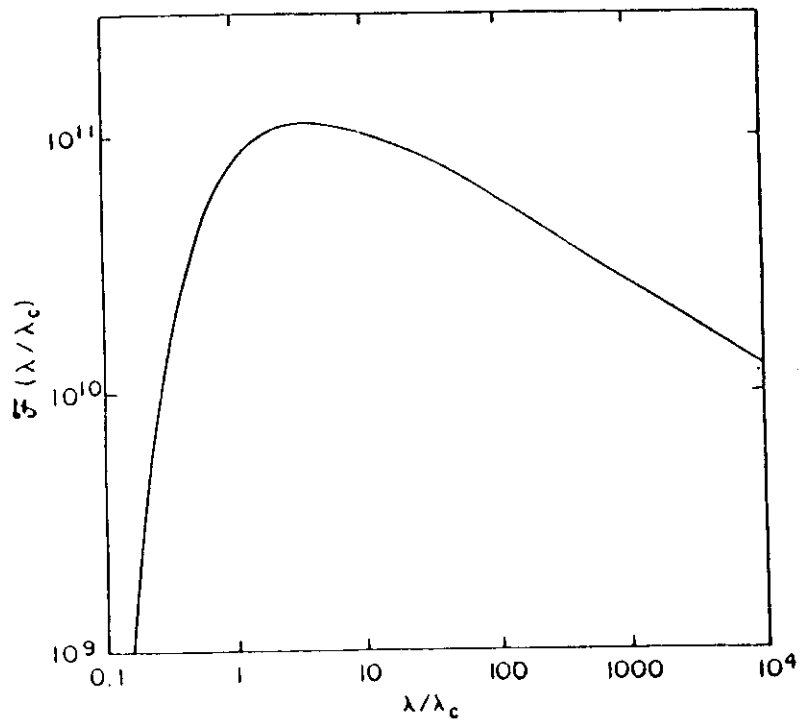

b) Function $\mathcal{F}(\lambda/\lambda_c)$ of eq. (11) for the photon flux integrated over all vertical angles ψ.

The function G_2 is shown in figure 2.2.1a [2.1] .

$$G_2 = \left(\frac{\lambda_c}{\lambda}\right)^2 \int_{\frac{\lambda_c}{\lambda}}^{\infty} K_{5/3}(\eta)d\eta \ , \quad G_{max} \cong \frac{2}{3}\lambda_c$$

f) Flux distribution (Photon/mrad·1 % BW)

$N = \gamma I F (\lambda/\lambda c)$ where **F** $(\lambda/\lambda c)$ is shown in figure 2.2.1b [2.1].

g) Polarisation:
Plane polarisation: see figures 2.2.2a, b
Circular polarisation: see figure 2.2.2c

2.3 Wavelength shifter (3 poles)

Similar to a dipole magnet with the corresponding B or ρ (see 2.2 above)

2.4 Multipole wiggler (N = No. of periods) see figure 2.4.1

Magnet field strength parameter, K

$$K = \delta\gamma = 0.934\ B\ \lambda_o$$

Wavelength of the wiggler/undulator radiation, λ

$$\lambda = \frac{\lambda_o}{2\gamma^2 k}\left(1 + \frac{K^2}{2} + \gamma^2\theta^2\right)$$

where B = Tesla
λ_o = length of one undulator period
δ = Deflection angle of the electron path with respect to the closed orbit.
γ = 1957 E [GeV]
θ = observation angle with respect to the closed orbit
k = number of the odd harmonic

Figure 2.2.2: Polarization Characteristics of Synchrotron Radiation [2.1, 2.9]

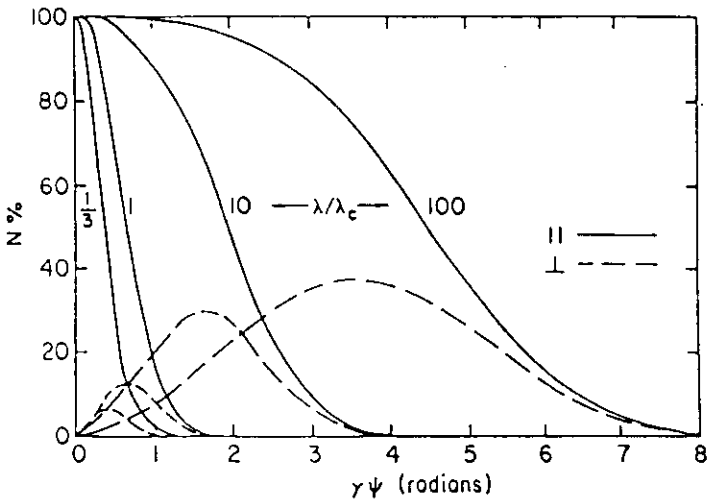

Fig. 3. Dependence on the vertical angle ψ of the intensities of the parallel (solid line) and perpendicular (dashed line) polarization components of the photon flux. The individual curves, plotted for $\lambda/\lambda_c = \frac{1}{3}$, 1, 10, and 100, are individually normalized to the intensity in the orbital plane ($\psi = 0$) at the respective λ/λ_c value. Note that the abscissa, ψ multiplied by the electron energy γ, makes these curves universal. **[2.1]**

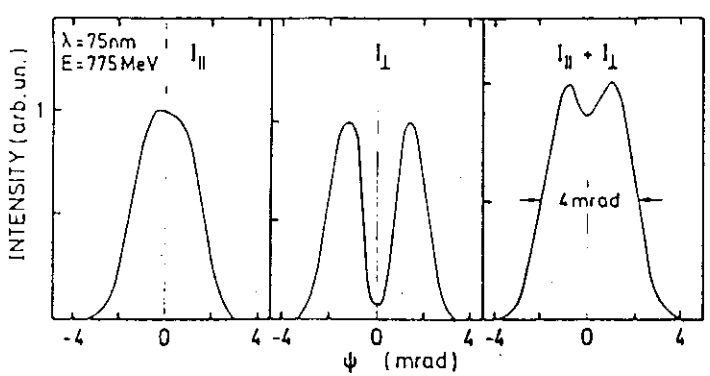

FIG. 9. Relative azimuthal intensity of the components, linearly polarized parallel and perpendicular with respect to the storage ring plane, and their sum measured at 75 nm. **[2.9]**

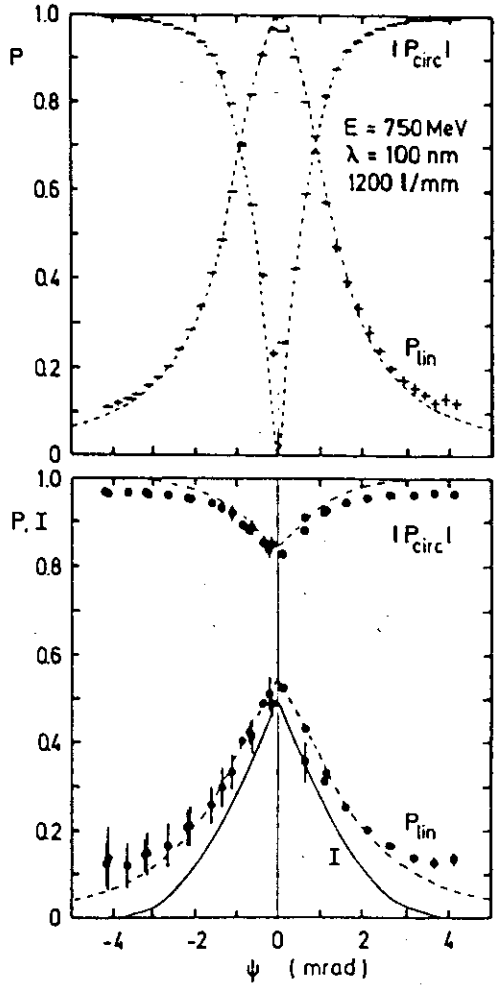

FIG. 10. Azimuthal dependence of the degree of the linear and circular polarization of 100-nm radiation. (a) Differential measurement with a vertical opening of 0.25 mrad (horizontal error bar).[37] (b) integral measurement with a slit from ψ to $\pm$ 5 mrad (error bars).[37] Full curve: ratio of the corresponding measured intensity of the radiation to the total radiation from $-$ 5 to $+$ 5 mrad. The dashed curves indicate the calculated polarization of the incident beam. **[2.9]**

a) Vertical opening angle of the radiation

$$\sigma'_{iv} = \left[\sigma'_{ev}{}^2 + \sigma'_{rv}{}^2\,(\text{Dipole})\right]^{1/2} \quad \text{see 2.2 a and 2.2c above}$$

b) Horizontal opening angle of the radiation

$$\sigma'_{ih} = \sigma'_{rh} \cong K/\gamma = \frac{0.934\, B\lambda_o}{\gamma}$$

c) Vertical source size [2.13]

$$\sigma_{iv} = \left[\sigma_{ev}{}^2 + \left(\frac{\sigma'_{ev}{}^2}{3} + \frac{\Delta\theta^2}{9}\right)\left(\frac{L}{2}\right)^2\right]^{1/2} .$$

where $L(\text{cm}) = N\,\lambda_o$

and $\Delta\theta$ = the half opening angle of the optical system.

(Optimally $\frac{L\sigma'_r}{2} \approx \sigma_{ev}$ and $\frac{L}{2} \approx \beta_y$, see 2.2 c)

d) Horizontal source size (zero dispersion [2.13])

$$\sigma_{ih} = \left[\sigma_{eh}{}^2 + x_o{}^2 + \left(\frac{\sigma'_{eh}{}^2}{3} + \frac{\Delta\theta^2}{9}\right)\left(\frac{L}{2}\right)^2\right]^{1/2} .$$

where $\Delta\theta$ = the half opening angle of the optical system

and $x_o = \frac{K}{\gamma} \cdot \frac{\lambda_o}{2\pi}$ (see "e" below)

e) Separation, $2x_o$, between the transverse source points:

where $x_o = \frac{K}{\gamma}\frac{\lambda_o}{2\pi}$

Figure 2.4.1: Layout of a Wiggler, Undulator

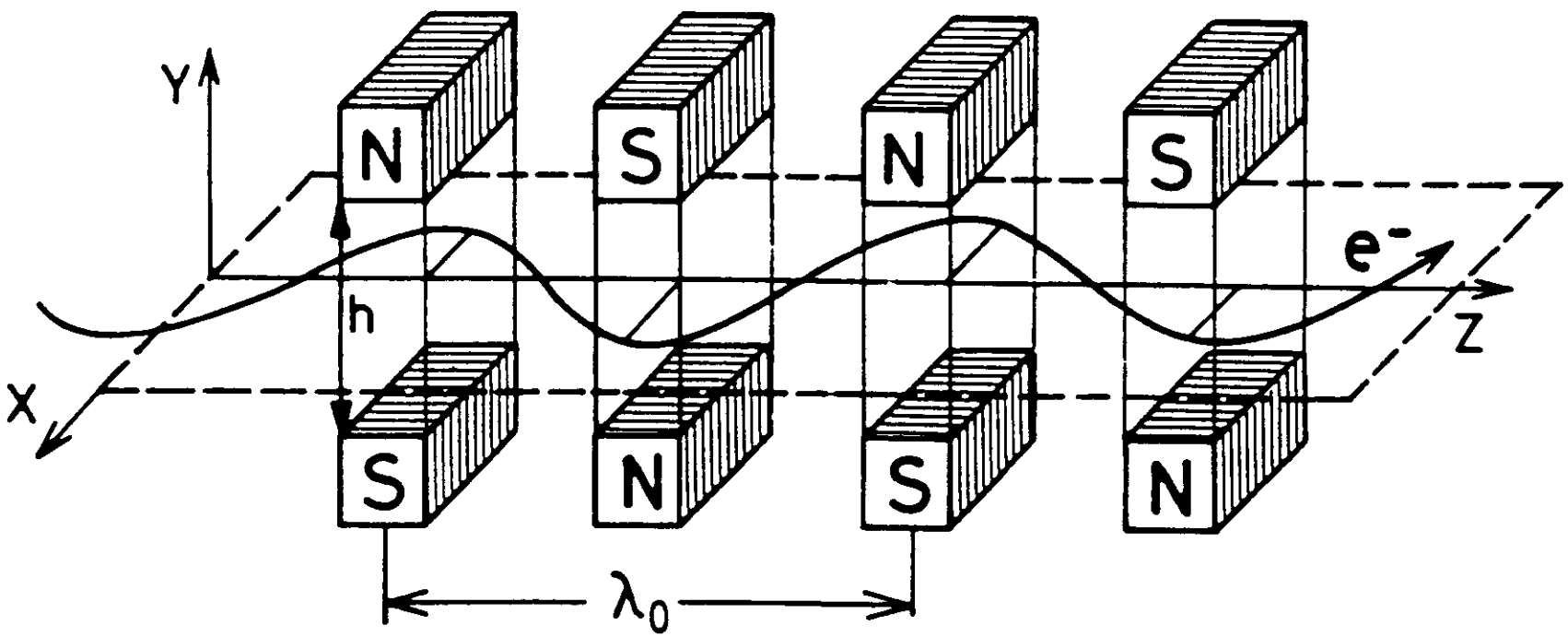

f) Total power

$$P_{tot}\,(W) \approx 1.9 \times 10^{-6}\, N\gamma^2 K^2 I/\lambda_o$$

or

$$P_{tot}\,(W) = 12.7\, E^2 < B^2 > LI$$

2.5 Undulator: $0 < K \lesssim 2 - 3$ see figure 2.4.1

$$K = \delta\gamma = 0.934\, B\lambda_o \quad ,$$

$$\lambda = \frac{\lambda_o}{2\gamma^2 k}\left(1 + \frac{K^2}{2} + \gamma^2\theta^2\right)$$ as above (sect. 2.4)

and $$P\,(Watt) = 1.9 \times 10^{-6} N\gamma^2 K^2 I/\lambda_o$$

Typical values of the total power delivered and its distribution for a typical storage ring of the third generation and for various types of ID's are given in table 2.5.2 and in figure 2.5.2. We shall see that the total power is not a good measure of the flux of the photons desired, except at small K values ($K < 0.5$). The total power must be kept in mind with regard to the heat loading of the optical components which can lead to their deformation and hence to an effective reduction of the brilliance of the complete system. It is just the brilliance of the odd harmonics of undulators that makes it possible to let most of their photons through while skimming off the unwanted photons which lie further away from the axis of the undulator. At higher K values, most of the power is in these unwanted photons making possible a beamline design which spares the optical components from unnecessary heat loading while transmitting the desired photons.

In addition, for reasons of resolution and economy, a knowledge of the horizontal and vertical divergences of an undulator source are essential for the design of an undulator beamline.

Unfortunately, these are quantities that are not easily calculated and the handy formulas usually encountered refer to the coherent core of a particular odd harmonic of the undulator radiation, i.e. the region around the central

Table 2.5.1: Source Characteristics for the Undulators at BESSY II [1.6b]

---

1. Characteristics of the electron beam in the straight sections

γ = 3327 (E = 1.7 GeV)
$\varepsilon_x = 6 \cdot 10^{-9}\pi$. m . rad
$\varepsilon_y = 0.1\ \varepsilon_x$
β_x = 8 m/rad
β_y = 3 m/rad
σ_x = 220 µm
σ_y = 42 µm
σ_x' = 27 µrad ⎤ not relevant
σ_y' = 14 µrad ⎦ see below

2. Depths of source: An average length of 4100 mm is used.

3. Minimum distance between middle of undulator and first optical element: 12000 mm.

Figure 2.5.2: Angular Distribution of the Power from W-2 and U-3 [1.6 b]

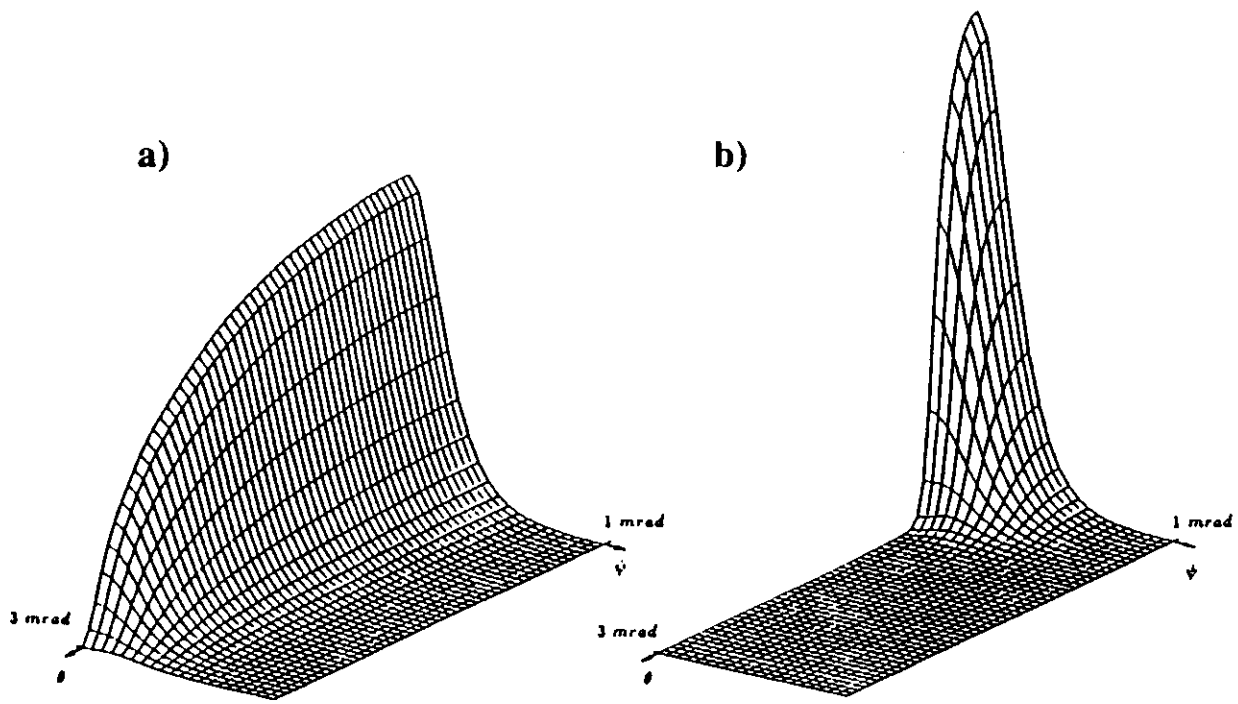

a) Angular distribution of the power for W-2/BESSY II (1.7 GeV) with 100 mA. The peak power is 371 Watt/mrad^2. K = 9.7

b) Angular distribution of the power for U-3/BESSY II as above. The peak power is 552 Watt/mrad^2. K = 1.6

axis of the undulator in which the relative phase shift of an odd harmonic at its maximum energy is small. This coherent core of radiation is much smaller than the solid angle into which the odd harmonic is emitted irrespective of phase. For most experiments, it is the flux of a particular energy radiation and not its coherence that is of interest. Thus, for a general purpose beamline, the acceptance should be based on the solid angle of emission of the harmonics irrespective of coherence. The horizontal and vertical opening angles will then determine the length of the mirrors and gratings required for general use. Should only the coherent core be desired, the acceptance of the beamline can easily be reduced with the help of apertures.

Of course, as one would expect, the solid angle depends upon the magnetic field strength at which the undulator is operating and upon the harmonic:

i.e. on K and on k.

Since both K and k vary over a fairly wide range for any undulator system, the solid angle must be chosen for maximum but reasonable conditions. In the case of k, this is simple: k = 1 has the largest opening angle for the odd harmonics. The even harmonics have a much lower brilliance than the odd ones: their maxima are distributed spacially around the the undulator axis and have a minimum on it. For this reason, they are generally of only secondary importance in the design. The transmission of both the odd and the even harmonics will be estimated by the procedure described below.

A common denominator for the value of K to be used for determining the solid angle of the beamline is a value of K = 2 or 2.5. Above these values the undulator radiation quickly becomes more wiggler like. i.e. the brilliance diminishes rapidly (see chapter 1.4.3 and figure 1.4.2).

In this section we describe how the effective opening angle of a particular harmonic, even as well as odd, can be estimated with the help of the computer program "SMUT" [2.3], "URGENT" [2.6] or "WAVE" [2.15]. At the end of the section, the elementary formulas are given by which the coherent core of the odd harmonics can be estimated.

Figure 2.5.1: Typical Undulator Spectra [2.10, 2.11]

a)

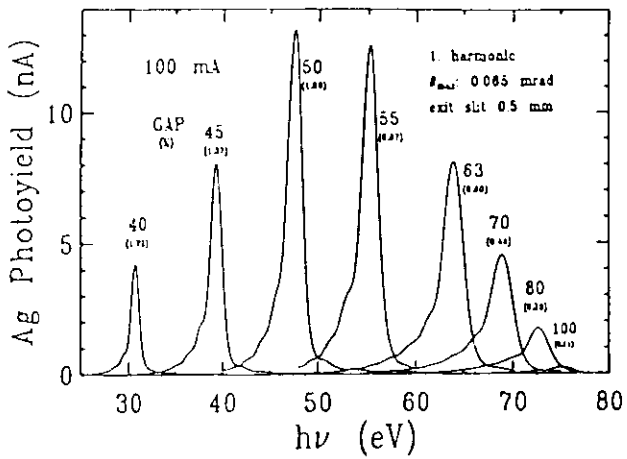

Spectra taken with the 800-line/mm grating. (a) First harmonic as a function of gap.

b)

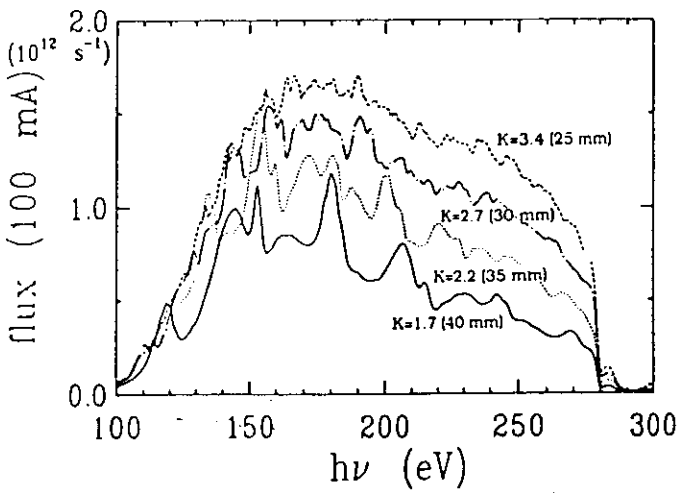

Measured intensities with the W/U and TGM-5 for various values of K. The gap in mm is also given. 100 mA ring current. The acceptance is $\sigma_h = \sigma_v = 125\ \mu$rad.

Spectra taken at higher energies.

c)

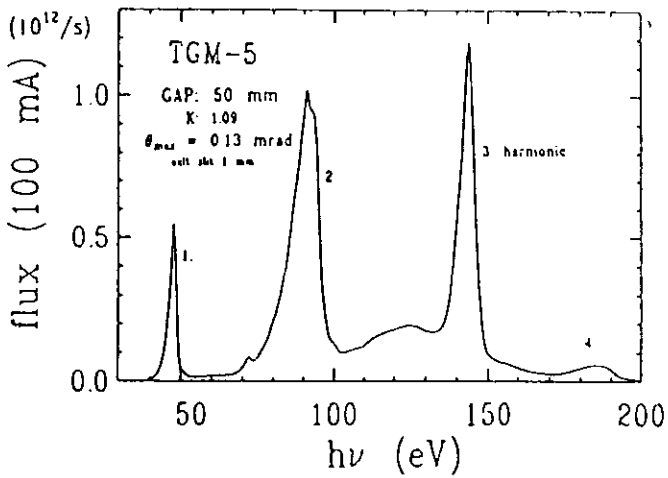

With the 1100-line/mm grating and pinhole.

d)

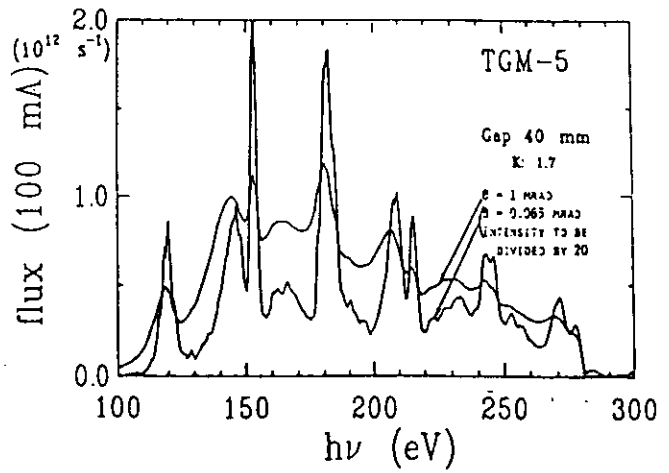

With the 1500-line/mm grating and two acceptances.

2.5.1. Opening angle

Using the program "SMUT" [2.3] with which the spectral characteristics of the radiation for a particular undulator can be calculated under realistic conditions, we have made studies of the opening angles of the radiation from the first 5 harmonics for three different, but typical undulators for a light source of the third generation. The studies consist simply of placing a circular pinhole at a distance of 10 meters from the center of the undulator and calculating the flux through it, employing, of course, the relevant emittance and beta functions for the source. By systematically increasing the diameter of the pinhole one can easily determine the spatial distribution of the flux. If the diameter is increased to a sufficiently large value, an asymptotic limit is found. In the case of the odd harmonics, this limit is rapidly reached. For the even harmonics, quite large pinholes must be used. Since the even harmonics are of less interest, we will save computer, and our own, time and just make rougher estimates of their asymptotes.

In figures 2.5.3.a and 2.5.3.b are shown the results of the calculation for an undulator with λ_0 = 52 mm on a storage ring with E = 1.7 GeV. This is a very common period length for a storage ring with 1.5 to 2.0 GeV electron energy. The characteristic energies of the radiation from such an undulator are given in table 2.5.3.b. There one can see that the photon energy range covered by such an undulator is 174 eV at K = 2.0 (and 127 eV at K = 2.5) to over 1000 eV with a photon flux > 1 x 10^{13} photons/s for 100 mA ring current.

The flux as a function of pinhole diameter for K = 0.5 is shown in figure 2.5.3.a while that for K = 2.0 is in figure 2.5.3.b. In both cases, the asymptote has been effectively reached by a pinhole area of 2 - 4 mm^2 for the odd harmonics. For K = 0.5, however, the 3, 4, and 5 th harmonics are hardly of importance, as one would expect. Hence, one should do these calculations at the upper limit of K as explained above. The results of these calculations for undulators with λ_0 = 100 mm and λ_0 = 30 mm are given in figures 2.5.3.c and 2.5.3.d.

With these figures, it is now possible to calculate a quasi-σ value for each harmonic as follows: The asymptote is introduced as a horizontal line and the flux for that particular undulator and harmonic determined. Then 95 %

of that value is taken and a second horizontal line which interesects the curve is drawn. The pinhole area at that intersection corresponds to the "4σ" value of a Gauß curve (see chapter 1 section 1.3.3 and table 1.3.1). Although we have not checked to see that the curve is indeed Gaußian, we assume that it is sufficiently similar that our "4σ" value is useful. A quick check of our curves for the odd harmonics will show that the Gauß approximation used here is not bad. From the σ values this obtained, a table can be created providing us with an overview of the situation for the various undulators. This is shown in table 2.5.4.

There is one more point that has to be made here. In making the "SMUT" calculations, one will determine that the energy of the odd harmonic decreases somewhat as the pinhole is enlarged. This is the "red" shift as expected from the equation for the undulator wavelength, λ, where θ is increasing (see beginning of this section, 2.5). The shift is small, but should be compensated for as the pinhole size is increased.

In table 2.5.4 we have defined a "hard edge half opening angle" of θ (μrad) as one half of the opening of the pinhole: i.e. 2 θ corresponds to diameter divided by the distance of the pinhole from the source, 10 m. The power emitted into such a pinhole can be calculated using formulas available in the literature [Kim, 2.14].

The result of all these calculations is now easily recognized: except for the second harmonic of all three undulators, more than 95 % of the flux of a particular harmonic is transmitted by a pinhole with an angular diameter of 2 θ = 160 μrad. At the same time, the power transmitted by such a pinhole is only 6 % of the total power emitted by the undulator. Thus, it is theoretically possible to eliminate 94% of the (unwanted, unused) power of the undulator and still have > 95 % of the photons desired!

That is the point of these calculations.

For the final design parameters, we can take two further steps in finalizing the horizontal and vertical opening angles, up to now the same since we used a circular pinhole.

1) To be on the safe side, and at the same time to allow more of the 2nd. harmonic pass through the system, we can make 2θ somewhat larger. Ultimately this will determine the lengths of the mirrors and gratings in grazing incidence (see section 4.4.7) and may at the time of their specification be revised. However, we may try $2\theta = 300$ μrad.

2) In order to eliminate unwanted undulator radiation, the maximum vertical opening angle can be reduced from the $2\theta = 160$ μrad value or from its nominal value of $1/\gamma$ at large K values by the square root of the bandwidth $(kN)^{-1/2}$.

$$\text{i.e. bandwidth} = \frac{\Delta\lambda}{\lambda} \approx \frac{1}{kN}$$

$$\text{Thus } \sigma'_{rv} \approx \frac{1}{\gamma(kN)^{1/2}} \text{ for odd harmonics.}$$

For $N = 80$, $k = 1$ and $\gamma = 1957 \times 1.7$ GeV $= 3330$,

$$\sigma'_{rv} = 30 \text{ μrad}$$

and for 95 % of the radiation, we take 4σ or 120 μrad.

Thus, we arrive at hard edge half opening angles of

$$\Theta_h = 150 \text{ μrad}$$
$$\text{and} \quad \Theta_v = 60 \text{ μrad.}$$

With these angles along with the previously determined source sizes, σ_{eh} and σ_{ev}, the necessary parameters for the ray trace program have been determined. These parameters will strongly influence the dimensioning of the monochromator.

2.5.2. The coherent core. Source size and opening angles.

Here we will simply state the formulas frequently encountered for estimating the parameters for a coherent source. The word "estimate" is particularly well taken here since, as already stated, the undulator source is not in detail

Table 2.5.2: Radiative Power And Beam Divergence of the B-II Undulators*

1)	U-1 (λ_0 = 100 mm, N = 40)	K = 0.5	K = 2.2
	Total power (W)	2.1	41
	Axial power (W/mrad^2)	15.6	84
	θ_h (mrad)/L_h (mm)+	0.31/6.2	0.72/14.4
	θ_v (mrad)/L_v (mm)+	0.50/10.0	0.50/10.0
2)	U-2.5 (λ_0 = 52 mm, N = 80)	K = 0.5	K = 2.2
	Total power (W)	8	156
	Axial power (W/mrad^2)	60	322
	θ_h (mrad)/L_h (mm)+	0.26/5.2	0.78/15.6
	θ_v (mrad)/L_v (mm)+	0.50/10.0	0.50/10.0
3)	U-3.0 (λ_0 = 30 mm, N = 110)	K = 0.5	K = 1.6
	Total power (W)	19.2	197
	Axial power (W/mrad^2)	143	552
	θ_h (mrad)/L_h (mm)+	0.30/6.0	0.60/12.0
	θ_v (mrad)/L_v (mm)+	0.50/10.0	0.55/11.0
4)	W-2 (λ_0 = 100 mm, N = 40)		K = 9.7
	Total power (W)		789
	Axial power (W/mrad^2)		371
	θ_h (mrad)/L_h (mm)+		2.94/58.8
	θ_v (mrad)/L_v (mm)+		0.55/11.0

* for 100 mA ring current and 1.7 GeV

+ Half opening angle for ca. 95% of the power delivered (ca. 2 σ-value). The equivalent opening in mm is given for a distance of 10 m from the middle of the undulator.

Figure 2.5.3: Undulator Flux Versus Pinhole Area

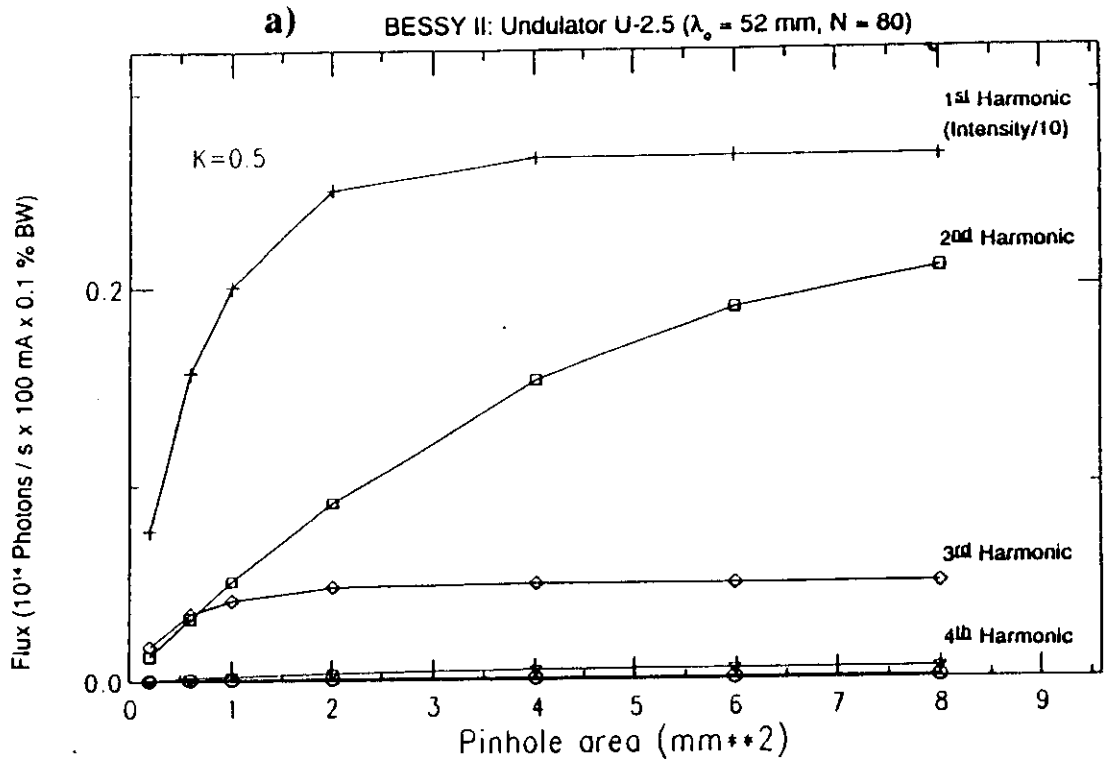

Peak intensities of the 1st to 5th Harmonic versus Pinhole size.
Pinhole is 10 m from the middle of the undulator.

θ (μrad) 56 98 126 149 169

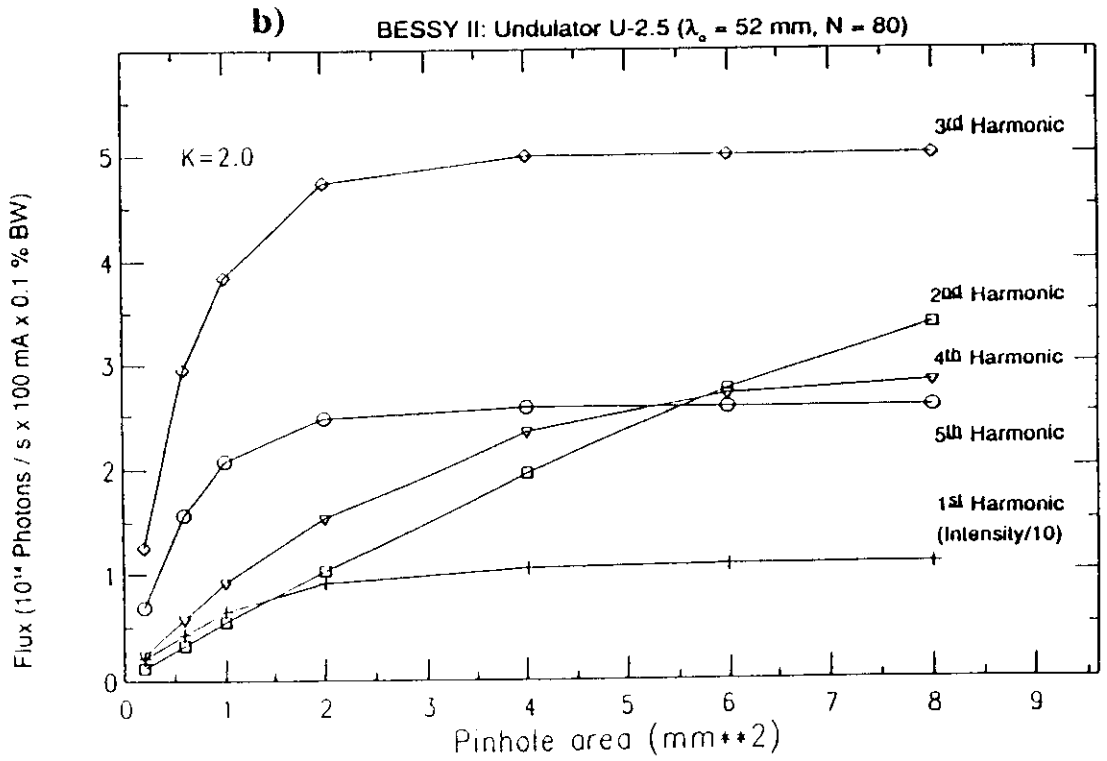

Peak intensities of the 1st to 5th Harmonic versus Pinhole size.
Pinhole is 10 m from the middle of the undulator.

θ (μrad) 56 98 126 149 169

Figure 2.5.3: Undulator Flux Versus Pinhole Area

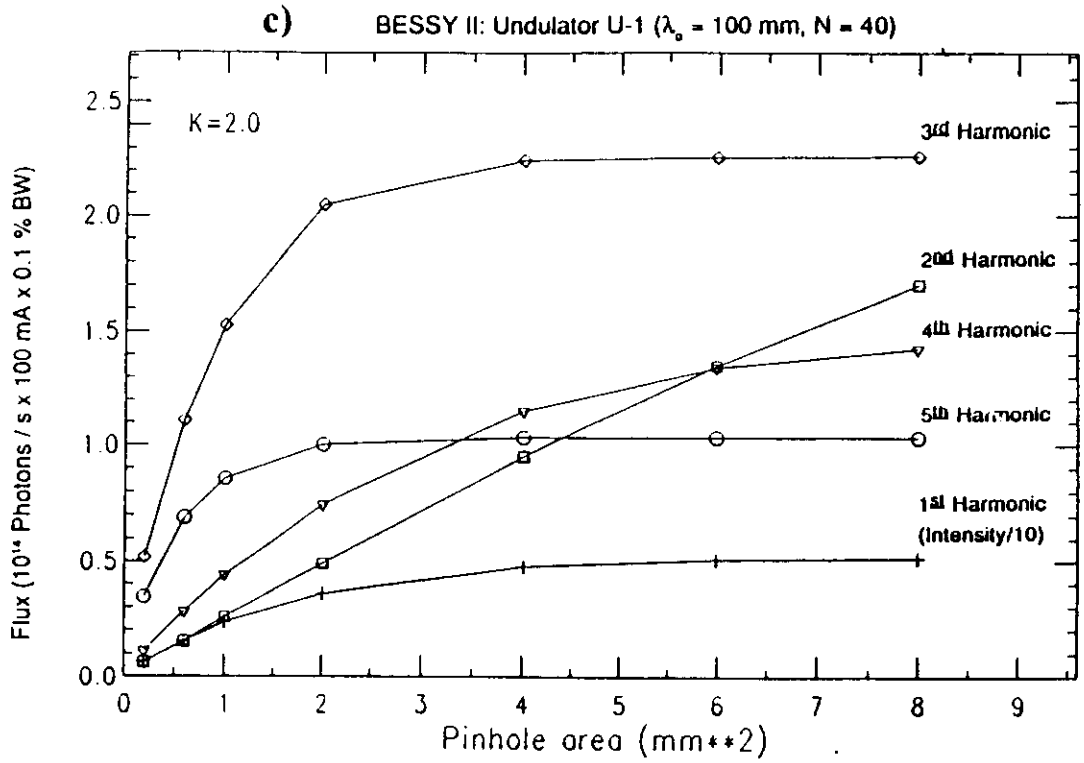

Peak intensities of the 1st to 5th Harmonic versus Pinhole size.
Pinhole is 10 m from the middle of the undulator.

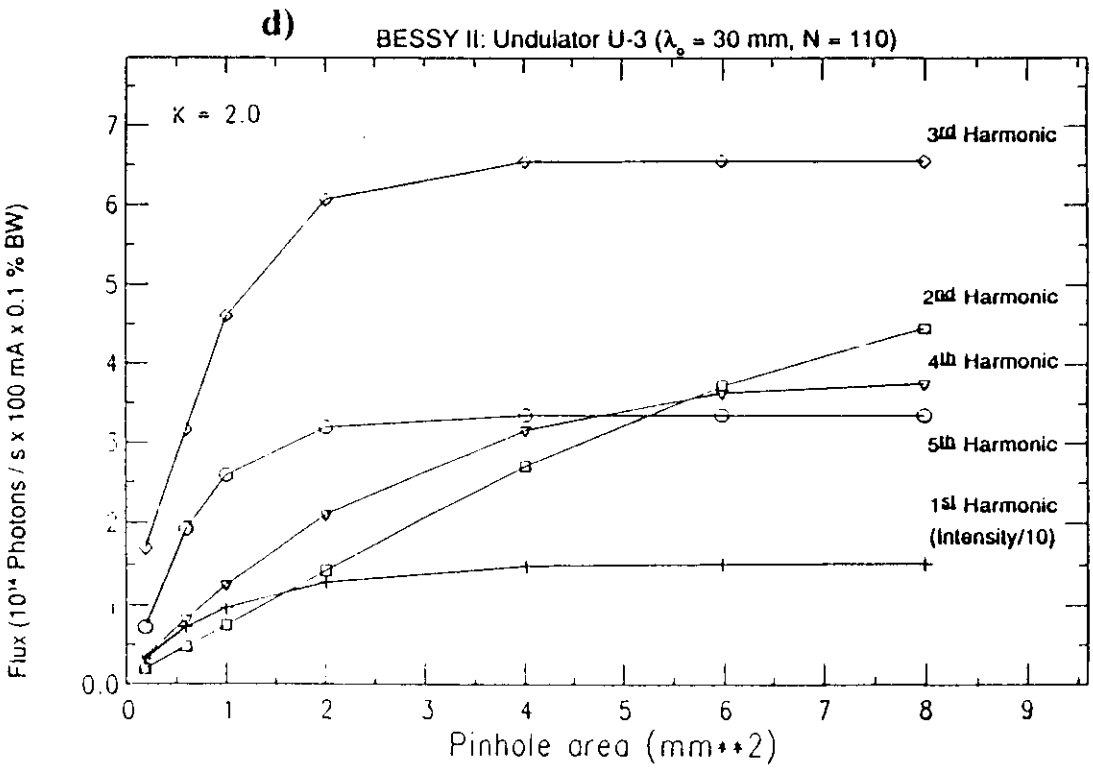

Peak intensities of the 1st to 5th Harmonic versus Pinhole size.
Pinhole is 10 m from the middle of the undulator.

Table 2.5.3 a: Undulator U - 1 (λ = 100 mm, N = 40)

Energy, Flux and Opening Aperture[+] of the First Five Harmonics[*] for K=0.5 and 2.0

	K = 0.5	K = 2.0
1st Harmonic, Energy (eV):	239	90
-Flux (photons/sec)	1.2×10^{14}	4.8×10^{14}
-Opening Aperture (R(mm))[+]	1.2	1.2
2nd Harmonic, Energy (eV):	431	164 (172)[#]
-Flux (photons/sec)	1.2×10^{13}	2.5×10^{14} (1.7×10^{14})
-Opening Aperture (R(mm))[+]	1.6	3.2 (1.6)
3rd Harmonic, Energy (eV):	728	273
-Flux (photons/sec)	2.3×10^{12}	2.2×10^{14}
-Opening Aperture (R(mm))[+]	0.8	1.2
4th Harmonic, Energy (eV):	932	353
-Flux (photons/sec)	2.8×10^{11}	1.4×10^{14}
-Opening Aperture (R(mm))[+]	1.2	1.6
5th Harmonic, Energy (eV):	1214	457
-Flux (photons/sec)	4.3×10^{10}	1.0×10^{14}
-Opening Aperture (R(mm))[+]	0.8	0.8

[*] For 100 mA ring current and 0.1% BW. Calculation used the beam parameters of BESSY II.

[+] The opening aperture is defined as the radius, R, of a circular aperture at 10 m from the source through which 95% of the radiation passes.

Case where the radius of the aperture is R/2 where R is defined above (only important for second harmonic).

Table 2.5.3 b: Undulator U - 2.5 (λ = 52 mm, N = 80)

Energy, Flux and Opening Aperture[+] of the First Five Harmonics[*] for K=0.5 and 2.0

	K = 0.5	K = 2.0
1st Harmonic, Energy (eV):	464	174
-Flux (photons/sec)	2.6×10^{14}	1.0×10^{15}
-Opening Aperture (R(mm))[+]	1.2	1.2
2nd Harmonic, Energy (eV):	843	326(332)#
-Flux (photons/sec)	2.1×10^{13}	$4.0 \times 10^{14}(3.4 \times 10^{14})$
-Opening Aperture (R(mm))[+]	1.6	3.2(1.6)
3rd Harmonic, Energy (eV):	1400	526
-Flux (photons/sec)	4.7×10^{12}	5.0×10^{14}
-Opening Aperture (R(mm))[+]	0.8	1.2
4th Harmonic, Energy (eV):	1792	682
-Flux (photons/sec)	5.7×10^{11}	2.8×10^{14}
-Opening Aperture (R(mm))[+]	1.4	1.6
5th Harmonic, Energy (eV):	2344	878
-Flux (photons/sec)	1.0×10^{11}	2.5×10^{14}
-Opening Aperture (R(mm))[+]	0.8	0.8

[*] For 100 mA ring current and 0.1% BW. Calculation used the beam parameters of BESSY II.

[+] The opening aperture is defined as the radius, R, of a circular aperture at 10 m from the source through which 95% of the radiation passes.

Case where the radius of the aperture is R/2 where R is defined above (only important for second harmonic).

Table 2.5.3 c: Undulator U - 3 (λ = 30 mm, N = 110)

Energy, Flux and Opening Aperture[+] of the First Five Harmonics[*] for K=0.5 and 2.0

	K = 0.5	K = 2.0
1st Harmonic, Energy (eV):	806	302
-Flux (photons/sec)	3.6×10^{14}	1.5×10^{15}
-Opening Aperture (R(mm))[+]	0.9	1.2
2nd Harmonic, Energy (eV):	1483	572 (578)[#]
-Flux (photons/sec)	2.7×10^{13}	4.9×10^{14} (4.4×10^{14})
-Opening Aperture (R(mm))[+]	1.6	3.2 (1.6)
3rd Harmonic, Energy (eV):	2427	910
-Flux (photons/sec)	6.7×10^{12}	6.5×10^{14}
-Opening Aperture (R(mm))[+]	0.8	1.2
4th Harmonic, Energy (eV):	3126	1185
-Flux (photons/sec)	7.8×10^{11}	3.8×10^{14}
-Opening Aperture (R(mm))[+]	1.4	1.6
5th Harmonic, Energy (eV):	4076	1520
-Flux (photons/sec)	1.2×10^{11}	3.2×10^{14}
-Opening Aperture (R(mm))[+]	0.8	0.8

[*] For 100 mA ring current and 0.1% BW. Calculation used the beam parameters of BESSY II.

[+] The opening aperture is defined as the radius, R, of a circular aperture at 10 m from the source through which 95% of the radiation passes.

Case where the radius of the aperture is R/2 where R is defined above (only important for second harmonic).

Table 2.5.4: Comparison of Divergence of Power and Flux [1.6b]

BESSY II Studie: 1.7 GeV

Comparison of the total emitted power of an undulator with the flux of the first five harmonics as a function of the hard edge half opening angle, θ, of an aperture.

	θ (μrad)	P+	F* 1.	2.	3.	4.	5.
	40	0.007	0.24	0.05	0.42	0.09	0.59
U-1	80	0.06	0.68	0.19	0.90	0.53	
(K = 2.0)	160	0.16		0.68			
λ_0 = 100 mm	320	0.50		0.95			
N = 40	640	0.92					
	40	0.007	0.34	0.07	0.50	0.16	0.51
U-2.5	80	0.06	0.84	0.25	0.95	0.53	0.96
(K = 2.0)	160	0.16		0.84		0.98	
λ_0 = 52 mm	320	0.50		0.95			
N = 80	640	0.92					
	40	0.008	0.40	0.08	0.42	0.18	0.49
U-3	80	0.07	0.83	0.29	0.92	0.53	0.95
(K = 1.6)	160	0.20		0.90		0.97	
λ_0 = 30 mm	320	0.59		0.95			
N = 110	640	0.95					

+ P = fraction of total power emitted

*F = fraction of the total flux of the harmonic. If F ≥ 0.99 no entry is made.

Table 2.5.5: Angular Divergences, σ'_r, for the Odd Harmonics

---

Angular divergence of the kth harmonic as compared with the divergence of the electron beam in the straight section.

BESSY: 755 MeV

$\varepsilon_x = 4.6 \times 10^{-8}$ π·m·rad; $\beta_x = 3.2$ m/rad
$\varepsilon_y = 3.5 \times 10^{-9}$ π·m·rad; $\beta_y = 15.5$ m/rad
$\sigma_x' = 0.12$ mrad (Section 2.1.1)
$\lambda_o = 70$ mm; N = 35

		k = 1	k = 9
K	0.5	0.086 mrad	0.029 mrad
	2.0	0.140 mrad	0.047 mrad

BESSY II: 1.7 GeV

$\varepsilon_x < 6.5 \times 10^{-9}$ π·m·rad; $\beta_x \leq 8$m/rad
$\varepsilon_y < 6.5 \times 10^{-10}$ π·m·rad; $\beta_y \leq 3$ m/rad
$\sigma_x' = 0.029$ mrad (Section 2.1.1)
$\lambda_o = 52$ mm; N = 80

N = 80		k = 1	k = 9
K	0.5	0.025 mrad	0.008 mrad
	2.0	0.041 mrad	0.014 mrad

described by a Gauß distribution and hence, several approximations are encountered in the literature all of which force the real source characteristics into a Gauß-like corsett.

Horizontal and vertical source size, σ_r:

$$\sigma_r = \frac{1}{4\pi}\sqrt{\lambda L} \quad \text{or} \quad \sigma_r = \frac{1}{2\sqrt{2}\pi}\sqrt{\lambda L}.$$

Which formula is used is a matter of taste, depending upon whether you live in the USA or Sweden! Note that the effective difference in the magnitudes is a factor $1/\sqrt{2}$. The coherent core of undulator radiation is axially symmetric for K values below about 5. The formula for the opening angle, $\sigma'_h \cong \sigma'_v$, results from the fundamental phase space relationship,

$$\sigma_r \cdot \sigma'_r = \frac{\lambda_{coh}}{4\pi} .$$

Hence, again depending upon your place of domicile, one has

$$\sigma'_r = \sqrt{\frac{\lambda}{L}} \quad \text{or} \quad \sigma'_r = \sqrt{\frac{\lambda}{2L}}.$$

In figure 2.5.4 is shown the realistic distribution of undulator radiation for an 83 period undulator with period length, λ_o (= λ_u) = 49 mm on a storage ring with E = 1.7 GeV. The curves were calculated with the program WAVE [2.15] for K = 1.0 and K = 2.5 . Under these conditions the first harmonic has the energy 373.5 eV and 135.8 eV respectively. In both cases, the distribution is axially symmetric. A Gauß curve has been fitted in each case using the least squares fit routine from "PAW" (CERN library). The fitted σ values are

K = 1.0, λ = 3.32 nm, σ'_r = 0.19 / 10000 = 19 x 10^{-6} rad
K = 2.5, λ = 9.13 nm, σ'_r = 0.34 / 10000 = 34 x 10^{-6} rad

By substituting the values used in the WAVE calculations (figure 2.5.4) into the above equations for opening angle, one obtains the following:

Figure 2.5.4: The Coherent Core of Undulator Radiation: The Gauß Fit

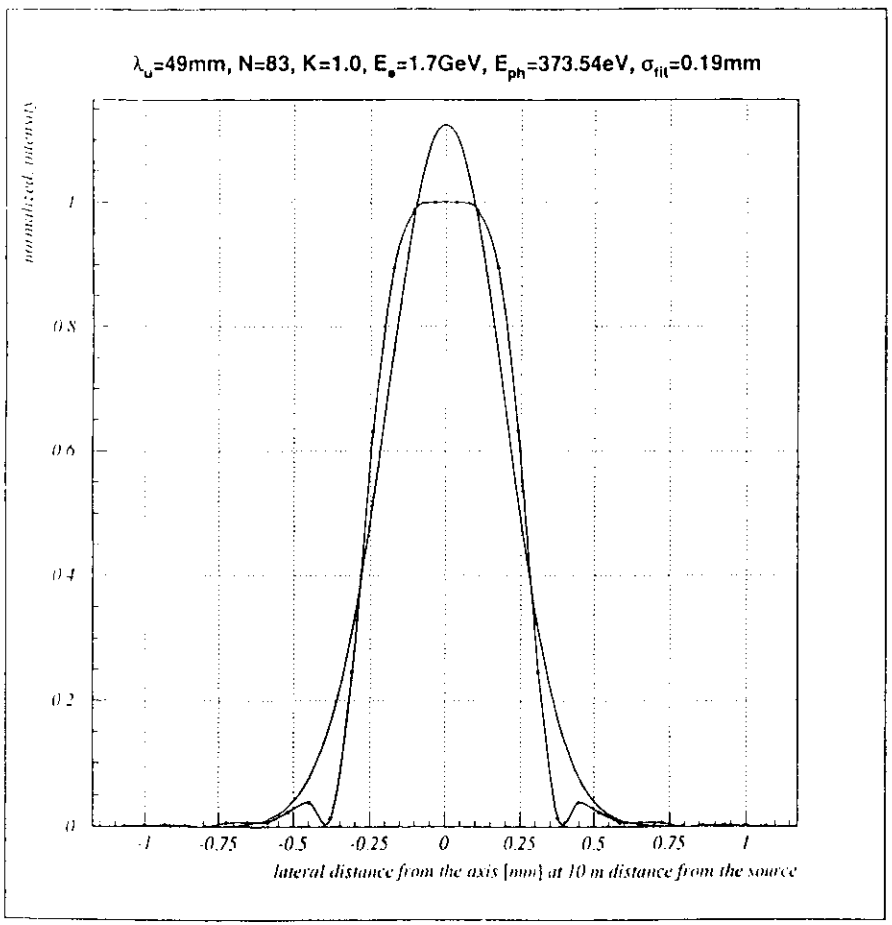

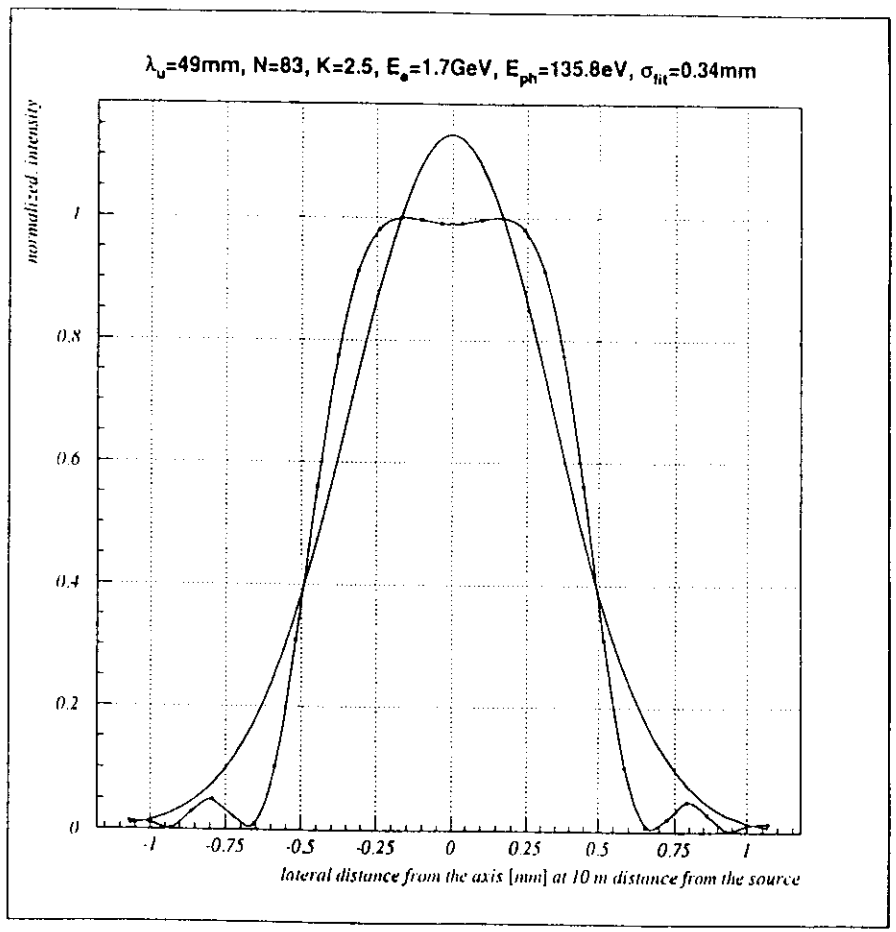

USA, K = 1.0, $\sigma'_r = 29 \times 10^{-6}$ rad

USA, K = 2.5, $\sigma'_r = 47 \times 10^{-6}$ rad

and

Sweden, K = 1.0, $\sigma'_r = 20 \times 10^{-6}$ rad

Sweden, K = 2.5, $\sigma'_r = 34 \times 10^{-6}$ rad

Without taking sides, one can say that the agreement in both cases is very acceptable. The usefulness of the Gauß approximation and of the simple formulations above are made evident by these comparisons.

For the beamline design, we should take the K = 2.5 value. The half hard edge opening would be twice the above , i.e. $\Theta = 68 \times 10^{-6}$ rad in both planes. The opening angles for non-coherent radiation were $\Theta_h = 150 \times 10^{-6}$ rad and $\Theta_V = 60 \times 10^{-6}$ rad.

Finally, for the effective source size and divergence, the corresponding parameters for the electron beam must be taken into account by taking the Gaußian sum of them:

$$\sigma_i = \sqrt{\sigma_e^2 + \sigma_r^2} \qquad \text{and} \qquad \sigma'_i = \sqrt{(\sigma'_e)^2 + (\sigma'_r)^2} \quad .$$

2.6 Determination of the direction and position of the light axis

The alignment of a beamline starts with the determination of the optical axis of the SR itself. Electron beam position monitors installed in the storage ring are essential for stable ring operation but are sufficient neither for checking the stability of the SR position/angle nor for aligning the beamline. Before the beamline is set up, but after completion of the front end, the fan of visible SR passing through a window flange can be used to determine the horizontal area into which the tangents to the electron orbit fall. The exact positions of the tangents can be determined by the shadow method: a plumb line is suspended near the front end and its shadow is observed further back. **Note: This can only be done with low currents in the ring and with approval of the radiation safety officer.** Higher currents can produce dangerous amounts of radiation and the heat of the SR can crack the window. The location of the observed SR axis or fan can be marked on the floor with surveying studs, for example.

Figure 2.6.1: **Determination of the Direction and Position of SR [6.14]**

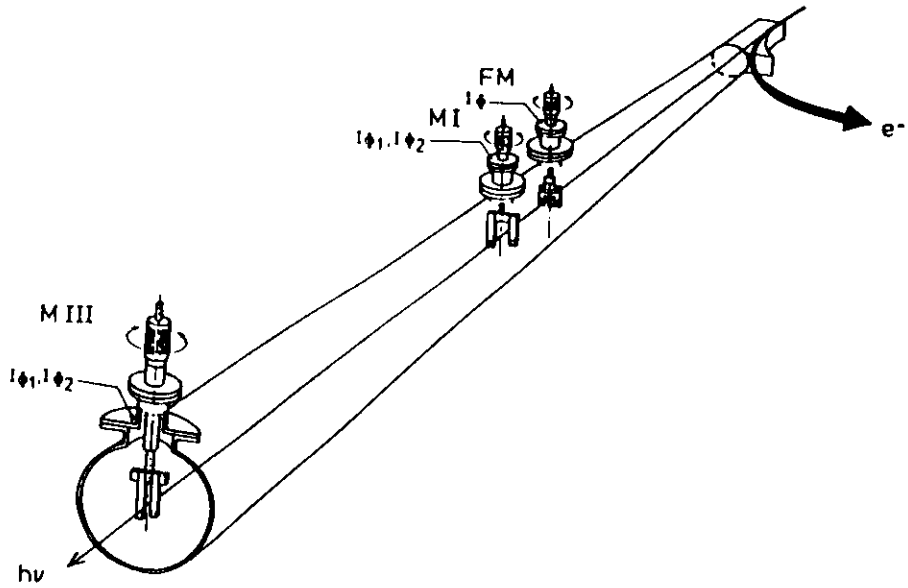

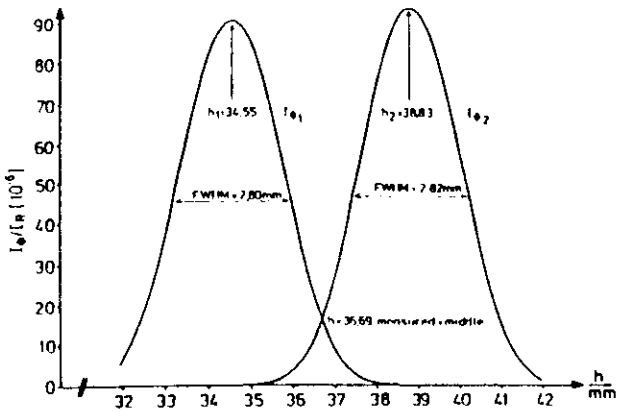

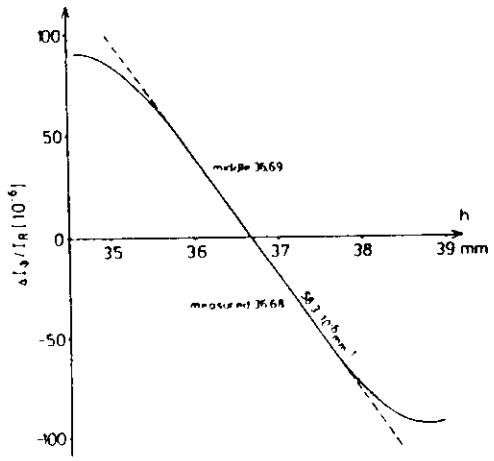

In designing a beamline for dipole radiation it is generally possible to use some of the SR just outside of the primary area for monitors. Most commonly plate or wire monitors are located just above and below the meridional plane and the difference signal used to detect changes in the height of this plane. By employing two sets of monitors in the beamline, the second at about twice the distance of the first from the source, the angle of emission of SR from the electron beam can be determined (see figure 2.6.1 [6.14]. The horizontal direction of the tangent to the bending radius is easily determined by placing a vertical wire early in the beamline and scanning through the position of its shadow at double the distance [6.11]. If the wires are fine enough, the horizontal source size can also be determined. It is strongly recommended that SR-position monitors for both the vertical and horizontal directions be installed as standard procedure in a beamline behind every front end. Diagnosing problems on the beamline is much more straightforward with than without them. The first goal of troubleshooting is to determine where the problem is located: in the storage ring, in the monochromator/beamline or at the experiment.

In addition to electronic SR-monitors in the beamline it is useful to have stratigically placed, moveable ground glass screens: in front of the entrance and exit slits for example using a phosphor (e.g. ZnS) where/when necessary to detect otherwise invisible undulator radiation. "Seeing is believing" and avoids spurious effects that occasionally crop up in electronic systems.

The above methods of locating and viewing the SR fan in a beamline are only of limited use in an undulator beamline. Photoemission from suitably designed four blade monitors (see reference 6.10 and figure 2.6.2 for example) along with a feedback circuit to steerer magnets to regulate the direction of the electron beam [6.5 - 6.9] are essential for high brightness undulators: the acceptance of a monochromator for undulator radiation is generally much smaller than that for dipole radiation. Since undulators tend to steer the electron beam with increasing K values, a high brightness undulator/monochromator would tend to be self-defeating without controlling monitors and feedback loops.

There are two fundamental differences between monitoring dipole radiation and monitoring undulator radiation:

a) For electrons of energy 700 MeV and higher, undulator radiation is not visible to the eye.
b) The neighboring dipole magnets, which bound the straight section containing the undulator, produce copious amounts of both visible and short wavelength light.

Figure 2.6.2: **An Example of a 4 Blade Detector for Undulator Radiation [6.10]**

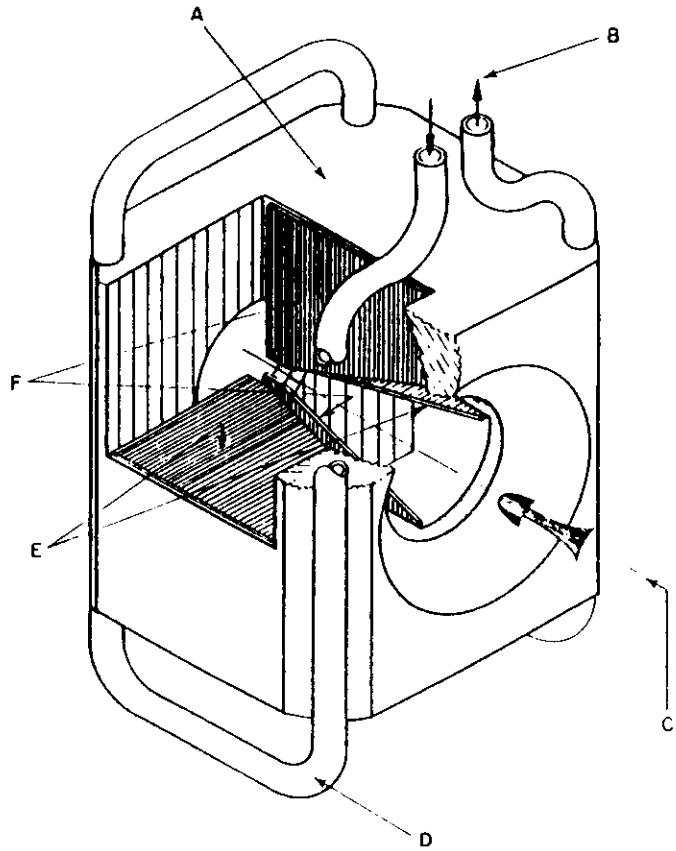

FIG. 2. Phantom view of the monolith showing the blades and the cooling tubes. A—copper monolith, B—cooling water flow, C—direction of photon beam, D—cooling water tubes, E—horizontal blades, and F—vertical blades.

Thus, what one sees in an undulator beamline is not undulator radiation at all, but is instead dipole radiation from sources far removed from the undulator. Photoelectric devices also "see" the dipole radiation and can yield misleading results. The nature of the undulator radiation must be exploited in order to separate the two types of radiation:

c) Undulator radiation is strongly collimated in both transverse directions.
d) Undulator radiation consists of discrete lines or peaks whose energy maximum lies on the optical axis of the undulator itself (see chapter 2.4).

The four blade monitor mentioned above [6.10] effectively exploits the first of these two characteristics of undulator radiation.

The latter characteristic (d above) is generally used to locate the undulator axis with the highest accuracy and certainty. A moveable pinhole of dimensions of the order of those of the electron beam is positioned on what is thought to be the undulator axis. An energy scan is then made on the monochromator. The pinhole is moved slightly (laterally) and the energy scan repeated. By systematically searching the area with the pinhole, the exact location of the undulator axis can be determined. It is the location which produces a spectrum of the first harmonic, for example, of the undulator spectrum which is shifted to the highest energy relative to the other spectra, of the first harmonic.

Such moveable pinholes or apertures are essential in an undulator beamline. They serve not only to set up the beamline initially but also to check the stability of the electron beam in the undulator against time or K value, for example. They can also be used as a fairly good check of the general alignment of the beamline in that the visible dipole radiation passing through a pinhole which is known to lie on the undulator axis simulates the path of the invisible undulator radiation quite well.

It is hoped that the reader is now so convinced of the necessity of SR and undulator radiation monitors in beamlines that he is willing to put the time and effort into planning and installing them.

Chapter 3: Fundamental considerations regarding the optical system

3.1 Fermat's Principle

The basic principle which explains the formation of an image in an optical system was expressed in 1661 by the French physicist, P. de Fermat, based on his Principle of Least Time (1657): The light path from point A to point B must be an extremum and is, more precisely, a minimum. From this postulate all laws of geometrical optics can be derived: reflection, refraction, diffraction, imaging, etc. [see ref. 3.9].

For a system with constant index of refraction, say n = 1, light must travel in a straight line, according to Fermat. Referring to figure 3.1.1, a light ray starting at point A, impinging on a mirror at point $P_{\xi,\omega,\ell}$ will be reflected to a point B in space. This is a completely general statement and is easily accepted. The question is, what happens if some number of light rays start out at A and impinge on the mirror at an equally large number of different points $P_{\xi,\omega,\ell}$ from whence they are reflected to a variety of $B_{x,y,z}$. Fermat's principle says, that if the point A is to be imaged at some point B, then all of the paths from A *via* the mirror surface, described by the function $P(\xi,\omega,\ell)$, to B will be equally long. In other words, the time taken by the light ray in going from the one point to the other will be the same. Thus, it is the job of the mirror, $P(\xi,\omega,\ell)$, to accomplish this! If the mirror has the correct geometry, the desired result will be achieved. If not, no image, or a poor one will be generated. In terms of the wave nature of light, an image is formed only when the individual rays constructively interfere. The only guarantee that this will happen continuously over the possible paths, is if the path lengths are the same. The general definition of "equally long" is that the path lengths lie within $\lambda/4$ of each other (Rayleigh criterion).

Thus, for some arbitrary path $F = \overline{AP} + \overline{PB}$

all paths *via* the mirror surface, $P(\xi,\omega,\ell)$, must fulfill the following:

$$\frac{\partial F}{\partial w} = 0 \quad \text{and} \quad \frac{\partial F}{\partial \ell} = 0 \quad .$$

Figure 3.1.1: The Optical Path Function

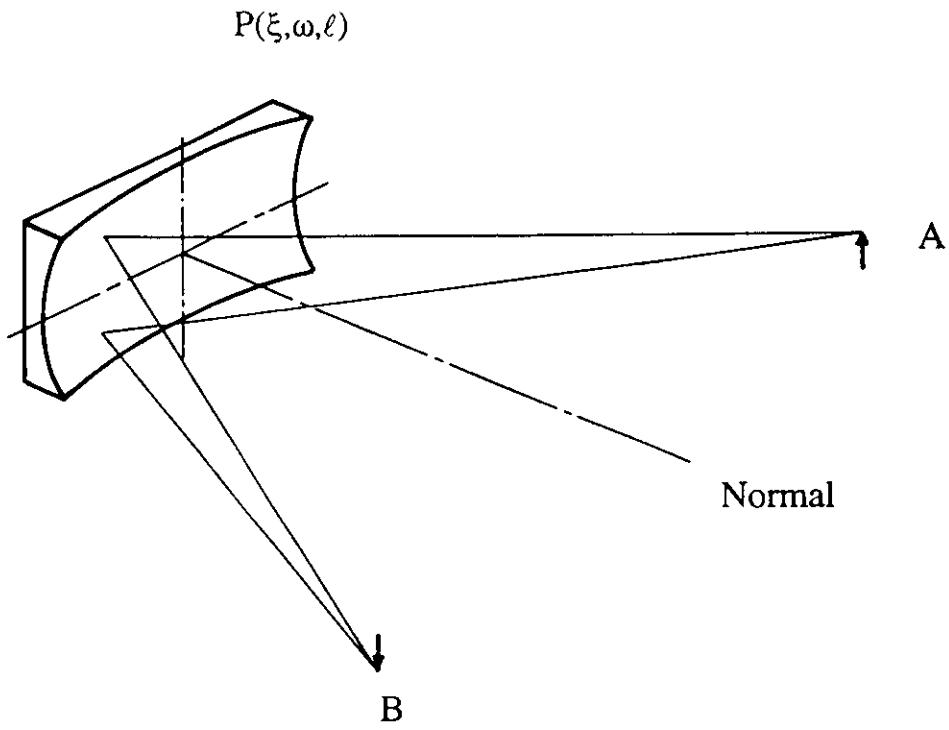

The only thing remaining is to define the surface, $P(\xi,\omega,\ell)$. This has been done in chapter 4 for geometries relevant to our needs: toroid (sphere), ellipsoid and paraboloid (See figure 4.2.2). The general form of the surface is expressed by the equation

$$\xi = \sum_{i=0}^{\infty} \sum_{j=0}^{\infty} a_{ij} \omega^i \ell^j$$

The coefficients a_{ij} for the aforementioned surfaces are provided in table 4.2.1.

We make the following substitutions:

$$x = r \cos \alpha \quad \text{and} \quad y = r \sin \alpha$$
$$x' = r' \cos \beta \quad \text{and} \quad y' = r' \sin \beta \ .$$

The sign convention for the angles is $\beta > 0$ if both $\overline{AP}$ and $\overline{PB}$ lie on the same side of the normal to the surface. Otherwise $\beta < 0$. This convention will be examined more closely in chapter 4 , where gratings are treated.

Then F is defined by the following series:

$$\begin{aligned} F = \quad & F_{000} \\ & + \omega F_{100} \\ & + 1/2\ \omega^2 F_{200} + 1/2\ \ell^2 F_{020} \\ & + 1/2\ \omega^3 F_{300} + 1/2\ \omega\ell^2 F_{120} \\ & + 1/8\ \omega^4 F_{400} + 1/4\ \omega^2\ell^2 F_{220} + 1/8\ \ell^4 F_{040} \\ & + \ell F_{011} + \omega\ell F_{111} + 1/2\ \omega F_{102} + 1/4\ \omega^2 F_{202} + 1/2\ \omega^2\ell \\ & F_{211} \\ & + ... \end{aligned}$$

Although this all appears to be very complicated, it turns out that most of the "dirty work" will be performed by the ray trace program, which is nothing else than an elaborate bookkeeper for keeping track of individual light paths, called rays!

In chapter four we will extend the above arguments to gratings. In chapter five, the simpler case of mirrors will be dealt with.

3.2. Boundary conditions for the design of the beamline

The designer and/or end user of the beamline must set the boundary conditions before the design can be started: energy range, resolution, polarisation of the radiation and coherence are just a few of the more obvious ones. The decisions to be made here must be consonant with (a) the experimental goals of the beamline user and (b) reality. The beamline designer is perhaps more concerned with the latter. It is essential that one or more of the future users of the beamline be involved in the design at this stage.

If for example the beamline is to be dedicated to one application or to one type of research, it is possible to optimize it in ways which differ from a general purpose beamline. For example, for near edge spectroscopy at the carbon, nitrogen and oxygen K-edges, three gratings can be chosen for best resolution at 284, 400 and 540 eV respectively and over the range of 60 - 80 eV above them. As a second example, monochromators for circularly polarized radiation from dipole magnets have been reported in the literature, using off-plane radiation from the storage ring and requiring two optical paths through the monochromator [4.23, 4.24, 4.25].

High flux designs where resolution plays a secondary role can also be designed. One application is as a wavelength "filter" for a subsequent zone plate system for x-ray microscopy. The possibilities are too numerous to list. The solution is, as stated above, to get the users involved at this stage. By this means, new types of monochromators for new types of experiments will be conceived and both the users and the beamline designers will be more satisfied.

3.3. Critical aspects of beamlines for 10-1000 eV photons

The main points to be considered here are given in table 3.3.1. The experienced designer will automatically know or think about most of them. Nevertheless, it doesn't hurt to go through them one last time before starting with the design!

Table 3.3.1: Critical Aspects of Sources and Monochromators for 10 - 1000 eV Synchrotron Radiation

1. The light source is fixed (point or point on an axis). The experiment is also fixed in general (points, axis/point). The optical system must connect these two points, axis/points. *For fixed experiments resolution and/or transmission may suffer from the use of additional optical elements.*

2. SR-Sources (Dipole, Wiggler, Undulator) are highly collimated and of small size (i. e. brilliant). *This makes possible optical designs of high transmission and high resolution.*

3. The vertical source size and, for a dipole or wiggler source, the opening angle of the radiation is much smaller than in the horizontal plane. *Hence, vertical dispersion is desirable.*

4. The source position and axis must be highly stable. *Dynamic feedback between beamline monitors and steering magnets is required for ID's.*

5. The ring current is not a reliable measure of the intensity of the SR behind the exit slit. *The latter should be monitored.*

6. The SR is linearly polarized in the plane of the storage ring. For low energies (< 50 eV) the "p" and "s" reflectivities are very different.

7. The reflectivity and the transmission of all optical materials in the 10 - 1000 eV range are poor. *Windowless optics, grazing angles of incidence and selected reflective coatings are required.*

8. In the 10 - 1000 eV range higher order radiation is a problem. *It should be determinable and/or suppressed.*

9. The optical elements, in particular the first one, are subject to radiation damage and/or heat loading. The heat loading from wigglers and undulators produces bends and local bumps on mirrors and gratings. *Cooling is required but requires extra work.*

10. Ultrahigh vacuum conditions ($P = 1 - 2 \times 10^{-9}$ mbar) are required: *(1) to be compatible with the vacuum requirements of the storage ring and the experiment; (2) to avoid contamination of the optical surfaces, especially with carbon.*

Chapter 4: Gratings

In this chapter some basic aspects of diffraction gratings are discussed and the relationship between optical aberrations and resolution developed. In addition, several equations and approximations are derived or stated which should be of use to the designer. Special emphasis is given to spherical gratings but most of the development is equally applicable to plane gratings.

In the field of reflective and dispersive optics there are several developments that should be mentioned even if not dealt with in these notes. All of them are presently (1995) in use, either as prototype systems or more routinely.

a) Variable line spacing gratings, both plane and concave. With such optical elements, higher order corrections can be included improving the performance of the basic grating type.

b) Multilayers. These are especially important in high heat load beamlines and as normal incidence reflectors at high energies. They have a bandwidth of $BW \approx 1/M$ where M is the number of layers that are reached by the radiation.

c) Multilayer gratings. An enhanced reflectivity can be achieved over a normal reflecting coating. It is also possible to design the multilayer/grating combination so that it always stays on blaze.

d) Bragg-Fresnel optics. Such systems make possible low aberration optics at high energies and normal incidence for a small bandwidth of radiation.

These subjects are very important for beamline design and should not be neglected even if they are not covered in these "Notes". The reader is referred to the proceedings of the various national and international conferences on instrumentation for synchrotron radiation for relevant and up to date references. In addition, relevant references are given in chapter 11 here in these "Notes". See especially the references to chapter 4.

4.1. Some of the basic considerations for the choice of grating

The following is a list of parameters relevant to the choice of the grating to be used. For the final decisions regarding the design of the entire beamline, a number of further questions will have to be raised and answered. This will be done in chapter 6. It may well turn out that at that time a different choice of grating will appear more suitable that that made here. It doesn't matter! The appropriate thinking processes for the choice must be developed and tuned.

-Energy range

-Resolution required

-Flux required

-The grating type: plane, toroidal, spherical, variable line spacing etc.

-Availability of the type of grating desired

-Cost of the grating(s)

-Space available for the beamline

-Complexity and cost of the mechanics

-Amount of manpower available to develop, build and maintain the beamline.

In order to answer these questions some knowledge of grating theory is required. For this, detailed calculations and ray traces will be a great and essential help. But equally important, a knowledge of the use for which the monochromator is to be designed is required. The end users should be brought into the picture at an early stage of designing the beamline. Only in this way, will be design be optimized from both points of view: the designer's and the user's.

In table 4.1.1 we have listed the points that the most ambitious designer would like to include in the design of a high resolution monochromator. Many of the terms in this list will be unfamiliar to the reader at this point. They will be defined here in chapter 4. We shall see this list again in chapter 6.

Table 4.1.1: The "Ideal" High Resolution Soft X-Ray Monochromator

1) Focussed for all λ ($F_{200} = 0$)
2) Coma corrected for all λ ($F_{300} = 0$)
3) Other aberrations minimized
4) Large energy range without grating change
5) Grating always on "blaze"
6) Higher orders suppressed
7) Fixed entrance and exit slits
8) Fixed entrance and exit directions
9) Perfect matching to source
10) Performance unaffected by heat load
11) High transmission
    Number of optical elements
    Quality of optical elements
12) Possible to align!
13) Possible to pay for!

4.2. Geometric Aberration Theory of Straight Ruled, Constant Spacing Diffraction Gratings

As we have already seen in chapter 3, Fermat's Principle of Least Time explains why optical systems function. There a mirror system was described and the path function defined. In the case of a diffraction grating, a further condition must be fulfilled if the system is to function: the monochromaticity condition: $Nk\lambda w$.

For a diffraction grating, light coming from point A (see figure 4.2.1) and impinging on an arbitrary point P (ξ, ω, ℓ) on a grating will contribute to an image at B only if the light path function is fulfilled:

$$F = \overline{AP} + \overline{PB} + Nk\lambda\omega \qquad (1)$$

where N is the line density
k is the order of diffraction $\pm 1, \pm 2$ etc.
λ is the wavelength of the light being diffracted
and ω is the position in the dispersion plane.

Thus, the rays of light coming from A will arrive at B with the same phase, yielding constructive interference and hence, an image. According to Rayleigh's criterion for constructive interference, $\Delta F \leq \lambda/4$. That is, there is a certain bandpass associated with the light path function, a fact which we will not pursue here any further.

According to Fermats' principle of least time, the conditions for focussing A at B are given by

$$\frac{\partial F}{\partial w} = 0 \qquad \text{(meridional focus)} \qquad (2)$$

and

$$\frac{\partial F}{\partial \ell} = 0 \qquad \text{(sagittal focus)} \qquad (3)$$

These three equations provide the basis for determining the optical properties of a given diffraction grating. More subtly, they can be used to decide on the characteristics of the diffraction grating, in particular, the shape of the surface and the groove density N in order to optimize the performance of the entire system. With regard to the latter point, various authors have determined that certain optical properties can be improved, or aberrations reduced, if N is variable across the surface of the grating [4.3 and references therein, 4.11, 4.16]. This possibility will not be developed

Figure 4.2.1: Grating Definitions

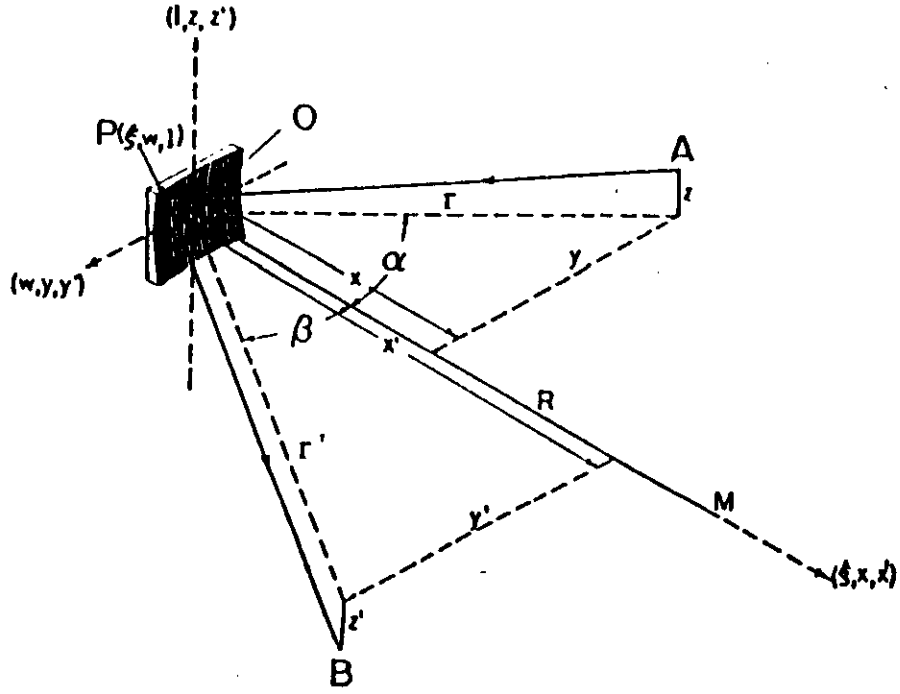

a) Coordinate systems [taken from Reference 4.1]

Whereas Beutler [4.1] uses the notation ξ, w, l for the grating and x, y, z, x', y', z' for the object and image respectively, Haber [4.2] uses x, y, z for the grating and x_a, x_b, x_c, x_b, y_b and z_b for the object and image. We use the Beutler notation as do references 4.3 and 4.10.

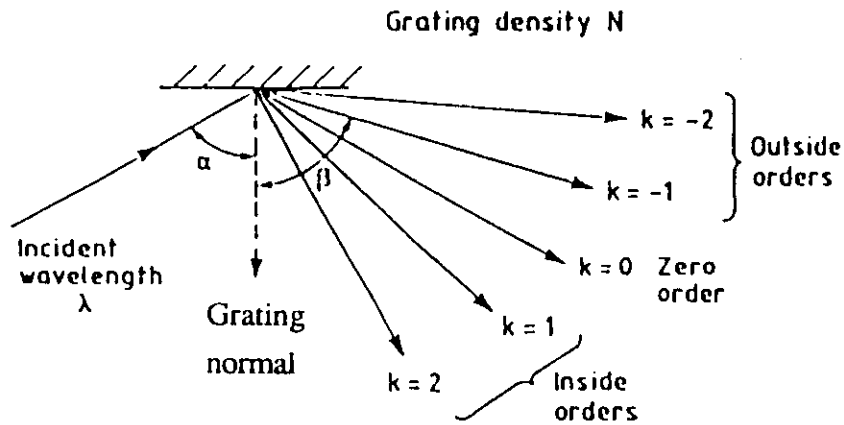

b) Grating orders [taken from Reference 3.4]. Note the sign convention for the angle β:

$\beta > 0$	when on the same side of the grating normal as α
$\beta < 0$	when on the opposite side of the grating normal

here, and we restrict ourselves to straight ruled, constant spacing diffraction gratings. Our goal here is to develop the relationship between the geometry of the optical system and the dispersion, $\Delta\lambda$, resulting from this geometry, the aberration dispersion.

The equations 1-3 above only gain a practical meaning if we define the surface under study. For the purpose at hand, it is most convenient to use a polynominal for the surface P (ξ, ω, ℓ):

where
$$\xi = \sum_{i=0}^{\infty} \sum_{j=0}^{\infty} a_{ij} \omega^i \ell^j$$

and

$$a_{00} = a_{10} = 0; \; j = \text{even}$$

as dictated by the choice of origin and the fact that the xy plane is a symmetry plane. We should like to point out here that this is not the usual way of defining surfaces and that, in the past, a considerable amount of work was required to achieve the series expansions from the familiar expressions (see for example references 4.1 and 4.2). We have obtained the coefficients with the help of a computer code [4.18] the results of which are given in table 4.2.1 for various surfaces (see figure 4.2.2).

Then,

$$\langle AP \rangle = \left[(x-\xi)^2 + (y-\omega)^2 + (z-\ell)^2\right]^{1/2}$$

$$\langle PB \rangle = \left[(x'-\xi)^2 + (y'-\omega)^2 + (z'-\ell)^2\right]^{1/2}$$

From figure 4.2.1 it can be seen that the following substitutions can be made:

$$x = r\cos\alpha \,, \; y = r\sin\alpha$$
$$x' = r'\cos\beta \,, \; y' = r'\sin\beta$$

and that
$$\frac{z}{r} = -\frac{z'}{r'}$$

where the signs of α and β are opposite if points A and B lie on opposite sides of the xz-plane. The grating dimensions are $\pm w_o$ in the y (dispersive) direction and $\pm \ell_o$ in the sagittal direction. The origin is in the middle of the grating. In the development of the geometric relations relating A, P and B,

Figure 4.2.2: **Three Geometries [3.4, 5.7]**

Toroid

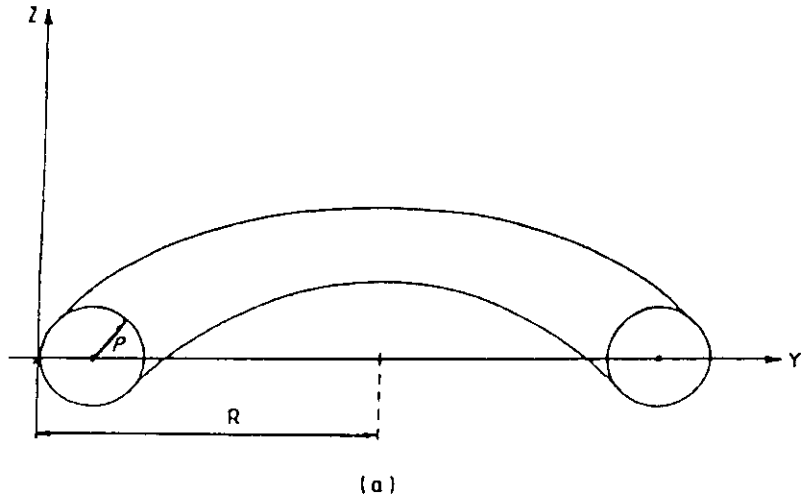

(a)

Parabola

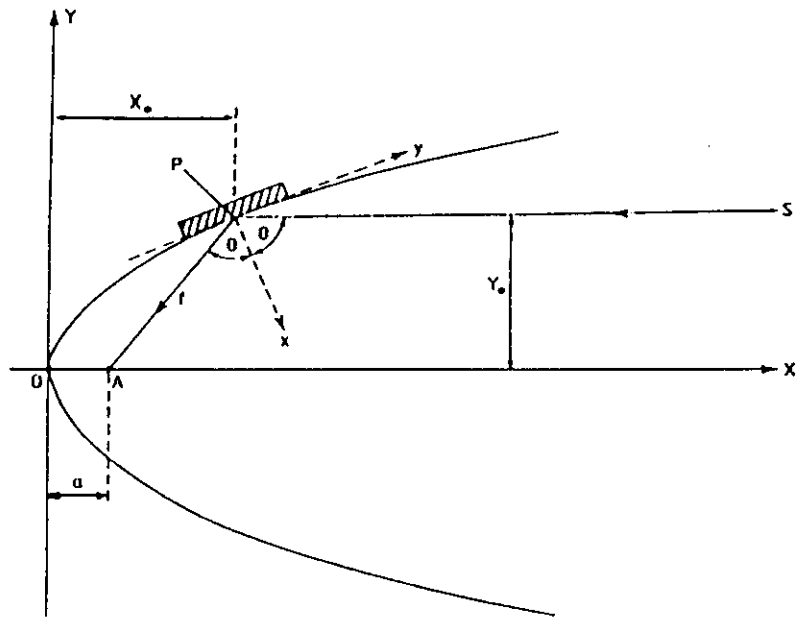

Ellipse

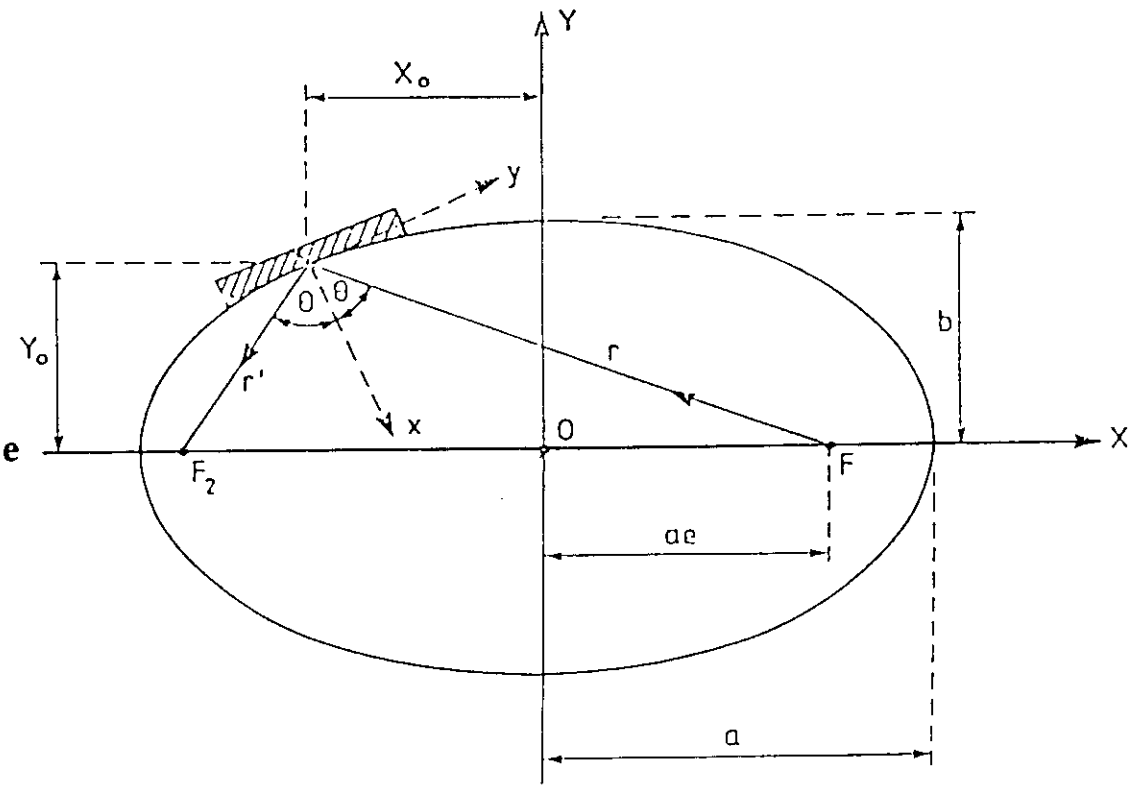

Table 4.2.1 The a_{ij} coefficients for various surfaces [4.18].
see figure 4.2.2 for definitions of terms.

Toroid Note: For a sphere, $\rho = R$

$$a_{02} = \frac{1}{2\rho} \qquad a_{20} = \frac{1}{2R} \qquad a_{22} = \frac{1}{4R^2\rho}$$

$$a_{40} = \frac{1}{8R^3} \qquad a_{04} = \frac{1}{8\rho^3}$$

Ellipsoid Note: $f = \left[\frac{1}{r} + \frac{1}{r'}\right]^{-1}$

$$a_{02} = \frac{1}{4f\cos\theta} \; ; \quad a_{20} = \frac{\cos\theta}{4f} \; ; \quad a_{04} = \frac{b^2}{64f^3\cos^3\theta}\left[\frac{\sin^2\theta}{b^2} + \frac{1}{a^2}\right]$$

$$a_{12} = \frac{\tan\theta(e^2 - \sin^2\theta)^{1/2}}{8f^2\cos\theta} \; ; \quad a_{30} = \frac{\sin\theta}{8f^2}(e^2 - \sin^2\theta)^{1/2}$$

$$a_{40} = \frac{b^2}{64f^3\cos\theta}\left[\frac{5\sin^2\theta\cos^2\theta}{b^2} - \frac{5\sin^2\theta}{a^2} + \frac{1}{a^2}\right]$$

$$a_{22} = \frac{\sin^2\theta}{16f^3\cos^3\theta}\left[\frac{3}{2}\cos^2\theta - \frac{b^2}{a^2}\left(1 - \frac{\cos^2\theta}{2}\right)\right]$$

Paraboloid

$$a_{02} = \frac{1}{4f\cos\theta} \; ; \quad a_{20} = \frac{\cos\theta}{4f} \; ; \quad a_{04} = \frac{\sin^2\theta}{64f^3\cos^3\theta}$$

$$a_{12} = -\frac{\tan\theta}{8f^2} \; ; \quad a_{30} = -\frac{\sin\theta\cos\theta}{8f^2}$$

$$a_{40} = \frac{5\cos\theta\sin^2\theta}{64f^3} \; ; \quad a_{22} = \frac{3\sin^2\theta}{32\cos\theta\, f^3}$$

Plane

$R = \infty$; $\rho = \infty$; $a_{ij} \equiv 0$!

the variables x, y, x', y' for A and B are eliminated as shown above and for a given surface geometry, P, ξ can be expressed in terms of the other variables and the various a_{ij}. After making these expansions and substitutions one can express F as follows:

$$F = F_{000} + wF_{100} + \tfrac{1}{2} w^2F_{200} + \tfrac{1}{2} \ell^2F_{020} + \tfrac{1}{2} w^3F_{300} + \tfrac{1}{2} w\ell^2F_{120}$$

$$+ \tfrac{1}{8} w^4F_{400} + \tfrac{1}{4} w^2\ell^2F_{220} + \tfrac{1}{8} \ell^4F_{040}$$

$$+ \ell F_{011} + w\ell F_{111} + \tfrac{1}{2} w F_{102} + \tfrac{1}{4} w^2F_{202} + \tfrac{1}{2} w^2\ell F_{211} + ...$$

selecting the most important terms [4.3, 4.10] and using the notation of Noda et al [4.3].

Thus, for r, r' >> z, z'

$F_{000} = r + r'$

$F_{100} = Nk\lambda - (\sin\alpha + \sin\beta)$ grating equation

$F_{200} = (\cos^2\alpha/r) + (\cos^2\beta/r') - 2a_{20}(\cos\alpha + \cos\beta)$ Meridional focus

$F_{020} = (1/r) + (1/r') - 2a_{02}(\cos\alpha + \cos\beta)$ Sagittal focus

$F_{300} = [T(r,\alpha)/r] \sin\alpha + [(T(r',\beta)/r'] \sin\beta - 2a_{30}(\cos\alpha + \cos\beta)$ Primary coma

$F_{120} = [S(r,\alpha)/r] \sin\alpha + [S(r',\beta)/r'] \sin\beta - 2a_{12}(\cos\alpha + \cos\beta)$ Astigmatic coma

$$F_{400} = [\,4T(r,\alpha)/r^2]\ \sin^2\alpha - [\,T^2(r,\alpha)/r]\ + [\,4T(r',\beta)/r'^2]\ \sin^2\beta$$

$$- [\,T^2(r',\beta)/r'] - 8a_{30}\left[\frac{1}{r}(\sin\alpha\cos\alpha) + \frac{1}{r'}(\sin\beta\cos\beta)\right]$$

$$- 8a_{40}(\cos\alpha + \cos\beta) + 4a^2{}_{20}\left[\frac{1}{r} + \frac{1}{r'}\right]$$

$$F_{220} = [\,2S(r,\alpha)/r^2\,]\ \sin^2\alpha + [\,2S(r',\beta)/r'^2\,]\ \sin^2\beta$$

$$- [\,T(r,\alpha)\,S(r,\alpha)/r\,] - [\,T(r',\beta)\,S(r',\beta)/r'\,]$$

$$+ 4a_{20}a_{02}\,(1/r + 1/r') - 4a_{22}\,(\cos\alpha + \cos\beta)$$

$$- 4a_{12}\left[\frac{1}{r}\,(\sin\alpha\cos\alpha) + \frac{1}{r'}\,(\sin\beta\cos\beta)\right]$$

$$F_{040} = 4a_{02}^2\,(1/r + 1/r') - 8a_{04}\,(\cos\alpha + \cos\beta) - [S^2(r,\alpha)/r] - [S^2(r',\beta)/r']$$

$$F_{011} = -\frac{z}{r} - \frac{z'}{r'}$$

$$F_{111} = -\frac{z}{r^2}\sin\alpha - \frac{z'}{r'^2}\sin\beta$$

$$F_{102} = \frac{z^2\sin\alpha}{r^2} + \frac{z'^2}{r'^2}\sin\beta$$

$$F_{202} = \left(\frac{z}{r}\right)^2\left[\frac{2\sin^2\alpha}{r} - T(r,\ \alpha)\right] + \left(\frac{z'}{r'}\right)^2\left[\frac{2\sin^2\beta}{r'} - T(r',\ \beta)\right]$$

$$F_{211} = \frac{z}{r^2}\left[T(r,\ \alpha) - \frac{2\sin^2\alpha}{r}\right] + \frac{z'}{r'^2}\left[T(r',\ \beta) - \frac{2\sin^2\beta}{r'}\right]$$

and $\quad T(r,\alpha) = (\cos^2\alpha/r) - 2a_{20}\cos\alpha$

$$S(r,\alpha) = (1/r) - 2a_{02}\cos\alpha$$

and analogously for $T(r',\beta)$, $S(r',\beta)$.

The F_{ijk} terms which are not identified above contribute to coma, line shape, and line inclination.

It is useful to divide the light path function, F, into two parts

$$F^* = F_{000} + wF_{100}$$

and $\quad F^{**} =$ the rest!

Application of Fermats' principle (eq. 2, 3) to F* yields the grating equation

$$Nk\lambda = \sin\alpha + \sin\beta.$$

Application of Fermats' principle to F** yields the expressions for the optical characteristics of the image at B for a given object at A and the surface P.

The main goal of this entire exercise is to determine the relationship between A, P and B on the one hand and the resolution, $\Delta\lambda$, that one can expect from a given system on the other. The dispersive contribution to resolution, $\Delta\lambda$, caused by aberrations stemming from F**, is derived as follows:

$$Nk\lambda = \sin\alpha + \sin\beta$$

$$\left(\frac{\partial \lambda}{\partial \beta}\right)_{\alpha=\text{const.}} = \frac{1}{Nk}\cos\beta$$

$$\frac{dy'}{r'} = d\beta$$

$$d\lambda = \frac{1}{Nkr'}\cos\beta\, dy'$$

The deviation of the path function in the dispersive direction is

$$\frac{\partial F**}{\partial \omega} = \delta(\cos\gamma_y) = d(\sin\beta) = \cos\beta\, d\,\beta = \frac{\cos\beta}{r'}\, dy'$$

and in the sagittal direction

$$\frac{\partial F**}{\partial \ell} = \frac{1}{r'}\, dz'$$

where δ ($\cos\gamma_y$) is the change in the direction cosine from the Gaussian value (see Howells, 1980).

Then

$$\Delta\lambda = \frac{1}{Nk}\,\frac{\partial F**}{\partial \omega}$$

and

$$\Delta\lambda = \frac{1}{Nk}\Big[wF_{200} + \frac{3}{2}w^2F_{300} + \frac{1}{2}\ell^2F_{120} + \frac{1}{2}w^3F_{400} + \frac{1}{2}w\ell^2F_{220} +$$

$$\ell F_{111} + \frac{1}{2}F_{102} + \frac{1}{2}wF_{202} + w\ell F_{211} \cdots \Big]$$

We have thus arrived at the goal of this section and need now simply to insert the geometric parameters, a_{ij}, in the F_{ijk} relations above to obtain the expression for $\Delta\lambda$ (w, ℓ, a, b, etc.) for a given surface.

4.3. Toroidal and Spherical Gratings

For toroidal grating monochromators, and for the special case of spherical grating monochromators, where $\rho = R$, the relevant expressions for the terms in the optical path function are as follows:

$$F_{020} = \frac{1}{r} + \frac{1}{r'} - \frac{1}{\rho}(\cos\alpha + \cos\beta) \qquad \text{sagittal focus}$$

$$F_{200} = \left(\frac{\cos^2\alpha}{r} - \frac{\cos\alpha}{R}\right) + \left(\frac{\cos^2\beta}{r'} - \frac{\cos\beta}{R}\right) \qquad \text{meridional focus}$$

$$F_{300} = \left(\frac{\cos^2\alpha}{r} - \frac{\cos\alpha}{R}\right)\frac{\sin\alpha}{r} + \left(\frac{\cos^2\beta}{r'} - \frac{\cos\beta}{R}\right)\frac{\sin\beta}{r'} \qquad \text{primary coma}$$

$$F_{400} = \frac{4}{r^2}\left(\frac{\cos^2\alpha}{r} - \frac{\cos\alpha}{R}\right)\sin^2\alpha - \frac{1}{r}\left(\frac{\cos^2\alpha}{r} - \frac{\cos\alpha}{R}\right)^2$$

$$+ \frac{4}{r'^2}\left(\frac{\cos^2\beta}{r'} - \frac{\cos\beta}{R}\right)\sin^2\beta - \frac{1}{r'}\left(\frac{\cos^2\beta}{r'} - \frac{\cos\beta}{R}\right)^2$$

$$- \frac{1}{R^3}(\cos\alpha + \cos\beta) + \frac{1}{R^2}\left(\frac{1}{r} + \frac{1}{r'}\right)$$

$$F_{120} = \left(\frac{1}{r} - \frac{1}{\rho}\cos\alpha\right)\frac{\sin\alpha}{r} + \left(\frac{1}{r'} - \frac{1}{\rho}\cos\beta\right)\frac{\sin\beta}{r'} \qquad \text{astigmatic coma}$$

$$F_{220} = \left(\frac{1}{r} - \frac{1}{\rho}\cos\alpha\right)\frac{2\sin^2\alpha}{r^2} + \left(\frac{1}{r'} - \frac{1}{\rho}\cos\beta\right)\frac{2\sin^2\beta}{r'^2}$$

$$- \frac{1}{r}\left(\frac{\cos^2\alpha}{r} - \frac{\cos\alpha}{R}\right)\left(\frac{1}{r} - \frac{\cos\alpha}{\rho}\right) - \frac{1}{r'}\left(\frac{\cos^2\beta}{r'} - \frac{\cos\beta}{R}\right)\left(\frac{1}{r'} - \frac{\cos\beta}{\rho}\right)$$

$$+ \frac{1}{\rho R}\left(\frac{1}{r} + \frac{1}{r'}\right) - \frac{1}{\rho R^2}(\cos\alpha + \cos\beta)$$

$$F_{040} = \frac{1}{\rho^2}\left(\frac{1}{r} + \frac{1}{r'}\right) - \frac{1}{\rho^3}(\cos\alpha + \cos\beta) - \frac{1}{r}\left(\frac{1}{r} - \frac{\cos\alpha}{\rho}\right)^2 - \frac{1}{r'}\left(\frac{1}{r'} - \frac{\cos\beta}{\rho}\right)^2$$

$$F_{202} = \left(\frac{z}{r}\right)^2\left[\frac{2\sin^2\alpha}{r} - \frac{\cos^2\alpha}{r} + \frac{\cos\alpha}{R}\right] + \left(\frac{z'}{r'}\right)^2\left[\frac{2\sin^2\beta}{r'} - \frac{\cos^2\beta}{r'} + \frac{\cos\beta}{R}\right]$$

$$F_{211} = \frac{z}{r^2}\left[\frac{\cos^2\alpha}{r} - \frac{\cos\alpha}{R} - \frac{2\sin^2\alpha}{r}\right] + \frac{z'}{r'^2}\left[\frac{\cos^2\beta}{r'} - \frac{\cos\beta}{R} - \frac{2\sin^2\beta}{r'}\right]$$

and F_{011}, F_{111} and F_{102} are as given above.

As shown in section 4.2, the resolution, $\Delta\lambda$, is related to the various terms by the following:

$$\Delta\lambda = \frac{1}{Nk}\left[wF_{200} + \frac{3}{2}w^2F_{300} + \frac{1}{2}\ell^2F_{120} + \frac{1}{2}w^3F_{400} + \frac{1}{2}w\ell^2F_{220} + \right.$$

$$\left. \ell F_{111} + \frac{1}{2}F_{102} + \frac{1}{2}wF_{202} + w\ell F_{211} \ldots\right]$$

The two focussing terms F_{200} , and F_{020} , arise from the fact that, for a single spherical optical element at other than normal incidence, two non-coincident focii are produced, one in the meridional plane and one in the sagittal. Thus, for a vertically deflecting spherical mirror

Figure 4.3.1: Sagittal and Meridional Focii

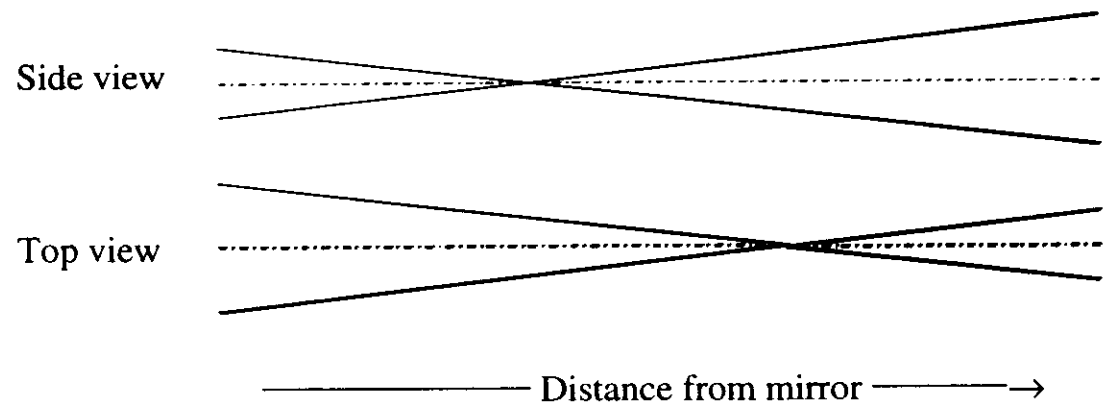

In a monochromator this is not necessarily a problem since only the focus in the dispersion plane affects the resolution. It can become a problem, however, if an absolute minimum of optical elements is required. This subject will be taken up again at a suitable point.

4.4. Some useful relationships

4.4.1. Slit limited resolution:

Entrance: $$\Delta\lambda_{ent} = \frac{1}{Nk}\frac{s}{r}\cos\alpha$$

Exit: $$\Delta\lambda_{exit} = \frac{1}{Nk}\frac{s'}{r'}\cos\beta$$

4.4.2. Contribution of rms tangent errors, σ_{TE}, to resolution:

$$\Delta\lambda_{Tan} = 2\,\lambda\,\sigma_{TE}\cot\sin^{-1}\left(\frac{Nk\lambda}{2\cos\theta}\right) = 2\,\lambda\,\sigma_{TE}\cot\phi$$

where $\theta = \frac{\alpha-\beta}{2}$ and $\phi = \frac{\alpha+\beta}{2}$.

4.4.3. Diffraction limited resolution:

$$\Delta\lambda_0 = \frac{\lambda}{2kNw_O}$$

N = lines/mm
w_O = half illuminated width in dispersive direction
k = diffraction order

4.4.4. Horizon wavelength:

$$\lambda_H = \frac{2}{Nk}\cos^2\theta$$

4.4.5. Grating equation: $Nk\lambda = \sin\alpha + \sin\beta = 2\cos\theta\sin\phi$

where

$$\theta = \frac{\alpha-\beta}{2} \quad ; \quad \phi = \frac{\alpha+\beta}{2}$$

N.B. Note the sign convention for α and β! (see fig. 4.2.1)

4.4.6. The determination of the length of a grazing incidence mirror/grating

The figure below illustrates the illumination of a mirror/grating of length w_1 to w_2 by radiation coming from the source, S, along the axis r.

Figure 4.4.1: Determination of the Length of a Grazing Incidence Mirror or Grating

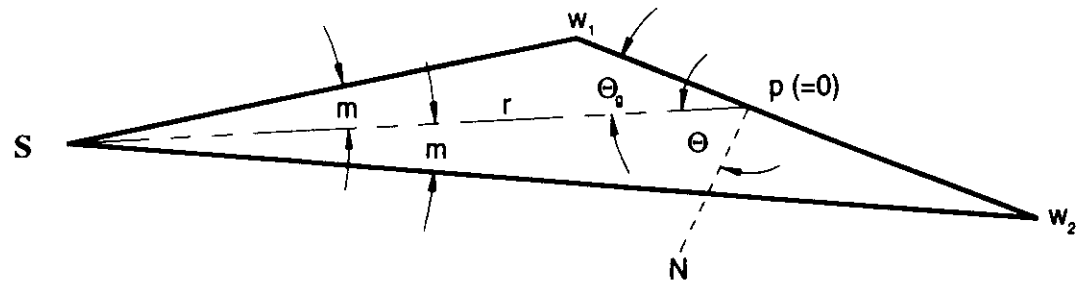

r = distance source to mirror
p = point of incidence of the central ray
± m = ± divergence of the light beam
w_1 , w_2 = nearer, farther illuminated length of mirror
$\theta_g = \pi/2 - \theta$ = grazing angle of incidence of light on mirror
N = normal to the mirror surface

from the sine law: $\frac{a}{\sin\alpha} = \frac{b}{\sin\beta} = \frac{c}{\sin\gamma}$

$$w_1 = \frac{r\sin m}{\sin(\pi - \theta_g - m)} = \frac{r\sin m}{\sin(\theta_g + m)}$$

$$w_2 = \frac{r\sin m}{\sin(\theta_g - m)}$$

and $$L = w_1 + w_2$$

For $\theta_g >> m$ $$L_{approx} \approx \frac{2\, r \sin m}{\sin\theta_g}$$

Example: r = 6500 mm, m = 2.5 mrad, $\theta_g = 2.5°$, w_1 = 354.1 mm, w_2 = 397.4 mm

L = 751.5 mm exactly or approximately $L_{approx.} \approx$ 749 mm.

4.4.7. Determination of a slit width or pinhole diameter

The width of a slit or the diameter of a pinhole may be determined by analysing the Fraunhofer diffraction pattern generated by the opening using coherent light (e.g. HeNe laser).

Figure 4.4.2: Determination of a Slit Width or Pinhole Diameter

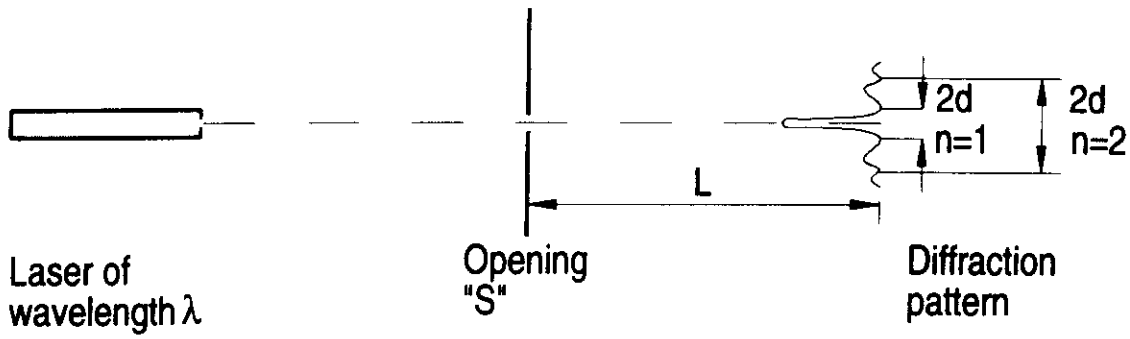

a) Slit (width much smaller than length): $\sin\left(\frac{d(n)}{L}\right) \approx \frac{d(n)}{L} = \frac{n\lambda}{S}$

Note:

1. 2 d(n) represents the distance between intensity minima i.e. dark bands. These are more easily and accurately determined than the middle of the bright bands. "n" is the number of the dark band, i.e. first, second etc. from the central maximum.

2. The diffraction pattern is perpendicular to the slit length. It can be used to determine that the slit is horizontal to an accuracy of about 1° with the help of a plumb line.

b) Pinhole of diameter S: $\sin\left(\frac{d(n)}{L}\right) \approx \frac{d(n)}{L} = \frac{X_n\lambda}{S}$

where X_n corresponds to the zero value of the Bessel function, $J_1(X_n)$ divided by π. X_n = 1.220; 2.233; 3.238; 4.241; 5.243; 6.244; 7.245; 8.245; 9.246; 10.246 for the first ten dark rings.

The central bright spot is known as the Airy disk, encountered in the Rayleigh definition of resolution. The relative intensities of the bright bands are of the order of 1 : 0.05 : 0.02 : 0.01 for slits and 1: 0.02 : 0.004 : 0.002 for pinholes.

4.4.8. The blaze angle of a diffraction grating

For a grating with a "saw tooth" groove profile, it is possible to choose the angle Ψ of the long side of the profile such that, for a particular wavelength, the diffraction direction coincides with the direction of specular reflection from the individual facets. This is shown in the figure below [3.1]. Note that N is the normal to the overall grating surface while N' is the normal to the individual facet. See figure below:

Figure 4.4.3: The Blaze Angle of a Diffraction Grating

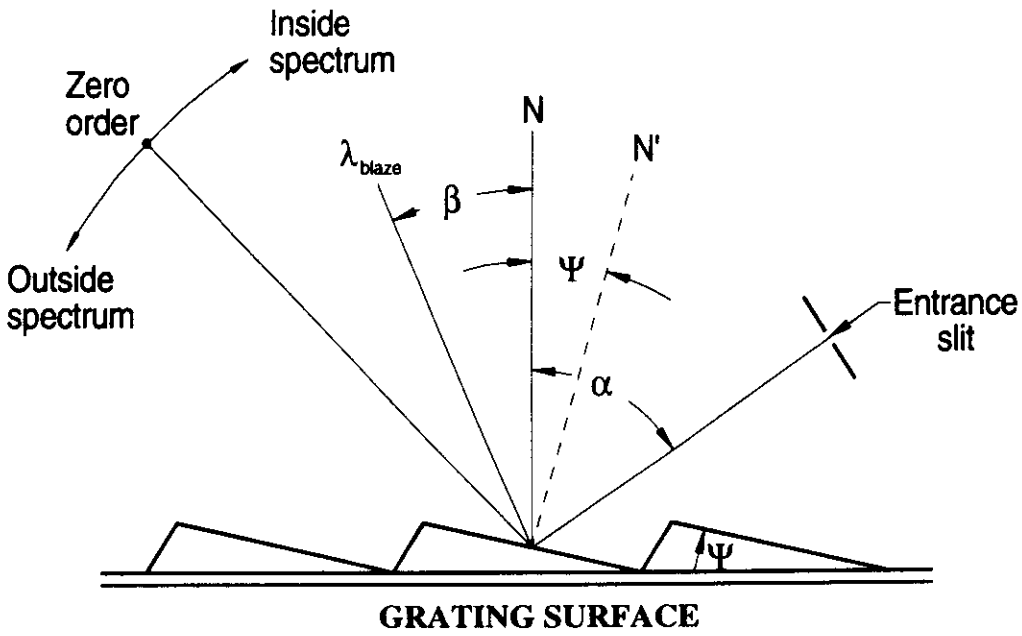

Evidently, the blaze condition is fulfilled

when $\alpha - \Psi = -\beta + \Psi$ (Note sign convention for β!)

Thus $\Psi = \frac{\alpha + \beta}{2}$.

Then, since $\lambda = \frac{2}{Nk} \cos\theta \sin\Psi$ (Eq. 4.4.6)

one finds $\lambda_{blaze} = \frac{2}{Nk} \cos(\alpha - \Psi) \sin\Psi$

Ignoring other effects, a grating blazed for the wavelength λ_1 in first order (k = 1) is blazed for $\frac{\lambda_1}{2}$ in second order (k = 2) etc.

4.4.9. Magnification within a monochromator, M (λ)

What is the optimal size of the exit slit for a given entrance slit or source size?

The meridional magnification is defined by $M(\lambda) = \frac{s'}{s}$

where s = entrance slit width and s' = exit slit width.

This is related to the optical parameters as follows:

$$\left(\frac{d\lambda}{d\alpha}\right)_\beta = \frac{\cos\alpha}{Nk} \qquad \text{and} \qquad \left(\frac{d\lambda}{d\beta}\right)_\alpha = \frac{\cos\beta}{Nk}$$

$$\Delta\alpha = \frac{s}{r}, \qquad \Delta\beta = \frac{s'}{r'}$$

$$\frac{\cos\alpha}{Nk}\Delta\alpha = \frac{\cos\beta}{Nk}\Delta\beta$$

$$\frac{s}{r}\cos\alpha = \frac{s'}{r'}\cos\beta$$

$$M(\lambda) = \frac{s'}{s} = \frac{r'}{r}\frac{\cos\alpha}{\cos\beta}$$

4.4.9.A: Magnification in a Rowland Circle Monochromator
For the description of the Rowland circle monochromator see chapter 6.3.

$$M = \frac{r'\cos\alpha}{r\cos\beta}$$

$r = R\cos\alpha$
$r' = R\cos\beta$ Rowland Conditions

$$\therefore M = \frac{R\cos\beta\cdot\cos\alpha}{R\cos\alpha\cdot\cos\beta} \equiv 1\ !$$

4.4.9.B: Magnification in a Petersen Plane Grating Monochromator.
The design principles and the definitions of the Petersen plane grating monochromator are shown in figure 4.4.4 . See chapter 6.4 as well.

a) $\frac{r'}{r} = - \frac{\cos^2\beta}{\cos^2\alpha}$ F_{200} for Plane Grating

b) $M_{Grating} = M_G = \frac{r'}{r}\frac{\cos\alpha}{\cos\beta}$

c) $M_{Mirror} = M_M = \frac{r''}{r'+d}$ see Fig. 4.5.2

d) $M = M_G \cdot M_M$

For constant focussing

$$\frac{r'}{r} = - \frac{\cos^2\beta}{\cos^2\alpha} = - c^2$$ (Petersen [4.9], c = 2.25)

then $$M = \frac{r'\cos\alpha}{r\cos\beta} \cdot \frac{r''}{r'+d} = \frac{r'}{rc} \cdot \frac{r''}{r'+d}$$

But $r' = - r c^2$

$$\therefore M = \frac{r''}{rc - d/c} \simeq \frac{r''}{rc}$$

Figure 4.4.4: Optical Design of the Petersen Plane Grating Monochromator [4.9]

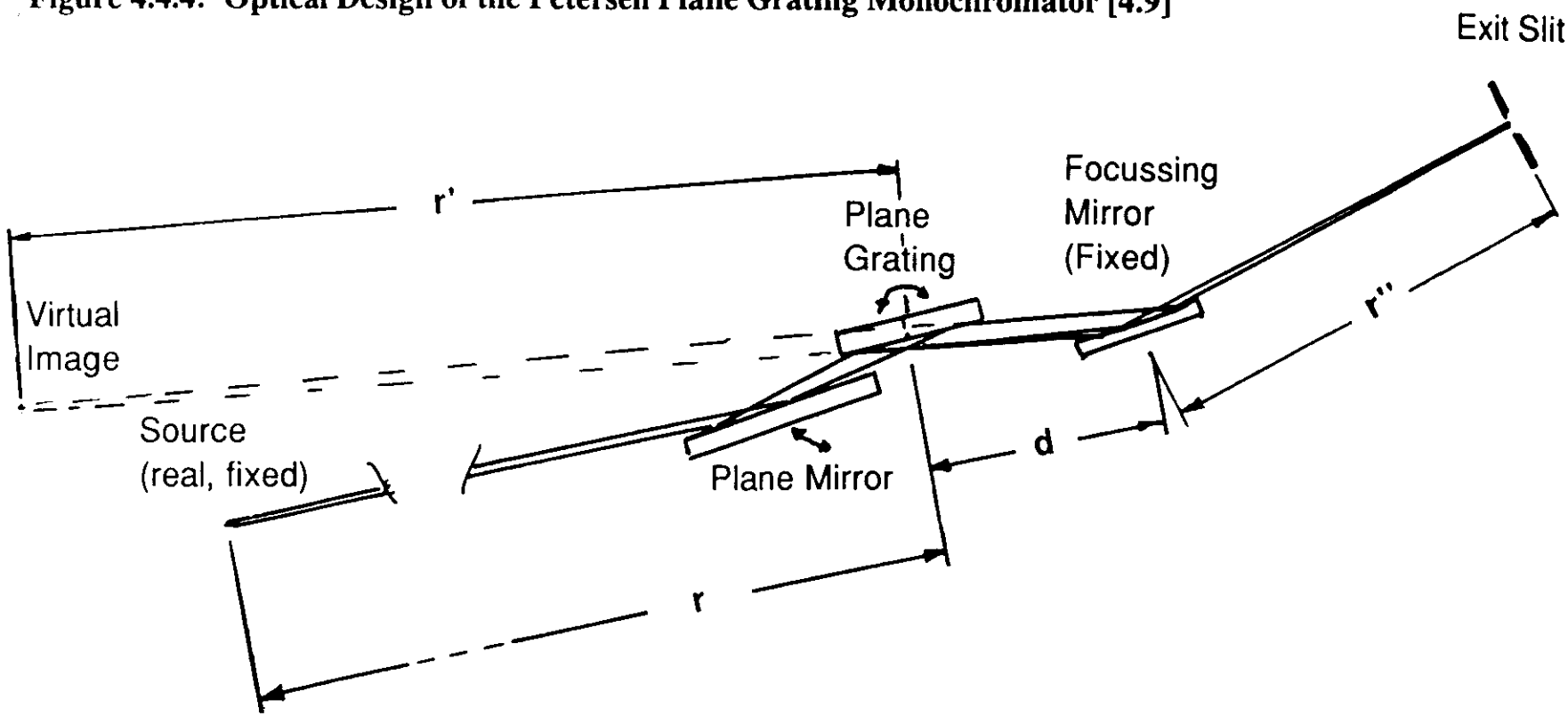

For Grating: $$-\frac{r'}{r} = \frac{\cos^2\beta}{\cos^2\alpha} = (2.25)^2 \quad \text{(Petersen)}$$

For Mirror: $$\left(\frac{1}{p} + \frac{1}{r''}\right)\frac{\cos\theta}{2} = \frac{1}{R} \qquad \text{where } p = r' + d$$

4.4.10. Groove depth for grating grooves

The efficiency of a grating is a function of the depth of the grooves, the shape and the uniformity of the grooves and of the coating material and its thickness. For the calculation of the depth of the grooves for laminar gratings, the most commonly produced holographic grating, the following equation can be used [see ref. 3.4 pp. 82-83. See also ref. 4.32]:

$$\left(\frac{1}{h} - \frac{1}{h_o}\right)^2 = \left(\frac{8\sin\alpha}{\lambda d}\right)m + \frac{1}{h_o^2}$$

where h = groove depth
α = angle of incidence
λ = the middle of the optimized wavelength region
$h_o = \lambda/2\cos\alpha$
d = groove spacing
and m = 1, 3, 5, ... the odd order in question

For 1:1 laminar gratings (see 4.4.11 below), the even orders have zero efficiency in normal incidence, theoretically. In fact they do disperse radiation and produce second order radiation which is often a problem. (see references to "chapter 8")

4.4.11. Groove width to groove period for laminar gratings

The most obvious relation between groove width and groove period is 1:2 or, as is more commonly expressed, groove width to land width 1:1. For this case in normal incidence, second order radiation is completely suppressed theoretically. As soon as the grating is tilted with respect to the incident radiation, the interference pattern changes because the radiation does not "see" the full width of the bottom of the grooves. This is the so-called shadow effect. The extent of the shadow effect is also affected by the penetration of the radiation through the corners of the lands, again when the grating is no longer at normal incidence.

In ordering laminar gratings the groove width to groove period ratio must be optimized for the wavelengths to be dispersed. For the details of this optimization see reference 4.32. This can usually be done by the manufacturer. In any case, it must be addressed.

4.4.12. Thickness of reflecting coatings for gratings and mirrors

The reflection efficiency of a coating is a function of the coating material, its roughness, its thickness, the angle of incidence and the wavelengths of the photons to be reflected. Basically, the thickness must be sufficient so that no interference occurs between the top and the bottom of the coating layer, where a change in the indices of refraction occurs at each interface. In other words, the extinction lengths of the photon wavelengths used must be shorter than the optical path in the coating so that the photons do not reach the second interface. The optimal thickness for the desired coating material and wavelength region can usually be calculated by the mirror manufacturer.

For coatings for photon energies above 100 eV it is important to specify that no subcoating be used. Such subcoatings have been used in the past to make the top coating stick better to the substrate. However, the radiation penetrates the top coating and is absorbed by the elements of the subcoating, producing dips in the spectrum. This is a particular nuisance with Cr, often used as such a subcoating. The Cr lines at 574 and 584 eV show up very clearly in the spectra. In recent years, some optical manufacturers have developed coating methods that make a subcoating superfluous. Basically, it is a question of the cleaning procedure employed before coating. Whether a subcoating is acceptable should be discussed with a grating or mirror manufacturer before ordering.

Chapter 5: Mirror Systems

It is the absorption coefficient of optical materials that makes the VUV and soft x-ray part of the spectrum so different from the visible: the high energy radiation (> 10 eV) interacts with essentially all materials with the result that nothing transmits and little reflects. Even air is opaque to the radiation between ca. 6 and 1000 eV. Thus, the entire optical system must be kept under vacuum. There are no windows (for vacuum), no lenses, prisms, quarter wave plates, etc. and only poorly reflecting mirrors. Only at increasingly grazing angles is a reflected wave observed with increasing photon energy. In this section we encounter the relationships necessary to determine reflectivities, polarisation effects, etc. In addition, the focussing properties of some standard (and eminently useful!) geometries are provided. Finally, manufacturing errors and limits and their consequences are discussed.

5.1. Reflectivity and Polarisation

The relationship between the optical constants of a surface, the angle of incidence and the reflectivity is given by the generalized Fresnel equations for reflection [3.1, 5.5]:

$R_S = [(a-\cos\theta)^2 + b^2] / [(a+\cos\theta)^2 + b^2]$
= Reflectivity of the component whose E vector is perpendicular to the plane of incidence

$R_P = R_S [(a-\sin\theta\tan\theta)^2 + b^2] / [(a+\sin\theta\tan\theta)^2 + b^2]$
= Reflectivity of the component whose E vector is parallel to the plane of incidence

where θ = Angle of incidence with respect to the surface normal

and
$$a^2 = \frac{1}{2}\{[(n^2-k^2-\sin^2\theta)^2 + 4n^2k^2]^{1/2} + (n^2-k^2-\sin^2\theta)\}$$
$$b^2 = \frac{1}{2}\{[(n^2-k^2-\sin^2\theta)^2 + 4n^2k^2]^{1/2} - (n^2-k^2-\sin^2\theta)\}$$

Hence, if one knows the optical constants of a material at some photon wavelength or energy, one can calculate the components of reflectivity at that energy.

i.e. $\tilde{n}(E) = n(E) + i\,k(E)$

where $\tilde{n}(E)$ is the complex index of refraction

$n(E)$ is the real part

and $k(E)$ is the imaginary part or extinction coefficient.

The optical constants for carbon, gold, platinum and nickel for energies between 100 - 1000 eV are shown in figure 5.1.2 [5.6].

Conversely, by measurements of the reflectivity and phase shift of s and p waves it is possible to determine the optical constants. Fortunately, for energies between ca. 30 eV and 10 keV, the optical constants for the elements can be calculated from the atomic scattering factors [5.4] Although the agreement between calculations and measurements is not always good [7.2, 7.3] (fig. 5.1.1) one can at least obtain a qualitative impression of the reflectivity from the calculations for elements for which measured data are lacking. The calculated reflectivities for many materials useful in the VUV and soft x-ray portion of the spectrum have been plotted in reference 7.4. Figure 5.1.3 illustrates the behavior to be found for carbon (C), gold (Au), platinum (Pt) and nickel (Ni) at angles of incidence of 80°, 82°, 84°, 86° and 88° for energies 100-1000 eV [5.6]. Note that at these energies and angles of incidence the Rs and Rp components are almost equal. At lower energies and steeper angles they differ dramatically (Fig. 5.1.4).

The degree of linear polarisation of radiation can be defined by

$$P = \frac{Is - Ip}{Is + Ip} \cdot$$

where Is, Ip are the intensities of the s and p polarized radiation respectively. Radiation produced in a storage ring is almost 100% polarized: in the plane of the ring it is plane polarized with the E vector also in the plane of the ring. Above and below the plane of the ring it is elliptically polarised: that is both s and p waves are produced and exhibit a constant phase difference of 90°.
For equal amplitudes and a 90° or 270° phase difference one talks of circularly polarised light. Various cases are shown in figure 5.1.5 [5.10].

Figure 5.1.1.A: Comparison of Calculated and Measured Reflectivities: C

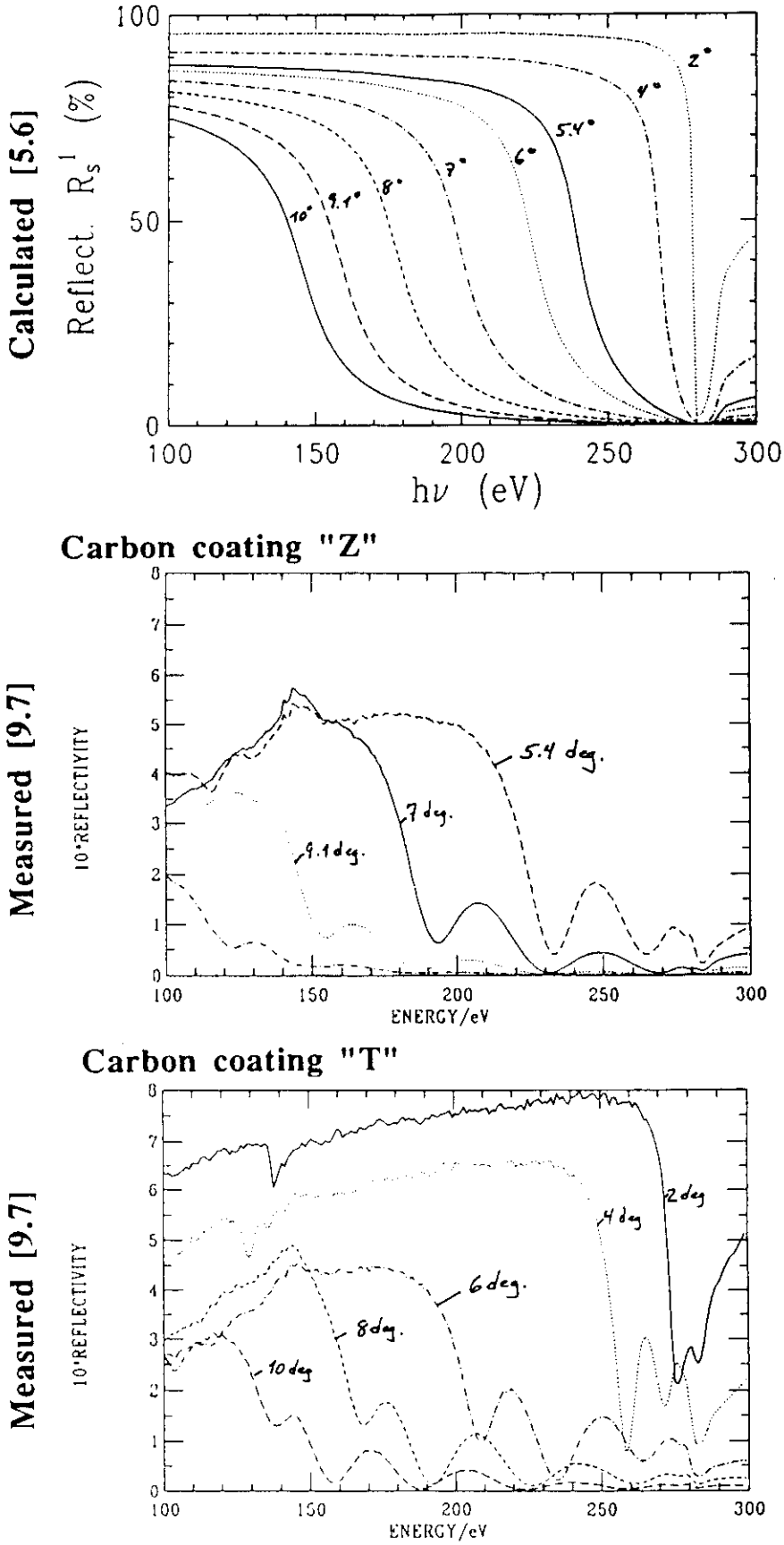

Grazing angles of incidence

Figure 5.1.1.B: Comparison of Calculated and Measured Reflectivities: Au [5.6]

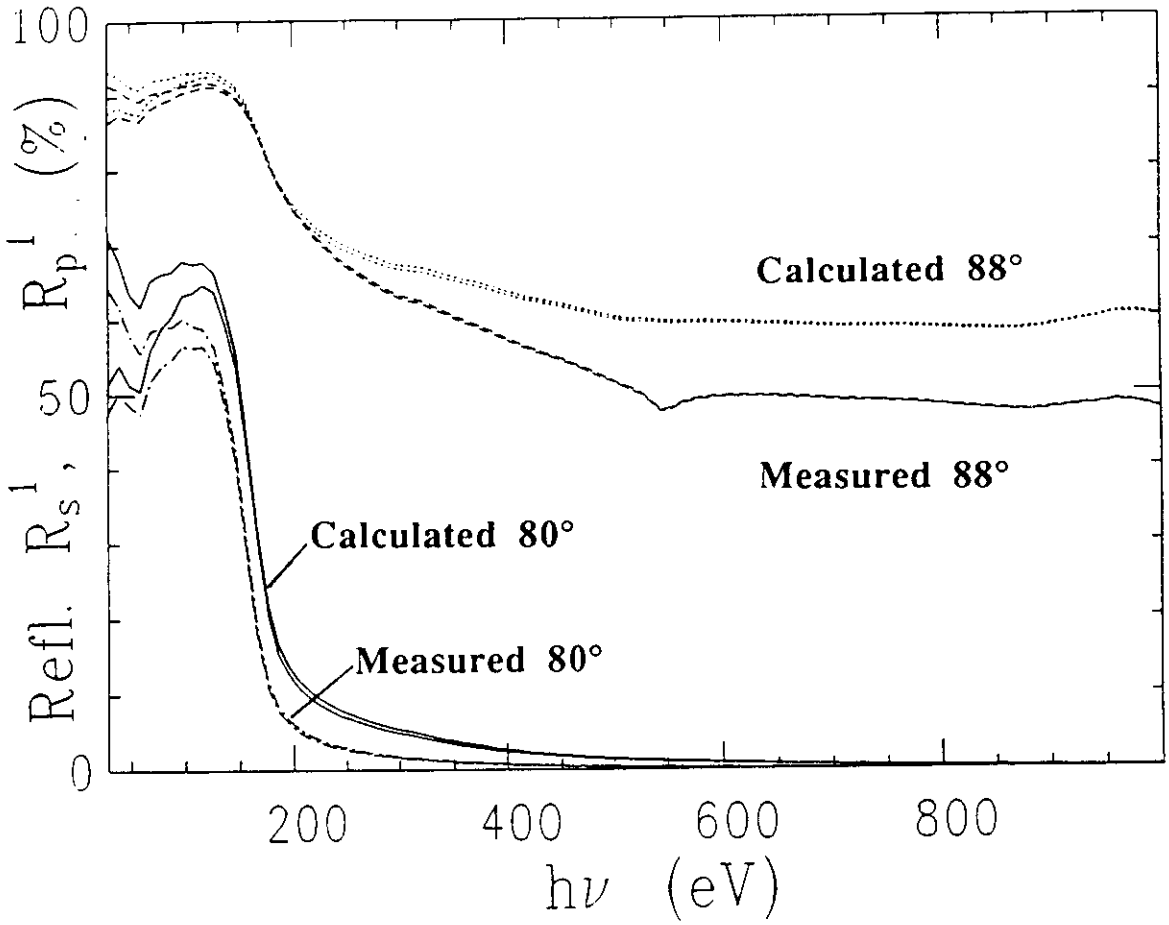

Figure 5.1.2: **The Optical Constants for C, Au, Pt, Ni [5.6]**

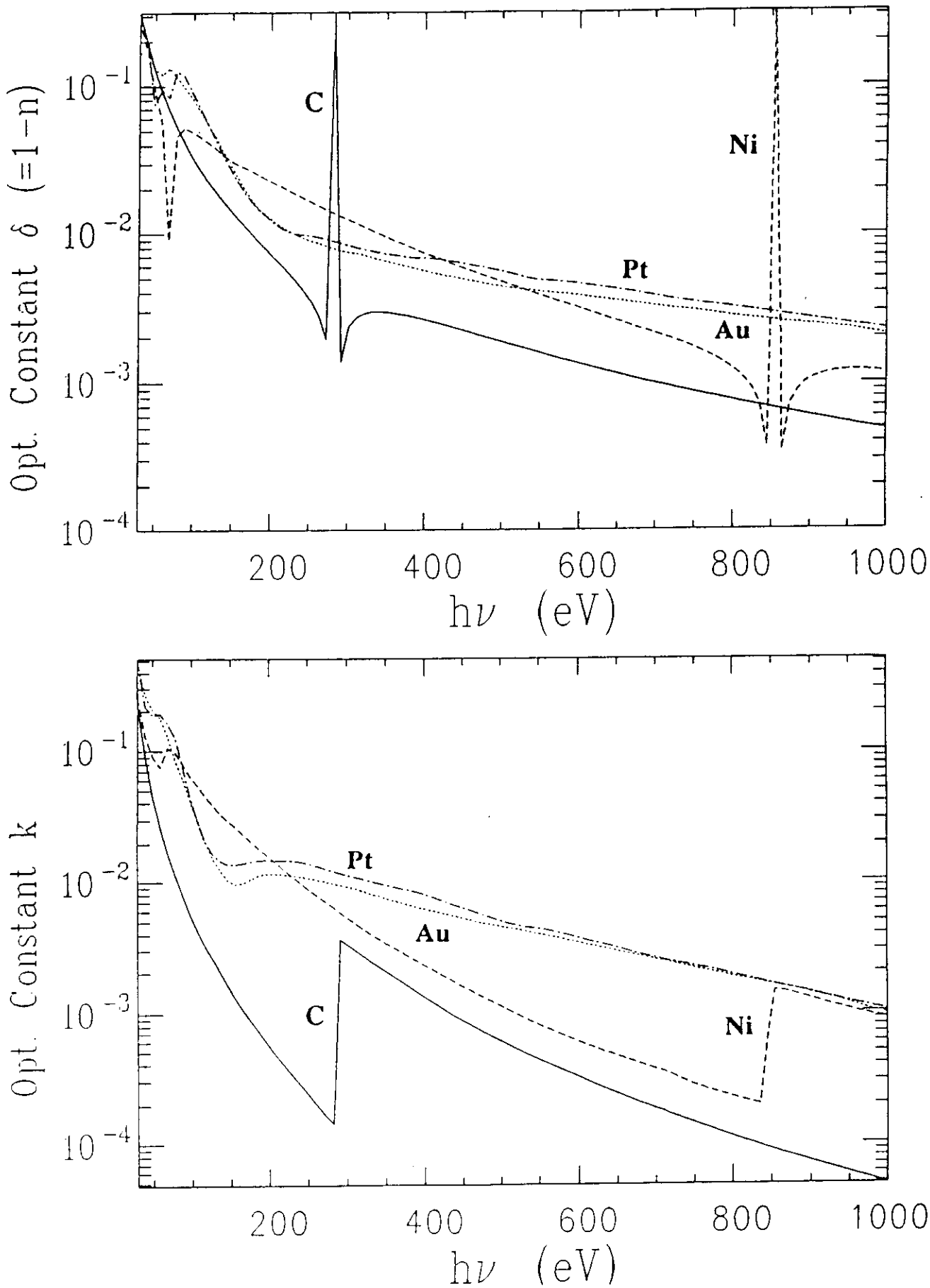

Figure 5.1.3: **Calculated Reflectivities of C, Au, Pt , Ni at Angles 80°, 82°, 84°, 86°, 88° [5.6]**

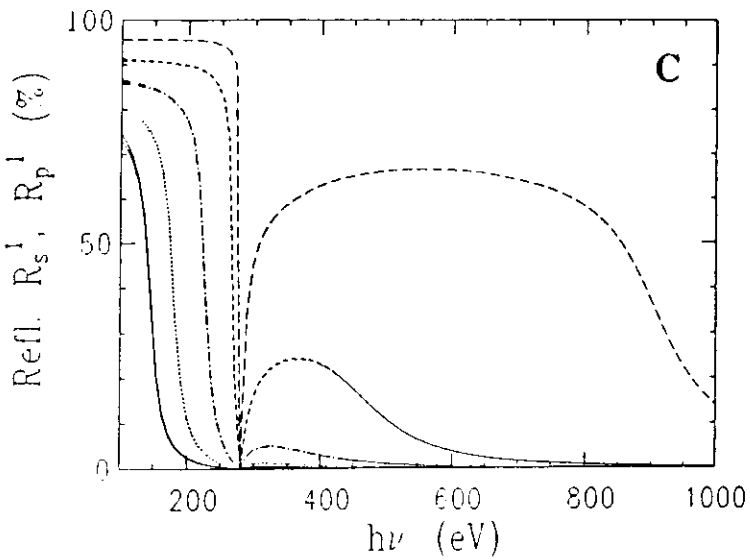

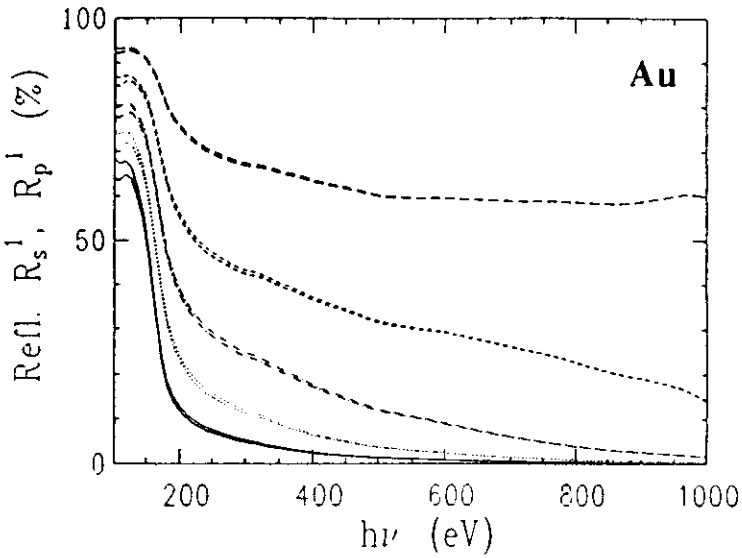

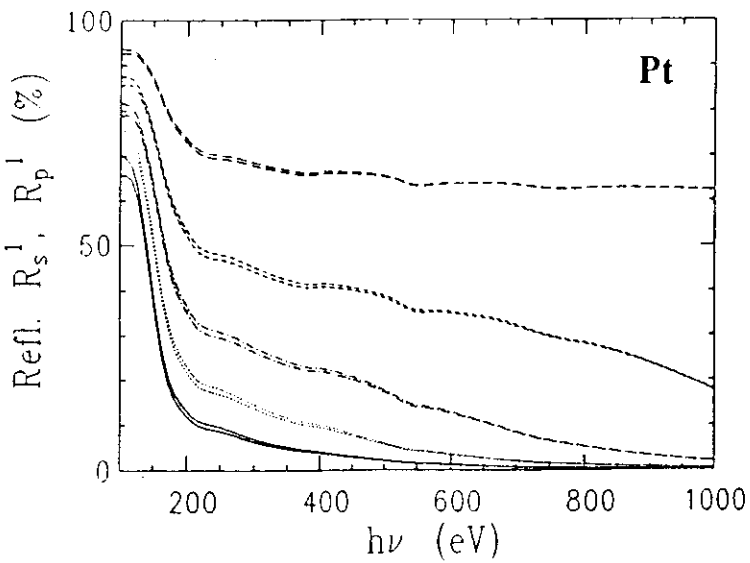

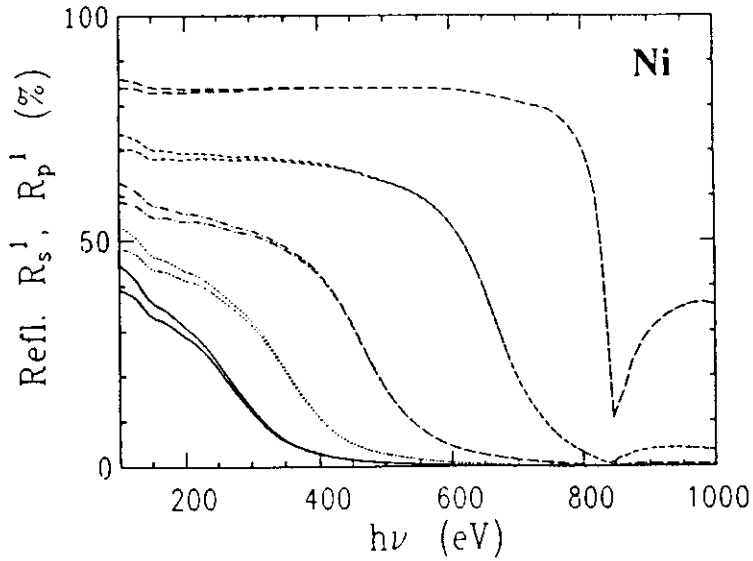

Figure 5.1.4: **Calculated Reflectivities of C, Au, Pt, Ni at Angles 50°, 60°, 70°, 80°, 88° [5.6]**

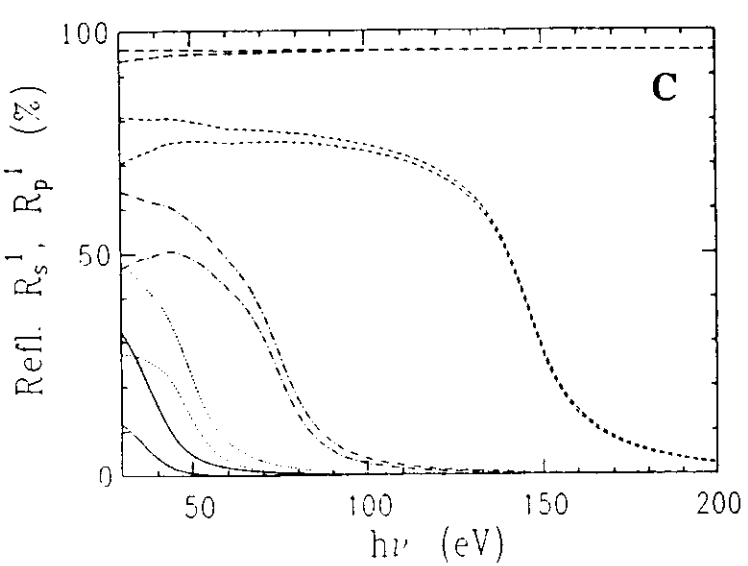

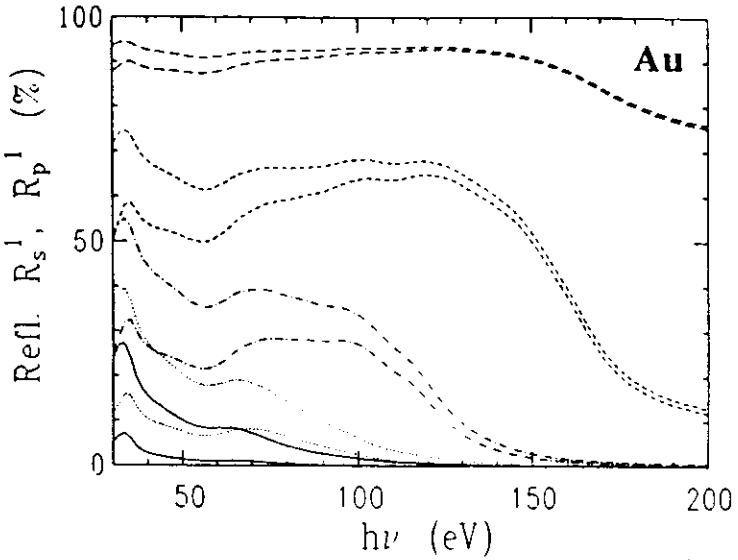

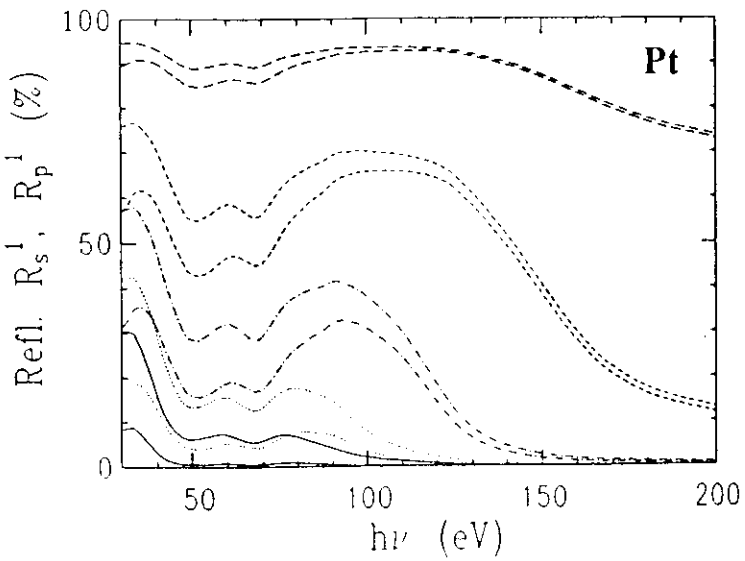

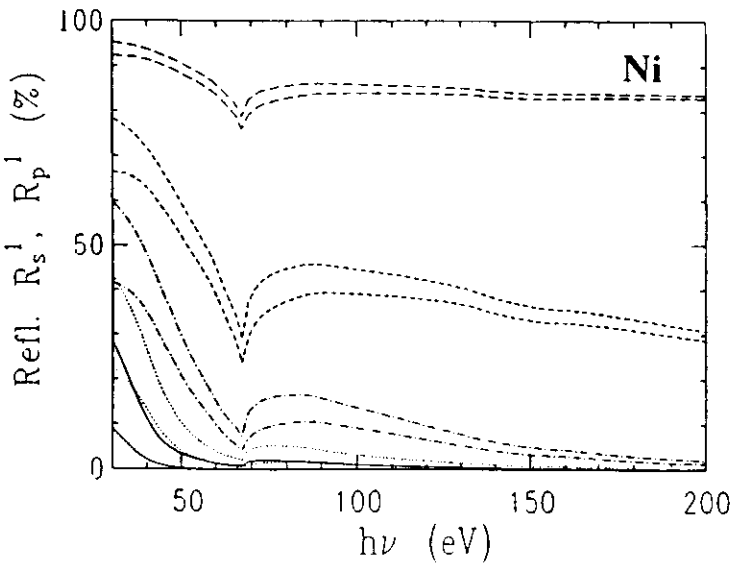

Figure 5.1.5: Elliptically Polarized Light: Various Cases [5.10]

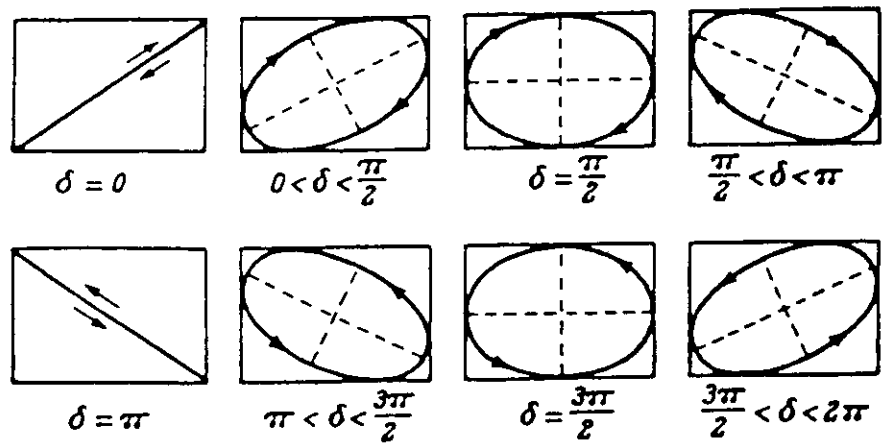

Table 5.1.1: Possible Observations with Polarized Light [5.19]

<table>
<tr><td colspan="3">A. No intensity variation with analyzer alone</td></tr>
<tr><td>I. If with λ/4 plate in front of analyzer</td><td colspan="2">II. If with λ/4 plate in front of analyzer one finds a maximum, then</td></tr>
<tr><td>1. One has no intensity variation,
one has
natural unpolarized light</td><td>2. If one position of analyzer gives zero intensity,
one has
circularly polarized light</td><td>3. If no position of analyzer gives zero intensity,
one has
mixture of circularly polarized light and unpolarized light</td></tr>
<tr><td colspan="3">B. Intensity variation with analyzer alone</td></tr>
<tr><td>I. If one position of analyzer gives</td><td colspan="2">II. If no position of analyzer gives zero intensity</td></tr>
<tr><td rowspan="2">1. Zero intensity,
one has
plane-polarized light</td><td colspan="2">2. Insert a λ/4 plate in front of analyzer with optic axis parallel to position of maximum intensity</td></tr>
<tr><td>a) If get zero intensity with analyzer,
one has
elliptically polarized light</td><td>b) If get no zero intensity,
(1) But the same analyzer setting as before gives the maximum intensity,
one has
mixture of plane-polarized light and unpolarized light
(2) But some other analyzer setting than before gives a maximum intensity,
one has
mixture of elliptically polarized light and plane-polarized light</td></tr>
</table>

Upon reflection, the relative phase of the two components, δ, is altered by, Δ, as given by [3.1, 5.6]:

$$\tan\Delta = \frac{-2b\ \sin\theta\tan\theta}{a^2+b^2-\sin^2\theta\tan^2\theta} .$$

It is therefore easily checked mathematically if a given optical system will alter the polarisation characteristics of the incident radiation. Although the state of polarisation is defined by the amplitudes of the two linear components, a_1, a_2, and their relative phase, δ, it is convenient to use a different definition which corresponds more closely to the measured parameters, the Stokes parameters [5.17] first defined in 1852. For monochromatic radiation they are:

$S_o = a_1^2 + a_2^2 = I\ (0,0) + I\ (90,0)$ = total intensity
$S_1 = a_1^2 - a_2^2 = I\ (0,0) - I\ (90,0)$ = erect component
$S_2 = 2a_1a_2\cos\delta = I\ (45,0) - I\ (135,0)$ = skew component
$S_3 = 2a_1a_2\sin\delta = I\ (45,90) - I\ (135,90)$ = circular component

The intensities indicated I (Ψ, Δ) refer to the orientation of a polariser, Ψ, which produces a phase shift of Δ as analysed by a second polariser [5.6].

For monochromatic radiation which is 100% polarised, there is a further relationship between the Stokes parameters:

$$S_o^2 = S_1^2 + S_2^2 + S_3^2$$

If non-polarized light is present, as indicated by being unable to find a position of zero intensity with any orientation of a polariser with and without a quarter wave plate, the above equality is no longer valid i.e.

$$S_o^2 > S_1^2 + S_2^2 + S_3^2$$

In this case, one can define the degree of polarisation as follows

$$P = \frac{1}{S_o}(S_1^2 + S_2^2 + S_3^2)^{1/2}$$

The determination of the Stokes parameters in the VUV and soft x-ray region of the spectrum is made difficult by the lack of quarter wave plates in this region. Multiple mirrors provide the usual way around this problem, but only up to about 90 eV [see 5.20]. Recently, multilayer systems have been developed which act as polarisers at energies above 90 eV.

Finally, in order to give a better "feel" and understanding for this subject we refer to Table 5.1.1 which explains the observations one can make with a polariser and a quarter wave plate [5.19].

5.2. Focussing properties of single geometries

The equations relating object distance, r, image distance, r', and angle of incidence, θ, for a toroid (sphere), parabola/paraboloid and ellipse/ellipsoid are given below. For definitions see figure 5.2.1 [3.4, 5.7].

5.2.1. Toroid. For a sphere $\rho = R$.

Meridional focus $$\left(\frac{1}{r}+\frac{1}{r'}\right)\frac{\cos\theta}{2}=\frac{1}{R}$$

Sagittal focus $$\left(\frac{1}{r}+\frac{1}{r'}\right)\frac{1}{2\cos\theta}=\frac{1}{\rho}$$

For r = r' the image is identically free of coma.

5.2.2. Parabola $\Psi^2 = 4\,aX$

Paraboloid $\Psi^2 + Z^2 = 4\,aX$

where $a = f\cos^2\theta$

The location of the pole of the mirror, P, is given by

$$X_O = a\tan^2\theta$$
$$Y_O = 2a\tan\theta$$

5.2.3. Ellipse $$\frac{X^2}{a^2}+\frac{Y^2}{b^2}=1$$

Ellipsoid $$\frac{X^2}{a^2}+\frac{Y^2}{b^2}+\frac{Z^2}{b^2}=1$$

Figure 5.2.1 **Three Geometries [3.4, 5.7]**

Toroid

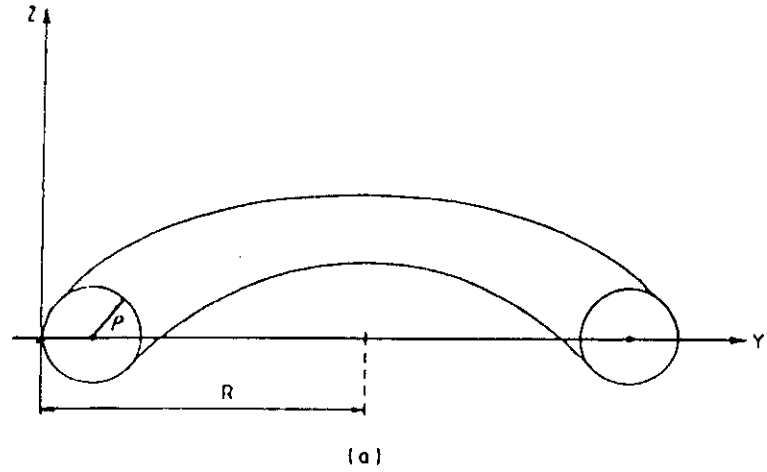

Parabola

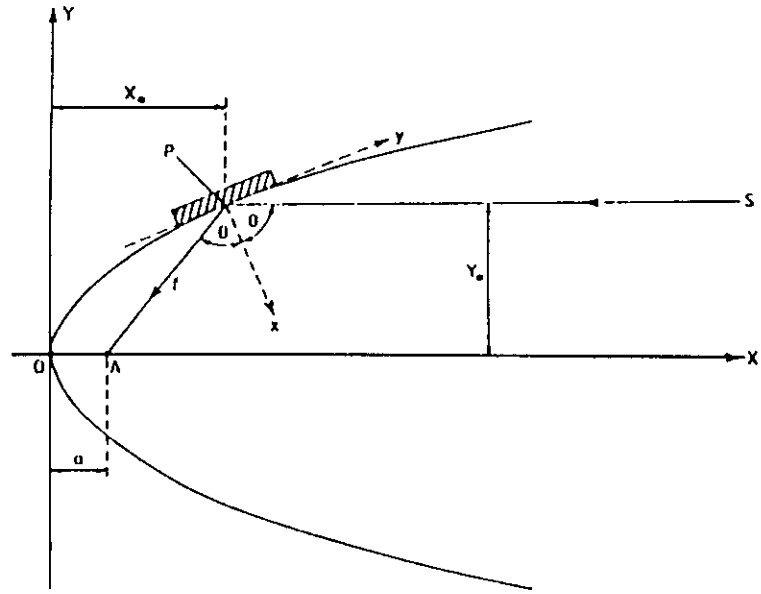

Ellipse

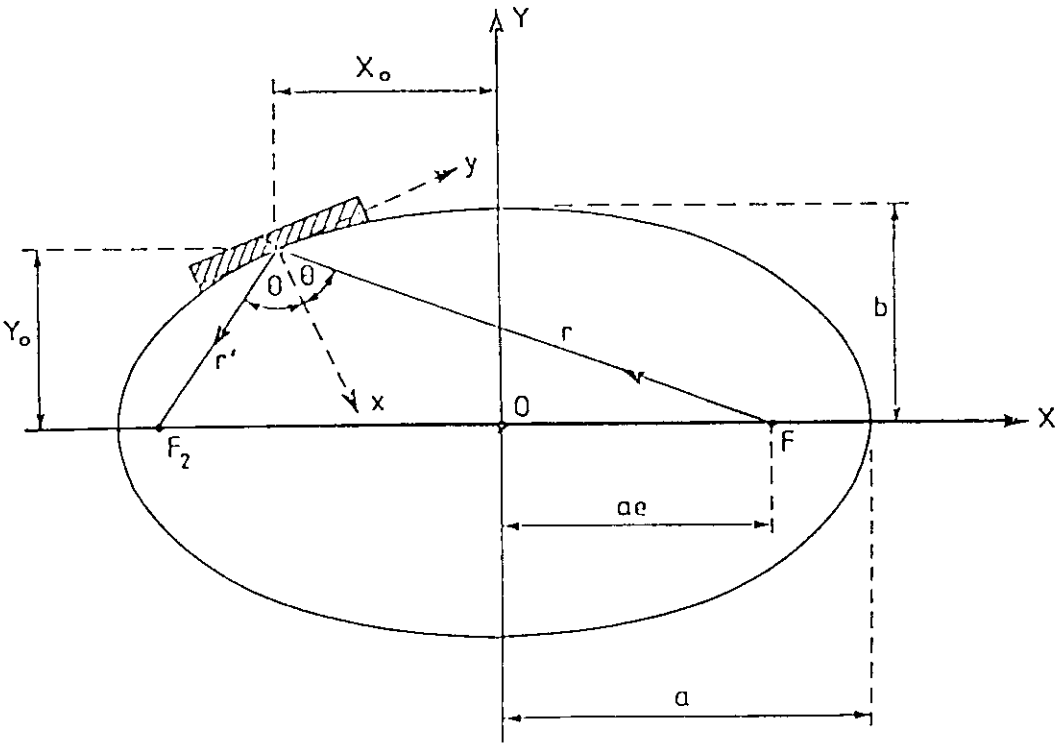

where $$a = \frac{r + r'}{2}$$

$$b = [a^2 (1-e^2)]^{1/2}$$

and the eccentricity, e, is given by

$$e = \frac{1}{2a} (r^2 + r'^2 - 2r\, r' \cos 2\theta)^{1/2}$$

The location of the pole of the mirror is given by

$$X_O = a \left(1 - \frac{Y_O^2}{b^2}\right)^{1/2}$$

$$Y_O = \frac{r\, r' \sin 2\theta}{2ae}$$

5.3. Two-Mirror Systems

Every optical system suffers from intrinsic optical aberrations which, in contrast to manufacturing limitations, can only be reduced by going to another system. A camera lens, for example, can be as simple as a pinhole, a triplett of lenses as in pocket cameras or a set of five or more individual lenses for more demanding uses. In this example, the main causes for the different systems are twofold: lens opening or f number and chromatic correction. The larger the transverse size of the lens, in comparison to the object or image distance, the more difficult the task of correcting for the intrinsic optical aberrations. Conversely, the smaller it is, the easier -- hence the pinhole lens!

In contrast to optical systems for visible light, we have seen that in the VUV and soft X-ray part of the spectrum no optical materials exist from which lenses can be made and only reflecting optics are available, and these with quite limited reflectivity (see sect. 5.1). Thus, the concept of "corrected" optical systems is of much more limited application than in the visible and,

in general, instead of 3 - 7 optical elements for a "corrected" system only two elements are practicable. As will be seen in section 5.5 on figure errors, the accuracy with which a particular geometry can be manufactured is limited, plane and spherical surfaces being easier to produce to a high figure accuracy than parabolic, hyperbolic or ellipsoidal geometries. Unfortunately, the latter are generally required for "corrected" systems at short wavelengths. Finally, the ease and stability of the alignment of the elements of an optical system also depends upon their geometry, planes and spheres being the easiest having no plane of symmetry.

For the above reasons then, we will limit the discussion of two-mirror systems, designed to correct or to avoid particular optical aberrations, to the Kirkpatrick-Baez design [5.1]. Wolter, Schwarzschild and other systems, requiring the use of two aspheric mirrors will not be discussed here in monochromator design. It should be noted that their application in purely imaging systems for soft X-rays is quite widespread. Furthermore, we will assume that the monochromator has an entrance slit and that the two-mirror system is intended to focus the source on this entrance slit in the dispersion plane of the monochromator. The arguments for using an entrance slit can be found in reference 4.20. Nevertheless, a two-mirror system is equally applicable to a monochromator with no entrance slit.

The Kirkpatrick-Baez arrangement [5.1] is shown in figure 5.3.1: two mirrors are employed to independently focus the object in the two orthogonal planes. Thus, it is possible to optimize geometry (intrinsic aberrations), figure accuracy and heat load aspects in the critical, resolution determining plane while solving or partially solving the "heat load" problem in the other plane. As will be seen in section 5.5 pp. 8 - 11, the influence of tangent errors of a mirror on the sagittal focussing characteristics of that mirror are reduced by the factor $\sin\theta_g$ where θ_g is the grazing angle of incidence on the mirror. For the application at hand θ_g is typically 2 - 3° and $\sin\theta_g$ is 0.035 - 0.052 or a factor of 29 or 19 respectively. That is, a mirror with a figure error of 1 arc sec will effectively have a figure error of $\frac{1}{29}$ or $\frac{1}{19}$ arc sec in the sagittal direction. The first mirror in a beamline, the one that receives the largest heat load, can be chosen to deflect and focus the source in the plane perpendicular to the resolution determining plane. Then, the geometrical errors of this mirror, caused by manufacturing deficiencies

Figure 5.3.1: The Kirkpatrick-Baez Optical System [5.1]

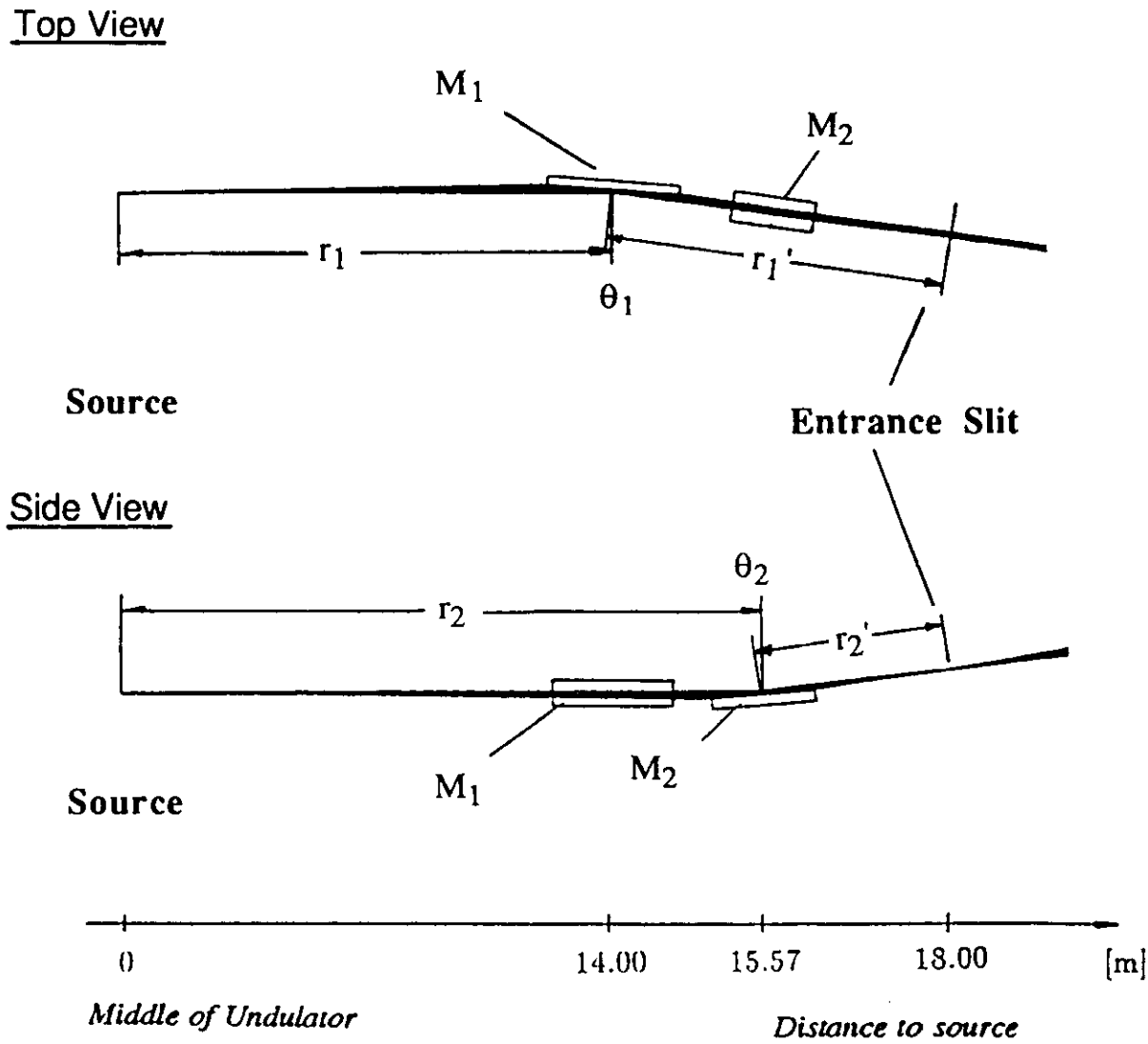

and by heat loading, are reduced by the factor $\sin\theta_g$ in that plane. The second mirror must intrinsically offer and, under illumination, should maintain an especially high geometric accuracy of its reflecting surface. Finally, and of great importance in the overall beamline design, the astigmatic errors of the rest of the beamline can be compensated for by the first mirror. In general, a small focus is desired at the experiment or on the exit slit of the monochromator. Thus, the first mirror can be designed to produce a focus in its plane at the rear of the beamline, if possible such that $r \approx r'$ which is free of coma in that plane. In addition, the light and heat density on the entrance slit of the monochromator are reduced, typically by a factor of 10 or so, thereby reducing the problem of deformation of the entrance slit by the heat load. Slit lengths of 10 - 30 mm do not produce new problems of consequence.

For the second mirror, one can choose between a cylindrical, a spherical or a plane elliptical mirror. The first two are essentially the same in their optical function: they produce a focus in their meridional plane according to equation 5.2.1. Sagittally, the cylinder produces no focus while the sphere focusses the source very weakly and negligibly in comparison to the other mirror in the system. The advantages of the sphere over the cylinder are that it can be produced to a higher figure accuracy and that it has no unique symmetry plane, making alignment easier.

The plane elliptical geometry can be used for relatively large acceptance angles and produces an image free of coma and spherical aberrations. It is, however, more difficult (and expensive!) to produce, cannot be produced with as high a figure accuracy and has a very critical plane of symmetry.

A possible way around the first two criticisms of the plane elliptical geometry is presented by the Namioka conjugate sphere system in which coma and some spherical aberrations are identically eliminated [5.3]. Two spherical mirrors are employed such that an intermediary focus is produced by the first which is than refocussed by the second sphere, the aforementioned optical aberrations of the first image being cancelled by the action of the second sphere (Figure 5.3.2). Thus, the second mirror of the Kirkpatrick-Baez system is replaced by two tightly coupled spherical mirrors which produce a focus in their meridional plane.

Figure 5.3.2: The Namioka Conjugate Sphere System [5.3]

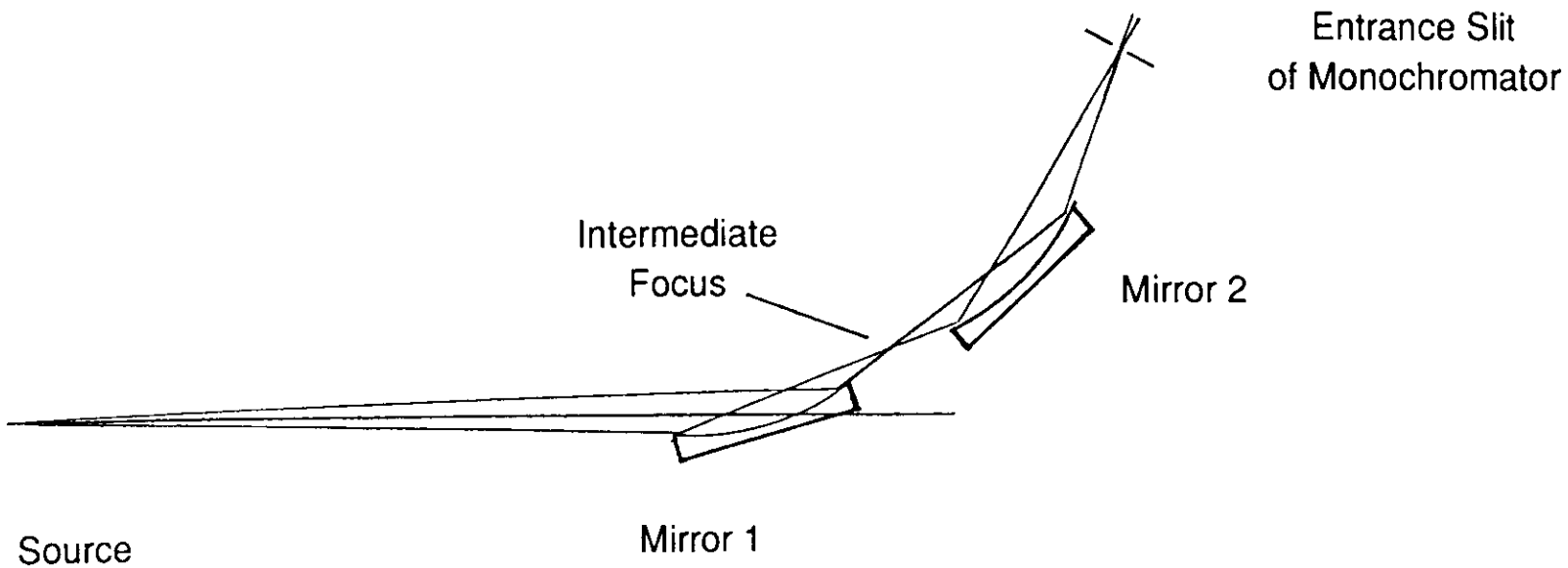

The focussing equations for the Namioka system are:

$$\frac{1}{R_1} = \left(\frac{1}{r_1} + \frac{1}{r_1'}\right)\frac{\cos\theta_1}{2}$$

and $$M_1 = \frac{r_1'}{r_1} = \text{demagnification}$$

where R_1, r_1, r_1' and θ_1 are as usually defined and refer to the first mirror of the pair. Similarly, R_2, r_2, r_2', θ_2 and M_2 are defined for the second mirror.

The nominal demagnification of the Namioka system is given by

$$M = M_1 \cdot M_2.$$

Finally, the parameters of the second mirror are coupled to those of the first by the following relation:

$$r_2 = r_1' \frac{\tan\theta_1}{\tan\theta_2} \cdot \frac{(1-M_1^2)M_2^2}{(M_2^2-1)} .$$

The focussing properties of the Namioka system are similar to those of a plane ellipse and are, for example, relatively independent of the acceptance of the system, in sharp contrast to a single sphere where coma dominates. An aperture can be located at the intermediate focus in order to mask out unwanted light. The disadvantages of this system are that two reflections are employed, that it has a plane of symmetry and that the relative position of the mirrors to each other is critical.

The optical characteristics of three Kirkpatrick-Baez arrangements are quantitatively discussed with the help of ray tracings in the next section.

5.4. Extreme Demagnifications

In the quest for resolution, the size of the source of synchrotron radiation, the electron beam itself, has been significantly reduced in each new generation of storage rings. Along with the lateral dimensions, the

divergence of the source has been reduced as well. That these two dimensions are coupled in the expression called emittance is an unavoidable fact (see chapter 2) and is an example of Liouville's theorem. The same holds true at the entrance slit of a monochromator: the emittance of the source cannot be reduced at the entrance slit, only the two quantities, lateral size and divergence, can be traded off against each other. Thus, in a beamline, the more the source size is reduced by an optical system, the larger the divergence of the light beam behind the slit. If no light is to be lost, the grating and mirrors in the monochromator must be made larger thereby increasing the problems of optical aberrations, figure errors and costs. This situation is shown in figure 1.1.1 of chapter 1. In addition to this, the ability of an optical system to reduce the size of the source decreases with increasing demagnifications. In order to illustrate this point, a ray-trace study has been made of three systems (Kirkpatrick-Baez) used to reduce the size of a realistic undulator source on a storage ring of the third generation. Only the dispersion plane is considered, the sagittal direction being irrelevant for the study. Although an extended source such as that in an undulator is more difficult to demagnify than a dipole source, the problematic is similar. The rest of this section is taken up with this study.

The source characteristics have been worked out for an undulator on a storage ring of the third generation and are given in table 2.5.1 of chapter 2. As shown there, the relevant parameters for ray trace studies are

σ_x	= 0.220 mm
σ_y	= 0.042 mm
z	= 4100 mm (not r.m.s.!)
σ'_{rh}	= 0.080 - 0.160 mrad
σ'_{rv}	= 0.055 - 0.110 mrad
r	= 17000 mm.

For the study two values of σ'_{rv} have been used in order to test the systems for sensitivity to divergence: σ'_{rv} = 0.040 and 0.080 mrad.

The idea is to determine the size of the entrance slit necessary to accept all of the SR from the source. Hence, the effective source size (95 % or 4 σ'_{rv}) is 0.168 mm. An effective demagnification of 10 would mean that the entrance slit must be opened to 17 μm. If a slitwidth of 10 μm is necessary

for the desired resolution, an effective demagnification of 17 is required. As shall be shown, the nominal demagnification, r/r', does not correspond well to the effective demagnification.

Shown in figure 5.4.1 are the point diagrams for a simple sphere with a nominal demagnification of 24. Immediately evident is a large coma tail resulting from the very asymmetric system (r/r' = 24). Equally evident is the fact that the extent of this tail is relatively independent of the figure error of the mirror, σ_{TE}. Since the coma aberration scales with the square of the illuminated length of the mirror, it should be significantly reduced if the acceptance, σ'_{rv}, is reduced. This is shown in figure 5.4.1c. The effective demagnifications are found to be 168/37 = 4.5, 168/53 = 3.2 and 168/35 = 4.8 for the three cases respectively. A perfect sphere (σ_{TF} = 0) and an acceptance of 0.040 mrad yields an effective demagnification of 168/15 = 11! These results are summarized in figure 5.4.4a. The difference between the nominal demagnification and the effective demagnification is apparent. One should not forget that the divergence of the SR behind the slit has been increased, in this case by a factor of roughly 24! This too is easily shown with the help of ray-traces. Thus, we conclude that a strong demagnification with a sphere is not only ineffective but impossible for the source under study!

The same approach was used for a plane elliptical mirror and the results shown in figure 5.4.2 and summarized in figure 5.4.4b. The line shape is much better than for a sphere because of the absence of coma but one must expect that the figure errors, σ_{TE}, are larger than for a sphere. Geometric errors resulting from a heat load would be the same in both cases making the effective figure error for the sphere more like that of the plane ellipse. Also seen in figure 5.4.4b is the insensitivity of the plane ellipse to acceptance, again resulting from the absence of coma. The best realistic effective demagnification is 168/29 = 5.8 for σ_{TE} = 1 sec. A perfect mirror would yield 168/12 = 14.

The data for the conjugate spheres are shown in figures 5.4.3 and 5.4.4c. As seen in the former, the line shape is similar to that of the system with the plane elliptical mirror, the coma aberration of each sphere cancelling with that of the other. Only a weak dependence on acceptance is to be seen. The

Figure 5.4.1: Focussing Characteristics of a Spherical Mirror

To the left the spot diagram. To the right, the integrated vertical profile.
The angle of incidence, θ , is 87.5° .

a) Demagnification = 24, σ_{te} = 0 , σ'_{rv} = 80 μrad
b) Demagnification = 24, σ_{te} = 1 sec , σ'_{rv} = 80 μrad
c) Demagnification = 24, σ_{te} = 1 sec , σ'_{rv} = 40 μrad

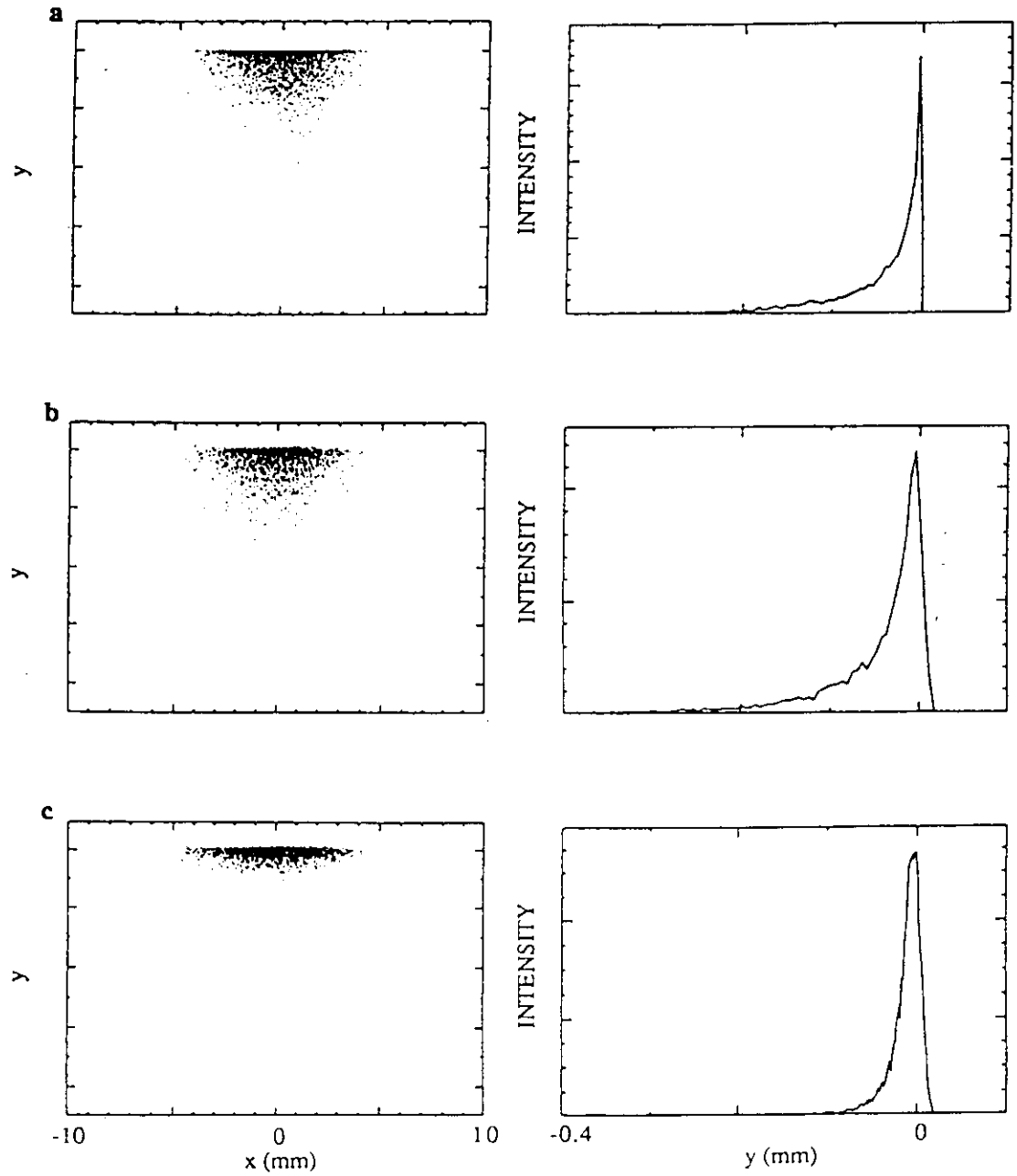

Figure 5.4.2: Focussing Characteristics of a Plane Elliptical Mirror

To the left the spot diagram. To the right, the integrated vertical profile.
The angle of incidence, θ , is 87.5° .

a) Demagnification = 24, $\sigma_{te} = 0$, $\sigma'_{rv} = 80$ μrad
b) Demagnification = 24, $\sigma_{te} = 1$ sec , $\sigma'_{rv} = 80$ μrad
c) Demagnification = 24, $\sigma_{te} = 2$ sec , $\sigma'_{rv} = 80$ μrad

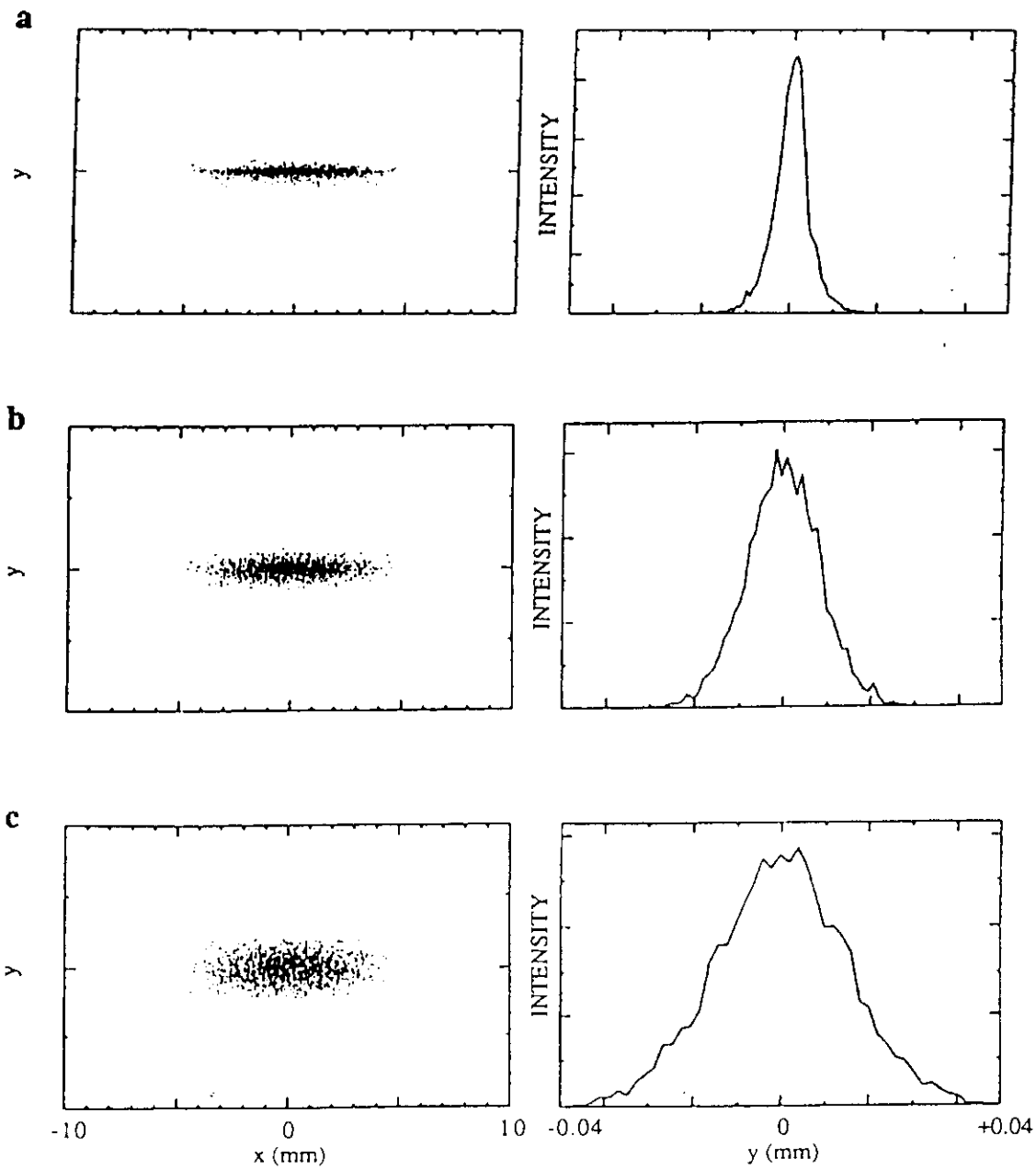

Figure 5.4.3: Focussing Characteristics of a Conjugate Sphere System

To the left the spot diagram. To the right, the integrated vertical profile.
The angle of incidence on each mirror , θ , is 88.0° .

a) Demagnification = 24, σ_{te} = 0 , σ'_{rv} = 80 μrad

b) Demagnification = 24, σ_{te} = 1 sec , σ'_{rv} = 80 μrad

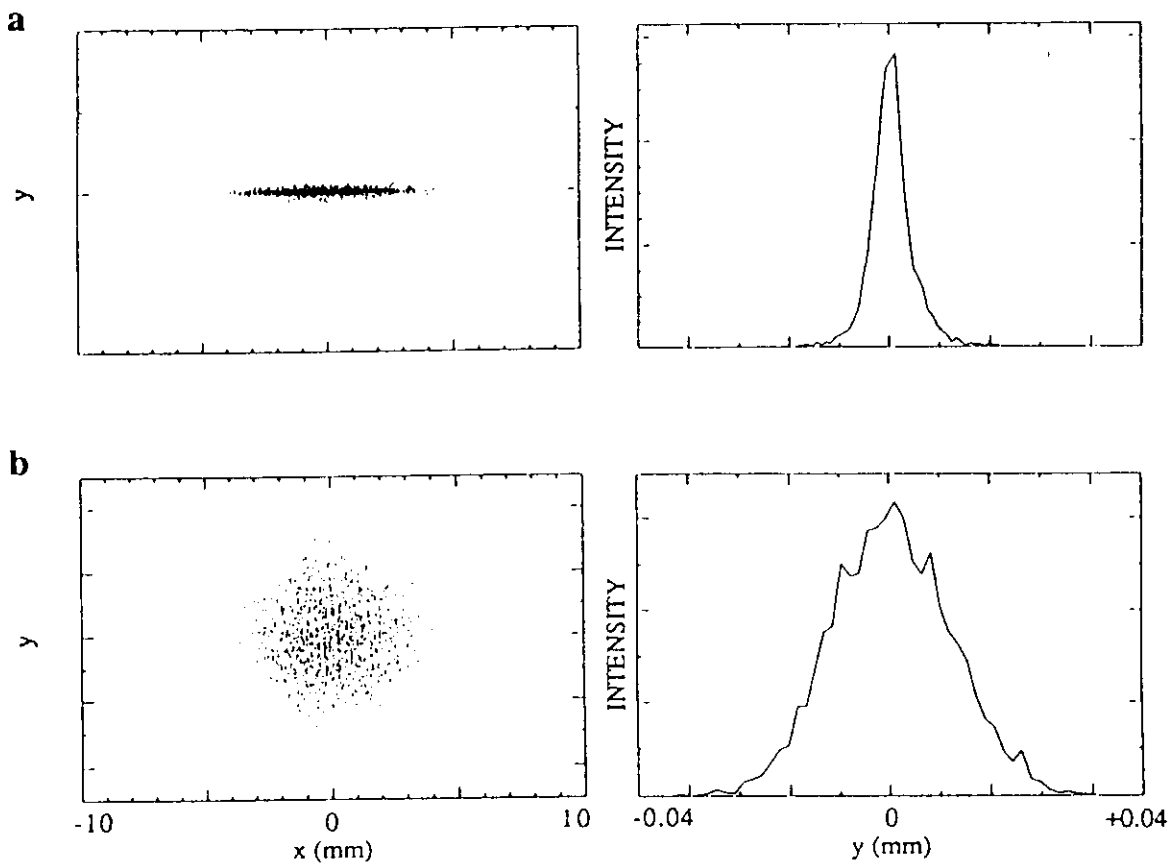

Figure 5.4.4: Demagnification of an Undulator Source on an Entrance Slit [1.6b]

Vertical image size as a function of demagnification for several tangent errors (σ_{te} and vertical acceptances (σ'_{rv}). Source characteristics are given in table 2.5.1. (a) Spherical mirror, (b) Plane elliptical mirror, (c) Conjugate spheres.

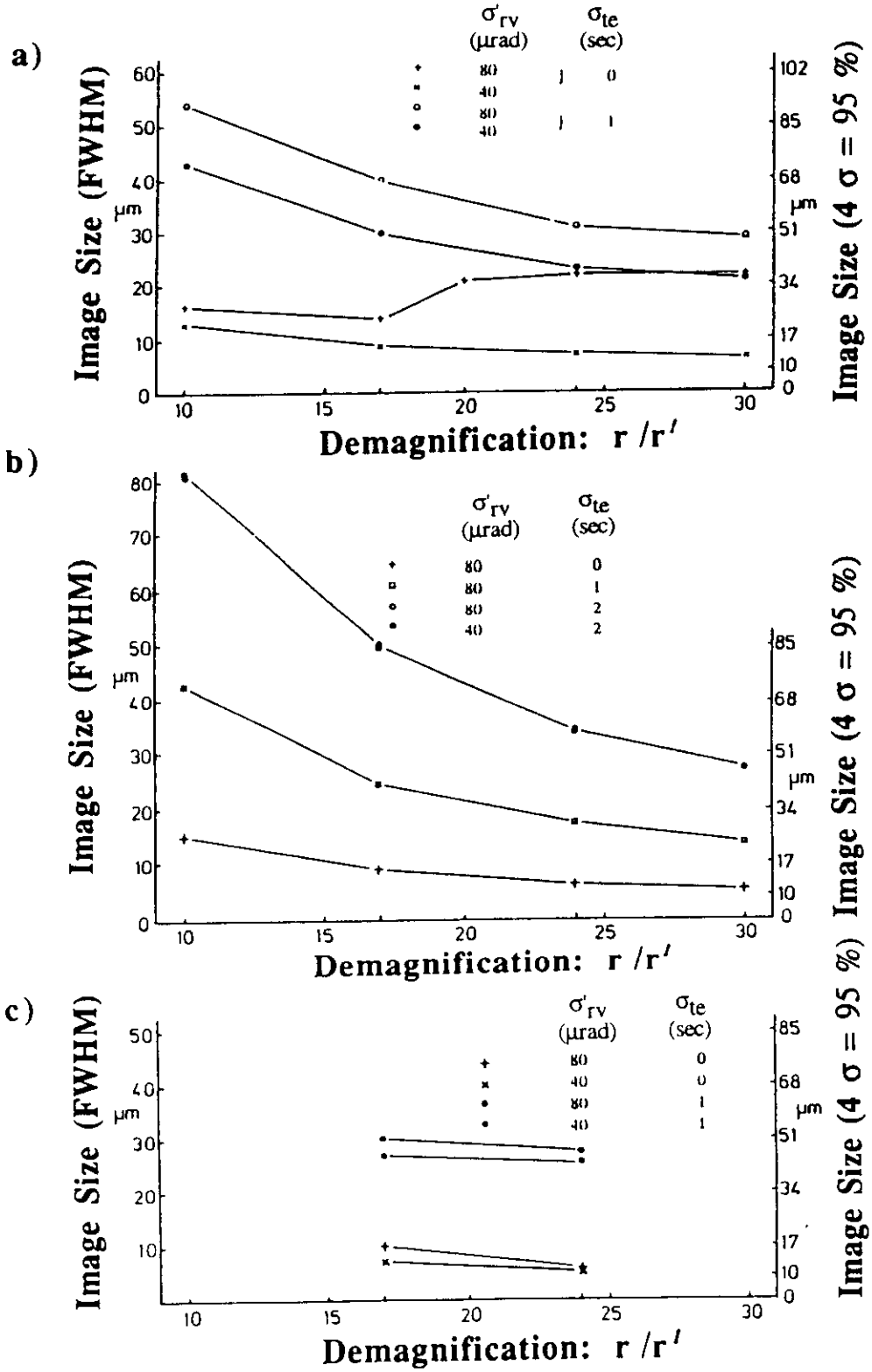

effective demagnifications are 168/48 = 3.5 (σ_{TE} = 1 sec) and 168/12 = 14 for perfect mirrors.

Making similar comparisons for a nominal demagnification of 10 yields the following results (with σ_{TE} = 1 sec and 0 sec respectively):

Spheres	168/89 = 1.9	effective demagnification
	168/28 = 6.0	effective demagnification
Plane ellipse	168/72 = 2.3	effective demagnification
	168/24 = 7.0	effective demagnification

In this case the resulting divergence is smaller and, in the case of the sphere, the line shape is much better.

In fact, it is to be recommended that a still smaller demagnification be employed in real systems. By choosing a demagnification of 5 - 8, one can easily show that a perfect sphere is almost as good as a perfect plane ellipse. Since the former can be manufactured with a better figure and at a lower cost than the latter and is more easily adjusted, there is little incentive to employ a plane ellipse for the premirror system to a monochromator. That the conjugate sphere system offers no advantage at such modest demagnifications should be evident from the foregoing.

5.5. Figure Errors

The equations given in other sections for describing mirror and grating geometries are for perfect surfaces. There we are confronted with optical aberrations stemming from the inability of particular geometries to produce a perfect image. In fact, however, it is not possible to obtain such surfaces from manufacturers and additional sources of optical aberrations must be considered. Thus, the designer of an optical system must evaluate the effect of deviations from a perfect geometry on the performance of the system. Such an evaluation is made difficult by the fact that often neither the manufacturer nor the user of the optical elements is in a position to determine the extent and nature of the imperfections - or only with great difficulty and incompletely. This is especially true in the vacuum ultraviolet

and soft x-ray regions of the spectrum. The following points highlight the new situation:

a) The optical relations are different from those relevant to the visible region resulting from the necessity of employing grazing angles of incidence instead of (near) normal angles of incidence.

b) The most relevant optical tests can only be made with light of the wavelengths of interest. Thus, sources, vacuum systems and corresponding detectors are required. Most manufacturers and indeed users do not have such systems at their ready disposal.

c) With the coming of synchrotron radiation sources, the failings of the optical fabrication techniques have been brought to light (!). The requirements on mirrors and gratings for VUV and soft x-ray optics have forced manufacturers and users alike to develop measuring and test methods for optical components.

d) The availability of fast and inexpensive computers has made possible the development and widespread use of programs which geometrically trace the path of a ray of light through arbitrarily complicated optical systems. With such ray trace programs it is possible to deal with complex geometries of sources and optical elements and with optical errors associated with the latter (see e.g. references 1.2, 1.3).

Coming back to the question of errors in the geometry, it is necessary to distinguish between two types of errors:

1. Errors whose period (length) is comparable to the dimensions of the optical element and
2. Errors whose period is irregular and is much shorter than the dimensions of the optical element.

Errors of the first type must be considered in terms of the geometry of the optical element: a spherical mirror is specified as having a radius of curvature of, say, 100 m but in fact has somewhat different radii depending upon what portion of the mirror is measured. This is not a random error and, hence, cannot be treated as such. By masking out certain portions of the

mirror it may be possible to achieve the performance of a nearly perfect mirror of R = 100 m.

Errors of the second type include such things as irregular machining marks on the one hand and residual roughness on the other. These two sorts of errors differ in their spatial frequency but can be displayed in a power spectrum of the surface (Fig. 5.5.1). If such data are available to the manufacturer, it may be possible to locate the source of a particular frequency in the manufacturing process and to reduce or eliminate it.

Errors of the first type are very common and cannot be treated in a statistical fashion. Each mirror or grating will have its own characteristics which cannot be extrapolated from general considerations. Its character may be discovered by examining its performance piecewise, by masking off the rest [5.7]. An example of such a case is shown in figure 5.5.2. In the 1980's highly precise measuring instruments were developed enabling one to ascertain this type of error [5.12, 5.13]. Such instruments are quite expensive but are becoming less so as the market for them develops. With the measurement data of such instruments the manufacturer can then rework the substrate thereby, iteratively, improving the basic geometry enormously. In practice, it is not uncommon for users to empirically find the best portion of a mirror or grating and to occlude the rest, when the additional performance is worth the cost in photon flux.

Errors of the second type are assumed to obey a Gauß distribution and can, therefore, be dealt with mathematically in a straightforward fashion [5.9 - 5.11, 5.14 - 5.16]. It is convenient to make a further subdivision of errors. Errors of the second type which contribute to the specular image we call, along with errors of the first type, figure or tangent errors. Thus we have systematic figure (tangent) errors (first type) and random figure (tangent) errors. Errors of the second type which do not contribute to the specular image but instead to scattered light we ascribe to surface roughness. Errors of this type will be discussed briefly in section 5.6.

Random figure errors are easily dealt with in ray-trace programs if their σ_{TE} or r.m.s. value of the random scatter of the tangents over the surface is known (see e.g. Ref. 1.3). Moreover, given σ_{TE}, one can readily estimate their effect on the image of a single optical element as shown below.

Figure 5.5.1: Power Spectrum of Surface Errors [5.11]

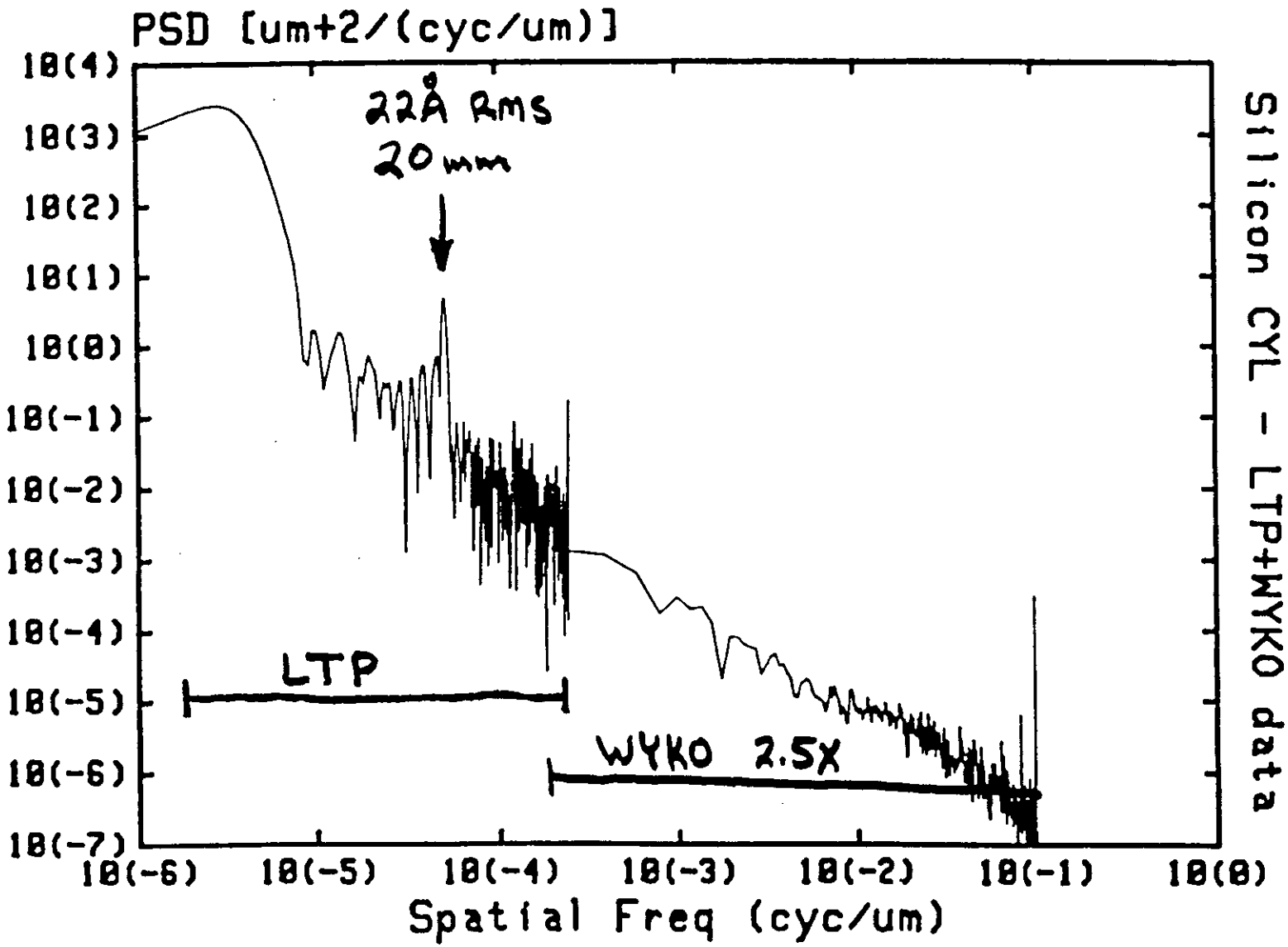

Figure 5.5.2: Example of Figure Error of the First Type [5.12]

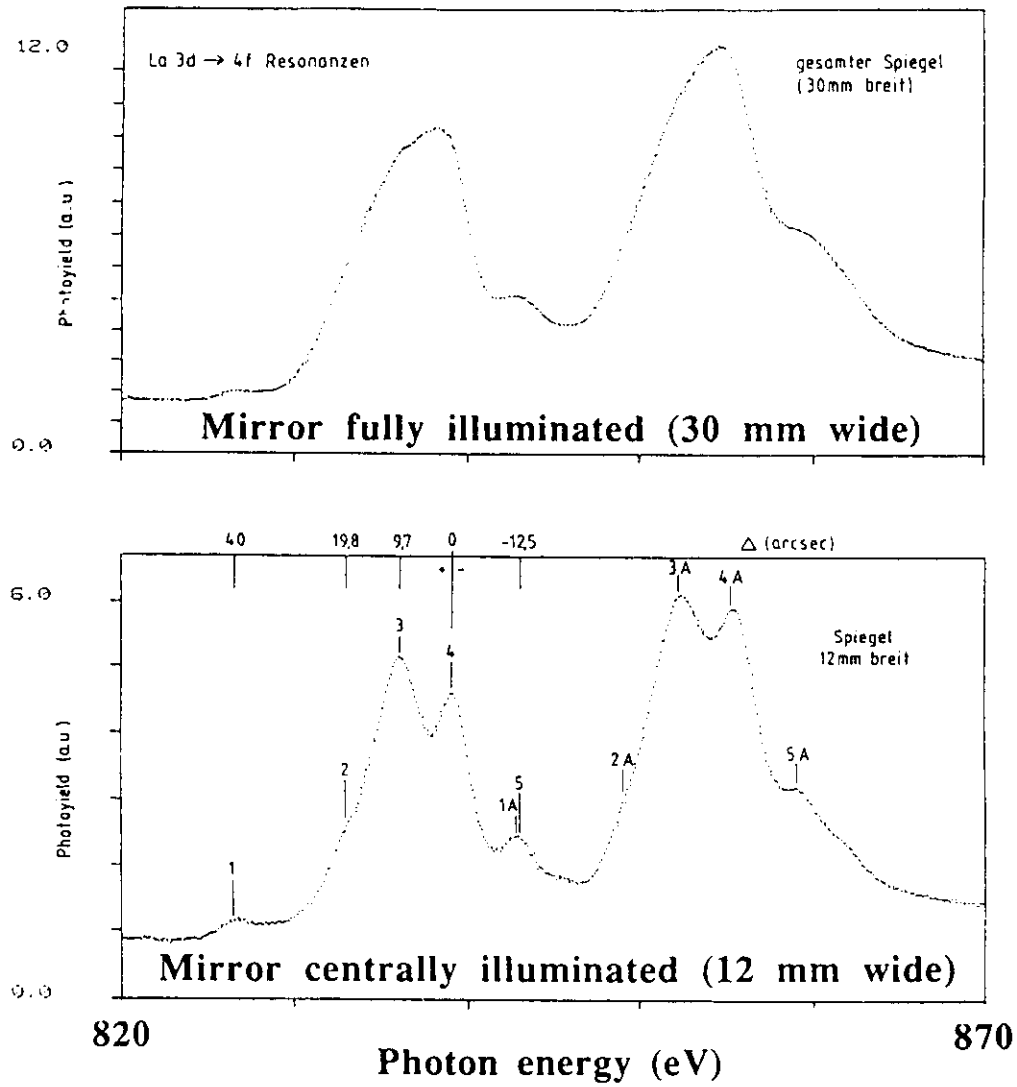

Photoyield spectrum of the La $3d_{3/2,\ 5/2} \rightarrow 4f$ resonances with a fully and a partially illuminated mirror. The well known spin-orbit pair is seen to appear five times. The corresponding (systematic) tangent error is indicated. The numbers correspond to the areas of the mirror given below [5.12].

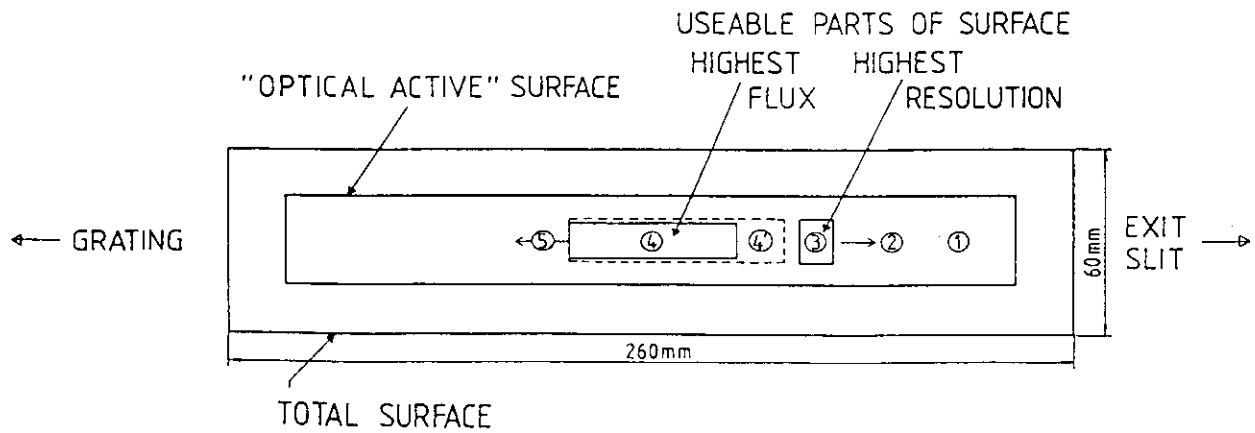

Figure 5.5.3: Meridional and Sagittal Tangent Errors

a) Meridional tangent error

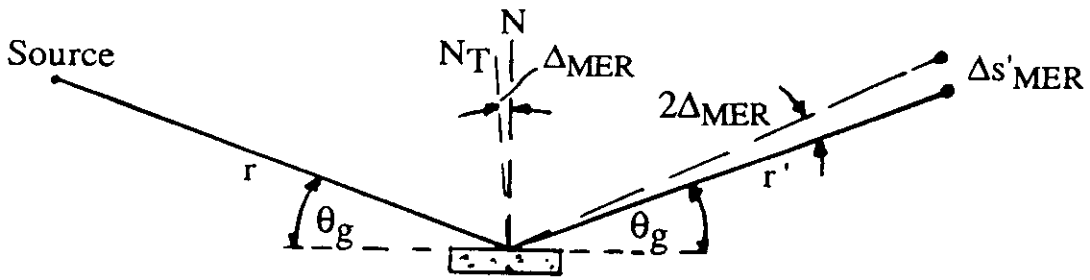

$$\Delta\, s'_{mer} = 2\, r'\, \Delta_{mer}$$

which is the same is if the source were at

$$\Delta\, s_{mer} = 2\, r\, \Delta_{mer}$$

b) Sagittal tangent error

$\Delta\, s'_{sag}$

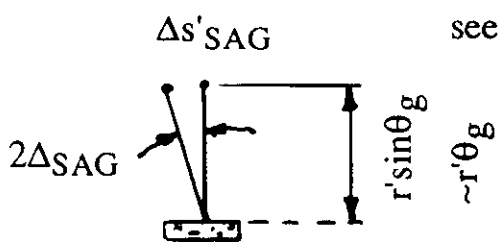

see picture above

end-on view

$$\Delta\, s'_{sag} = 2\, \Delta_{sag} \cdot r' \sin \theta_g$$

$$\approx 2\, \Delta_{sag} \cdot r' \theta_g$$

(good to < 0.5 % for $0 < \theta_g < 10°$)

Figure 5.5.4: Effect of Tangent Errors on Line Width: Ray Trace Results

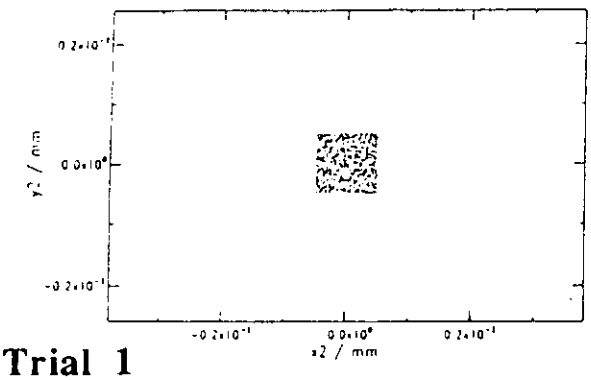

Trial 1

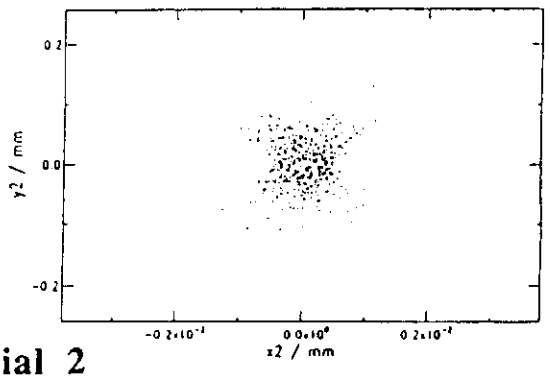

Trial 2

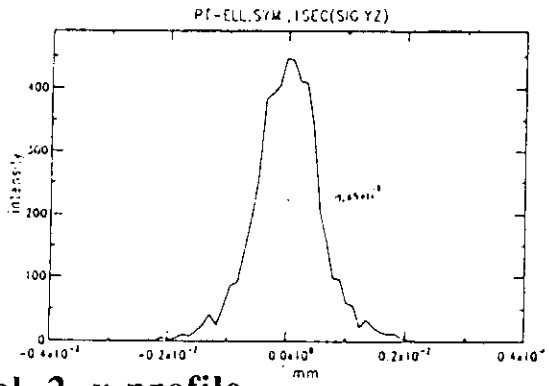

Trial 2 x-profile

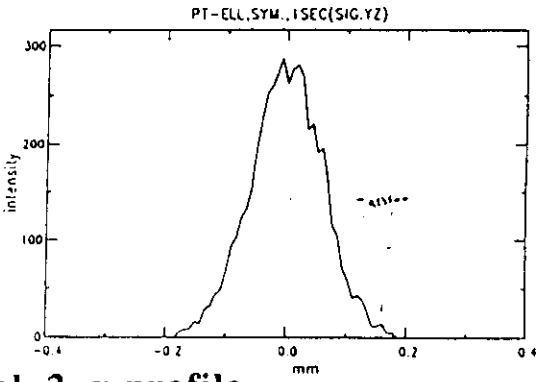

Trial 2 y-profile

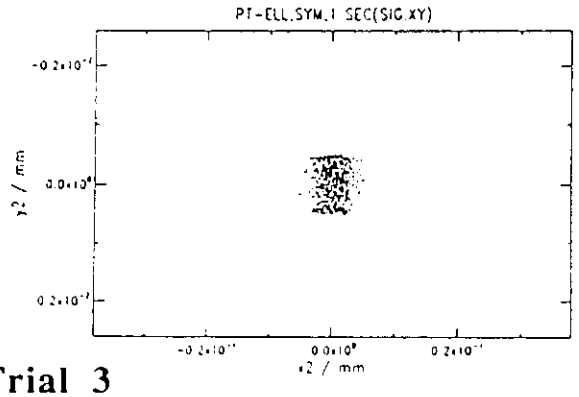

Trial 3

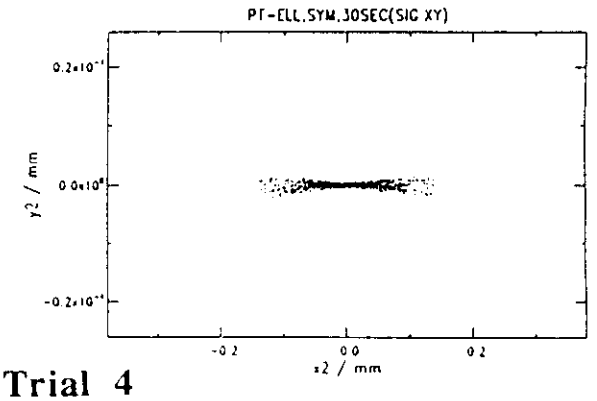

Trial 4

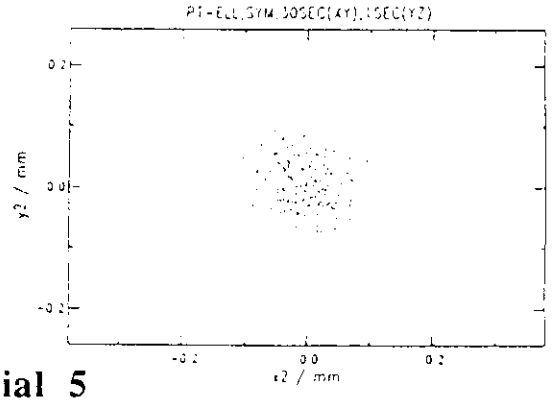

Trial 5

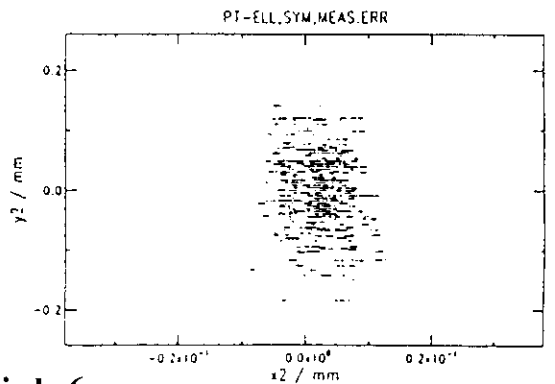

Trial 6

First, however, it should be pointed out that there is a significant difference in the effectiveness of meridional tangent errors, σ_{mer}, and sagittal tangent errors, σ_{sag}, in disturbing the image. This is easily explained as seen in the following figure (fig. 5.5.3):

The relative magnitudes of Δ_{mer} and Δ_{sag} which produce the same $\Delta s'$ is given by

$$\frac{\Delta s'_{mer}}{\Delta s'_{sag}} \equiv 1 \approx \frac{2r'\Delta_{mer}}{2r'\theta_g \Delta_{sag}}$$

$$\theta_g = \frac{\Delta_{mer}}{\Delta_{sag}}$$

$$\theta_g = 5.73° = 0.1 \text{ rad}$$
$$\Delta_{sag} = 10\ \Delta_{mer}$$

$$\theta_g = 2° = 3.5 \times 10^{-2} \text{ rad}$$
$$\Delta_{sag} = 29\ \Delta_{mer}$$

Thus, for example, for a monochromator with a vertical dispersion plane mirrors which produce a horizontal deflection need not be as high quality as those producing a vertical deflection, or, it may be possible for a manufacturer to produce a more accurate finish in one direction than in the other: e.g. a mirror might be ground or cut in one direction rather in the other. In this case differing tangent errors will be produced and the mirror should be specified so as to yield a satisfactory tangent error in the dispersion plane.

Before we apply these equations, we'll examine the results of ray-trace calculations set up for the same purpose: to determine the effect of meridional and sagittal tangent errors on an image. Six trials are made, in which, for a symmetric optical system with an ellipsoidal focussing mirror and a point source, the image is generated with various values of tangent errors. The parameters and results are given in Table 5.5.1. The ray-trace diagrams are shown in Fig. 5.5.3. The image is also calculated for zero tangent error as reference (trial 1). Note that the effect of the errors is

Table 5.5.1: Effect of Tangent Error on Line Width as Determined with Ray Traces

			Ray Traces*	
Trial	σ_{sag} (sec)	σ_{mer} (sec)	$FWHM_{sag}$ (mm)	$FWHM_{mer}$ (mm)
1	0	0	1.0×10^{-3}	1.0×10^{-3}
2	0	1	1.1×10^{-3}	0.134
3	1	0	4.9×10^{-3}	1.0×10^{-3}
4	30	0	0.14	1.1×10^{-3}
5	30	1	0.14	0.14
	measured tangent errors from a real mirror			
6	~ 2	~ 0.9	$8 - 11 \times 10^{-3}$	~ 0.11

* Ray-trace parameters

Source: $0.001\ mm^3$ x, y, z
1 mrad FWHM Divergence in the x and y planes
Isotropic distribution of source points and emission angles

Mirror: Ellipsoid
$r = r' = 6000$ mm
$\theta_g = 2° = 3.5 \times 10^{-2}$ rad $= \frac{1}{29}$ rad

essentially orthogonal: meridional tangent errors have little effect on the sagittal halfwidth and vice-versa.

Now we can take the formulas given above and calculate the image halfwidths resulting from the various tangent errors chosen.

2nd trial: $\Delta s'_{mer}$ $= 2\, r' \Delta_{mer}$
$= 2 \cdot 6000 \cdot 1.14 \times 10^{-5}$ rad $= \underline{0.14 \text{ mm}}$

3rd trial: $\Delta s'_{sag}$ $= 2\, r' \theta_g\, \Delta_{sag}$
$= 2 \cdot 6000 \cdot 3.5 \times 10^{-2}$ rad $\cdot\ 1.1 \times 10^{-5}$ rad
$= 4.8 \times 10^{-3}$ mm

4th trial: $\Delta s'_{sag}$ $= 2\, r' \theta_g\, \Delta_{sag}$
$= 2 \cdot 6000 \cdot 3.5 \times 10^{-2}$ rad $\cdot\ 3.4 \times 10^{-4}$ rad
$= \underline{0.14 \text{ mm}}$

5th trial : $\sigma_{mer} = 1$ sec

$$\theta g\, \sigma_{sag} = \frac{1}{29} \cdot 30 \cong 1 \text{ sec}$$

The aberrations should be comparable (see trials 2 and 4 above).

6th trial: $\Delta s'_{mer} \cong 0.11 = 2 \cdot 6000\, \Delta_{mer}$
$\sigma_{mer} = \underline{0.81 \text{ sec}}$

$\Delta s'_{sag} \cong 9.5 \times 10^{-3} = 2 \cdot 6000 \cdot 3.5 \times 10^{-2}\, \Delta_{sag}$
$\sigma_{sag} = \underline{2.0 \text{ sec}}$

Similar trials were made for a 6:1 demagnifying system. The agreement between the σ's and the FWHM (ray trace) was as good as found above.

5.6. Surface Roughness

In contrast to the specular reflectance of a mirror at angles around $-\theta$, where θ is the angle of incidence, the intensity observed at other angles is not easily calculated. Such scattered reflectance results from the microroughness of the mirror surface (Figure 5.6.1 [5.11]). An useful

Figure 5.6.1: Surface Roughness : Theory and Experiment [5.11]

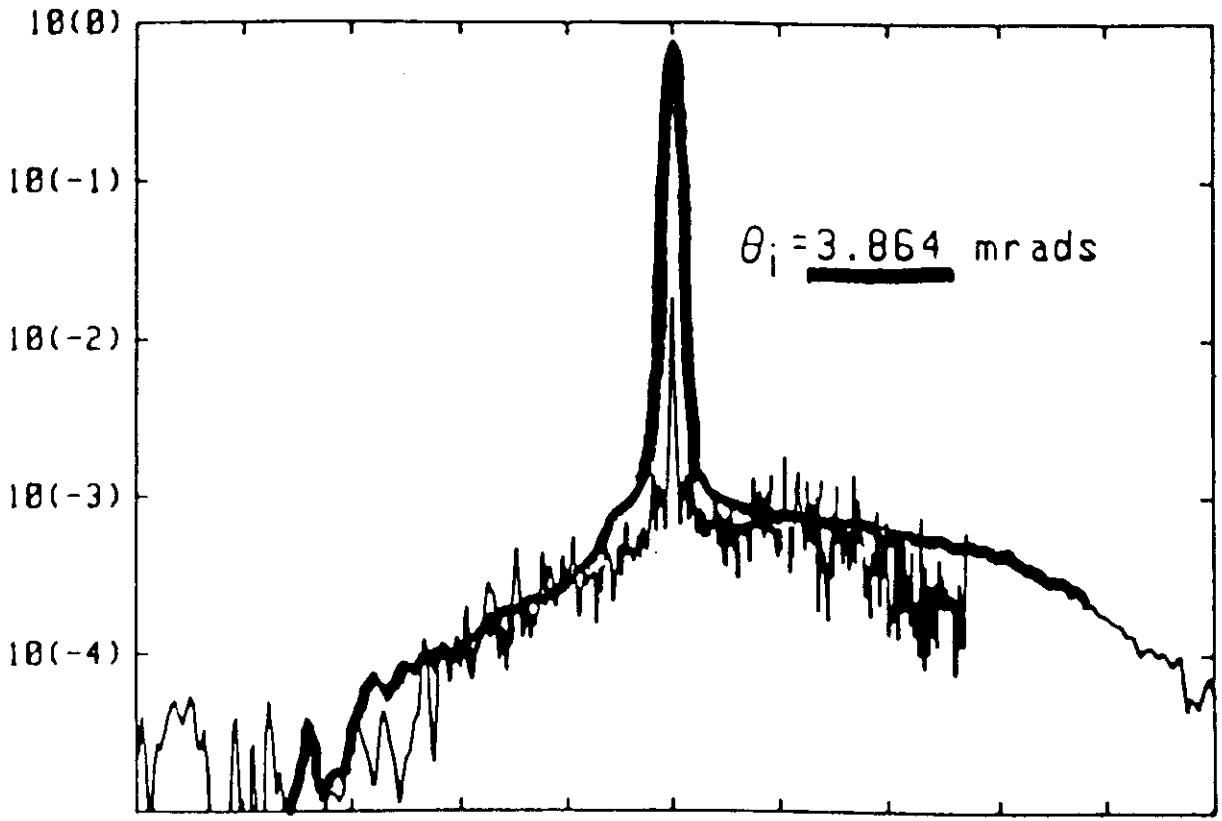

relation for the reduction in reflectivity at a given wavelength and grazing angle of incidence is [5.18]

$$R = R_0 \exp - \left(\frac{4\pi \sigma \sin \theta_g}{\lambda} \right)^2$$

where R_0 = smooth surface reflectivity
R = attenuated reflectivity
θ_g = grazing angle of incidence
λ = Wavelength of incident light
σ = rms surface roughness .

Attention is drawn to the references (5.8 - 5.11).

In general, surface roughness and figure error are coupled perversely: in the manufacturing process, the process that produces a better (smaller) rms microroughness simultaneously makes the figure worse. In recent years an rms microroughness of < 10Å is commonly available, with values down to 3 Å not uncommon.

In summary, the best proof of the quality of an optical element are direct measurements of the surface geometry with a profilometer and of the microroughness with an interferometric microscope. The second best proof is to find someone with such diagnostic tools who will make the measurements for you, even if it costs. There is no third best proof!

Chapter 6: Monochromators and Beamlines

Now that the preliminaries to beamline design have been touched on, all that remains is for the designer to proceed with the detailed design of the complete beamline. Since the beamline will be intended for particular experiments, a knowledge of the requirements of these experiments is necessary. The prospective users of the beamline should be requested to specify their particular needs.

The first question that should be raised is (1) the energy range required. The second is (2) should it be layed out for highest resolution or (3) highest flux at the experiment. The priority of the remaining questions is not unique. However, if the user "requires" the highest resolution and the highest flux and the widest energy range, all within the budget of a used Ford, don't dispair. Your's is a very common problem.

The best solution to this problem is to make the user(s) an active part of the design team so that he becomes thoroughly acquainted with the real problems at hand. Give him specific tasks so that the (successful) completion of the beamline directly and in some significant way depends upon his performance. If he happens to be the director of an institute or a full professor somewhere, have him designate one of his postdocs as full time member of the design team. Get him involved at all costs!

So, with this preamble, the "team" must determine the parameters listed in the next section.

6.1. On the optimization of the beamline

The following parameters must be established:

- Energy range

- Resolution required

- Number of gratings to be used for the above

- Flux required

- Entrance slit to be used?

- Means and location of sagittal focussing

- The grating type: plane, toroidal, spherical, variable line spacing, etc.

- Availability of the optical components desired

- Cost of the optical components

- The size of the monochromator as determined by total space available, space required for the experiments, monochromator design, etc.

- Is heat loading a factor?

- Complexity and cost of the mechanics

- Amount of manpower available to develop, build and maintain the beamline.

- The deflection angle, α - β, must be chosen. This is done on the basis of the maximum photon energy, E_{max}, to be transmitted with (say) 50% reflectance. If possible, α - β should increase with increasing energy.

-Means of suppression of higher order light.

-Minimization of optical aberrations: they are strongly dependent on α_{max} and grating length (see sections 4.2 and 4.3):

a) α_{max} (β_{max} if k = -1) is determined by

$$\frac{\lambda_2}{\lambda_1} = \frac{\sin\phi_2}{\sin\phi_1} \text{ where } \phi = \frac{\alpha + \beta}{2}$$

($\phi_2 - \phi_1$ = angular scanning range of grating for the wave length range $\lambda_1 - \lambda_2$)

b) Grating length $\cong$ 2 r sin m/sin θg;
$\theta g = 90° - \alpha$ = grazing angle of incidence
$\pm$ m = vertical acceptance
r = distance between entrance slit and grating

If the goal of the design team is to achieve the highest resolution along with the highest spectral purity (minimization of higher order light) and good flux, the following list will summarize the design points to be addressed (table 6.1.1).

In the subsequent sections the main types of soft x-ray monochromators used at synchrotron radiation laboratories around the world are described. For monochromators which are intended exclusively for energies below 40 eV, the normal incidence and Seya-Namioka monochromators, see chapter 11 sections 3 and 4 for suitable references. They will not be handled here.

Table 6.1.1: The "Ideal" High Resolution Soft X-Ray Monochromator

1) Focussed for all λ ($F_{200} = 0$)
2) Coma corrected for all λ ($F_{300} = 0$)
3) Other aberrations minimized
4) Large energy range without grating change
5) Grating always on "blaze"
6) Higher orders suppressed
7) Fixed entrance and exit slits
8) Fixed entrance and exit directions
9) Perfect matching to source
10) Performance unaffected by heat load
11) High transmission
    Number of optical elements
    Quality of optical elements
12) Possible to align!
13) Possible to pay for!

6.2. The toroidal/spherical grating monochromator

In chapter 4 the equations for a toroidal/spherical grating were explicitly given (see section 4.3). With these equations and with the desired geometry of the monochromator, the exact details of the beamline can be determined.

The designation "toroidal/spherical grating monochromator" is meant to describe the most simple type of soft x-ray monochromator: Except for a rotation of the grating, everything is fixed in space. Of course, variations on this theme, which compensate for some particular problem or optical aberration, have been made. This is the most commonly found type of monochromator at the synchrotron radiation laboratories around the world. We explicitly exclude the Rowland circle monochromator described in section 6.3 which represents a significant improvement on the spherical grating monochromator design but which is significantly more complicated.

What is the desired geometry of the monochromator? In particular:

- will a premirror system and entrance slit will be used?
- will a refocussing mirror behind the exit slit be used?
- what is the total length?
- what angle of deviation on the grating is required(energy range)?

6.2.1. Toroidal grating monochromators

A typical layout of a TGM for photon energies from ca. 15 to 160 eV is shown in figure 6.2.1. In this case, an elliptical torus premirror is employed to focus the dipole radiation source on the entrance slit. The grating focusses (poorly) the dispersed radiation on the exit slit. An ellipsoidal refocussing mirror refocusses the light at the exit slit on the experiment. Thus, two mirrors, (three) gratings and two slits make up the optical elements of this beamline. The theoretical and experimentally determined characteristics of this beamline are shown in figure 6.2.3. [6.2].

A still simpler TGM is shown in figure 6.2.2: a high energy toroidal grating monochromator for a dipole source. In this case, the main emphasis was put on the energy range, 180 to 1100 eV, and on maximizing the flux behind the exit slit. Thus, the design calls for only two optical elements: a grating and

Figure 6.2.1: A TGM for Photon Energies from ca. 15 to 160 eV

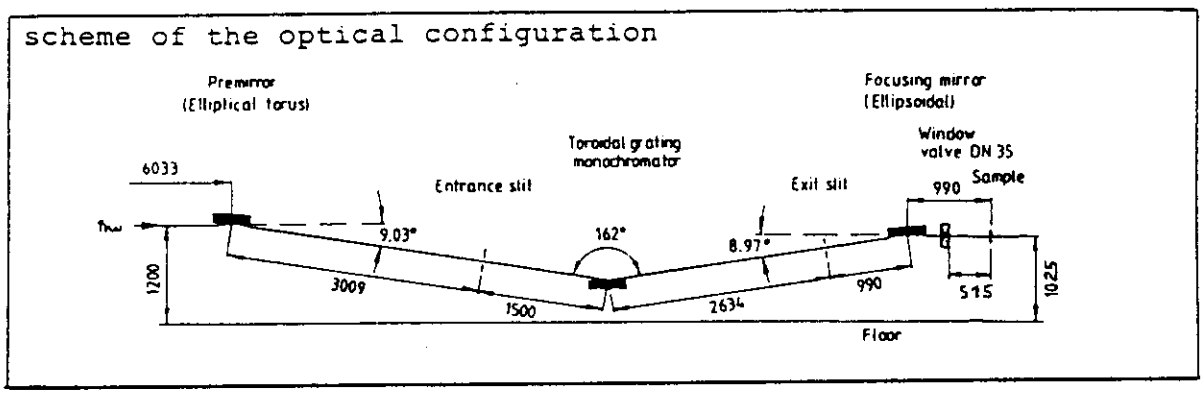

Figure 6.2.2: A TGM for Photon Energies from ca. 180 to 1100 eV [6.3]

TOROIDAL GRATINGS

MAJOR RADIUS : 116 000 mm

MINOR RADIUS : 483 mm

DIMENSION (ruled area) : 100 × 30 mm^2

DIVERGENCE BEHIND EXIT SLIT : < 2.6 mrad

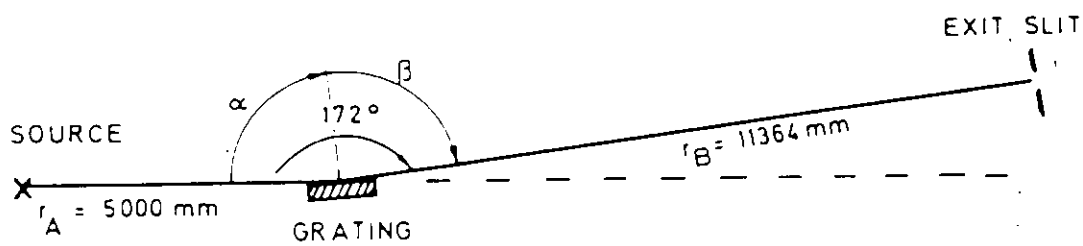

Figure 6.2.3: The Characteristics of a TGM for 15-160 eV Photons

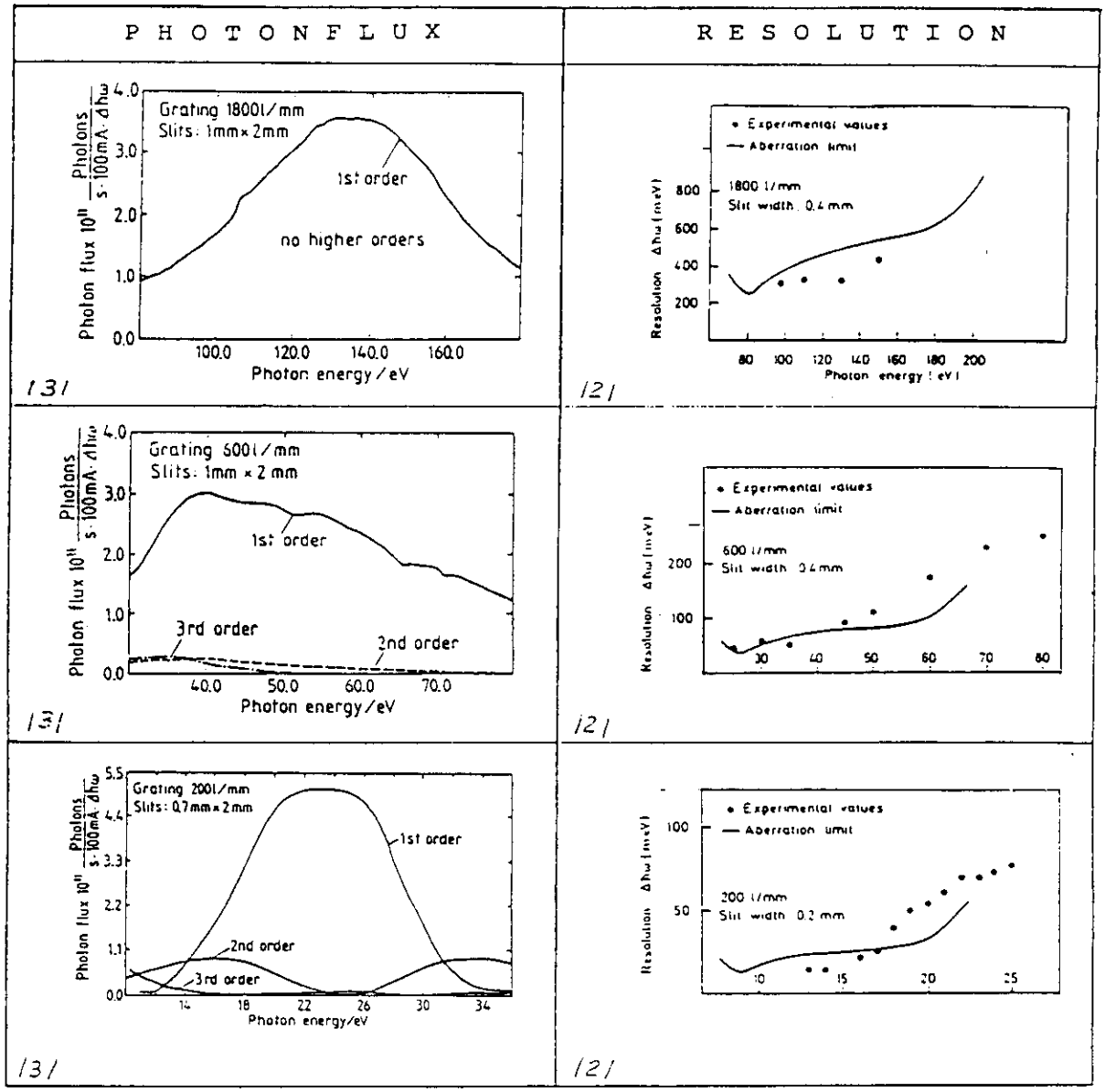

an exit slit. In order to cover the energy range, one of two gratings is moved laterally into its operating position. The toroidal grating provides focussing (poorly) in both the sagittal and the meridional planes. The measured characteristics of this monochromator are given in figure 6.2.4 [6.2, 6.3].

For toroidal grating monochromators, the most important expressions for the terms in the optical path function are as follows (for all of the F_{xyz} terms see chapter 4):

$$F_{020} = \frac{1}{r} + \frac{1}{r'} - \frac{1}{\rho}(\cos\alpha + \cos\beta) \qquad \text{sagittal focus}$$

$$F_{200} = \left(\frac{\cos^2\alpha}{r} - \frac{\cos\alpha}{R}\right) + \left(\frac{\cos^2\beta}{r'} - \frac{\cos\beta}{R}\right) \qquad \text{meridional focus}$$

$$F_{120} = \left(\frac{1}{r} - \frac{1}{\rho}\cos\alpha\right)\frac{\sin\alpha}{r} + \left(\frac{1}{r'} - \frac{1}{\rho}\cos\beta\right)\frac{\sin\beta}{r'} \qquad \text{astigmatic coma}$$

The resolution, $\Delta\lambda$, is most strongly related to the two terms, meridional focus and astigmatic coma [ref 4.6], the other terms given in chapter 4 being comparitively small. That the other terms are not so important may appear to be surprising, but is easily explained: the resolution of a toroidal grating monochromator is at best modest. Because of the wavelength dependence of the meridional focus, the monochromator is only focussed at one wavelength. In addition, because of the small radius for sagittal focussing, ρ, the image is very poor. Finally, it is very difficult to manufacture toroidal gratings with a tangent error less than 1 arc second. Nevertheless, toroidal grating monochromators have been serving the scientific community since the late 1970's.

The usual method of optimizing the specification of the toroidal grating itself is the following:

1) The abbreviated equation for the resolution (below) is minimized using a least squares routine. In this way, a resolution curve is obtained showing two minima. These are placed at strategic energies so that the user has the best resolution/wavelength compromise. Such an optimization is shown in figure 6.2.4.A. where the two minima are clearly to be seen [6.4].

Figure 6.2.4: The Characteristics of a TGM for 180-1100 eV Photons [6.3]

A. Optimization curves for a toroid grating with 1800 ℓ/mm

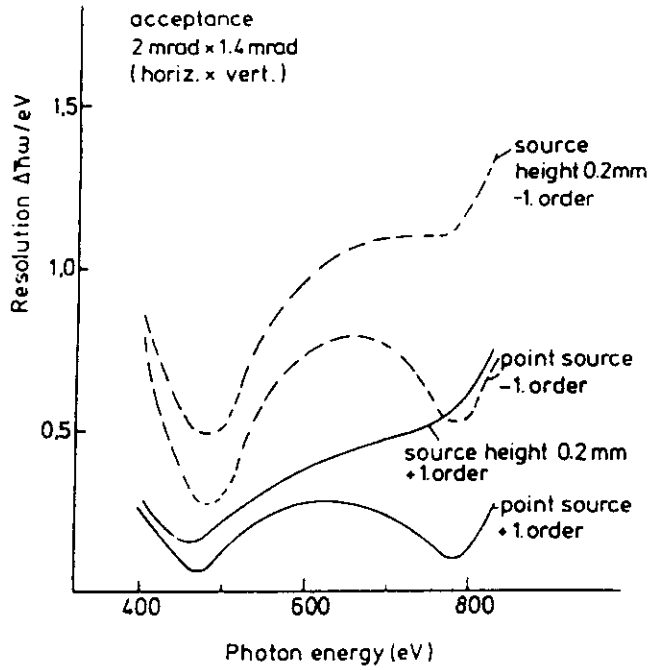

B. Measured data

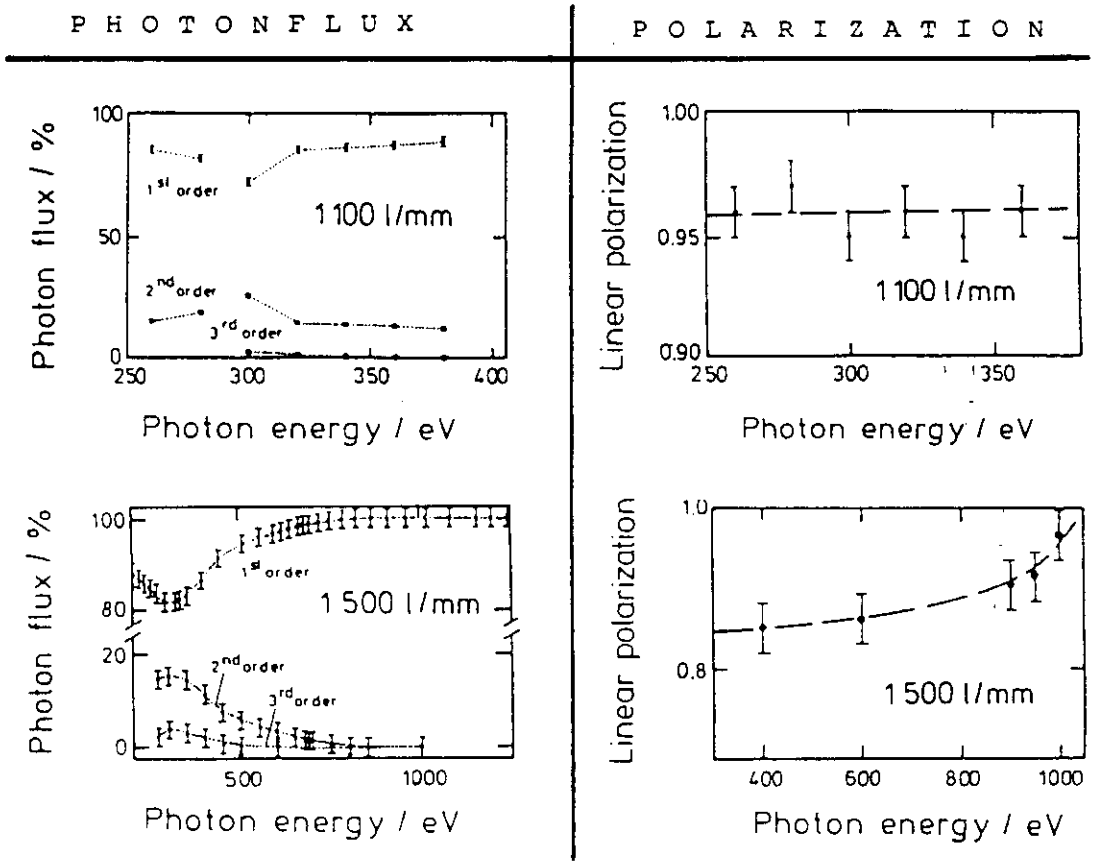

$$\Delta\lambda \approx \frac{1}{Nk}\left[wF_{200} + \frac{1}{2}\ell^2 F_{120} \right]$$

where $$F_{200} = \left(\frac{\cos^2\alpha}{r} - \frac{\cos\alpha}{R}\right) + \left(\frac{\cos^2\beta}{r'} - \frac{\cos\beta}{R}\right)$$

and $$F_{120} = \left(\frac{1}{r} - \frac{1}{\rho}\cos\alpha\right)\frac{\sin\alpha}{r} + \left(\frac{1}{r'} - \frac{1}{\rho}\cos\beta\right)\frac{\sin\beta}{r'}$$

2) If possible, one grating is used for each doubling of photon energy. Thus, for the energy range 25 to 200 eV, three gratings would be employed: 25-50 eV, 50-100 eV and 100-200 eV. This does not mean that the optimized energies (see 1 above) should lie at 25, 50, 100, and 200 eV. The optimization should be worked out so that the three ranges have a "suitable" overlap and that the six energies with best resolution are "good". What are "suitable" and "good" ? The user in the design team must help decide this!

6.2.2. Spherical grating monochromators

An improvement in resolution can be won by replacing the toroidal grating with a spherical one and providing an additional mirror for the sagittal focussing. This additional mirror can be vertically deflecting or horizontally deflecting. In the former case, it will be a cylindrical mirror which is also difficult to manufacture to a very high figure. In the latter case, the mirror can be spherical, which is less expensive and available with a very good figure. As seen in chapters 4 and 5 the horizontal deflection has the further advantage that the influence of its figure error on the resolution is reduced by the sine of the grazing angle of incidence (figure 5.5.3). However, if this mirror is to intercept a large number of milliradians from the storage ring it will be correspondingly large (section 4.4.6).

With the spherical grating the F_{120} term is no longer significant, because the very small radius of curvature has been eliminated: i.e. $\rho = R$. In addition, because of the larger radius, the F_{120} , F_{111} and the F_{102} terms tend to cancel each other [4.10]. Then, the main terms contributing to the resolution function are F_{200} and F_{300} , meridional focus and coma. These two terms can be minimized basically by fulfilling the Rowland conditions for a small evergy range. Then, because of the availability of very high quality

spherical gratings, and by the elimination of astigmatic coma, a very high resolution can be achieved at the optimized wavelengths [4.10 , 4.14]. This is the design principle of the "Dragon Monochromator" which has delivered a resolution, $\Delta E/E > 5000$ at 400 eV [4.14b].

Further improvements can be achieved by incorporating a moveable exit slit in the design. In this way, the monochromator can be made to focus over a larger range of wavelengths. The movement need not be continuous nor simultaneous with the wavelength scan. For experiments at fixed energies, the monochromator can be set up with the exit arm at the optimal wavelength and the experimental apparatus then attached. A moveable entrance slit is more complicated. The premirror(s) provide an optimal vertical focus at a particular location. Moving the extrance slit away from this location means a loss of flux. The "Grasshopper" monochromator and its relatives ("Locust" etc.) is a further example of an improved spherical grating monochromator design [1.4, 6.8]. Another means of improving the performance significantly is described in the next section.

6.2.3. The exactly focussed spherical grating monochromator

It is possible to exactly fulfill the F_{200} condition exactly and for all wavelengths if the monochromator has one degree of freedom more than just the rotation of the grating. As mentioned in the previous section, providing a moveable exit slit will accomplish this goal, but is cumbersome to carry out: the slit movement must remain exactly on the optical axis otherwise the energy calibration will be lost. In addition, the illumination of the experiment will be dependent upon the position of the exit slit.

Instead of having a moveable exit slit, one can employ a variable angle of deviation across the grating, α-β, in order to make $F_{200} = 0$ for all wavelengths. In this way, the exit slit and the experiment remain at fixed positions, and to the eye, nothing moves. How this can be accomplished without having to sweep the exit arm of the monochromator through space is illustrated in figure 6.2.5. Here a plane mirror is made to move in such a way that it always deflects the central ray of light coming from the entrance slit up to the center of the grating where it is dispersed and the desired energy directed to the exit slit. At first glance it would appear that only by translating and rotating the mirror such an effect could be realized, a relatively complicated mechanical arrangement for an ultra high vacuum

Figure 6.2.5: Optical Layout of a Focussing Spherical Grating Monochromator [6.4]

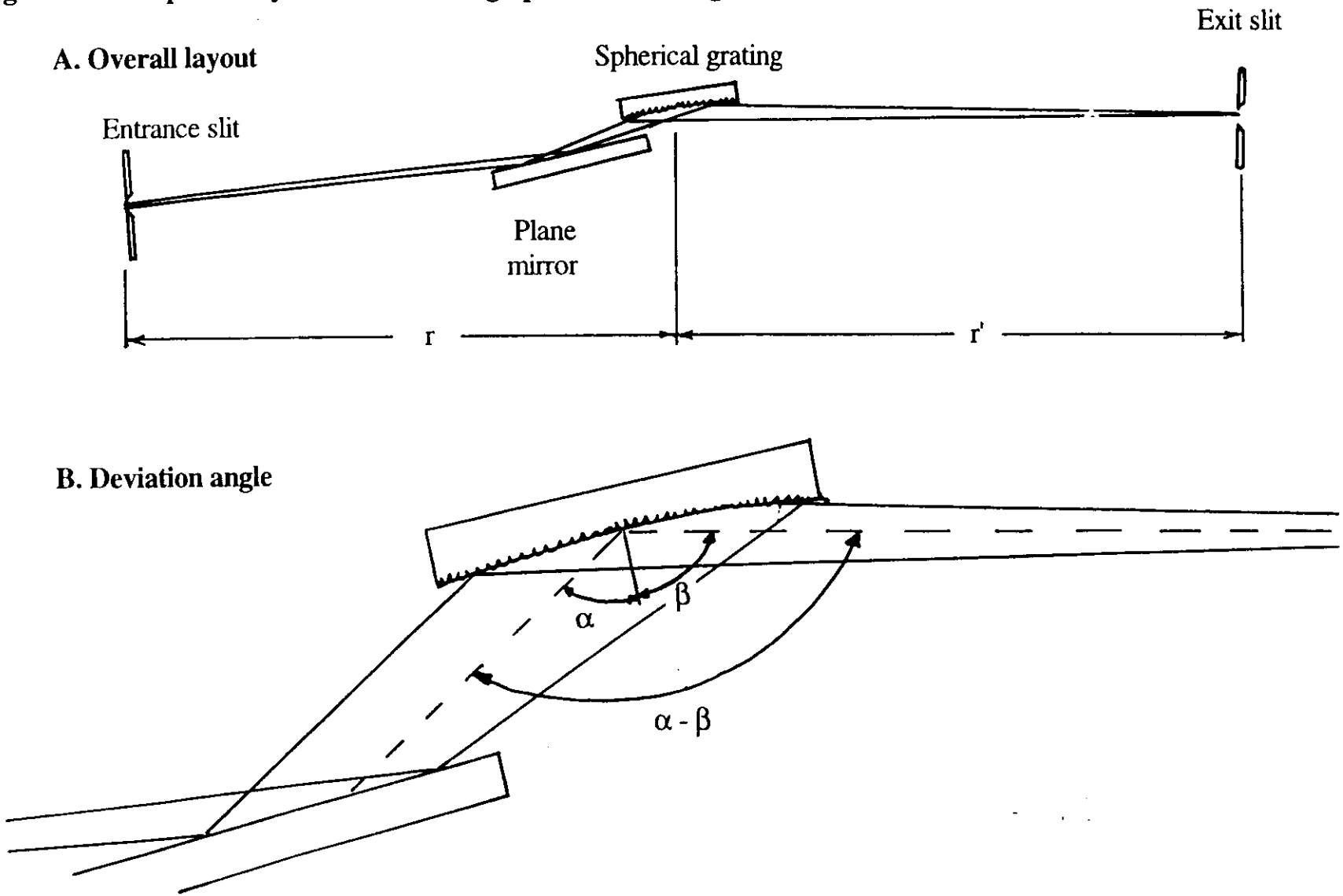

Figure 6.2.6: The Complete Beamline for the Focussing SGM [6.4]

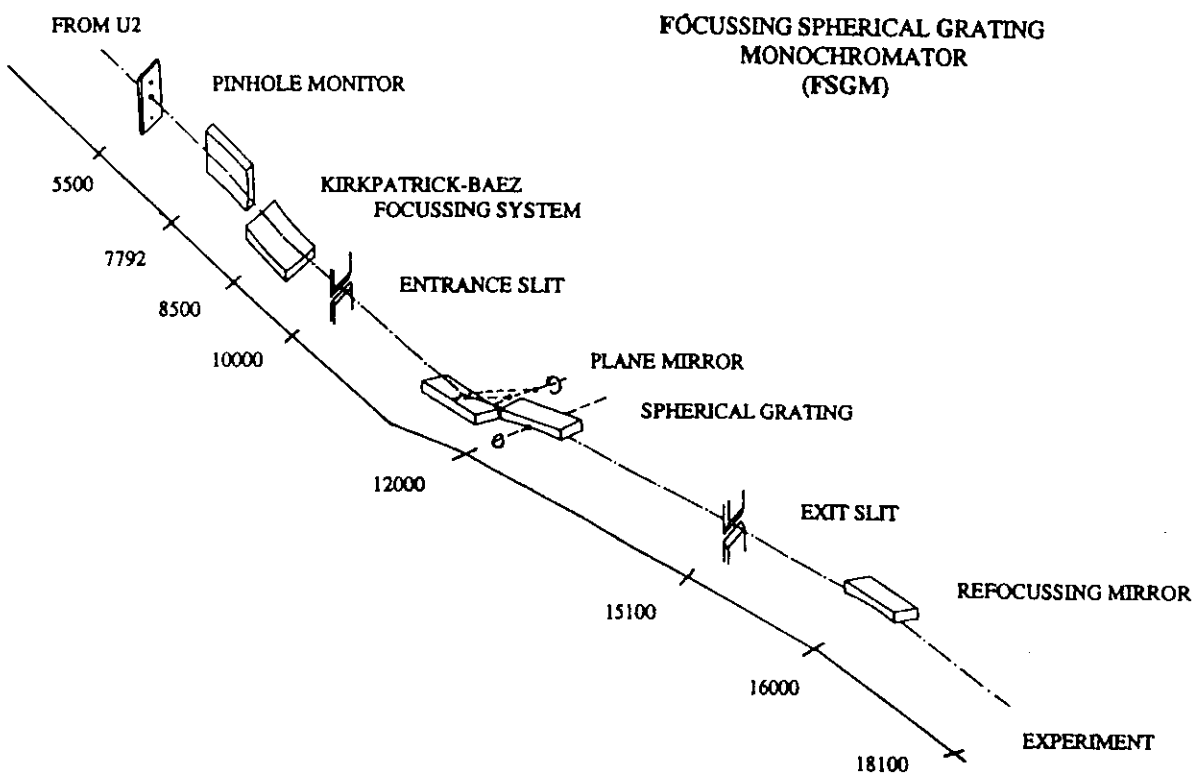

FIG. 1. Components of the FSGM beamline. In contrast to an ordinary SGM the deflection angle across the spherical diffraction grating can be varied by means of a rotating plane mirror.

Table 6.2.1: The Parameters of a Focussing SGM [6.4]

TABLE I. The parameters of the crossed field undulator U2.

First undulator	Planar, λ_u=84 mm, N=6.5, horizontal deflection, $2 \geq K \geq 0.5$
Modulator	three poles, horizontal deflection
Second undulator	planar, λ_u=84 mm, N=7.5, vertical deflection, $2 \geq K \geq 0.5$
Electron beam	$E_{electron}$=800 MeV, σ_x=0.4 mm, σ_y=0.1–0.3 mm
Energy range	first harmonic: 20–65 eV, third harm.: 60–126 eV, fifth harm: 100–195 eV

TABLE II. The Kirkpatrick–Baez mirror system.

First mirror (spherical)	horizontally deflecting; source distance: 7792 mm; image distance: 10 000 mm; Θ=86.1°; R=129 000 mm; $\sigma_m \leq 4$ s; microroughness$\leq$0.8 nm; mirror dimensions: 300×70×50 mm^3; optical surface:280×50 mm^2; material: CVD SiC on refel SiC; Coating: 300×35 mm^2 gold, 300×35 mm^2 CVD SiC
Second mirror (spherical)	vertically deflecting; source distance 8500 mm; image distance: 1500 mm; Θ=87.5°; R=60 000 mm; $\sigma_m \leq 1$ s; microroughness$\leq$0.8 nm; mirror dimensions: 300×70×50 mm^3; optical surface:280×50 mm^2; material: CVD SiC on refel SiC; Coating: 300×35 mm^2 gold, 300×35 mm^2 CVD SiC

TABLE III. The basic parameters of the focusing spherical grating monochromator.

	First grating	Second grating	Third grating
Grating profile	laminar,1:1	laminar,1:1	laminar,1:1
Energy range (eV)	20–100	37–150	80–220
Optimized energy range (eV)	35–60	60–100	100–160
Groove density $1/d$ (ℓ/mm)	500	750	1050
Deviation angle Θ (°)	158.3–160.0	160.7–161.5	162.9–164.4
Entrance arm length r (mm)	2000	2000	2000
Exit arm length r' (mm)	2900–3300	2900–3300	2900–3300
Grating radius R (mm)±(mm) rms	14 000±20	15 400±50	17 200±20
Grating coating	CVD SiC	gold	gold
$E/\Delta E_{max}$ (theoretical, 10 μm slits)	25 000	20 000	15 000

Figure 6.2.7: The Characteristics of the Focussing SGM [6.4]

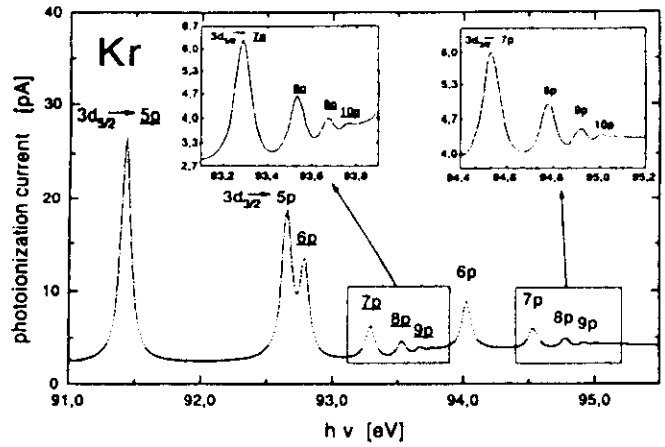

FIG. 4. Photoionization spectrum of krypton close to the Kr $M_{4,5}$ threshold recorded with grating 3 (1050 ℓ/mm) in first order (slit width 50 μm, full illumination of the optical components). The Kr $(3d_{5/2}^{-1}\, np)$ states, converging to the M_5 thresholds, are underlined. The $n=10$ structures could be resolved for the first time.

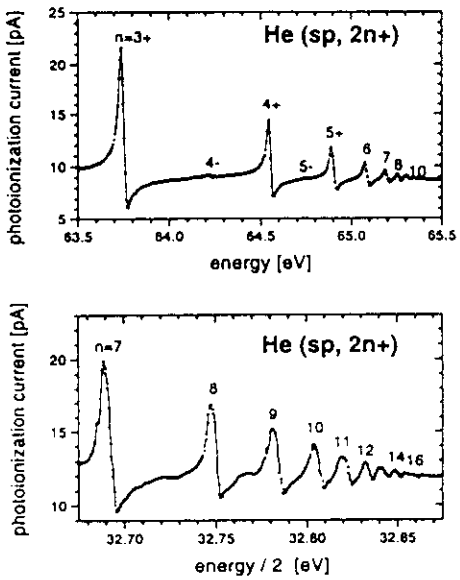

FIG. 2. Photoionization spectra of the $N=2$ series of the autoionization double-excitation states of He: $1s^2 \rightarrow (2snp \pm 2pns)$. (a) Measured with grating 1 (500 ℓ/mm) in first order. (b) Expanded high n region measured with grating 1 (500 ℓ/mm) in second order.

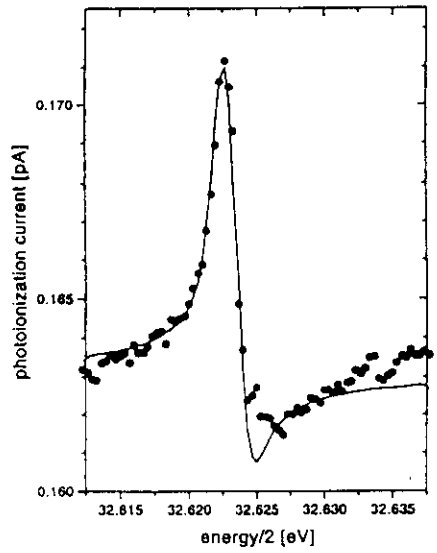

FIG. 3. The $n=8$ peak of the He $(sp, 2n+)$ series measured (●) in second order: grating 1, 500 ℓ/mm, slit widths 7 μm, full illumination of the optical components. The solid curve represents a Fano profile convoluted with a Gaussian profile, where $\sigma_{Gauss}=0.792$ meV, $E_{Res}=32.62317$ eV, $\Gamma=0.240$ meV, and $q=-2.500$, indicating a resolution of $E/\Delta E=17\,500$.

system. However, by using a sufficiently long plane mirror and rotating it about a particular axis, the same effect can be achieved, the light beam running up and down the long plane mirror as it is rotated. It can be shown that the error in directing the ray to the center of the grating over a turning range of over 10° is negligible. Thus, the angle of deviation, α-β, of the monochromator can be varied over a 10° range or more without having to move any external parts of the monochromator. In this case, there are simply two precision rotation axes with their associated drives. This principle was first employed on the Petersen plane grating monochromator in 1980 [4.9, 6.5].

The relevant relationship for the angle of deviation is derived from the F_{100} and F_{200} terms given in chapter 4 for a spherical grating:

$$F_{100} = 0 = Nk\lambda - \sin\alpha + \sin\beta\,, \qquad \text{the grating equation}$$

$$F_{200} = 0 = \left[\frac{\cos^2 a}{r} - \frac{\cos a}{R}\right] + \left[\frac{\cos^2 b}{r'} - \frac{\cos b}{R}\right], \qquad \text{the meridional focus}$$

Since r, r', R, N and k are known for a particular system and λ is the desired wavelength, it is easy to obtain λ as a function of α and β by solving these two equations simultaneously. Thus, both of the "F" terms are kept at zero and the deviation across the grating, α-β, is a known variable.

This principle has been incorporated in the exactly focussing spherical grating monochromator [6.4]. The beamline layout for this monochromator is shown in figure 6.2.6. The basic parameters of the beamline are presented in table 6.2.1. This monochromator was designed for very high resolution and is mounted on a crossed field undulator which produces circularly polarized undulator radiation. Measured results are shown in figure 6.2.7.

6.3. The Rowland circle monochromator

Over one hundred years ago, in his theoretical analysis of the aberrations of a spherical grating, the spectroscopist H.A.Rowland worked out the most complete solution to minimizing the aberrations of such a grating. His solution, now known as the Rowland conditions, is (now) simply derived. One must remember, however, that he was the first to derive the analytical solution to the aberrations of the grating, i.e. the expressions now given conveniently in the form of the F-terms.

$F_{100} = Nk\lambda - \sin\alpha + \sin\beta$ grating equation

$$F_{020} = \frac{1}{r} + \frac{1}{r'} - \frac{1}{\rho}(\cos\alpha + \cos\beta)$$ sagittal focus

$$F_{200} = 0 = \left[\frac{\cos^2\alpha}{r} - \frac{\cos\alpha}{R}\right] + \left[\frac{\cos^2\beta}{r'} - \frac{\cos\beta}{R}\right]$$ meridional focus

$$F_{300} = \left(\frac{\cos^2\alpha}{r} - \frac{\cos\alpha}{R}\right)\frac{\sin\alpha}{r} + \left(\frac{\cos^2\beta}{r'} - \frac{\cos\beta}{R}\right)\frac{\sin\beta}{r'}$$ primary coma

$$F_{400} = \frac{4}{r^2}\left(\frac{\cos^2\alpha}{r} - \frac{\cos\alpha}{R}\right)\sin^2\alpha - \frac{1}{r}\left(\frac{\cos^2\alpha}{r} - \frac{\cos\alpha}{R}\right)^2$$

$$+ \frac{4}{r'^2}\left(\frac{\cos^2\beta}{r'} - \frac{\cos\beta}{R}\right)\sin^2\beta - \frac{1}{r'}\left(\frac{\cos^2\beta}{r'} - \frac{\cos\beta}{R}\right)^2$$

$$- \frac{1}{R^3}(\cos\alpha + \cos\beta) + \frac{1}{R^2}\left(\frac{1}{r} + \frac{1}{r'}\right)$$

etc.

Rowland identified the following terms which are common to the main sources of aberration:

$$\left[\frac{\cos^2\alpha}{r} - \frac{\cos\alpha}{R}\right] \quad \text{and} \quad \left[\frac{\cos^2\beta}{r'} - \frac{\cos\beta}{R}\right].$$

Furthermore, he solved each of them independently of the other, thereby making a general solution to the aberration equations. The solutions are

$$r = R \cos \alpha \qquad \text{and} \quad r' = R \cos \beta \ .$$

These are the Rowland conditions for a spherical grating monochromator.

Inserting them into the F-terms, one finds the following:

$F_{100} = Nk\lambda - \sin \alpha + \sin \beta$ grating equation

$$F_{020} = \frac{1}{r} + \frac{1}{r'} - \frac{1}{\rho}(\cos \alpha + \cos \beta)$$ sagittal focus

$F_{200} \equiv 0$ meridional focus

$F_{300} \equiv 0$ primary coma

$$F_{400} = - \frac{1}{R^3}(\cos \alpha + \cos \beta) + \frac{1}{R^2}\left[\frac{1}{r} + \frac{1}{r'}\right]$$

Parts of the remaining F terms also vanish while at the same time the terms themselves decrease in magnitude. The virtues of the Rowland conditions are obvious. What do these conditions mean in terms of the monochromator design?

The classical Rowland circle monochromator is depicted in figure 6.3.1. Here one sees why the name Rowland circle is apt. The grating radius is equal to the diameter of the circle, while the position of both slits is given by the circle. Many monochromator designs are based on this basic principle, especially in the normal incidence region of the spectrum. At higher photon energies, the poor reflectivity of the optical components forces the use of grazing angles of incidence. Furthermore, in order to "connect" the fixed source (storage ring) with a fixed experiment, additional mirrors must be used in order to keep the slits on the Rowland circle. This further reduces the throughput.

Figure 6.3.1: The Rowland Circle Monochromator

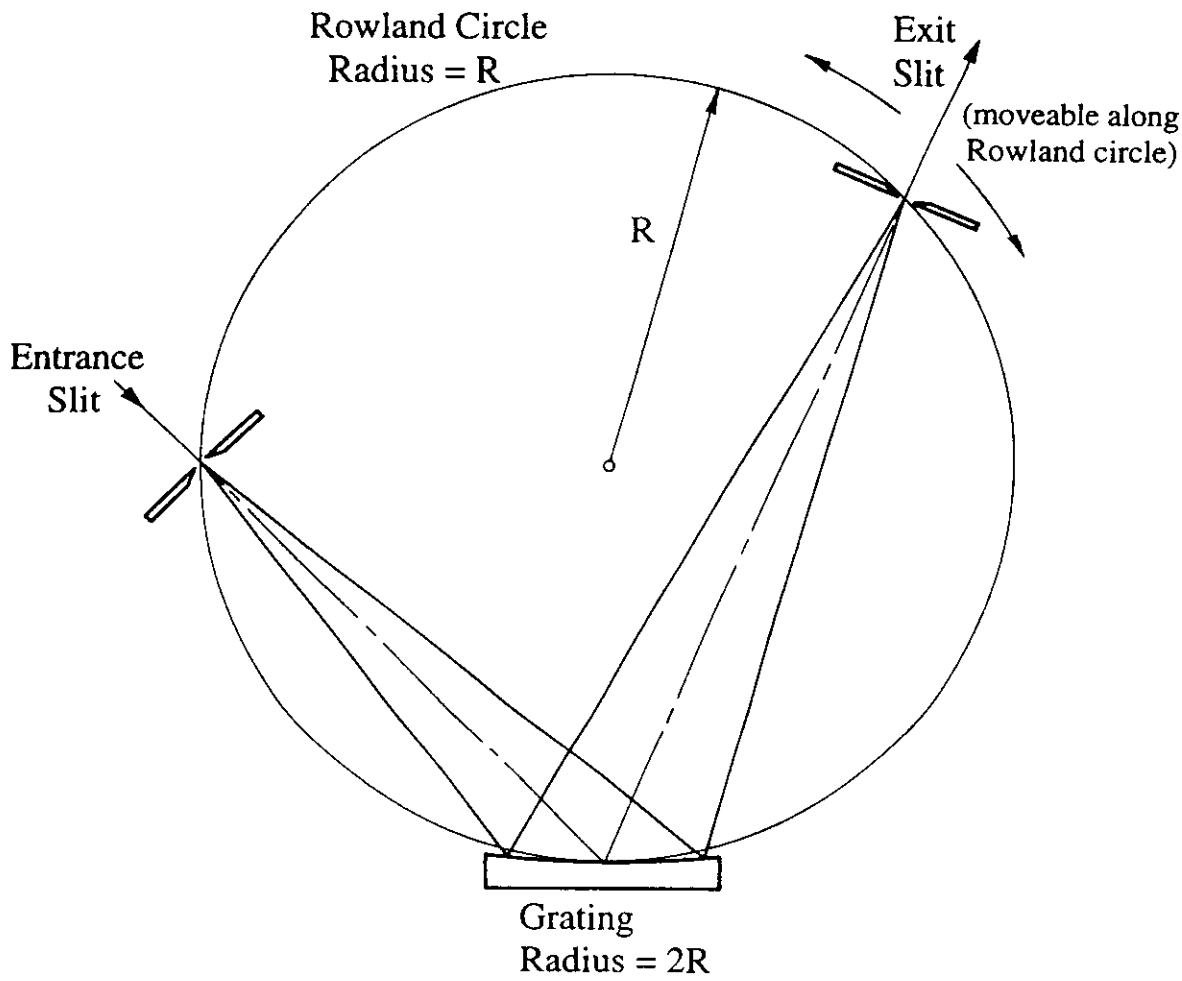

Recently, a Rowland circle design for the grazing incidence region of the spectrum has been developed and built [4.19 , 4.20]. The design requires the use of a premirror system for the sagittal focussing and one plane mirror in order to fulfill the Rowland conditions. Otherwise, only a simple rotation of the grating is required. The layout is shown in figure 6.3.2 [4.20]. As seen there, the input and output axes of the monochromator are parallel to each other. The positions of the extrance and exit slits are fixed and for a wavelength scan, the grating / plane mirror combination travel in their ultrahigh vacuum chamber between the slits. Thus, it is possible to fulfill the Rowland conditions with few optical components at grazing incidence!

One last point should be made (again, see chapter 4.4.9.A) in regard to the Rowland circle monochromator: the magnification. As we saw in section 4.4.9, the magnification in any monochromator is given by

$$M(\lambda) = \frac{s'}{s} = \frac{r'}{r} \cdot \frac{\cos\alpha}{\cos\beta}$$

When we substitute in the Rowland conditions we obtain

$$M(\lambda) = \frac{s'}{s} = \frac{r'}{r} \cdot \frac{r\,R}{R\,r'} \equiv 1 \,.$$

Thus, it is not possible to do anything about the source *size* within a Rowland circle monochromator. The situation is very different for the following monochromator.

6.4. The Petersen plane grating monochromator

As the name implies, a plane grating monochromator employs a plane grating for dispersing the radiation, while requiring additional, non-plane elements for sagittal and meridional focussing. As seen above, the sagittal focussing is relatively easily accomplished be various means and is therefore secondary to this discussion for the time being. The problem lies in the meridional focussing. In particular, the problem is that the plane grating itself weakly focusses the radiation in the meridional plane as a function of wavelength. Thus, the work of the primary focussing elements is done in by

Figure 6.3.2: The Constant Length Rowland Circle Monochromator

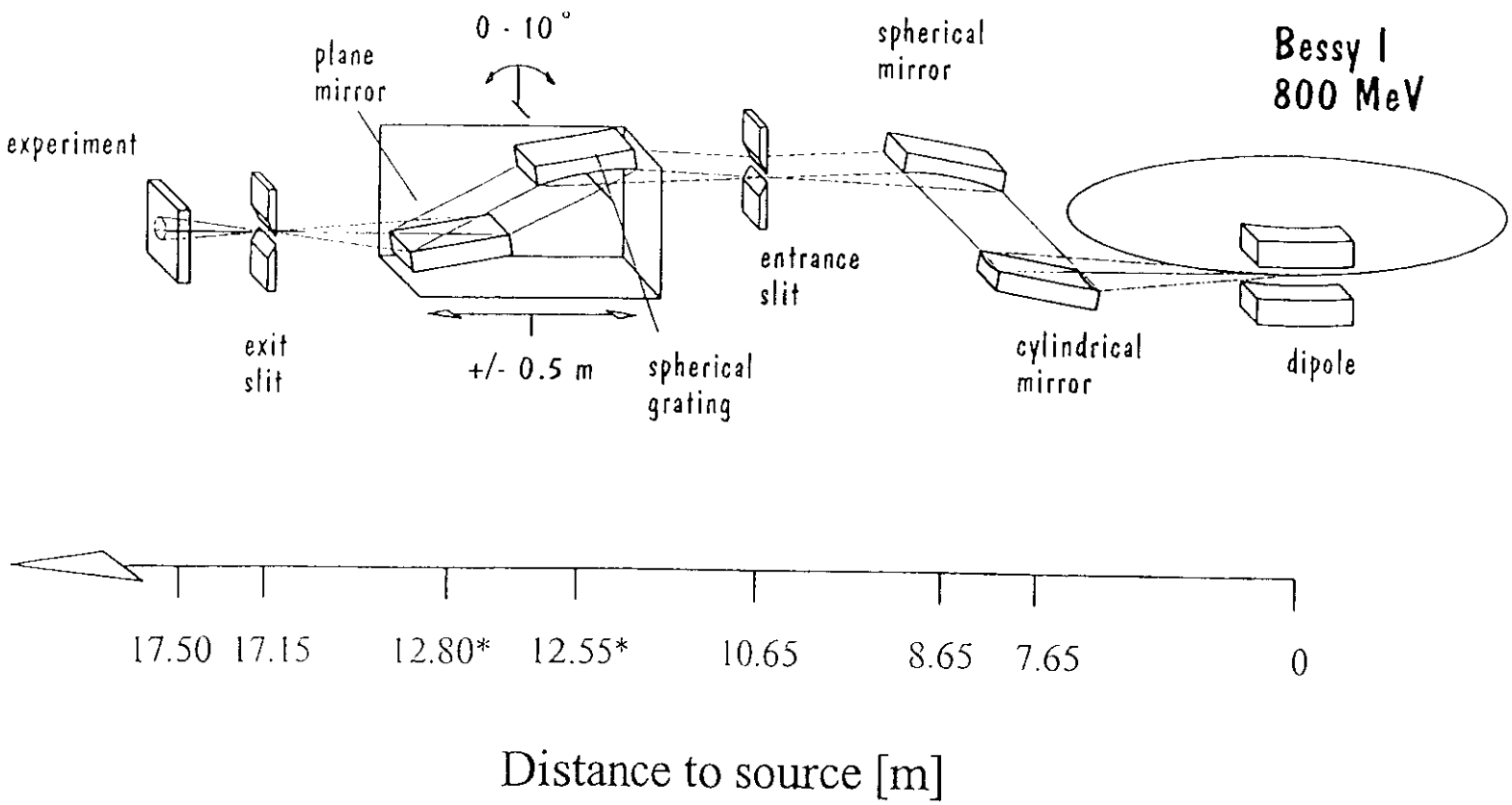

the variable focussing effect of the grating during a wavelength scan. The focussing effect of the plane grating is evident from the F_{200} term for a spherical grating!

$$\text{Thus, } F_{200} = \left[\frac{\cos^2 \alpha}{r} - \frac{\cos\alpha}{R}\right] + \left[\frac{\cos^2 \beta}{r'} - \frac{\cos\beta}{R}\right] \qquad \text{meridional focus}$$

Since we are dealing with a plane grating $R = \infty$ and $\cos \alpha / R = 0$! The same is true for the β term leading to

$$F_{200} = \left[\frac{\cos^2 \alpha}{r}\right] + \left[\frac{\cos^2 \beta}{r'}\right]$$

In order to eliminate the focussing effect of the grating this term must be made zero for all wavelengths, i.e. for all α and β values.

The solution for this problem was worked out by H. Petersen in 1979 and is as follows [4.9]:

$$\frac{r'}{r} = - \left(\frac{\cos \beta}{\cos \alpha}\right)^2 = - c_{ff}^2 \qquad \text{where } c_{ff} \text{ is a constant.}$$

Thus, the ratio of the input and output armlengths is a constant for all values of α and β . i.e. the focussing effect of the grating is a constant for all wavelengths (seen chapter 4.4.9.B). Figure 6.4.1 shows the original form of the Petersen fixed focus plane grating monochromator, built and marketed by the company C.Zeiss , Oberkochen, Germany under the name SX-700. In this version, the primary focussing both sagittally and meridionally is accomplished by means of one ellipsoidal mirror. Because of the difficulty of manufacture of such aspheric mirrors, the tangent errors limit the performance of the monochromator, later designs employ a two spherical mirrors for the sagittal and the meridional focussing, respectively [6.5, 6.6, 6.7]. Such a design is shown in figure 6.4.2. The measured spectra for the energy regions around 250 eV, 400 eV and 860 eV are shown in figure 6.4.3. The resolutions achieved at these energies are also given there.

Figure 6.4.1: Optical Layout of the Original Petersen Plane Grating Monochromator

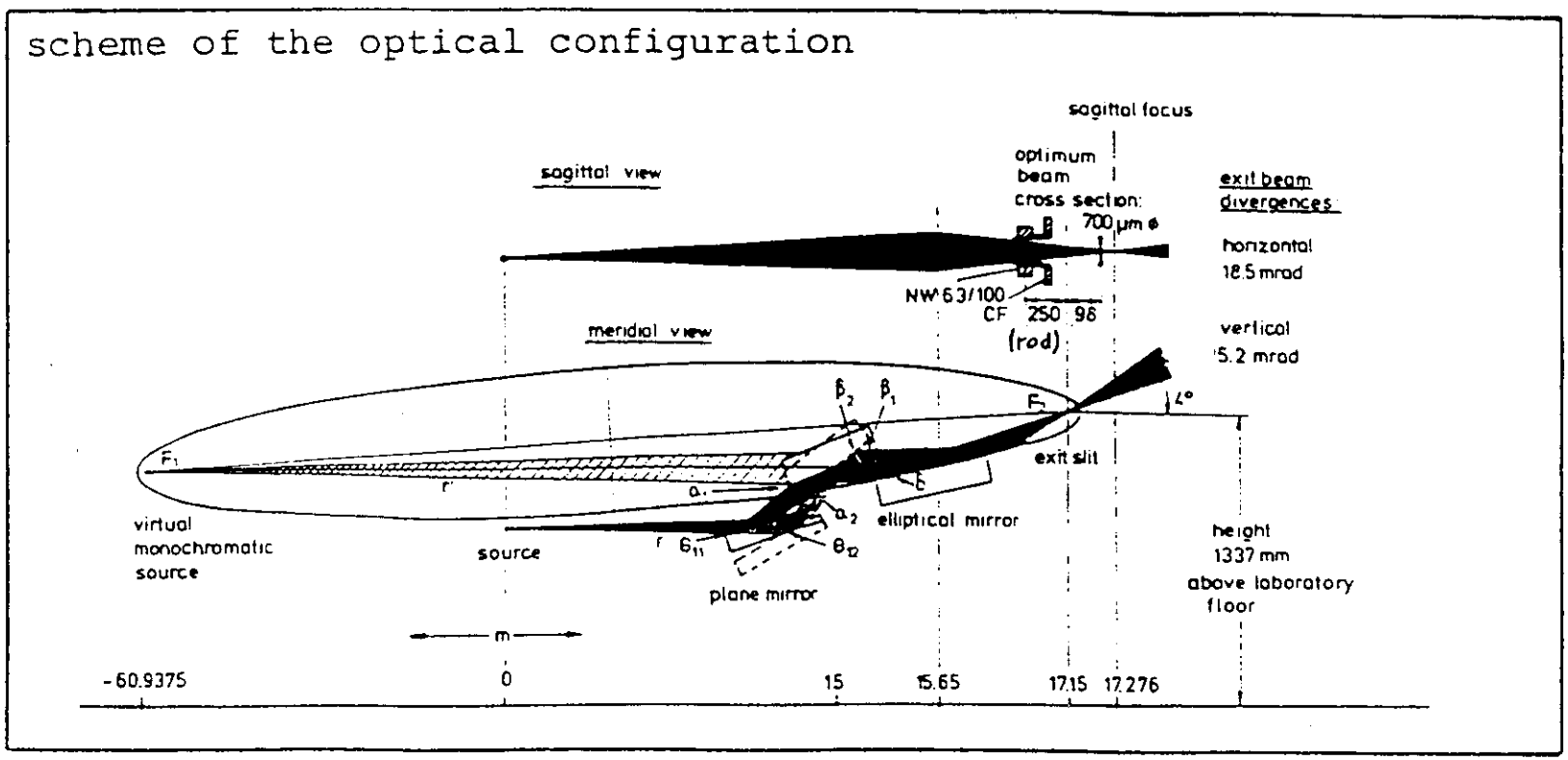

Figure 6.4.2: Optical Layout of the Petersen-PGM with Spherical Mirrors

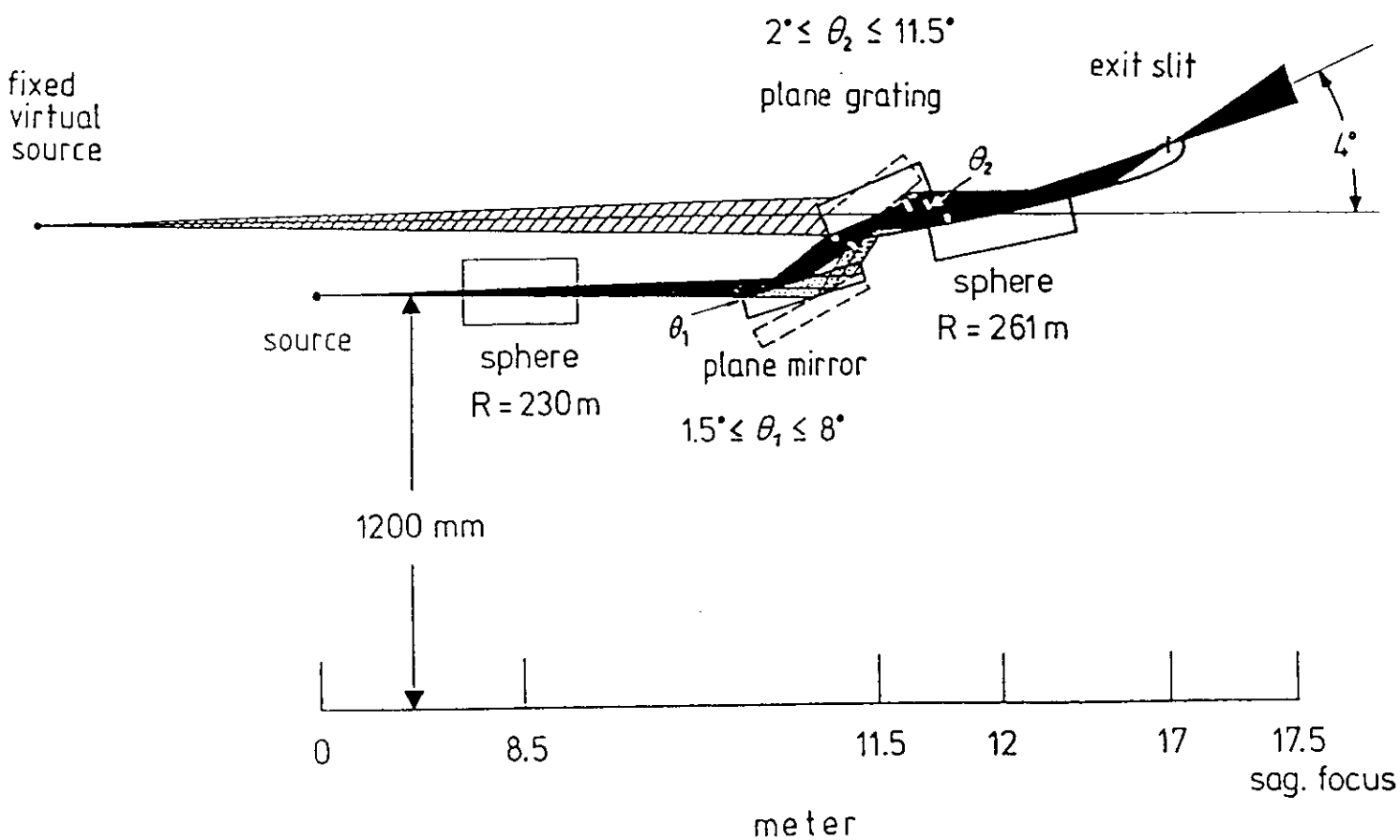

Figure 6.4.3: The Characteristics of a Petersen PGM with Spherical Mirrors [6.5]

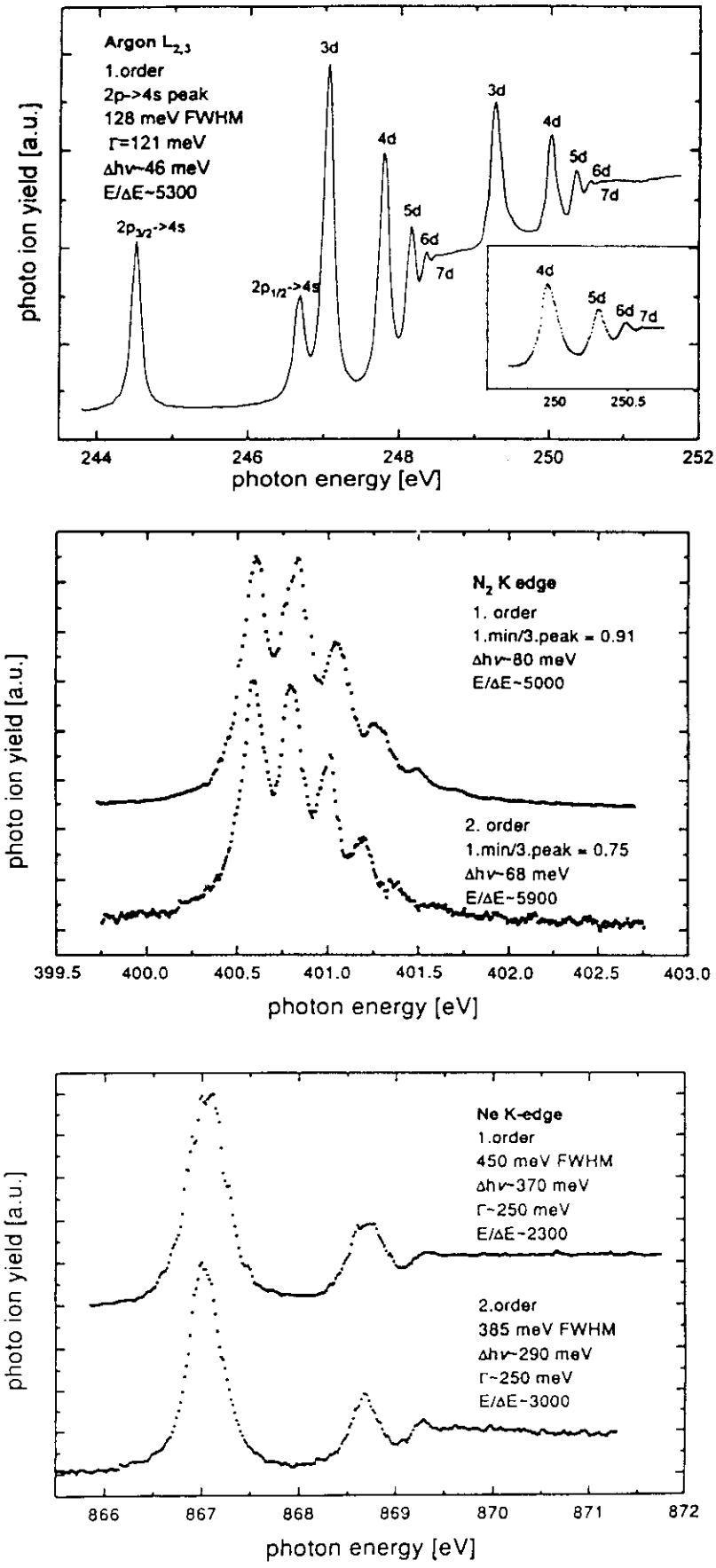

In his papers on this fixed focus plane grating monochromator design, Petersen also discussed the choice of the constant c_{ff} [4.9, 6.5]. Basically, he showed that, for an optimal resolution/flux product, a value of 2.25 should be taken. With this value, the grating remains in its most efficient operating region. If resolution should be increased at the cost of flux, larger values of c_{ff} can be employed. This has indeed been done and the improvement verified by experiment [see 6.5 for details].

Finally, the Petersen plane grating monochromator inherently demagnifies the image of the source at the exit slit. This has been derived in chapter 4.4.9.B. As shown there, the magnification is given be the expression

$$M = \frac{r''}{r c_{ff} - d / c_{ff} / c} \cong \frac{r''}{r c_{ff}}$$ (see figure 4.4.4. for definitions).

For usual conditions and $c_{ff} = 2.25$ (see for example ref. 6.5) a demagnification of 5.6 obtains.

6.5. A comparison between a Rowland circle-SGM and a Petersen-PGM

The question is often raised, which is "better", a spherical grating monochromator or a plane grating monochromator. One must first decide upon the criteria for "better". In planning for BESSY II, a study was made of exactly this question [6.7]. It may be useful for the reader to see what the boundary conditions were for this study and what conclusions could be drawn from it. In addition, it makes, perhaps, a fitting epilogue to this set of "Notes on Beamline Design".

Goal: To define a high resolution monochromator for undulator radiation

1. Energy range: 90 - 800 eV

2. Boundary conditions: see table 6.5.1.

3. Criteria
    a. Ray trace transmissions used
    b. Reflectivities and grating efficiencies included

4. Types of Monochromator compared:
    a. Rowland circle spherical grating monochromator
    b.Petersen plane grating monochromator

5. Comparisons made:
    a. Resolution for the same transmission
    b. Maximum resolution at the cost of transmission

Of concern here are the Rowland circle spherical grating monochromator and the Petersen plane grating monochromator. The layouts compared are shown in figure 6.5.1.

Table 6.5.1: Boundary Conditions: High Resolution Monochromators for Photon Energies 90-800 eV [6.7]

1)	Total length: middle of undulator to exit slit	26	m
2)	Length occupied by storage ring	9	m
3)	Undulator source characteristics		
	$E = 1.7$ GeV ;	$L = \lambda_O N =$	4100 mm
	$\sigma_H' (e\ell) = 0.029$ mrad ;	$\sigma_H (e\ell) =$	0.200 mm
	$\sigma_V' (e\ell) = 0.015$ mrad ;	$\sigma_V (e\ell) =$	0.040 mm
		$\sigma_H' (SR) =$	0.200 mrad
		$\sigma_V' (SR) =$	0.080 mrad
4)	Lengths of optical components:		
	Vertical mirrors	≤ 300	mm
	Horizontal mirrors	≤ 1000	mm
	Gratings	≤ 160	mm
5)	Tangent errors assumed (rms)		
	Planes, Spheres	0.1	sec
	Ellipse	0.25	sec
	Horizontal elements	0.4	sec
6)	Slits	≥ 4	μm
7)	Grating line density	≤ 1600	ℓ/mm
8)	Types of monochromator considered:		
	Rowland Circle-SGM (RC-SGM)		
	Petersen-PGM (P-PGM)		

Figure 6.5.1: The Layouts of the Monochromators to be Compared [6.7]

A. Grazing Incidence Rowland Circle Monochromator

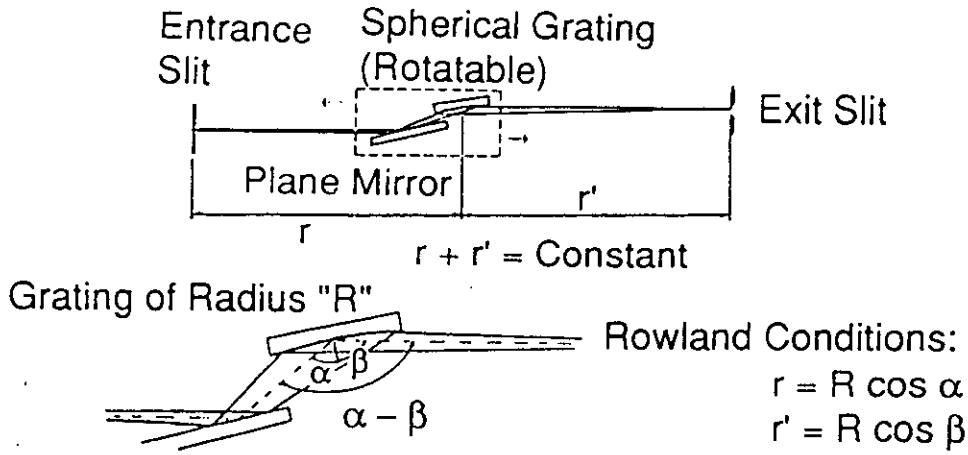

B. Petersen Plane Grating Monochromator

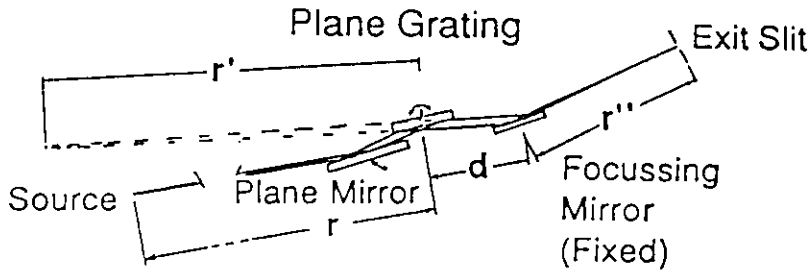

For Exact Focussing at all Wavelengths

$$-\frac{r'}{r} = \frac{\cos^2\beta}{\cos^2\alpha} = \text{Constant}$$

Figure 6.5.2: Ray Trace Comparison of a Rowland Circle-SGM and a Petersen-PGM [6.7]

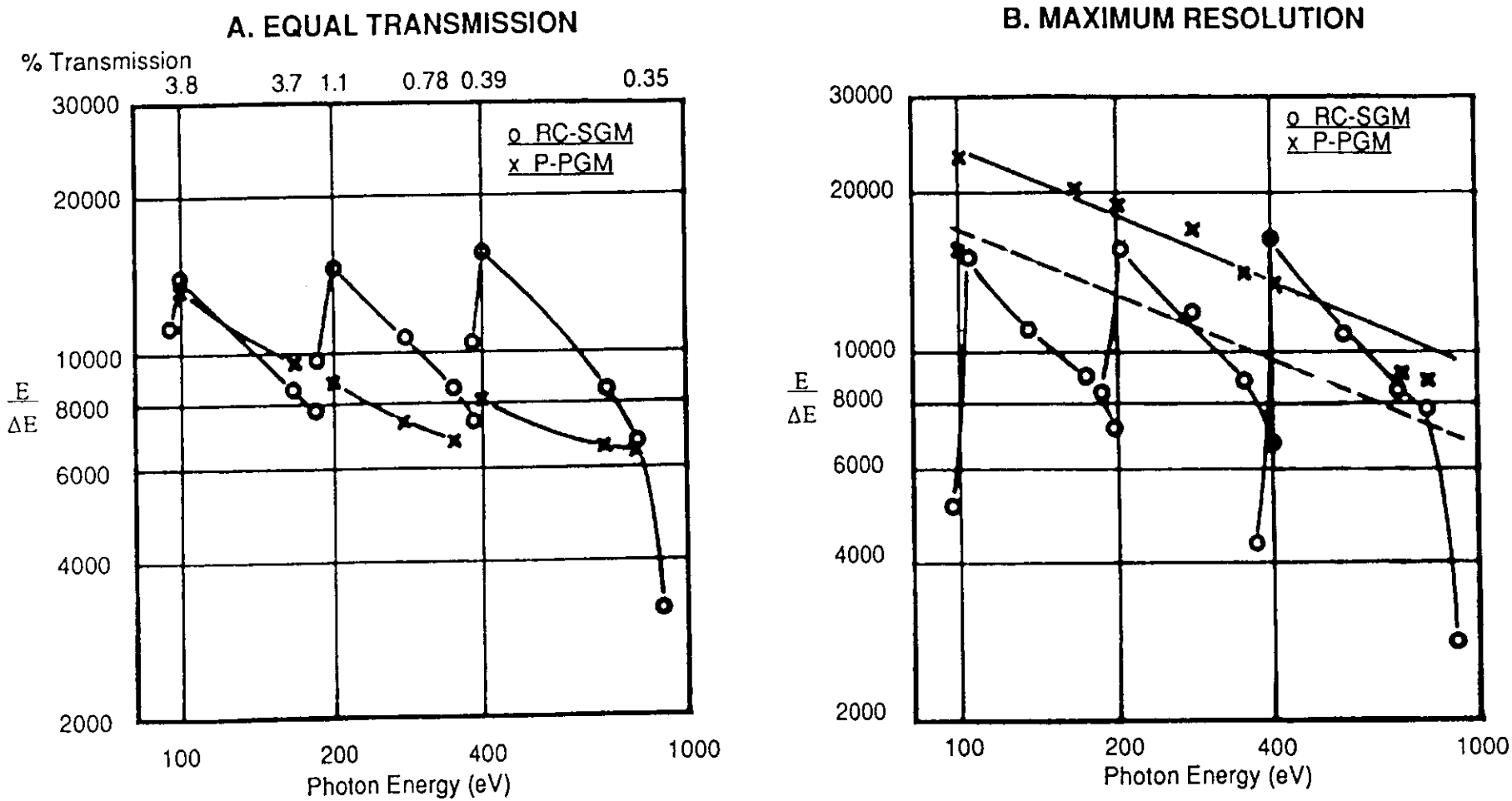

A. Resolution for Equal Transmission

1) RC-SGM: 10 μm slits; K-B preoptics of sphere and plane ellipse with 1/M = 6.4; Gratings (174°) 265 ℓ/mm, 530 ℓ/mm, 1060 ℓ/mm; Monochromator length = 8.0 m

2) P-PGM: 10 μm exit slit; spherical focussing mirror; Grating (174°) 1200 ℓ/mm, 1/M = 7.3 Monochromator length = 26.0 m. For "B" a 2400 ℓ/mm grating was used or 1200 ℓ/mm in second order.

B. Resolution maximized at cost of Transmission.

Table 6.5.2: Monochromator Comparison: Tally Sheet

	Rowland Circle SGM			**Petersen PGM**	
1)	Small entrance slit with preoptics	~ 97 % loss of photons	1)	„Small source" ring operation (lower current, shorter lifetime)	~ 50 % loss of photons
2)	Spherical grating	tan. err. small	2)	Plane grating	tan. err. small
3)	Measurements at optimized energy e.g. 400 eV	mono. focussed at this one energy	3)	Ellipsoidal mirror masked to reduce tan. errors	95 % loss of photons
4)	Vertical acceptance „blow up" due to demagnifying preoptics		4)	Very small vertical acceptance	
5)	„Optimal" interpretation of data	_____	5)	„Optimal" interpretation of data	_____
	Maximum resolution at 65 eV	**$\gtrsim$ 15 000**			**$\gtrsim$ 15 000**

From table 6.5.2 in which the performance of these two types of monochromator is compared step for step from source to experiment, what comes out at the end.....

the bottom line!

I hope that these "Notes 95 " have been useful!

W.B.Peatman
Berlin, November 1995

"NOTES 95": Some Notes on the Design of Beamlines for Soft X-ray Synchrotron Radiation Sources of the 3rd Generation

W.B. Peatman, BESSY, Berlin, BRD

11. References
(given by section)

1. Introduction

1. For both general and specific treatments of the problems encountered here see the proceedings of the various national and international Synchrotron Instrumentation Meetings.
2. B. Lai, F. Cerrina, "Shadow: A Synchrotron Radiation Ray Tracing Program", Nucl. Instr. and Meth. A246, 337 (1986). For information contact Franco Cerrina, Center for X-Ray Lithography and Electrical and Computer Engineering Dept., University of Wisconsin, Madison, WI 53706, USA
3. Raytrace program RAY, J. Feldhaus, Fritz-Haber-Institute, MPG, Berlin; F. Schäfers, BESSY, Berlin. For information contact F. Schäfers, BESSY, Lentzeallee 100, D-1000 Berlin 33, Germany.
4. An example of a complete system, from multi-undulator to experiment.
   a) R.Z. Bachrach, R.D. Bringans, B.B. Pate, R.G. Carr, "The SSRL Insertion Device beam line 'WUNDER'", SPIE Proc. 582, 251-267 (1985)
   b) R.Z. Bachrach, R.D. Bringans, L.E. Swartz, I. Lindau, B.B. Pate, R.G. Carr, N. Nower, B. Youngman, H. Morales, P. Pianetta, "Multi-Undulator Beam Line V at SSRL: A Progress Report", Nucl. Instr. Meth. A266, 83 (1988)
5. a) G. Isoyama, S. Yamamoto, T. Shioya, H. Ohkuma, S. Sasaki, T. Mitsuhashi, T. Yamakawa, H. Kitamura, "Construction of a Multiundulator, Revolver No. 19, at the Photon Factory", Rev. Sci. Instrum. 60, 1863 (1989)
   b) A. Kakizaki, H. Ohkuma, T. Kinoshita, A. Harasawa, T. Ishii, "Simultaneous Scanning of Revolver Undulator and Monochromator at BL-19A of the Photon Factory", Rev. Sci. Instrum. 63, 367-370 (1992)
6. "BESSY II, an Optimized Wiggler/Undulator Storage Ring Light Source for the VUV and XUV Spectral Regions" BESSY, Berlin (in German)
   (a) Part 1 1986 (b) Part 2 1989
7. U. Menthel, W.B. Peatman, F. Senf, "Conservation of Brightness in Undulator Beamlines", Rev. Sci. Instrum. 63, 481-484 (1992)
8. R.T. Avery, "Thermal Problems on High Flux Beam Lines", Nucl. Inst. Meth. 222, 146 (1984)

2. Characteristics of synchrotron radiation sources

1. S. Krinsky, M.L. Perlman, R.E. Watson, "Characteristics of Synchrotron Radiation and of its Sources" in "Handbook on Synchrotron Radiation", vol. 1, E.-E. Koch, Editor, North Holland, Amsterdam, 1983, chapter 2.
2. G. Brown, K. Halbach, J. Harris, H. Winick, "Wiggler and Undulator Magnets - A Review", Nucl. Instr. Meth. 208, 65-77 (1983)
3. C. Jacobsen, "SMUT" Undulator spectrum program with finite electron beam dimensions. Lawrence Berkeley Laboratory, Center for x-ray optics
4. C. Jacobsen, H. Rarback, "Predictions on the Performance of the Soft X-Ray Undulator", SPIE 582, 201-212 (1985)
5. H. Maezawa, Y. Suzuki, H. Kitamura, T. Sasaki, "Spectral Characterization of Undulator Radiation in the Soft X-Ray Region", Appl. Opt. 25, 3260-3268 (1987)
6. R.P. Walker, B. Diviacco "URGENT" Undulator spectrum program with finite electron beam dimensions. Sincrotrone Trieste, Italy
7. K. Molter, G. Ulm "Absolute Measurement of the Spectral and Angular Properties of Undulator Radiation with a Pinhole Transmission Grating Monochromator", Rev. Sci. Inst. 63, 1296-1299 (1992)
8. J.M. Machado, P. Kuske "Horizontal Beam Profile at the BESSY Storage Ring" BESSY Technical Report TB 106/87 (1987) (in German)
9. F. Schäfers, W. Peatman, A. Eyers, Ch. Heckenkamp, G. Schönhense, U. Heinzmann "High-flux normal incidence monochromator for circularly polarized synchrotron radiation", Rev. Sci. Instrum. 57, 1032 (1986)
10. W. Peatman, J. Bahrdt "Undulator Radiation: Promises and Problems", Nucl. Instr. and Meth. A282, 448 (1989)
11. W. Peatman, C. Carbone, W. Gudat, W. Heinen, P. Kuske, J. Pflüger, F. Schäfers, T. Schroeter "The BESSY wiggler/undulator-TGM-5 beamline", Rev. Sci. Instrum. 60, 1445 (1989)
12. "An ALS Handbook" Lawrence Berkeley Laboratory Publication PUB-643 Rev. 2, April 1989
13. R.P. Walker "Multipole Wiggler Brilliance and Effective Source Size", Sincrotrone Trieste Technical Report ST/M-TN-89/24
14. K.-J.Kim "Angular Distribution of Undulator Power for an Arbitrary Deflection Parameter K*", Nuc. Inst. Meth. A246, 67 (1986)
15. M.Scheer "WAVE" , Insertion device code: differential spectra, power, stokes parameters, for any magnet field : wiggler, undulator, wavelength shifter, dipole, etc.. Also interaction of magnet field with the storage ring, tracking. BESSY Berlin 1994.

3. Requirements of the optical system:

Reviews and new developments of monochromators, mirrors, etc. for SR

1. J.A.R. Samson, "Techniques of Vacuum Ultraviolet Spectroscopy", Wiley, New York (1967), Chapters 2, 3
2. W. Gudat, C. Kunz, "Instrumentation for Spectroscopy and Other Applications" in "Topics in Current Physics", vol. 10, C. Kunz, Editor, Springer, Berlin, 1979, chapter 3
3. R.L. Johnson, "Grating Monochromator and Optics for the VUV and Soft X-Ray Region" in "Handbook on Synchrotron Radiation", Vol. 1, E.-E. Koch, Editor, North Holland, Amsterdam, 1983, chapter 3
4. J.B. West, H.A. Padmore, "Optical Engineering" in "Handbook on Synchrotron Radiation", Vol. 2, G.V. Marr, Editor, North Holland, Amsterdam, 1987
5. T. Namioka, K. Ito, "Modern Developments in VUV Spectroscopic Instrumentation", Phys. Scripta 37, 673-681 (1988)
6. D. Attwood, K. Halbach, K.-J. Kim "Tunable Coherent X-Rays", Science 228, 1265-1272 (1985)
7. M.R. Howells, M.A. Iarocci, J. Kirz "Experiments in X-Ray Holographic Microscopy Using Synchrotron Radiation", J. Opt. Soc. Am. A 3, 2171-2178 (1986)
8. E. Spiller "Soft X-Ray Optics and Microscopy" in "Handbook on Synchrotron Radiation", Vol.1 E.E.Koch Editor, North Holland, Amsterdam, 1983, Chapter 12
9. A.Gaupp, W.Peatman "Instrumentierung für den Vakuum-Ultravioletten Spektralbereich" in 23. IFF-Ferienkurs: Synchrotronstrahlung zur Erforschung Kondensierter Materie, 1992, Jülich, Chapter 2 (in German)
10. Proceedings of the International Workshop "High Performance Monochromators and Optics for Synchrotron Radiation in the Soft X-Ray Region", Ed. W.Gudat, M. Howells, BESSY/LBL, 26-28 March 1991 in Berlin

4. Gratings and optics

1. H.G. Beutler, "The Theory of the Concave Grating", J. Opt. Soc. Am. 35, 311-350 (1945)
2. H. Haber, "The Torus Grating", J. Opt. Soc. Am. 40, 153-165 (1950)
3. H. Noda, T. Namioka, M. Seya, "Geometric Theory of the Grating", J. Opt. Soc. Am. 64, 1031-1036 (1974)
4. T. Namioka, M. Seya, H. Noda, "Design and Performance of Holographic Concave Gratings", Jap. J. Appl. Phys. 15, 1181-1197 (1976)

5. M. Nevière, P. Vincent, D. Maystre, (Efficiency of Conical Diffraction), Appl. Opt. 17, 843-845 (1978)
6. W.R. McKinney, M.R. Howells, "Design Optimization of 'Straight Groove' Toroidal Grating Monochromators for Synchrotron Radiation", Nucl. Instr. Meth. 172, 149-156 (1980)
7. M.R. Howells, "Vacuum Ultra Violet Monochromators", Nucl. Instr. Meth. 172, 123-131 (1980)
8. M.R. Howells, "Plane Grating Monochromators for Synchrotron Radiation", Nucl. Instr. Meth. 177, 127-139 (1980)
9. a.) H. Petersen, BESSY Technical Report TB29 (1980) unpublished
   b.)H. Petersen, "The Plane Grating and Elliptical Mirror: A New Optical Configuration for Monochromators", Opt. Commun. 40, 402-406 (1982)
10. H. Hogrefe, M.R. Howells, E. Hoyer, "Application of Spherical Gratings in Synchrotron Radiation Spectroscopy", SPIE Proc. 733, 274-285 (1986)
11. T. Harada, M. Itou, T. Kita, "A Grazing Incidence Monochromator with a Varied-Space Plane Grating for Synchrotron Radiation", SPIE Proc. 503, 114-118 (1984)
12. H. Petersen, "Plane Grating Monochromators: The Working Curve Concept as Implemented in the SX-700", SPIE Proc. 733, 262-264 (1986)
13. M. Pouey, "Dedicated Undulator Monochromators", Nucl. Instr. Meth. A 246, 256-259 (1986)
14. a.) C.T. Chen, "Concept and Design Procedure for Cylindrical Element Monochromators for Synchrotron Radiation", Nucl.Instr.Meth. A256, 595-604 (1987)
   b.) C.T.Chen, F. Sette, "Performance of the Dragon Soft X-Ray Beamline" Rev. Sci. Instrum. 60, 1616 (1989)
   c.) C.T.Chen, Y. Ma, F.Sette, "K-shell Photoabsorption of the N_2 Molecule", Phys. Rev. A, 40, 6737-6740 (1989)
15. J.B. West, H.A. Padmore, "Optical Engineering" in "Handbook on Synchrotron Radiation", Vol. 2, G.V. Marr, Editor, North Holland, Amsterdam, 1987, Chapter 2
16. M.C. Hettrick, J.H. Underwood, P.J. Batson, M.J. Eckart, "Resolving Power of 35000 (5 mA) in the extreme Ultraviolet Employing a Grazing Incidence Spectrometer", Appl. Opt. 27, 200-201 (1988)
17. For several new monochromator designs see "Proceedings" of SRI-88, SRI-91 and SRI-94 in "Review of Scientific Instruments", 1989, 1992, 1995.
18. REDUCE 3.3, A General Purpose Algebra System
   © A.C. Hearn (the RAND Corp.), 386 Based Computer Version, H. Melenk, W. Neun, Konrad Zuse Zentrum Berlin (1990)

19. E. Ishiguro, M. Suzui, J. Yamazaki, E. Nakamura, K. Sakai, O. Matsudo, N. Mizutani, F. Fukui, M. Watanabe "Constant Deviation Monochromator for the Range 100Å < λ < 1000Å" Rev. Sci. Inst. 60, 2105 (1989)20.
20. F. Senf, F. Eggenstein, W.B. Peatman "Simple, Constant Length Rowland Circle Monochromators for Undulator Radiation "Rev. Sci. Inst. 63, 1326-1329 (1992).
21. W. Werner, H. Visser "X-Ray Monochromator Designs Based on Extreme Off-Plane Grating Mountings" Appl. Opt. 20, 487-492 (1981)
22. C. Buckley, H. Rarback, R. Alforque, D. Shu, H. Ade, S. Hellman, N. Iskander, J. Kirz, S. Lindaas, I.McNulty, M. Oversluizen, E. Tang, D. Attwood, R. DiGennaro, M. Howells, C. Jacobsen, Y. Vladimirsky, S. Rothman, D. Kern, D. Sayre "Soft-x-ray imaging with the 35 period undulator at the NSLS" Rev. Sci. Instrum. 60, 2444-2447 (1989)
23. F. Schäfers, W. Peatman, A. Eyers, Ch. Heckenkamp, G. Schönhense, U. Heinzmann "High-flux normal incidence monochromator for circularly polarized synchrotron radiation" Rev. Sci. Instrum. 57, 1032-1041 (1986)
24. Chien-Te Chen, F. Sette, N.V. Smith "Double-headed Dragon monochromator for soft x-ray circular dichroism studies" Appl. Optics 29, 4535-4536 (1990)
25. H. Petersen "Circularly Polarized Light in the 30-2000 eV Photon Energy Range at the SX700/3" Proceedings of the International Workshop High Performance Monochromators and Optics for Synchrotron Radiation in the Soft X-Ray Region held at BESSY GmbH, Berlin, Germany 26th - 28th March 1991
26. V.V.Aristov "Bragg-Fresnel Optics: Principles and Prospects of Applications" in X-Ray Microscopa II, ed. D.Sayre, M.Howells, J. Kirz, H. Rarback, Springer-Verlag, 1988, pp 108-117
27. V.V.Aristov, A.I.Erko, B.Vidal, "Diffraction X-Ray Optics", IOP Publishing, London, 250 pages, in press (1995)
28. A.I.Erko, "Synthesized Bragg-Fresnel Multilayer Optics", J. X-Ray Science and Tech. 2, 297-316 (1990)
29. A.Erko "Multilayer Bragg-Fresnel Optics: Design, Technology and Applications", J.Physique IV C9, Vol.4, 245-251 (1994)
30. P.Dhez, A.I.Erko, E.Khzmalian, B.Vidal, "Kirkpatrick-Baez Microscope Based on Bragg-Fresnel X-Ray Multilayer Lenses" Appl.Optics, 31, 6664 (1991)
31. A.Erko, V.V.Martynov, D.V.Roshchupkin, A.Yuakshin, B.Vidal, P.Vincent, M. Brunel, "Multilayer Diffraction Grating Properties", J.Physique III, V.4, 1649-1658 (1994)
32. G.M.Bennett," X-Ray Grating Evaluation and Development" Ph.D. Thesis, Imperial College London, Department of Physics, 1971.

33. J.Bahrdt "Fourth-Order Optical Aberrations and Phase-Space Transformation for Reflection and Diffraction Optics", Appl.Opt 34, 114-127 (1995)
34. H.Petersen, F.Senf, F.Schäfers, J.Bahrdt, "Monochromators for the Undulator U49 at the BESSY II Storage Ring", Rev. Sci. Instrum. 66, 1777-1779 (1995)
35. J.Bahrdt, U.Flechsig, F.Senf, "Beamline Optimization and Phase Space Transformation", Rev. Sci. Instrum. 66, 2719-2723 (1995)

5. Mirror systems

1. P. Kirkpatrick, A.V. Baez, "Formation of Optical Images by X-Rays", J. Opt. Soc. Am. 38, 766-774 (1948)
2. W.A. Rense, T. Violett, "Method of Increasing the Speed of a Grazing-Incidence Spectrograph", J. Opt. Soc. Am. 49, 139-141 (1959)
3. T. Namioka, H. Noda, K. Goto, T. Katayama, "Design Studies of Mirror-Grating Systems for Use with an Electron Storage Ring Source at the Photon Factory", Nucl. Instr. Meth. 208, 215-222 (1983)
4. a) B.L. Henke, P. Lee, T.J. Tanaka, R.L. Shimabukuro, B.K. Fujikawa, "Low-Energy X-Ray Interaction Coefficients: Photoabsorption, Scattering and Reflection", Atomic Data Nucl. Data Tab. 27, 1 (1982)
   b) B.L. Henke, J.C. Davis, E.M. Gullikson, R.C.C. Perera, Lawrence Berkeley Laboratory, Berkeley, CA, LBL-26259 UC-411 (1988)
5. W.R. Hunter, "Measurement of Optical Constants in the Vacuum Ultraviolet Spectral Region" in "Handbook of Optical Constants of Solids", Ed. Palik, Academic, New York (1985) chapter 4
6. F. Schäfers "Description of the program REFLEC" BESSY Technical Report No. 157/1990 (in German)
7. M.R. Howells "Some Geometrical Considerations Concerning Grazing Incidence Reflectors", Brookhaven National Laboratory Report BNL-27416 (1980)
8. H. Petersen "Plane Grating Monochromators: Adjustment, Aspheric Mirror Analysis, Effects of Source Instabilities", BESSY Technical Report No. 118/1987 (in German)
9. E.L. Church, P. Takacs, "The Interpretation of Glancing Incidence Scattering Measurements", SPIE Proc. 640, 126-133 (1986)
10. P.Z. Takacs, E.L. Church, "Figure and Finish of Grazing Incidence Mirrors", Nucl. Instr. and Meth. A291, 253 (1990)
11. P.Z. Takacs, K. Furenlid, E.L. Church "Measurement of Surface Finish and Figure Accuracy" in Proceedings of the international workshop "High Performance Monochromators and Optics for Synchrotron Radiation in the Soft X-Ray Region" BESSY, Berlin 26th - 28th of March 1991

12. K. Becker, K. Beckstette "M 400 and P 400 - A Pair of Machines for Computer-Controlled Fine Correction of Optical Surfaces" in "Ultraprecision in Manufacturing Engineering", Springer, Berlin 1988
13. K. Beckstette, "Fabrication and Test of X-Ray Optics", SPIE 1140, 316 (1989)
14 H.E. Bennett, "Techniques for Evaluating the Surface Finish of X-Ray Optics", SPIE Proc. 184, 153-166 (1979)
15. K.H. Guenther, P.G. Wierer, J.M. Bennett, "Surface Roughness Measurements of Low-Scatter Mirrors and Roughness Standards", Appl.Opt. 23, 3820-3836 (1984)
16. H. Hogrefe, C. Kunz, "Soft X-Ray Scattering from Rough Surfaces: Experimental and Theoretical Analysis", Appl. Opt. 26, 2851-2859 (1987)
17. M. Born, E. Wolf "Principles of Optics", Pergamon Press Oxford, (1980)
18. E. Spiller "Soft X-Ray Optics and Microscopy" in "Handbook on Synchrotron Radiation", Vol.1 E.-E. Koch, Editor, NorthHolland,Amsterdam, 1983 chapter 12
19. F.A. Jenkins, H.E. White "Fundamentals of Optics", 4th Edition, McGraw-Hill, New York, 1976
20. A. Gaupp, M. Mast "First Experimental Experience with a VUV Polarimeter at BESSY", Rev. Sci. Instrum. 60, 2213 (1989)
21. A.G. Michette "Optical Systems for Soft X-Rays" Plenum, New York 1986

6. Monochromators and beamlines

1. H.A.Rowland, Philosophical Magasine 13, 469 (1882); ibid 16, 197 (1883)
2. Ch.Jung, Editor, "Research at BESSY: A User's Handbook", Nov. 1993
3. E.Dietz, W.Braun, A.M.Bradshaw, R.L.Johnson "A High Flux Toroidal Grating Monochromator for the Soft X-Ray Region" Nucl.Instr.Meth.A239,359-366 (1985)
4. W.B.Peatman, J.Bahrdt, F.Eggenstein, G.Reichardt, F.Senf "The Exactly Focusing Spherical Grating Monochromator for Undulator Radiation at BESSY" Rev. Sci. Instrum. 66, 2801-2806 (1995)
5. H.Petersen, C.Jung, C.Hellwig, W.B.Peatman, W.Gudat "Review of Plane Grating Focusing for Soft X-Ray Monochromators" Rev.Sci.Instrum. 66, 1-14 (1995)
6. a) H.Padmore, "Optimization of Soft X-Ray Monochromators" Rev. Sci. Instrum. 60, 1608-1615 (1989)
   b) R.Reiniger, V.Saile, Nucl. Instrum. Meth. A288, 343 (1990)
7. W.B.Peatman, F.Senf "High Resolution Monochromators for Undulator Radiation" Vacuum Ultraviolet Radiation Physics, Proceedings of the 10th VUV Conference (Paris,July1992), Ed. F.J.Wuilleumier, Y.Petroff, I.Nenner, 1993,pp.73-84
8. F.C.Brown, R.Z.Bachrach, N.Lien "The SSRL Ultrahigh Vacuum Grazing Incidence Monochromator: Design Considerations and Operating Experience" Nuc. Instr. Meth. 152, 73-79 (1978)

7. Source stability

1. R.O. Hettel, "Beam Steering at the Stanford Synchrotron Radiation Laboratory", IEEE Trans. Nucl. Sci. NS-30, 2228 (1983)
2. L.H. Yu, J. Nawrocky, J. Galayda, "Studies of Positional Stability of the Electron Beam in the NSLS Storage Ring", IEEE Trans. Nucl. Sci. NS-32, 3394 (1985)
3. K. Huke, "Correlation Between the Movement of the Light Source Building and the Vibration of the Synchrotron Radiation Axis", Photon Factory Preprint KEK 86-48 (1986)
4. M.A. Green, E.I. Majer, V.D. More, R.D. O'Connell, R.C. Shilling, "Ground Motion Measurements at the LBL Light Source Site, the Bevatron and at SLAC", Lawrence Berkeley Laboratory Report LBL-21519 (1986)
5. T. Katsura, Y. Kamiya, K. Haga, T. Mitsuhashi, "Beam Position Monitoring and Feedback Steering System at the Photon Factory", Part. Accl. Conf. 1987, IEEE Catalog No. 87CH2387-9, p. 538
6. W. Brefeld, "Beam Position Control System at DORIS II", Nucl. Instr. Meth. A 261, 22-26 (1987)
7. R.O. Hettel, "Beam Steering and Stabilizing Systems: Present Status and Considerations for the Future", Nucl. Instr. Meth. A 266, 155-163 (1988)
8. R.J. Nawrocky, J.W. Bittner, Li Ma, H.M. Rarback, D.P. Siddons, L.H. Yu, "Automatic Beam Steering in the NSLS Storage Rings Using Closed Orbit Feedback", Nucl. Instr. Meth. A 266, 164-171 (1988)
9. K.J. Kleman, "Beam Diagnostics and Control at ALADDIN", Nucl. Instr. Meth. A 266, 172-176 (1988)
10. E.D. Johnson, T. Oversluizen "Compact High Flux Photon Beam Position Monitor", Rev. Sci. Instrum. 60, 1947 (1989)
11. E.D. Johnson, T. Oversluizen "UHV Photoelectron X-Ray Beam Position Monitor", Nucl. Instr. Meth. A291, 427 (1990)
12. T.Warwick, D.Shu, B.Rodricks, E.D.Johnson "Prototype Photon Position Monitors for Undulator Beams at the Advanced Light Source" Rev. Sci. Inst. 63, 550-553 (1992)
13. F.-P. Wolf, W. Peatman "Synchrotron Radiation Diagnostics at BESSY", Nucl. Instr. Meth. A246, 408 (1986)
14. F.-P. Wolf, W. Peatman "Precise, Continuous Determination of Source Position and Emission Angle in Synchrotron Radiation Sources", Nucl. Instr. Meth. A278, 598 (1989)

8. Light of higher orders

1. E.S. Gluskin, E.M. Trachtenberg, A.S. Vinogradov, "A Simple System of the Short-Wave SR Prevention in the 30 Å to 180 Å Wavelength Range", Nucl. Instr. Meth. 152, 133-134 (1978)
2. R.J. Bartlett, D.R. Kania, R.H. Day, E. Källne, "Mirror Filter Systems for the Soft X-Ray Region", Nucl. Instr. Meth. 222, 95 - 98 (1984)
3. K. Ito, T. Namioka, Y. Morioka, T. Sasaki, H. Noda, K. Goto, T. Katayama, M. Koike, "High-Resolution VUV Spectroscopic Facility at the Photon Factory", Appl. Opt. 25, 837-847 (1986)
4. W. Peatman, "High-Order-Light Suppressor for Monochromators", BESSY Technical Report TB 160/90, 1990
5. M. Krumrey, E. Tegeler, "Self-Calibration of Semiconductor Photodiodes in the Soft X-Ray Region", Rev. Sci. Inst. 63, 797-801 (1992)
6. B.S.Itchkawitz, B.Kempgens, H.M.Köppe, J.Feldhaus, A.M. Bradshaw, W.B.Peatman "Absolute Photoabsorption Cross-Section Measurements of Simple Molecules in the Core-Level Region" Rev. Sci. Instrum. 66, 1531-1533 (1995).

9. Heat loading and radiation damage

1. T. Ohta, T. Fujikawa, "Computer Simulation of the Heating Effect on Mirrors by Synchrotron Radiation", KEK Technical Report (Japan, in english) KEK 81-10
2. V. Rehn, "Optics for Insertion-Device Beam Lines", SPIE Proc. 582, 238-250 (85)
3. R. Di Gennaro, W.R. Edwards, E. Hoyer, "Predicting Thermal Distortion of Synchrotron Radiation Mirrors with Finite Element Analysis", SPIE Proc. 582, 273-280 (1985)
4. R.T. Avery, "Thermal Problems on High Flux Beamlines", Nucl. Instr. Meth. 222, 146-158 (1984)
5. P.Z. Takacs, T.L. Hursman, J.T. Williams, "Application of Silicon Carbide to Synchrotron Radiation Mirrors", Nucl. Instr. Meth. 222, 133-145 (1984)
6. J.B. Kortright, P. Plag, R.C.C. Perera, P.L. Cowan, D.W. Lindle, B. Karlin, "Multilayer Coated Mirrors as Power Filters in Synchrotron Radiation Beamlines", Nucl. Instr. Meth. A 266, 452-456 (1988)
7. W. Peatman, J. Bahrdt, "Undulator Radiation: Promises and Problems", Nucl. Instr. Meth. A 282, 448 (1989)

10. Contamination of optical components

1. K. Boller, R.-P. Haelbick, H. Hogrefe, W. Jark, C. Kunz, "Investigation of Carbon Contamination of Mirror Surfaces Exposed to Synchrotron Radiation", Nucl. Instr. Meth. 208, 273-279 (1983)
2. W.R. McKinney, P.Z. Takacs, "Plasma Discharge Cleaning of Replica Gratings Contaminated by Synchrotron Radiation", Nucl.Instr.Meth. 195, 371-374 (1982)
3. T. Koide, S. Sato, T. Shidara, M. Niwano, M. Yanagihara, A. Yamada, A. Fujimori, A. Mikuni, H. Kato, T. Miyahara, "Investigation of Carbon Contamination of Synchrotron Radiation Mirrors", Nucl. Instr. Meth. A 246, 215-218 (1986)
4. T. Koide, T. Shidara, M. Yanagihara, S. Sato, "Resuscitation of Carbon-Contaminated Mirrors and Gratings by Oxygen Discharge Cleaning. 2: Efficiency Recovery in the 100 - 1000 eV Range", Appl. Opt. 27, 4305-4313 (1988)
5. E.D. Johnson, R.E. Garrett, "In Situ Reactive Cleaning of X-Ray Optics by Glow Discharge", Nucl. Instr. Meth. A 266, 381-385 (1988)
6. R.A. Rosenberg, D.B. Crossley, "Oxygen RF-Discharge Cleaning: Plasma Characterization and Implementation on a Grasshopper Beam Line", Nucl. Instr. Meth. A 266, 386-391 (1988)
7. B.R. Müller, F. Schäfers, F. Eggenstein, J. Feldhaus "Cleaning of Carbon Contaminated VUV-Optics: Influence on Surface Roughness and Reflectivity" Rev. Sci. Inst. 63, 1428-1431 (1992)